Smouldering and Thermal Remediation Effects on Properties and Behaviour of Porous Media

Stephanie Gabriele Zihms

Submitted for the degree of Doctor of Philosophy

University of Strathclyde

Department of Civil & Environmental Engineering

August 2013

Declaration of Authenticity

This thesis is the result of the author's original research. It has been composed by the author and has not been previously submitted for examination which has led to the award of a degree.

Signed:

Date: 01st August 2013

ABSTRACT

Smouldering and thermal remediation processes can achieve rapid removal of organic contaminants from soils but these processes expose soils to high temperatures for extended periods of time. Wild fire research shows changes in soil properties, when exposed to temperatures up to 850°C. Based on temperatures achieved during smouldering, this work aims to investigate how high temperature thermal and smouldering treatments affect soils.

Laboratory experiments on simple soils prepared from silica sand and silica sand-kaolin show that thermal treatments affect soil particle size distribution, mass, pH, mineralogy, liquid limits, and plastic limits. Properties such as particle density and bulk density remain unchanged after exposure to elevated temperatures.

In silica sand, shear strength decreases with increasing temperature and smouldering whereas it increases with increasing temperature in the sand-kaolin soil. High temperatures and smouldering may smooth the sand particle surfaces and reduce interparticle friction. The presence of kaolin may protect the sand grains from this effect and affect the shear strength through mineralogical changes. Kaolin addition has similar effects on hydraulic conductivity. Samples containing 10% kaolin show a relationship between hydraulic history, microstructure and hydraulic conductivity. Samples treated by smouldering have lower saturated hydraulic conductivities compared to furnace treatments. For silica sand no changes in hydraulic conductivity were observed. These changes in dynamic response were linked to changes on a particle scale such as chemistry, mineralogy, and composition.

ÜBERSICHT

Schwelbrand und Thermalsanierungsprozesse können kohlenstoffhaltige Schadstoffe schnell entfernen jedoch setzen diesen den Boden für längere Zeiträume hohen Temperaturen aus. Die Waldbrandforschung zeigt Veränderungen in Böden die Temperaturen bis zu 850℃ ausgesetzt s ind. Basierend auf den Temperaturen welche durch die Schwelbrandsanierung erreicht werden ist es das Ziel dieser Studie zu erforschen wie hohen Temperaturen der Schwelbrände und Thermalsanierungen den Boden verändern.

Laborversuche an einfachen Böden aus Quarzsand und Quarzsand-Kaolin zeigen, dass thermische Prozesse die Partikelgrößenverteilung, Masse, pH, Mineralogie, Fließ- und Plastizitätsgrenze beinflussen. Eigenschaften wie Partikel- und Rohdichte sind nach der thermischen Behandlung unverändert.

In Quarzsand verringert sich die Scherfestigkeit mit steigender Temperatur und nach einer Schwelbrandbehandlung. Im Vergleich zeigt sich ein ansteigende der Scherfestigkeit im Quarzsand-Kaolin bei steigender Temperatur. Hohe Temperaturen und Schwelbrände können die Oberfläche von Sandpartikeln glätten und damit die Reibkraft zwischen Partikeln verringern. Durch den Zusatz von Kaolin ist es möglich, die Sandpartikel hiervor zu schützten ausserdem beeinflussen die mineralogische Veränderungen im Kaolin die Scherfestigkeit zusätzlich. Ein ähnlicher Effekt last die Zugabe von Kaolin beim Bodendurchlässigkeitswert erkennen. Die Proben mit 10% Kaolinanteil zeigen eine Beziehung zwischen hydraulischer Vergangenheit, Mikorstruktur und Bodendurchlässigkeit. Proben, die mit Schwelbrand behandelt wurden haben eine niedrigere wassergesättigte Bodendurchlässigkeit als Proben die im Brennofen behandelt wurden. Bei Quarzsand wurden keine Veränderungen in der Bodendurchlässigkeit beobachtet.

Veränderungen im dynamischen Verhalten wurden mit Veränderungen auf Partikelebene so wie Chemie, Mineralogy und Aufbau gekoppelt.

Auf diese Beobachtungen basierend können Böden nach einer Sanierung nicht als identisch zu Böden vor Verunreinigung und Sanierung angesehen werden. Weiterhin kann nicht davon ausgegangen werden dass Sanierungenen die Urzustände in Böden wieder herstellen. Kontrollen der Bodeneigenschaften und des Verhaltens während und nach einer Sanierung mit hohen Temperaturen ist zwingend erforderlich um zu dokumentieren dass Veränderungen der Bodeneigenschaften und das dynamische Verhalten erkannt werden, und, wenn erforderlich, Stabilisierungsmaßnahmen ergriffen werden können um somit die sichere Wiederverwendung der sanierten Böden zu gewährleisten.

DEDICATION

In liebevoller Erinnnerung an meine Oma

ACKNOWLEDGEMENTS

I would like to thank my supervisor Christine Switzer for this interesting and very cool project. Thank you for your encouragement, insights and endless patience.

Thanks also to Minna Karstunen who provided geo-engineering input in the early stages and extra financial support in the final stage. And thanks to Alessandro Tarantino who provided meticulous attention to detail and invaluable input into the geotechnical experimental set up and theory.

Thanks must also go to Peter Cormack for the opportunity to have a dip into the chemical side of my project.

My main funding was provided by the Faculty of Engineering and the Department of Civil & Environmental Engineering of the University of Strathclyde for which I am very appreciative.

I thank all my friends for their support, understanding, and for showing me the importance of good coffee. You made sure my work-balance never became too unhealthy.
John – thanks for being my Hide&Write buddy during the final stage and I am sorry that I cannot repay the favour.

Susan – thanks for being a true inspiration and an amazing friend. I cannot tell you how much your friendship means to me.

I also want to thank my and Will's family.

Jane and Walter – thank you for all your support and interest in this project. I truly enjoyed our discussions and all of Walter's questions.

Mum and Dad – your constant support, encouragement, interest and challenges enabled me to follow my own path. It is because of you that I look back without any regrets. I will never be able to repay you for this.

Finally my greatest thanks go out to William – even countries away you manage to keep me sane, excited and encouraged. Having you as my lifeline throughout the four years of this PhD has made it possible. I could not have done this without you.

DANKSAGUNG

Hiermit möchte ich meiner Supervisorin Christine Switzer für dieses interessante und sehr coole Pojekt danken. Danke für deine Anregungen, Einblicke und endlose Geduld.

Ein Dankeschön auch an Minna Karstunen, die zu der frühen Geo-Ingenieur Phase beitrug und für Ihre extra finanzielle Unterstützung am Ende des Pojektes. Dank auch an Alessandro Tarantino für seine akribische Aufmerksamkeit für jedes Detail und seinen wertvollen Beitrag zu den geotechnischen Experimenten und Theorien.

Ein Dank auch an Perter Cormack, für die Möglichkeit die chemische Seite meines Projektes etwas genauer zu Erkunden.

Meine finanzielle Unterstützung kam hauptsächlich von der Fakultät für Ingenieurwissenschaften und dem Institut für Bau- und Umweltingenieurwissenschaften der Universität Strathclyde wofür ich sehr dankbar bin.

Ich möchte all meinen Freunden für ihre Unterstützung und Verständins danken und dass sie mir die Bedeutung von gutem Kaffee gezeigt haben. Ihr habt immer für einen gesunde Balance zwsichen Arbeit und Leben gesorgt.

John – danke dass du mein Hide&Write Kumpel in der letzten Phase warst und es tut mir leid dass ich mich nicht bei dir revangieren kann.

Susan – danke dass du eine echte Inspiration und eine großartige Freundin bist. Ich kann dir nicht sagen wie viel deine Freundschaft mir in den lezten vier Jahre geholfen hat.

Ich möchte mich auch bei meiner und Wills Familie bedanken.

Jane und Walter – danke für eure Unterstützung und Interesse an diesem Projekt. Ich habe unsere Diskussionen und Walters Fragen sehr genossen.

Mama und Papa – eure andauernde Unterstützung, Ermutigung, Interesse und Herausforderungen haben es mit ermöglicht meinen eigenen Weg zu gehen. Euretwegen schaue ich auf diesen Weg ohne Bedauern zurück. Ich werde euch nie genung dafür danken können.

Und zum Schluss mein größter Dank. Er geht an William – auch von weiter Ferne hast du es geschafft mir Ausgewogenheit zu gebe, mich zu ermutigen und zu begeistern. Dich als Anker in den letzten vier Jahre zu haben hat es mir ermöglicht diese Doktorarbeit zu meistern. Ich hätte dies ohne dich nicht geschafft.

ATTRIBUTION

This dissertation consists of four self-contained chapters (Chapters 2-5). Chapter 2 has been published in the peer-reviewed journal Engineering Geology. This attribution page is for introducing the co-authors and clarifying their contribution to this chapter.

Chapter 2: Dr Christine Switzer and Professor Minna Karstunen[1], Department of Civil & Environmental Engineering, University of Strathclyde, United Kingdom and former post-graduate student James Irvine are co-authors of this research article. This article was prepared by Stephanie Zihms. Dr Christine Switzer and Professor Minna Karstunen reviewed and revised the article. The modified falling head test was undertaken by James Irvine, however the data interpretation was done by Stephanie Zihms.

[1] Now at Department of Civil & Environmental Engineering, Chalmers University, Sweden

Contents

Declaration of Authenticity ii

ABSTRACT iii

ACKNOWLEDGEMENTS vii

ATTRIBUTION x

List of Figures xvi

List of Tables xix

1. Introduction 21

1.1. Smouldering Remediation 21

1.1.1. Organic Contaminants and Aggressive Remediation Technologies 21

1.1.2. Effects of Smouldering on Soil 23

1.1.3. Aims and Objectives 25

1.2. Literature Review 26

1.2.1. Wild Fires, Geological Disposal, and Thermal Remediation 26

1.2.2. Physical Properties 28

1.2.3. Hydraulic Conductivity and Wettability 32

1.2.4. Influence of Chemical Changes on Soil Physical Properties 33

1.3. Summary of Key Points Relevant to Remediation of Contaminated Sites 35

1.4. References 37

2. Effects of High Temperature Processes on Physical Properties of Silica Sand 43

2.1. Introduction 43

2.2. Materials and Methods 47

2.2.1. Sample Preparation and Heat Treatment....48
2.2.2. Laboratory Testing....49
2.3. Results and Discussion....53
2.3.1. Mineralogy....53
2.3.2. Particle and Bulk Densities....56
2.3.3. Particle Size Distribution....57
2.3.4. Preliminary Water Dynamic Tests....62
2.3.5. Summary and implications of soil changes....65
2.4. Conclusions....66
2.5. References....68
3. Changes to Shear Strength of Thermally Treated Soils and its Consideration for Remediation strategy....73
3.1. Introduction....73
3.2. Materials and Methods....76
3.2.1. Sample Preparation and Heat Treatment....77
3.2.2. Laboratory Testing....78
3.2.3. Direct Shear Box Testing....79
3.2.4. Image Analysis of Silica Sand Grain Photos and Thin Section Scans 82
3.3. Data Analysis and Friction Angle Determination....84
3.3.1. Silica Sand....84
3.3.2. Silica Sand + 10% Kaolin....90
3.4. Results and Discussion....90

3.4.1. Friction Angle Changes from Heat Treatment in Silica Sand.....90

3.4.2. Friction Angle Changes from Smouldering Remediation of Silica Sand 94

3.4.3. Friction Angle Changes in Silica Sand-Kaolin.....94

3.4.4. Discussion.....97

3.5. Conclusions.....98

3.6. References.....99

4. Unsaturated and Saturated Hydraulic Response of Silica Sand and Silica Sand-Kaolin after Thermal and Smouldering Treatments.....104

4.1. Introduction.....104

4.2. Materials and Methods.....107

4.2.1. Sample Preparation and Heat Treatment.....107

4.2.2. pH Testing.....108

4.2.3. Hydraulic Conductivity Testing.....108

4.2.4. Limitations and Assumptions.....110

4.2.5. Calculations.....112

4.3. Results and Discussion.....115

4.3.1. Saturated Hydraulic Conductivity.....116

4.3.2. Influence of Mineralogy on Saturated Hydraulic Conductivity.....120

4.3.3. Links between Changes in Particle Size to Changes in Pore Size...122

4.3.4. Transient Hydraulic Conductivity.....124

4.3.5. Mobilisation of Fines.....128

4.4. Conclusions 131

4.5. References 133

5. Analysis of Wettability of Heat Treated and Smouldered Silica Sands and Silica Sand-Kaolin 137

5.1. Introduction 137

5.1.1. Relationship between Wettability and Hydraulic Behaviour 141

5.2. Contact Angle Determination 144

5.2.1. Capillary Rise Method after Bachmann et al (2003) 146

5.2.2. Effective Radius Method 148

5.2.3. Effective Radius Determination 150

5.3. Materials and Methods 150

5.3.1. Sample Preparation and Heat Treatment 151

5.3.2. Modified Capillary Rise Experimental Set up and Method 151

5.3.3. Data processing 153

5.4. Validation of Contact Angle Determination Methods 156

5.4.1. Method after Bachman et al (2003) 156

5.4.2. Effective Radius Method 157

5.5. Results and Discussion 158

5.5.1. Silica Sand 158

5.5.2. Silica sand – kaolin 161

5.5.3. Discussion 163

5.6. Conclusion 164

5.7. References 166

6. Conclusions & Future Work 171

6.1. Conclusions 171

6.2. Future Work 175

6.3. Recommendations for Practice 176

Appendix A: Published Papers

Appendix B: Direct Shear Test Data

List of Figures

Figure 1.1. Variation of the plastic limit with temperature for two Turkish clays (Tan et al., 2004).....29

Figure 2.1. Schematic diagram of the modified falling head test apparatus.....52

Figure 2.2. Colour change observed in silica sand grains after heat treatment. 53

Figure 2.3. X-ray diffraction spectra for silica sand after thermal and smouldering treatments.....54

Figure 2.4. Mobilisation of particles smaller than 0.600mm from sand exposed to heat at 250, 500, 750, and 1000℃. Particles betwee n 0.600 and 2.36mm make up 99.7 – 99.9% of the particle size distribution in all cases.....59

Figure 2.5. Percentage of sand and sand/clay sample masses retained on the 1.18mm sieve after heat treatment and dry sieving.....61

Figure 2.6. Head loss (mm) observed over time in untreated sand, heat-treated sand, and sand after contamination with coal tar and smouldering remediation.....62

Figure 3.1 Pluviator design and shear box placement.....80

Figure 3.2 5kN s-type load cell calibration.....82

Figure 3.3. Calibration curves for vertical and horizontal displacement transducers82

Figure 3.4. Grain photograph original (A) and binary image for analysis (B) 83

Figure 3.5. Thin section scan conversion to binary image for use with ImageJ software. A: original scan, B: scan after selected grains have been coloured in, C: binary image of selected grains 83

Figure 3.6. Example shear box data for silica sand treated at 250℃ and 750℃ sheared with a normal stress of 100kPa. 1-1: displacement inflection point, 1-2: peak shear stress, 2-1: ultimate shear stress, 3-1: slope of dilatancy.....85

Figure 3.7. Example shear box data for silica sand treated at 250℃ and 750℃ sheared with a normal stress of 150kPa. 1-1: displacement inflection point, 1-2: peak shear stress, 2-1: ultimate shear stress, 4-1: start of non-typical test behaviour 86
Figure 3.8. Ultimate shear stress vs normal stress graph for Untreated silica sand.87
Figure 3.9. Peak shear stress vs effective normal stress for silica sand after different heat treatments.....88
Figure 3.10. Ultimate shear stress vs effective normal stress for silica sand after different heat treatments.....89
Figure 3.11. Example shear box data for silica sand + 10% kaolin treated at 500℃ sheared with a normal stress of 50kPa. 1-1: 55mm displacement, 2-1: ultimate shear stress.....90
Figure 3.12. Peak and ultimate friction angle values of silica sand for various treatment temperatures.....91
Figure 3.13. Example shear box data for silica sand treated with small scale smouldering (SM-2) sheared with a normal stress of 50kPa 92
Figure 3.14. Thin section Images for different thermal treatment temperatures.....93
Figure 3.15. Ultimate Friction Angle values (standard error) for sand-kaolin (10%) for different thermal treatment temperatures 95
Figure 3.16. XRD results for kaolin clay powder for different heat treatments 96
Figure 4.1. Hydraulic conductivity test – experimental set-up.....110
Figure 4.2. Experimental set-up and value definition for unsaturated hydraulic conductivity determination 114
Figure 4.3. Mass of water entering the column over the duration of the experiment 115
Figure 4.4. Average coefficient of hydraulic conductivity for silica sand 117

Figure 4.5. Saturated hydraulic conductivity for silica sand + 10% kaolin (5%MC) after different heat treatments.....119
Figure 4.6. Transient hydraulic conductivity of silica sand (corrected for the change of saturated sample length and hydraulic head).....125
Figure 4.7. Transient hydraulic conductivity of silica sand + 10% kaolin (corrected for the change of saturated sample length and hydraulic head) 127
Figure 4.8. Time lapse photographs during infiltration of silica sand + 10% kaolin sample (105-2). Showing the formation of a gap in the sample (1 A-E) and the removal of fines (2 A-E) 129
Figure 5.1. Representation of a liquid droplet on a surface under different wetting conditions. Relationship between wettability and contact angle (modified after Kumar and Prabhu (2007).....139
Figure 5.2. Rise of a liquid into a capillary; modified after (Smith, 2009) 143
Figure 5.3. Data for Silica Sand Untreated (2) showing the mass gain w^2 for the test duration 147
Figure 5.4. Linear proportion of the capillary rise experiment for Silica sand Untreated (2) 148
Figure 5.5. Capillary rise method – experimental set up.....153
Figure 5.6. Data for Silica Sand Untreated (2) experiment.....154
Figure 5.7. Data for Silica sand Untreated (2) experiment after discarding the filling data 155
Figure 5.8. Data for Silica Sand Untreated (2) after calculating mass gain of the sample for the experiment duration.....155
Figure 5.9. Relationship of final capillary rise height and capillary rise velocity for silica sand.....156

Figure 5.10. Relationship of final capillary rise height and capillary rise velocity for silica sand + 10% kaolin 157
Figure 5.11. Contact angle values for silica sand based on maximum (0.26mm) and minimum (0.06mm) effective capillary radius after different thermal treatments 159
Figure 5.12. Contact angle values for silica sand-kaolin mixtures based on maximum (0.26mm) and minimum (0.06) effective capillary radius after different thermal treatments.....161
Figure 6.1. Sketch of silica sand grain and silica sand grain + 10% kaolin with increasing thermal treatment (not to scale) 171
Figure 6.2. Links between particle scale changes and sample bulk response for silica sand and silica sand + 10% kaolin investigated in this study.....174

List of Tables

Table 1.1. Examples of thermal remediation techniques.....22
Table 2.1. Possible maximum temperatures of exemplar in-situ and ex-situ moderate to high remediation techniques 45
Table 2.2. Heat treatment conditions for silica sand.....49
Table 2.3. Exemplary mineralogy of points on sand grain surfaces after selected heat treatments.....55
Table 2.4. Particle density, minimum and maximum bulk density, particle size distribution, and mass loss observed in silica sand after exposure to elevated temperatures or smouldering remediation.....58
Table 2.5. Capillary rise height, void ratio, saturated hydraulic conductivity, and pH values for silica sand retained on the 1.18mm sieve 63
Table 3.1. Smouldering experiment summary for large and small scale set-up.....77
Table 3.2. Heating patterns for silica sand and silica sand-kaolin samples 78

Table 3.3. Image analysis results for full grains and thin section grains of silica sand 93
Table 3.4. Liquid and plastic limits for dry powder kaolin after different heat treatment temperatures.....97
Table 4.1. Summary of silica sand properties after different thermal treatments ...105
Table 4.2. Heating and cooling programme for silica sand + 10% kaolin samples 107
Table 4.3. Reynolds number (Re) for silica sand and silica sand + 10% kaolin for different treatment temperatures.....112
Table 4.4. Bulk densities and void ratios silica sand and silica sand + 10% kaolin samples 118
Table 4.5. pH values for kaolin, silica sand and silica sand + 10% kaolin after different thermal treaments 121
Table 4.6. Equivalent diameter for silica sand + 10% kaolin after different treatment temperatures 123
Table 4.7. Wetting front height for untreated and smouldered silica sand 126
Table 4.8. Sample height loss after infiltration for silica sand + 10% kaolin samples after heat treatment of 105 and 250℃..... 130
Table 5.1. Summary of properties of silica sand + 10% kaolin clay after different thermal treatments.....141
Table 5.2. Summary of pH and plastic and liquid limits of kaolin clay after different thermal treatment.....141
Table 5.3. Summary of properties for n-hexane and water.....144
Table 6.1. Summary of physical and chemical properties tested and how they are affected (T: temperature exposure independent of treatment; T<S: treatment dependent; N: not affected) 172

1. Introduction

1.1. Smouldering Remediation

Smouldering combustion is a novel, recently-patented remediation tool for soils contaminated with hazardous organic liquids. It has been particularly effective for coal tar and other high molecular weight contaminants, which are among the most difficult to treat. In-situ smouldering has been demonstrated across a wide range of soil and contaminant conditions and greater than 99.9% remediation has been observed in most cases, leaving behind clean, inert soil for reuse (Switzer et al., 2009). The aim of this research is to understand the effects that in-situ smouldering has on soil properties and soil behaviour, and determine how post-remediation soils differ from pre-remediation soil.

1.1.1. Organic Contaminants and Aggressive Remediation Technologies

Hazardous organic liquid contaminants are comprised of light and dense non-aqueous phase liquids (NAPLs), so named for their low miscibility with water. NAPLs are products or by-products of industrial processes and due to their long history of extensive use they pose a worldwide contamination problem (Vergnoux et al., 2010). The European Union (EU) specifically targets the re-use of large scale contaminated sites to reduce land consumption and further re-use of contaminated sites after remediation (McKnight and Finkel, 2013). The restoration of all large brownfield sites in the EU could cost up to €100 billion (Schädler et al., 2012). In the UK, in 1999, approximately 100 000 sites were identified as potentially contaminated and 10 000 sites are estimated to be definitely contaminated. These numbers include any range of contamination including waste, industrial and military sites (EEA, 2000). In the same year 1430 sites in the US were en identified as hazardous

waste and 600 contained poly aromatic hydrocarbons (Peters et al., 1999) and 60% of contaminated sites in Canada contain petroleum hydrocarbons (Sanscartier et al., 2009). These toxic and potentially carcinogenic pollutants enter the subsurface as oily liquids and because of their ability to adsorb on to solids they persist in the environment for long durations (Khalladi et al., 2009). This combination of contaminant chemistry and longevity makes them a risk to environmental and human health. Safe and effective removal of these contaminants is therefore necessary to protect the environment and create sites that are safe for redevelopment (Gan et al., 2009; Khalladi et al., 2009; Pironi et al., 2009).

A range of remediation methods is used to treat this kind of contamination, including thermal techniques, such as microwave, soil vapour extraction or incineration (Table 1.1).

Table 1.1. Examples of thermal remediation techniques

Remediation Technique	Maximum observed temperature (℃)	Approximate exposure duration (min)	Reference
Hot water extraction	300	20	Kronholm et al., 2002
Thermal desorption (low temperature)	112	47,570	Webb and Phelan, 1997
Thermal desorption (high temperature)	750	300	Chang and Yen, 2006
Heated soil extraction	300	50,400	Gan et al., 2009
Incineration	850	60	Lee et al., 2008
Smouldering remediation	600-1100[a]	60-3600[a]	Switzer et al., 2009

[a] Temperature range and exposure duration depend on the fuel

These thermal treatments either require removal of the soil for ex-situ treatment like incineration (Lee et al., 2008) or removing the contaminants as mobilised vapour (Webb and Phelan, 1997; Kronholm et al., 2002; Chang and Yen, 2006; Lee et al., 2008; Gan et al., 2009). The extracted vapour needs to be collected and treated ex-situ in addition to the removal from the soil. Smouldering remediation however uses the contaminants as part of the combustion process and therefore destroys them in place within the soil (Switzer et al., 2009). Exposure to elevated temperatures appears to affect stability and hydraulic conductivity, can lead to water repellent soil surfaces and alter the mineralogical composition of the soil (DeBano, 2000; Doerr et al., 2000; Certini, 2005; Goforth et al., 2005). In addition it is reported to affect the plasticity of clays causing cracking during firing processes (Colina et al., 2002; Tan et al., 2004; Ptáček et al., 2012).

1.1.2. Effects of Smouldering on Soil

To understand possible changes to soils due to exposure to elevated temperatures and smouldering remediation, research from related fields can provide insights. Soils exposed to elevated temperatures during wildfires (500-850℃) change properties. Chemical changes such as pH decrease with increasing temperature and are linked to ash formation during burning and the loss of organic acids (Ketterings and Bigham, 2000; Terefe et al., 2008). Physical changes such as increase in coarse sand fraction or increase in aggregate stability after burning are also observed (Ketterings and Bigham, 2000; Terefe et al., 2008; Are et al., 2009). However, wild fire research aims to understand effects of burning and the impact on forests, plants and their re-growth. Properties and behaviour of interest to geotechnical engineering are investigated but the way they are reported is often not in an engineering context or using non-engineering definitions. Therefore adding difficulty to comparison between studies and relating findings to geotechnical

engineering problems such as thermal remediation. Linking these findings to remediation research is important to improve both research areas. Wild fires occur on the soil surface, usually do not heat the soil above 500℃ and only affect the upper 20cm of the soil (Certini, 2005). Laboratory experiments are therefore conducted in this temperature range and focus on impact that relates to the soil surface, e.g. run-off after rainfall. Since smouldering remediation can reach gas phase temperatures of up to 1100℃, the changes observed during wildfires show that further investigation is necessary to complete the temperature profile encountered during smouldering remediation to better understand the impact of temperatures above 500℃.

High temperature (<1000℃) heating experiments on clay samples are done to understand the firing process and issues related to cracking in ceramic production. Although the temperature range is close to that of smouldering testing does not include engineering properties such as strength or hydraulic behaviour. Changes in clay mineralogy are observed with kaolinite transforming into mullite through sintering and dehydroxylation processes. Changes to mineralogy through sintering are reflected by an increase in particle size observed for kaolin treated with temperatures >550℃ (Fabbri et al., 2013). An increase of plasticity is also observed with increasing treatment temperature (Tan et al., 2004). These changes show that clay properties are also affected by exposure to elevated temperatures. It is very likely that the silt and sand fractions are affected in a similar way by these high temperatures. Thermal remediation research tends to focus on remediation success, technique novelty or the contaminant fate. It rarely includes post-treatment testing of the soil. Considering the aim of remediation is the removal of contaminants to allow a safe re-use of the treated soil, e.g. for housing or planting of energy crops, the fate of the soil needs be included.

1.1.3. Aims and Objectives

The aim of this research is to investigate and compare the effects of high-temperature thermal and smouldering treatments on soil properties and behaviour. To achieve these aims, simple soils involving silica sand and silica sand-kaolin mixtures are used to understand any links between micro-scale changes (e.g. mineralogy) and macro-scale behaviour (e.g. shear strength). The specific objectives of this research are:

1) Classification of physical and chemical properties of silica sand and kaolin clay related to elevated temperature exposure.
2) Determination of shear strength and friction angle of silica sand and silica sand-kaolin mixtures with exposure to elevated temperatures.
3) Analysis of unsaturated and saturated hydraulic response of silica sand and silica sand-kaolin mixtures with exposure to elevated temperatures.
4) Analysis of wettability by contact angle measurements for silica sand and silica sand-kaolin mixtures with exposure to elevated temperatures.
5) Development of links between physical and chemical properties and observed mechanical and hydraulic response.

Based on the findings for the sand and sand-clay materials, it will be possible to make inferences about the impacts of thermal and smouldering remediation on soils. Investigation of soil behaviour will focus on mechanical response during shearing and hydraulic response during infiltration. For the classification of physical and chemical properties the British Standard guidelines for laboratory testing are used and accompanied by methods from mineralogy (e.g. X-ray diffraction). The hydraulic and mechanical behaviour are investigated using geotechnical engineering methods, such as direct shear test and constant head test. These tests are

accompanied by methods used in soil science research such as the capillary rise test.

1.2. Literature Review

1.2.1. Wild Fires, Geological Disposal, and Thermal Remediation

Previous literature has shown that temperatures up to 500℃ affect the soil in some form (Ketterings and Bigham, 2000; Certini, 2005; Goforth et al., 2005; Hatten et al., 2005; Terefe et al., 2008; Are et al., 2009). However temperatures above 500℃ are investigated less and most properties reported are related to forest management like re-growth and soil damage. This broad discussion in the literature highlights that elevated temperatures do affect the soil and effects of smouldering combustion on soil properties should therefore be investigated, especially when used for in-situ remediation. This research is backed by literature published on heat treatments of clay showing the effects of temperatures up to 1000℃.

High level radioactive waste is proposed to be stored in deep geological repositories to ensure radionuclides do not affect environmental and human health. The heat generated by the radioactive waste is of concern for the barriers, buffer and backfill materials and is widely investigated (Gens et al., 2002; Min et al., 2005; Rempe, 2007; Yang and Yeh, 2009). The aim is to understand the implications to hydraulic and mechanical response of the barrier material, usually bentonite and the surrounding host rock after long term exposure to temperatures <100℃ (Gens et al., 2002; Yang and Yeh, 2009). Due to the design of the barrier material the temperature in the repository should not exceed 100℃ and there is little research on effects if this temperature is exceeded within the repository. But long term exposure experiments (<3 years) and simulations (<1 year) using temperatures

around 100℃ show a decrease in hydraulic conductivity over time. And if the stress state of the repository is close to its critical value exposure to elevated temperatures can cause shear dilation in the rock (Min et al., 2005). Research based on high temperatures can help understand changes to the barrier material and host rock and help predict repository performance should the temperature exceed 100℃.

Research considering various thermal remediation techniques (Table 1.1) tends to report the contaminant type and its fate and the cost related to the technique (McGowan et al., 1996; Chang and Yen, 2006). Remediation success is based on decreasing contamination to the desired level without considering any changes to the soil itself (Kronholm et al., 2002). Techniques are also considered environmentally friendly if they do not use organic solvents or additives to the soil, however changes to the soil like infiltration or particle mobilisation are not considered (Kronholm et al., 2002; Pironi et al., 2011). If changes to the soil are reported they tend to be based on visiual examination and are not reported on in more detail (Pironi et al., 2009; Switzer et al., 2009). This shows a gap with regards to soil and its fate after thermal remediation.

The properties affected can be split into three categories: physical, chemical and biological properties. Literature shows that temperatures reached during wild fires or used for heat treatment affect all of the above listed properties. The reasoning for these effects varies for different authors. The first two categories listed are discussed in more depth below.

Water repellency was initially investigated but found to not be occurring for the materials used in this study. Likely due to the lack of organic matter linked to water repellency in wild and forest fires (DeBano, 1981). The effects on biological

properties are out with the scope of this research and are therefore not discussed any further.

1.2.2. Physical Properties

The properties of interest and affected by wild fires or heat treatment are in regards to the soil strength. These comprise of particle size, shear strength, liquid limit, plastic limit and bulk density.

After exposure to low and moderate temperatures (200℃ to 300℃), soil strength has been observed to increase (Certini, 2005; Rein et al., 2008). The initial increase in strength is due to the increase in cementing or baking together clay sized particles. This coincides with a measured increase of sand particles with increasing temperatures. But when temperatures reach 500℃ or higher the soil strength decreases dramatically. This reduction in strength is linked to the loss of organic cements (Certini, 2005). A comparison of soil strength before and after burning (without an indication of burning temperatures) by Are et al (2009) shows a slight but not significant increase in soil strength combined with an increase in bulk density for the top 0.05m of the soil. The change in bulk density is due to the disruption of soil aggregation and loss of organic matter. A slight reduction of clay particles is also noted, which suggests aggregation of particles to create larger sized ones as observed by Certini et al (2005) and Rein et al (2008). This effect is also reported by Terefe et al (2008), however they also observe a change in soil texture where temperatures between 300℃ and 500℃ produce less s table aggregates. The above described property changes are good indicators to the effects smouldering could have on soil. Since wild fire temperatures rarely reach over 600℃ and therefore do not cover the whole temperature range encountered by smouldering remediation, filling this temperature gap is of high importance.

Research published on clay treated with temperatures of up to 1000℃ (Tan et al., 2004), shows a detailed list of property changes with temperatures. For low and medium temperatures, 100℃ to 400℃ and high temper atures 400℃ to 1000℃ the plastic and liquid limit of clay decreases, as well as specific gravity and optimum water content. The optimum water content decrease is significant between 100℃ and 400℃, where it drops from 36.0% to 17.6% but t hen remains almost constant around 16.0% at 1000℃ (Tan et al., 2004). This tre nd of higher effects for the low and medium temperatures is also observed for the other properties.

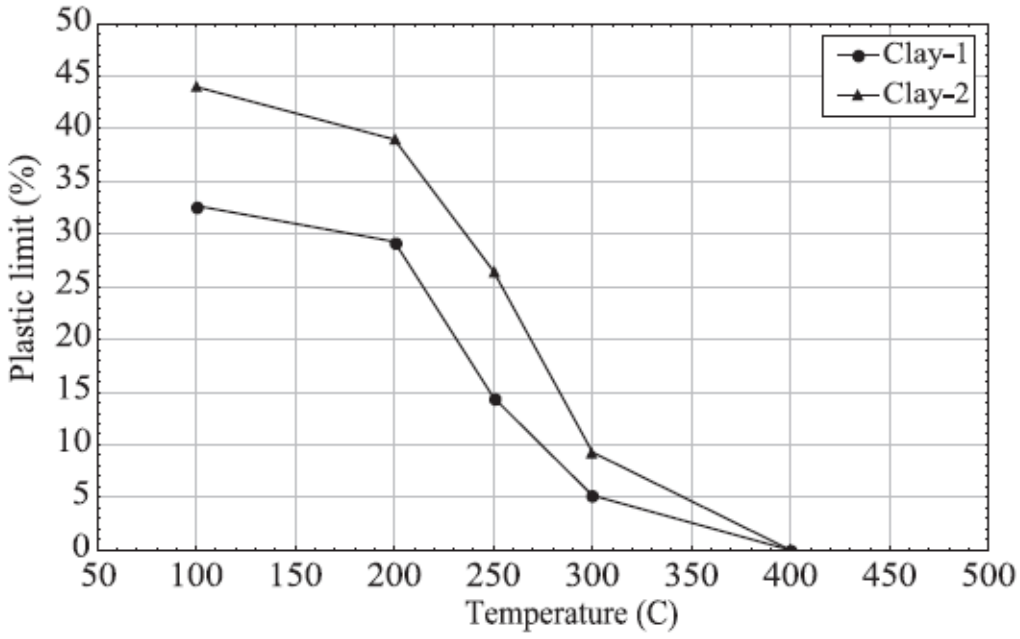

Figure 1.1. Variation of the plastic limit with temperature for two Turkish clays (Tan et al., 2004)

Plastic (Figure 1.1) and liquid limit decreases drastically between 100℃ and 300℃ with the clay becoming non-plastic at 400℃ (Tan et al., 2004). This is due to the loss of moisture causing the particles to become non-cohesive. The loss of the plastic ability of the soil has a major effect on the soil strength. Tan et al (2004) covers a higher temperature range and shows that temperatures above 400℃ do

not have a major effect on the soil. The research only covered clay soils but it shows the effects on clay by temperatures between 100℃ a nd 400°. Since this research is looking into soil remediation a better understanding of all soil components is important.

1.2.2.1. Shear Strength

As an engineering property soil strength is defined by a cohesion and an angle of shearing resistance which are both dependent on the stress environment of the material (e.g. soil) see Equation 1.1.

$$\tau = c + \sigma \tan \Phi \qquad \text{(Eq. 1.1)}$$

Where τ is the shear stress (or shear strength) (kPa), c is the cohesion, σ is the normal stress (kPa) and Φ is the friction angle (°).

In wild and forest fire research soil or aggregate stability are used to show temperature effects on soils. In this context stability is not properly defined or under what stresses the stability is tested. From an engineering perspective, it is important to include soil strength, as this is a property likely to be affected by temperatures. The definition given above (Eq. 1.1) enables comments and comparisons between different materials.

The direct shear test or so called shear box test is a quick and simple way to test the shear strength of sand and granular soils and gives a first insight in variations in strength due to medium and high temperatures. Results given by shear strength testing on the frictional strength of the sand and its development with increasing temperature can also be useful to other areas of research e.g. forest and wild fires, other remediation techniques producing heat or tunnel fires and their effects on

surrounding soil. Tarantino (2010) states that unsaturated materials effect the mechanical testing due to the presence of bulk and meniscus water within the sample (Tarantino, 2010). This effect can be eliminated by testing dry sand samples in the shear box. The samples have to be kept in a perfectly dry environment after heat treatment and prior to testing. This will help to determine solely the effects of temperature. The direct shear test and its results can also be influenced by characteristics of the material used. Those include but are not limited to particle shape, particle size, sample preparation and grain crushing, which are described in more detail below.

1.2.2.2. Effect of Particle Shape and Size

Direct shear testing results can be influenced by particle shape and size. Santamarina and Cho (2004) describe how larger grains have a higher probability of imperfections and are therefore more likely to show brittle fracturing during testing. Particle size also determines the relative arrangement of the sample and interparticle forces of the grains. For larger grains packing is mostly determined by gravitational forces and is in a bulky matter (Santamarina and Cho, 2004). Particle shape controls the behaviour of the sample before and or during shearing e.g. rounded grains can cause grain rolling whereas angular or subangular grains can cause grain interlocking. Grain rolling decreases the shear strength of the sample whereas grain interlocking can increase the shear strength (Mair et al., 2002), interlocking grains can also affect the volume of the sample tested (Li and Aydin, 2010). This agrees with research by Mair et al. (2002) who shows that spherical grains have a lower frictional strength than subangular grains. Research also shows that grain shape is more important than the particle size distribution or surface roughness (Mair et al., 2002). However, research by Bagherzadeh-Khalkhali 2009 shows that particle size and particle size distribution affect the direct shear test. He

compared various preparation techniques to compare these effects. It shows that the friction angle (a way to describe a samples shear strength) increases with overall particle size of the sample (Bagherzadeh-Khalkhali and Mirghasemi, 2009).

1.2.3. Hydraulic Conductivity and Wettability

The hydraulic conductivity describes how easily porous media such as rocks or soils can transmit a fluid. It is a complex phenomenon influenced by the scale of the medium (Fallico et al., 2010). Porous media have hydraulic conductivities in saturated and unsaturated ranges and changes to both are of interest in post-remediation soils. Smouldering and thermal remediation processes displace water during operation. During smouldering, this displacement occurs mainly within the treatment zone but also at a rim surrounding the target area. During thermal remediation, where operating time is on the order of weeks to months, water displacement in the subsurface may be more extensive. With removal of soil water, the treatment zone becomes unsaturated. The unsaturated hydraulic conductivity describes how a fluid flows in an unsaturated soil. The saturated hydraulic conductivity describes water flow through the soil once it is fully saturated. It is important to understand how thermal and smouldering remediation processes impact water movement through the soil following exposure to elevated temperatures during remediation or other high temperature processes.

The wettability of a soil and its changes are important for the overall water balance. Understanding and being able to predict changes to the water balance or the behaviour of the water recharge are important, especially for remediated sites. A change in water recharge or the water balance can have significant effects on run-off, fingered infiltration and contaminant transport (Wang et al., 2000; Lipsius and Mooney, 2006; Cuthbert et al., 2010). Wettability can be described by the contact

angle (CA), which in turn can be determined by capillary rise methods(Czachor, 2006). The capillary rise method is widely used to determine contact angles for soils and soil aggregates. Glass beads are also used in fundamental studies to investigate changes like surface roughness and its effect on the contact angle (Dang-Vu et al., 2006; Kumar and Prabhu, 2007; Ramírez-Flores et al., 2008; Chau et al., 2009; Ramírez-Flores et al., 2010). Some research on wettability is done on active sites but due to the variable nature, time scales and efforts these contributions are rather scarce, but nevertheless give a good insight into infiltration and drainage behaviour on a real scale and real conditions (Lipsius and Mooney, 2006; Cuthbert et al., 2010). Most experiments into understanding wettability changes are done in laboratories and investigate the contact angle by the capillary rise method. Especially fundamental studies on glass beads provide a good insight into changes due to changes to the porous media e.g. surface roughness. Physical and chemical factors affect the soils wettability and its response to wetting. An increasing surface roughness enhances the already existing characteristics of the soil. A hydrophobic soil becomes even more hydrophobic and a hydrophilic soil more hydrophilic. The penetration speed also increases for rougher surfaces compared to smooth ones, as does the nature of the penetration. Uneven water penetration has been observed for glass beads with smooth surfaces compared to an even penetration for rough surfaces. (Dang-Vu et al., 2006; Ramírez-Flores et al., 2008; Chau et al., 2009; Ramírez-Flores et al., 2010).

1.2.4. Influence of Chemical Changes on Soil Physical Properties

Forest and wild fire literature record chemical properties of soils such as composition, colour, pH, organic matter and magnetic susceptibility as affected by temperature. Even though they do not influence the soil strength as majorly as the physical property changes described in Section 1.2.2, they are included as

engineering properties of soils, e.g. the pH value determines the type of concrete suitable for a site.

The composition of soils can change with increasing temperatures due to the decomposition of magnesium carbonate, oxidation of iron and decomposition of clay minerals. The decomposition of magnesium carbonate starts at temperatures above 300℃ (Terefe et al., 2008) and increases the pH va lue of the soil.

The organic content of the soil also influences the soil pH. Soils with high organic content show an increase in pH values compared to soils with a lower organic content (Terefe et al., 2008). At temperatures from 450℃ to 500℃ the denaturation of organic acids causes the soil pH to increase drastically (Certini, 2005). Knowing the composition of the soil before remediation is important to make more precise predictions about the soil pH value change due to remediation. Due to the low reactivity of kaolin the effects of pore water chemistry are not included in this study.

1.2.4.1 Mineralogy

Impact of elevated temperature on the mineralogical composition of the soil may be important as well. Mineralogical changes of soil particles, especially clay minerals, starts at temperatures above 550℃ (Certini, 2005). These temperatures are rarely reported for wild and forest fire, but temperatures up to 1100℃ can be achieved during smouldering remediation (Pironi et al., 2009; Switzer et al., 2009). Colour change in soils has been observed after wild fires and after smouldering remediation. In most cases it changes from yellowish brown to reddish brown. This is due to the oxidation of soil iron content from goethite to maghemite or hematite (Ketterings and Bigham, 2000; Goforth et al., 2005). Goforth et al (2005) observe

the colour change for severely burned soil experiencing temperatures between 300℃ and 500℃, whereas Ketterings and Bigham (200 0) observe the same type of colour change for temperatures >600℃. The higher t emperatures recorded by Ketterings and Bigham (2000) show that the duration of exposition to elevated temperatures is important, too. The change in iron oxides during the burning or heating of the soil has an effect on the magnetic susceptibility of the soil and can actually be measured (Goforth et al., 2005). For temperatures between 300℃ and 500℃ Goethite (α-FeO(OH)) transforms into anti-ferromagnetic hematite (α-Fe_2O_3) and more abundantly to ferromagnetic maghemite (γ-Fe_2O_3).

1.3. Summary of Key Points Relevant to Remediation of Contaminated Sites

As part of the Code of practice for investigations an assessment into the changes that may arise in the ground and environmental conditions (naturally or due to the planned work) is required and stated as one of the primary objectives of the planned investigation (BS 5930:1999).

Proposing a relatively quick and cost effective in situ remediation technique for a broad range of nonaqueous phased liquids (NAPLs) will help fill a remediation need and improve remediation of these most frequently occurring subsurface contaminants within the industrialised world (Pironi et al., 2009; Switzer et al., 2009; Pironi et al., 2011). Understanding the process of self-sustaining smouldering combustion for in situ remediation as early as possible in the remediation process is vital to identify any risks to treated sites and their integrity. Usually new remediation techniques are investigated into their remediation effectiveness and cost to potential users. Considering the aim of this new technique to provide an in situ solution for

heavily contaminated sites with no limitation to size of the treated area, it is important to include changes to the treated soil as well as the effectiveness of the remediation itself. The remediation potential of this new technique is investigated by other researchers and results from bench scale proof of concepts experiments are investigated and published (Pironi et al., 2009; Switzer et al., 2009; Pironi et al., 2011).

1.4. References

Are, K.S., Oluwatosin, G.A., Adeyolanu, O.D., Oke, A.O., 2009. Slash and burn effect on soil quality of an Alfisol: Soil physical properties. Soil and Tillage Research, 103(1): 4-10.

Bagherzadeh-Khalkhali, A., Mirghasemi, A.A., 2009. Numerical and experimental direct shear tests for coarse-grained soils. Particuology, 7(1): 83-91.

Certini, G., 2005. Effects of fire on properties of forest soils: a review. Oecologia, 143(1): 1-10.

Chang, T.C., Yen, J.H., 2006. On-site mercury-contaminated soils remediation by using thermal desorption technology. Journal of Hazardous Materials, 128(2-3): 208-217.

Chau, T.T., Bruckard, W.J., Koh, P.T.L., Nguyen, A.V., 2009. A review of factors that affect contact angle and implications for flotation practice. Advances in Colloid and Interface Science, 150(2): 106-115.

Colina, F.G., Esplugas, S., Costa, J., 2002. High-Temperature Reaction of Kaolin with Sulfuric Acid. Industrial & Engineering Chemistry Research, 41(17): 4168-4173.

Cuthbert, M.O., Mackay, R., Tellam, J.H., Thatcher, K.E., 2010. Combining unsaturated and saturated hydraulic observations to understand and estimate groundwater recharge through glacial till. Journal of Hydrology, 391(3-4): 263-276.

Czachor, H., 2006. Modelling the effect of pore structure and wetting angles on capillary rise in soils having different wettabilities. Journal of Hydrology, 328(3–4): 604-613.

Dang-Vu, T., Hupka, J., Drzymala, J., 2006. Impact of roughness on hydrophobicity of particles measured by the Washburn method. Physicochemical Problems of Mineral Processing, 40: 45-52.

DeBano, L.F., 1981. Water Repellent Soils: a state-of-the-art. Pacific Southwest Forest and Range Experiment Station, General Technical Report PSW-46.

DeBano, L.F., 2000. Water repellency in soils: a historical overview. Journal of Hydrology, 231: 4-32.

Doerr, S.H., Shakesby, R.A., Walsh, R.P.D., 2000. Soil water repellency: its causes, characteristics and hydro-geomorphological significance. Earth-Science Reviews, 51(1-4): 33-65.

EEA, 2000. European Environment Agency, Management of Contaminated Sites in Western Europe, Topic Report No. 13/1999.

Fabbri, B., Gualtieri, S., Leonardi, C., 2013. Modifications induced by the thermal treatment of kaolin and determination of reactivity of metakaolin. Applied Clay Science, 73: 2-10.

Gan, S., Lau, E.V., Ng, H.K., 2009. Remediation of soils contaminated with polycyclic aromatic hydrocarbons (PAHs). Journal of Hazardous Materials, 172(2-3): 532-549.

Gens, A., Guimaraes, L.d.N., Garcia-Molina, A., Alonso, E.E., 2002. Factors controlling rock–clay buffer interaction in a radioactive waste repository. Engineering Geology, 64(2–3): 297-308.

Goforth, B.R., Graham, R.C., Hubbert, K.R., Zanner, C.W., Minnich, R.A., 2005. Spatial distribution and properties of ash and thermally altered soils after high-

severity forest fire, southern California. International Journal of Wildland Fire, 14(4): 343-354.

Hatten, J., Zabowski, D., Scherer, G., Dolan, E., 2005. A comparison of soil properties after contemporary wildfire and fire suppression. Forest Ecology and Management, 220(1-3): 227-241.

Ketterings, Q.M., Bigham, J.M., 2000. Soil color as an indicator of slash-and-burn fire severity and soil fertility in Sumatra, Indonesia. Soil Science Society of America Journal, 64(5): 1826-1833.

Khalladi, R., Benhabiles, O., Bentahar, F., Moulai-Mostefa, N., 2009. Surfactant remediation of diesel fuel polluted soil. Journal of Hazardous Materials, 164(2-3): 1179-1184.

Kronholm, J., Kalpala, J., Hartonen, K., Riekkola, M.-L., 2002. Pressurized hot water extraction coupled with supercritical water oxidation in remediation of sand and soil containing PAHs. The Journal of Supercritical Fluids, 23(2): 123-134.

Kumar, G., Prabhu, K.N., 2007. Review of non-reactive and reactive wetting of liquids on surfaces. Advances in Colloid and Interface Science, 133(2): 61-89.

Lee, W.-J. et al., 2008. Thermal treatment of polychlorinated dibenzo-p-dioxins and dibenzofurans from contaminated soils. Journal of Hazardous Materials, 160(1): 220-227.

Li, Y.R., Aydin, A., 2010. Behavior of rounded granular materials in direct shear: Mechanisms and quantification of fluctuations. Engineering Geology, 115(1-2): 96-104.

Lipsius, K., Mooney, S.J., 2006. Using image analysis of tracer staining to examine the infiltration patterns in a water repellent contaminated sandy soil. Geoderma, 136(3–4): 865-875.

Mair, K., Frye, K.M., Marone, C., 2002. Influence of grain characteristics on the friction of granular shear zones. Journal of Geophysical Research, 107(B10, 2219): EVC 4-1 - EVC 4-9.

McGowan, T.F., Greer, B.A., Lawless, M., 1996. Thermal treatment and non-thermal technologies for remediation of manufactured gas plant sites. Waste Management, 16(8): 691-698.

McKnight, U.S., Finkel, M., 2013. A system dynamics model for the screening-level long-term assessment of human health risks at contaminated sites. Environmental Modelling & Software, 40(0): 35-50.

Min, K.-B., Rutqvist, J., Tsang, C.-F., Jing, L., 2005. Thermally induced mechanical and permeability changes around a nuclear waste repository—a far-field study based on equivalent properties determined by a discrete approach. International Journal of Rock Mechanics and Mining Sciences, 42(5–6): 765-780.

Peters, C.A., Knightes, C.D., Brown, D.G., 1999. Long-Term Composition Dynamics of PAH-Containing NAPLs and Implications for Risk Assessment. Environmental Science & Technology, 33(24): 4499-4507.

Pironi, P., Switzer, C., Gerhard, J.I., Rein, G., Torero, J.L., 2011. Self-Sustaining Smoldering Combustion for NAPL Remediation: Laboratory Evaluation of Process Sensitivity to Key Parameters. Environmental Science & Technology, 45(7): 2980-2986.

Pironi, P. et al., 2009. Small-scale forward smouldering experiments for remediation of coal tar in inert media. Proceedings of the Combustion Institute, 32: 1957-1964.

Ptáček, P. et al., 2012. The kinetics and mechanism of kaolin powder sintering I. The dilatometric CRH study of sinter-crystallization of mullite and cristobalite. Powder Technology, 232: 24-30.

Ramírez-Flores, J.C., Bachmann, J., Marmur, A., 2010. Direct determination of contact angles of model soils in comparison with wettability characterization by capillary rise. Journal of Hydrology, 382(1–4): 10-19.

Ramírez-Flores, J.C., Woche, S.K., Bachmann, J., Goebel, M.-O., Hallett, P.D., 2008. Comparing capillary rise contact angles of soil aggregates and homogenized soil. Geoderma, 146(1-2): 336-343.

Rein, G., Cleaver, N., Ashton, C., Pironi, P., Torero, J.L., 2008. The severity of smouldering peat fires and damage to the forest soil. CATENA, 74(3): 304-309.

Rempe, N.T., 2007. Permanent underground repositories for radioactive waste. Progress in Nuclear Energy, 49(5): 365-374.

Sanscartier, D., Zeeb, B., Koch, I., Reimer, K., 2009. Bioremediation of diesel-contaminated soil by heated and humidified biopile system in cold climates. Cold Regions Science and Technology, 55(1): 167-173.

Santamarina, J.C., Cho, G.C., 2004. Soil behaviour: The role of particle shape. Advances in Geotechnical Engineering: The Skempton Conference, 1: 604-617.

Schädler, S., Morio, M., Bartke, S., Finkel, M., 2012. Integrated planning and spatial evaluation of megasite remediation and reuse options. Journal of Contaminant Hydrology, 127(1–4): 88-100.

Switzer, C., Pironi, P., Gerhard, J.I., Rein, G., Torero, J.L., 2009. Self-Sustaining Smoldering Combustion: A Novel Remediation Process for Non-Aqueous-Phase Liquids in Porous Media. Environmental Science & Technology, 43(15): 5871-5877.

Tan, Ö., Yilmaz, L., Zaimoglu, A.S., 2004. Variation of some engineering properties of clays with heat treatment. Materials Letters, 58(7-8): 1176-1179.

Tarantino, A., 2010. Basic concepts in the mechanics and hydraulics of unsaturated geomaterials. New Trends in the Mechanics of unsaturated Geomaterials(3-28).

Terefe, T., Mariscal-Sancho, I., Peregrina, F., Espejo, R., 2008. Influence of heating on various properties of six Mediterranean soils. A laboratory study. Geoderma, 143(3-4): 273-280.

Vergnoux, A., Malleret, L., Asia, L., Doumenq, P., Theraulaz, F., 2010. Impact of forest fires on PAH level and distribution in soils. Environmental Research, doi:10.1016/j.envres.2010.01.008.

Wang, Z. et al., 2000. Effects of soil water repellency on infiltration rate and flow instability. Journal of Hydrology, 231–232(0): 265-276.

Webb, S.W., Phelan, J.M., 1997. Effect of soil layering on NAPL removal behavior in soil-heated vapor extraction. Journal of Contaminant Hydrology, 27(3-4): 285-308.

Yang, S.-Y., Yeh, H.-D., 2009. Modeling transient heat transfer in nuclear waste repositories. Journal of Hazardous Materials, 169(1–3): 108-112.

2. Effects of High Temperature Processes on Physical Properties of Silica Sand

2.1. Introduction

Soils can be exposed to elevated temperatures naturally through wild, forest or peat fires or through thermal remediation processes designed to mitigate high concentrations of hazardous organic contaminants. Most research on soil properties and their heat dependency is based on forest fires and therefore concentrates on erosion rates, ground stability and nutrients affected by fire severity. The effects of exposure to temperatures up to 500℃ have been stud ied widely (Are et al., 2009; Certini, 2005; De Bruyn and Thimus, 1996; Rein, 2009; Rein et al., 2008).`. Literature published on heat treatments of clay evaluates the effects of temperatures up to 1000℃ (Tan et al., 2004). Exposures of 200 – 850℃ have been observed in soils during wildfires (Certini, 2005; DeBano, 2000; Mataix-Solera and Doerr, 2004; Rein et al., 2008). Moderate (300-400℃) and high (>450℃) temperature processes, such as hot water extraction, thermal desorption, soil heated vapour extraction, incineration or smouldering are widely used to treat contaminated soils (Araruna Jr et al., 2004; Chang and Yen, 2006; Gan et al., 2009; Kronholm et al., 2002; Lee et al., 2008; McGowan et al., 1996; Pironi et al., 2011; Pironi et al., 2009; Switzer et al., 2009; Webb and Phelan, 1997). Previous studies on the effects of non-aqueous phase liquid (NAPL) contamination on soil properties shows a net reduction in soil stability as NAPL content increases (Khamehchiyan et al., 2007). NAPLs displace soil moisture and thus change the interactions between soil particles. Most research on soil remediation techniques focuses on the remediation result and less on the effects the technique has on the soil properties itself. In some cases, the effects on

soil properties may be a criterion for selection of the remediation technique (Chang and Yen, 2006; Pironi et al., 2011) or the soil properties may influence the results (Webb and Phelan, 1997). There is little research on the effects of thermal remediation processes on soil physical properties. High temperature remediation displaces soil moisture and removes or destroys NAPL content. In order to establish whether the soil can recover strength and stability after remediation, it is important to establish the changes these remediation processes have on fundamental soil properties. The maximum temperatures observed in contaminant remediation vary by the process that is used (Table 2.1). Thermal desorption and soil heated vapour extraction use electric resistant heating either on the soil surface or through steel walls. The current transforms the groundwater and soil water into steam which in turn evaporates any harmful chemicals. The vapours are collected and treated or disposed (Araruna Jr et al., 2004; Chang and Yen, 2006). Hot water extraction uses pre-heated and pressurised water, which is injected into the soil, to extract and react with the targeted chemicals (Kronholm et al., 2002). In practice, maximum temperature is related to the soil conditions, process operating conditions and in some cases, the contaminant that is being treated.

Table 2.1. Possible maximum temperatures of exemplar in-situ and ex-situ moderate to high remediation techniques

Remediation Technique	Maximum observed temperature (℃)	Reference
Hot water extraction	300	Kronholm et al., 2002
In-situ Thermal desorption (low temperature)	112	Webb and Phelan, 1997
In-situ Thermal desorption (high temperature)	750	Chang and Yen, 2006
Heated soil extraction	300	Gan et al., 2009
Ex-situ Incineration	850	Lee et al., 2008
In-situ / Ex-situ Smouldering remediation	600-1100[a]	Switzer et al., 2009

[a] Maximum temperature is associated with contaminant type and treatment

With the exception of smouldering remediation, all of these remediation techniques use heat or heated water to volatilise the contaminant within the soil to enable its extraction. Maximum temperatures for these technologies are typically adjacent to the heat source with more moderate target temperatures of 80-100^{o}C achieved within the wider treatment zone. The contaminant must be collected and treated (Chang and Yen, 2006; Gan et al., 2009; Kronholm et al., 2002; Lee et al., 2008; McGowan et al., 1996; Webb and Phelan, 1997). These processes maintain high

temperatures in the soil for weeks to months or longer. In contrast, smouldering remediation uses the contaminant itself as fuel for the combustion reaction (Pironi et al., 2011; Pironi et al., 2009; Switzer et al., 2009). In laboratory studies, the soil particles are exposed to high temperatures on the order of 1000℃ for coal tars and 600-800℃ for oils for up to 60 minutes. Field scale efforts may result in exposure durations on the order of hours or longer.

Elevated temperatures have been shown to alter the mineralogical composition of soil. These effects have been studied extensively in relation to the effects of wildfires on soil properties. Colour change in soils has been observed after wildfire and after smouldering remediation. In most cases it changes from yellowish brown to reddish brown. This is due to the oxidation of soil iron content from goethite to maghemite or hematite (Goforth et al., 2005; Ketterings and Bigham, 2000). Decomposition of soil particles, especially clay minerals, starts at temperatures above 550℃ (Certini, 2005). These temperatures are rarely reported for wild and forest fire, but temperatures up to 1200℃ can be achieved during smouldering remediation (Pironi et al., 2009; Switzer et al., 2009).

In previous work, soil stability (strength of inter- and intra-particle bonds (North, 1976)) has been observed to increase with exposure to low and moderate temperatures as cementation of the clay particles occurs (Certini, 2005; Rein et al., 2008). This coincides with a measured increase of sand particle size with increasing temperatures in this range (Terefe et al., 2008). In clay-rich soils, bulk density and compressive strength were observed to increase as temperature was increased above ambient conditions whereas shear strength, liquid limit, and plasticity were observed to decrease (De Bruyn and Thimus, 1996). As exposure duration increases, clay cracking is observed as moisture is lost. This drying process has two distinct stages: constant evaporation as moisture is lost from the surface followed by

decreasing evaporation as the drying front propagates inward (Tang et al, 2010). Cracks form as a result of tensile stresses at the surface and can grow rapidly as moisture depletes.

At temperatures of 500℃ or higher, the soil stabil ity has been observed to decrease dramatically. This reduced stability is linked to the loss of organic cements (Certini, 2005). Wild fire temperatures can reach temperatures up to 850℃ at the soil-litter interface but temperatures at 0.05m depth are unlikely to exceed 150℃ (DeBano, 2000). Therefore, wild fire temperatures do not cover the temperature range encountered by thermal and smouldering remediation processes. It is necessary to understand possible impacts to soil from exposure to the whole temperature range of thermal remediation treatments.

This study aims to characterise the effects of moderate and high temperatures as well as smouldering on physical soil properties to determine the impact any changes will have to the soil and therefore predict possible complications during or after remediation treatment. Silica sand is used as a simple soil with relatively homogenous mineralogy and internal pore structure. These aims are achieved by comparing clean, heat-treated and smouldered silica sands with untreated and oven-dried sands. After each treatment, fundamental properties of the sand are tested and compared to determine the impacts of the treatment conditions.

2.2. Materials and Methods

Coarse silica sand (Leighton Buzzard 8/16, Sibelco, Sandbach, UK) was used as the base soil for all of the experiments. The sand contains 99% silicon-dioxide, has a mean grain size of 1.34mm and a bulk density of 1.7g/cm^3 (Switzer et al., 2009).

All sand was accepted as received and subjected to the same pre-treatment. A programmable muffle furnace (Nabertherm L9/11/SKM, Nabertherm GmbH, Lilienthal, Germany) was used for all heating experiments. The sands evaluated after smouldering remediation were prepared in a $3m^3$ experiment involving coal tar mixed with coarse sand. The concentration of this mixture was 31000 ± 14000 mg/kg total extractable petroleum hydrocarbons before treatment and the average concentration after smouldering remediation across the majority of the vessel was 10 ± 4 mg/kg. A 25L sample of the post-treatment material was collected and set aside for characterisation. Kaolin (Whitchem Ltd, UK) was used as an exemplar, non-swelling clay in a limited number of experiments. The smouldering experiment and set-up are described in detail in Pironi et al, 2009, Pironi et al, 2011 and Switzer et al, under review.

2.2.1. Sample Preparation and Heat Treatment

The silica sand was washed and wet sieved using a 0.63µm sieve to eliminate any loose fines and then air dried for several days. For each test the required amount of samples were placed in a ceramic crucible heated in the muffle furnace, following the heat treatment profiles listed in Table 2.2. Maximum temperatures of 105, 250, 500, 750, and 1000℃ were investigated. Each sample was subjected to a rapid increase in temperature, held at the peak temperature for 1 hour, cooled, and transferred for testing. After the heating period the samples were removed from the muffle furnace and placed in a desiccator to cool. Samples heated to temperatures above 500℃ were allowed to cool in the furnace to 200℃ before transfer to the desiccator. The necessary pre-treatment meant that all samples were disturbed by

handling steps. Therefore, only characteristics unrelated to soil structure were investigated in this study.

Table 2.2. Heat treatment conditions for silica sand

Maximum exposure temperature (℃)	Heating pattern		
	Pre-heating duration (min)	Peak temperature exposure duration (min)	Cooling period duration (min)
Untreated	-	-	-
105	30	1440	0
250	30	60	0
500	30	60	~ 60[a]
750	60	60	~ 180
1000	60	60	~ 240

[a] Cooling period varied for each batch so approximate duration is shown.

2.2.2. Laboratory Testing

Particle density was measured using the gas-jar method suitable for coarse soils (BS1377-2:1990). A sample of 1000g mass was placed in a 1L gas jar with approximately 500mL of water. The sample was set aside for 4hr and then shaken end-over-end for 30 min. The gas jar was filled with water fully. The average particle

density was determined based on the mass of the sand, mass of the water and volume of water displaced by the sand.

Minimum density was measured using 1000g of sand in a 1L glass measuring cylinder with 20mL graduation (BS1377-4:1990). The cylinder was shaken to loosen the sand and inverted four times. The cylinder was then inverted until all of the sand was at rest, returned to the initial position and carefully placed on a flat surface. The volume was recorded at the mean level of the surface to the nearest 10ml. The test was repeated 10 times with the same sample. The minimum density was calculated using the greatest volume reading in the cylinder (BS1377-4:1990).

Maximum density was determined using the vibrating hammer method (BS1377-4:199). Approximately 3000g of sand were placed in a bucket with warm water and thoroughly stirred to remove any air bubbles. The sand was left to cool overnight. A 1L compaction mould was used for all density measurements. The mould was placed in a water tight container on a solid base. Water was poured into the mould to 50mm depth in the mould body and the surrounding container. A portion of the sand-water mixture was carefully added to the mould, approximately filling a third of the mould after compaction. Water was added to the surrounding container to match the water level in the mould. The vibrating hammer used a circular tamper was to compact the sand for at least 2min using a force between 300N and 400N on the sample. This process was repeated for the other 2 layers to fill the mould. The masses of sand and water in the mould were used to determine the maximum density.

Particle size distribution for the sand was determined using a dry sieving method (BS1377-2:1990). Approximately 200g of each sample was placed into the top of set of sieves that included 1.18mm, 600µm, 425µm, 300µm and 212µm sieve sizes.

The set of sieves was shaken for 10 min. The mass of sand retained on each sieve was used to determine the particle size distribution. Particle size distribution was carried out in triplicate for each material.

The overall mass loss was determined by comparing the mass of samples before and after heat treatment. The samples tested were silica sand + 5% moisture content, silica sand + 10% kaolin + 5% moisture content, and silica sand + 10% kaolin dry. The samples were mixed by hand and stored in aplastic bag for 4 hours before heat treatment following the heat treatment shown in Table 2.2.

The silica sand pH was tested using 30g of silica sand and 75mL of distilled water in 100mL glass beaker. The mixture was agitated, covered and left overnight at 19℃ room temperature. The mixture was agitated again right before the measurement of pH with a pH meter (Mettler Toledo Ltd, Leicester, UK) with an accuracy of ± 0.004.

A modified falling head test was used to measure infiltration profile and falling head rate as a preliminary investigation in hydraulic effects after thermal treatment. A cylindrical tube (50cm H x 6cm OD) was filled with sand to height of 30cm. Using a funnel and diffuser system, a volume of 170mL of distilled water, which corresponded to a head of water of 60mm, was added to the top of the cylinder and allowed to flow into the sand. Falling head was measured as the time of this 60mm head of water reaching fixed increments on the column as it infiltrated into the sand column. The set-up for this experiment is shown in Figure 2.1.

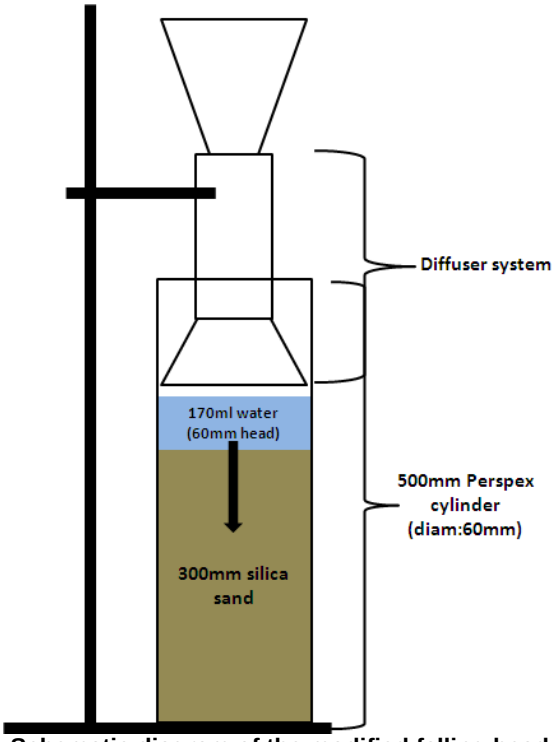

Figure 2.1. Schematic diagram of the modified falling head test apparatus

Also as a preliminary investigation, capillary rise was tested using a cylindrical tube (9.3cm H x 2cm OD) with a fine mesh fitted over the bottom. The cylinder was filled with approximately 50g of sand, placed above a reservoir filled with water and slowly lowered until it made contact with the water surface. To ensure a stable set up the tube was held in place with a clamp system. The water was drawn into the sand through capillary forces and the final height was measured once the water level in the tube was observed to remain constant for 2min. Capillary rise measurements were carried out in triplicate for each material. Only final rise height was measured during this test.

The mineralogical composition of the silica sands was tested by BRUKER D8 ADVANCE with DAVINCI (2010) powder X-Ray Diffraction (XRD) on crushed samples. Vibrational spectroscopy using Raman measurements were taken on individual silica sand grains to measure the crystal structure and bonds. The Raman

spectra were measured suing a Renishaw inVia Raman Microscope running from 240 to 2000cm^{-1} argon beam of 514nm, 2400 l mm^{-1} (vis) grating, 10 exposure times, 1 accumulation and 10% power (cross-polar) was used for excitation.

2.3. Results and Discussion

2.3.1. Mineralogy

During the heat treatment testing and after smouldering remediation, a colour change of the silica sand was observed (Figure 2.2). Exposure of this material to high temperatures results in colour change from yellowish brown to reddish brown with increasing temperature for the silica sand grains and a change from yellow to pinkish red for the crushed silica sand. This colour change is associated with the dehydration reaction of goethite with increasing temperatures to form hematite or maghemite.

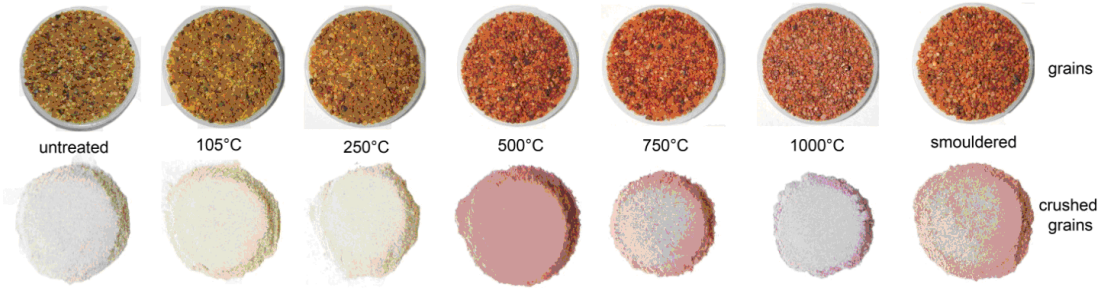

Figure 2.2. Colour change observed in silica sand grains after heat treatment.

During the dehydration reaction of goethite, the density of the iron-hydroxide increases from 4.3 mg/m^3 for goethite to 5.2 mg/m^3 for hematite (Wenk and Bulakh, 2004). The sand is comprised primarily of silicon dioxide; iron oxides make up a small fraction of its composition. High temperatures may cause additional changes

in mineralogy that may be less likely to be detected by visual examination (Goforth et al., 2005; Pomiès et al., 1998). Similar effects may occur within the silicon dioxide, which becomes unstable with high temperatures and forms silica polymorphs such as trydimite or cristobalite (Hand et al., 1998; Wenk and Bulakh, 2004). Thermal treatments (100-1200℃) on fly ash s howed that cristobalite becomes present in the samples and that smaller particles had a more glassy composition due their faster cooling time (Mollah et al., 1999).

Analysis of the silica sands by x-ray diffraction showed that both, iron oxide and quartz minerals are affected by heat treatment and smouldering remediation (Figure 2.3). Due to the high quartz content, the signal of the iron-oxides is small, but shifts are apparent. Shifts in quartz are apparent in the smouldered samples. For example, the quartz peaks from 2θ = 36 to 46 are very low for the smouldered samples. Glass is amorphous and cannot be excited by XRD analysis.

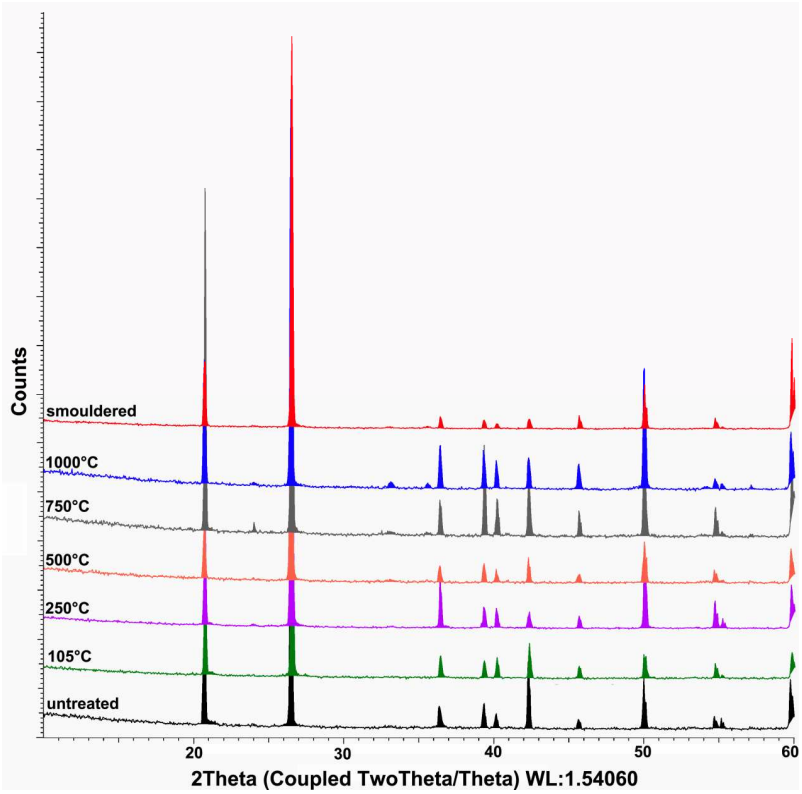

Figure 2.3. X-ray diffraction spectra for silica sand after thermal and smouldering treatments

The quartz in the sand grains exposed to smouldering remediation may be losing its crystal structure. Due to the nature of the excitement in XRD analysis, XRD cannot distinguish between quartz and its polymorphs as they have the same composition with a different structure. The formation of polymorphs was examined by Raman spectroscopy, a technique that excites the crystal structure with a laser and therefore allows a more targeted analysis of the grain surfaces (Komorida et al., 2010). After exposure to 1000℃, trydimite and hema tite were observed and after smouldering remediation, trydimite, crystobalite, dumortierite, and hematite were observed (Table 2.3).

Table 2.3. Exemplary mineralogy of points on sand grain surfaces after selected heat treatments

Sample	Grains	Analysis points	Number of detections of each mineral					
			Quartz	Tridymite	Cristobalite	Dumortierite	Goethite	Hematite
Untreated	5	9	9					
500	3	5	3				2	
1000	3	9	5	2				2
Smouldered (large scale)	12	37	12	6	3	8	5	2

Trydimite and cristobalite have flatter structures than α-quartz. Mineralogy changes were not observed in Raman measurements at lower temperatures, though small shifts were apparent in x-ray diffraction spectra. Raman analysis on thin sections prepared of sand grains showed no polymorphs, suggesting that the effect remains at the surface.

Use of the Bruker XRD instrument required crushing of the sand grains, effectively diluting any surface changes. Raman spectroscopy was carried out under

microscope and limited by the selection of single points for analysis. The extent of changes seems to be increasing with increasing temperature, as expected. More analysis is necessary to fully understand the exposure conditions that trigger these changes to the grain surfaces and how these changes may affect the grain-grain and grain-water interactions, particularly in more complex soils.

2.3.2. Particle and Bulk Densities

In contrast to mineralogy, elevated temperatures did not seem to affect the particle density or minimum/maximum bulk densities of the silica sand (Table 2.4). No real relationship was apparent between treatment temperature and density. For the particle density, the values are consistently near 2.65Mg/m^3, which is a value that is widely used in geotechnical engineering calculations. The maximum and minimum densities are equally unaffected by heat treatment or smouldering.

These observations are not consistent with the literature on wild and forest fire effects on soil properties, which suggests that bulk density would increase with temperature (Are et al., 2009; Certini, 2005). The lack of organic matter may explain the contrast. Organic matter is highly-affected by elevated temperature and thus organic-rich soils may exhibit density changes after exposure. Temperatures in the range of 260 – 370℃ are linked with melting and de composition of organic matter and temperatures in excess of 370℃ are linked with complete or near-complete destruction (DeBano, 1981; DeBano, 2000; Robichaud and Hungerford, 2000). The results in this study, which show no significant change in density, suggest that the changes in soil density that are observed after wildfires are associated primarily with effects on organic matter and potentially the smaller silt and clay–sized particles.

2.3.3. Particle Size Distribution

Particle size analyses suggest that heat treatment has a small but appreciable effect on grain distribution (Table 2.4). The sieve analyses show that the sample retained on the 1.18mm sieve increases from 94.4%±0.7% for the untreated sample to 95.5%±1.2% for treatment at 250°. After this initia l increase, the sample retained on the 1.18mm sieve decreases to 94.0%±0.4% and 93.3%±0.9%, as exposure temperature is increased to 500℃ and 1000℃, respe ctively. Corresponding measurements on sieves <1.18mm show an initial decrease from 5.3%±0.6% to 4.1%±1.2% for the untreated sample to 250℃ heat tr eatment, followed by an increase to 5.6%±0.4% and 6.2%±0.8%, for 500℃ and 1000℃, respectively.

Table 2.4. Particle density, minimum and maximum bulk density, particle size distribution, and mass loss observed in silica sand after exposure to elevated temperatures or smouldering remediation

Sample	Densities			Sieve Analysis						Mass loss
	Particle	Minimum	Maximum	1.18mm	600µm	425µm	300µm	212µm	<212µm	Sample mass loss
	Mg/m^3			% retained						%
Untreated	2.68	1.45	1.65	94.6 ± 0.7	5.3 ± 0.6	0.00	0.00	0.00	0.00	0.00
105	2.62	1.44	*untested*	*untested*	*untested*	*untested*	*untested*	*untested*	*untested*	4.21
250	2.66	1.43	1.67	95.8 ± 1.2	4.1 ± 1.2	0.00	0.00	0.00	0.00	4.74
500	2.69	1.45	1.68	94.3 ± 0.4	5.6 ± 0.4	0.02 ± 0.001	0.01 ± 0.004	0.00	0.00	5.10
750	2.7	1.44	1.65	*untested*	*untested*	*untested*	*untested*	*untested*	*untested*	5.37
1000	2.71	1.45	1.69	93.5 ± 0.9	6.2 ± 0.8	0.09 ± 0.0003	0.07 ± 0.004	0.03 ± 0.002	0.06 ± 0.005	5.63
Smouldered (large scale)	2.68	1.46	1.68	*untested*	*untested*	*untested*	*untested*	*untested*	*untested*	*untested*

Figure 2.4 shows the impact of temperature on the fines fraction <600µm, which increases with increasing temperature. Collection of the sand samples after smouldering remediation involved multiple handling steps, all of which resulted in visually -apparent mobilisation of fines. Thus, these sands were not tested for particle size distribution. Mobilisation of fines is defined as clay sized particles becoming detached from the sand grains either due to thermal treatment or mechanical effects such as during transportation.

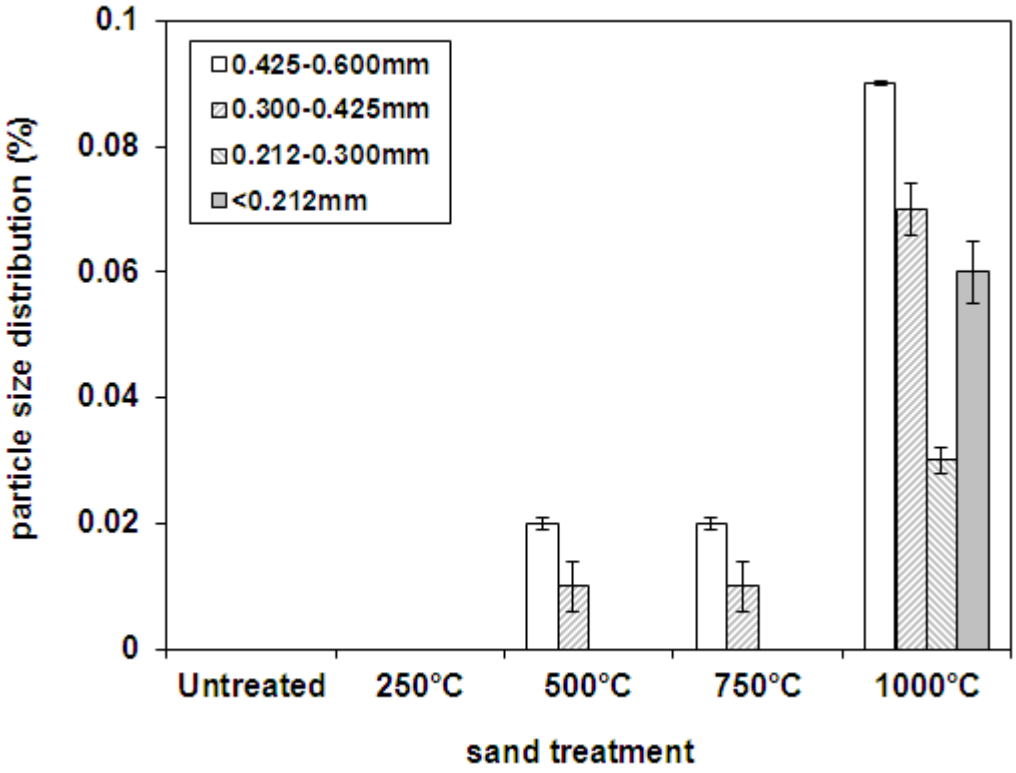

Figure 2.4. Mobilisation of particles smaller than 0.600mm from sand exposed to heat at 250, 500, 750, and 1000℃. Particles between 0.600 and 2 .36mm make up 99.7 – 99.9% of the particle size distribution in all cases.

The variation in particle size distribution may be linked to the loss of mass beyond the initial moisture content (Table 2.4). In the mass loss tests, samples were prepared to 5% moisture content and then treated according to the temperature

specified. As temperature increases, mass loss increases, exceeding the initial 5% added moisture for temperatures above 500℃. Althou gh there is a dehydration reaction from goethite to hematite, the fraction of iron oxide relative to the total composition of the sand is too small for this reaction alone to account for the whole additional mass loss. Other mineralogical reactions are likely to contribute to this loss in sample mass. Further investigation is necessary to identify and quantify the mineral changes that are occurring. The changes in particle size distribution can affect larger-scale behaviour of soil such as compaction.

Further fractionation of the sand after heat treatment shows that as temperature increases, fines are recovered across a wider range of size fractions (Table 2.4). These results show that with increasing temperature the particle size distribution of the sand is extended, which is in accordance with results from thermal desorption tests on sands (Araruna Jr et al., 2004). Based on the same mineralogical composition of fines after the thermal desorption, Araruna Jr. et al (2004) argue that the fines are the product of grains breaking with exposure to higher temperatures. This is a possibility, but not the only explanation that should be considered here.

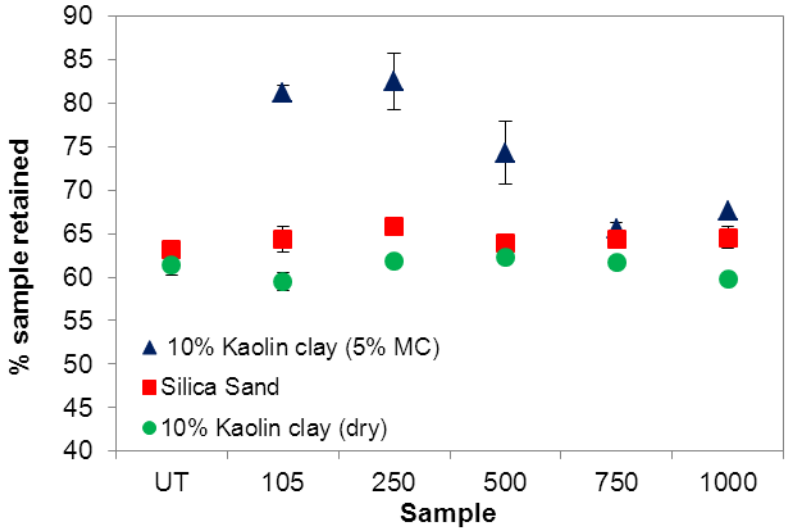

Figure 2.5. Percentage of sand and sand/clay sample masses retained on the 1.18mm sieve after heat treatment and dry sieving

Mobilisation of clay deposits on the sand grains, which would lose their bonds with the sand particles during thermal treatment, may affect the particle size distribution. The potential for clay mobilisation was explored with a set of experiments involving sand-clay mixtures. With moisture, clay was observed to coat the sand grains for temperatures up to 500℃ and that this coating is l ost for temperatures above 750℃ (Figure 2.5). This supports the theory that the bond between the fines and sand grains is lost and that this causes the extension in particle size distribution. This bond appears to be driven by presence or loss of moisture. It is therefore likely that this effect can occur during thermal and smouldering treatment. At this point, the data are inconclusive to eliminate the potential for breaking of the grains under high temperature, particularly as handling steps release fines into the air as dust, but the clay experiments illustrate the potential that increased fines can result from clay mobilisation.

2.3.4. Preliminary Water Dynamic Tests

Water dynamics in the sand was measured with two separate but interrelated tests: falling head and capillary rise. These tests were conducted to show how temperature and smouldering affect interaction of silica sand and water. The falling head test results show that heat treatment has a minimal effect on the sand permeability. For the untreated and heat treated samples, the change in head over time follows approximately the same profile. In contrast, the smouldered sample shows a much steeper profile (Figure 2.6). Water moves much more rapidly through the smouldered sand. The entire column of water disappears into the sand in 7s and drainage from the column is observed after less than 20s. The delay in the first measurement of head height for the smouldered sand is due to this rapid infiltration.

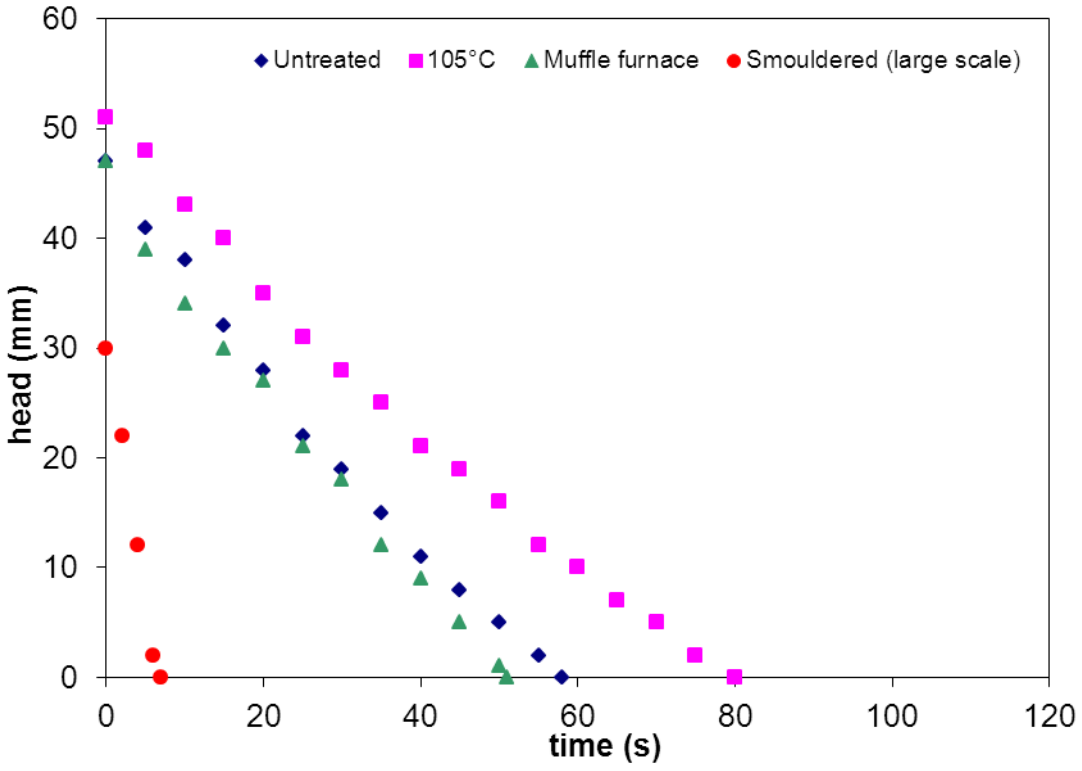

Figure 2.6. Head loss (mm) observed over time in untreated sand, heat-treated sand, and sand after contamination with coal tar and smouldering remediation

Approximately 50% of the total volume of water infiltrates into the sand as the total volume is delivered to the top of the sand column. In contrast, 17-22% of the total volume of water infiltrates during initial delivery to the other treated and untreated sand columns. In addition, drainage from the smouldered sand is noticeably discoloured with particulates. Channelling is observed in the column and lateral propagation is not evident, though some water is retained in the pore space after infiltration and excavation. These differences in falling head behaviour are not represented in the correlating hydraulic conductivity values, which are on the order of 10^{-4}m/s for all samples (Table 2.5).

Table 2.5. Capillary rise height, void ratio, saturated hydraulic conductivity, and pH values for silica sand retained on the 1.18mm sieve

Sample	Capillary Rise Height (mm)		Void ratio		Hydraulic conductivity k (m/s)	pH
	Uncompacted	Compacted	Uncompacted	Compacted		
Untreated	20.63 ± 4.13	20.63 ± 1.38	0.67	0.63	$9.6 \pm 0.6 \times 10^{-4}$	8.2
105	20.63 ± 4.13	20.63 ± 1.38	0.66	0.63	$7.0 \pm 0.5 \times 10^{-4}$	8.1
250	22.00 ± 0.00	23.38 ± 2.37	0.67	0.64	$5.2 \pm 0.7 \times 10^{-4}$	8.0
500	22.00 ± 2.75	23.38 ± 1.59	0.67	0.68	$5.5 \pm 0.7 \times 10^{-4}$	7.8
750	23.38 ± 1.27	23.38 ± 1.59	0.67	0.64	$5.0 \pm 0.6 \times 10^{-4}$	7.9
1000	22.63 ± 0.00	26.13 ± 1.38	0.67	0.61	$5.0 \pm 1.0 \times 10^{-4}$	7.8
Smouldered (large scale)	16.50 ± 3.50	19.25 ± 0.00	0.70	0.63	$7.3 \pm 0.4 \times 10^{-4}$	6.1

Differences are observed in the capillary rise test when comparing the heat-treated and smouldered sand samples (Table 2.5). While capillary rise is present in all samples, the capillary rise is lower in the smouldered sample. As the temperature of thermal treatment is increased, the resulting capillary rise after cooling and exposure to the water bath increases as well. Capillary rise is consistent or greater in

compacted samples, which may reflect the presence of small clay aggregates in the pore space, which is consistent with the changes observed in particle size distribution. The voids between the grains may have decreased to some extent and therefore caused the capillary forces to increase. In the smouldered sample, the capillary rise in both uncompacted and compacted states is below that observed in all other samples. This difference suggests greater void spaces between the grains, potentially changed contact angles, and less capillary forces, all of which may be influenced by the mobilisation of fines and other potential changes to the grain surfaces.

Heat treatment showed slight influence on the silica sand pH, which remained slightly alkaline between 7.8 and 8.2 (Table 2.5). The pH of the sand after smouldering remediation had shifted to slightly acidic. This change in pH is likely to be caused by the coal tar contamination present before smouldering and the chemical reactions that take place during smouldering. Decreased pH is associated with decreased cation exchange capacity in the soil, which is, in turn, linked to water holding capacity. Based on the heat treatment results, similar effects are expected in soil treated by smouldering remediation, though the presence of organic matter in the soil and its potential melting or destruction during remediation will affect pH as well. Though soil pH affects grain-water interactions, the changes in infiltration cannot be explained by pH change alone, particularly as saturated hydraulic conductivity is not observed to change as a result of high temperature exposure or smouldering remediation (Table 2.5). Sand after smouldering has small amounts of chemical residue, typically below detection limits (Switzer et al., 2009). The nature and extent of the residue is unknown, which challenges the decoupling of physical and chemical influences on water infiltration. Although hydraulic conductivity was not observed to be affected by heat treatment or smouldering, the mobilisation of fines

was apparent in the effluent water of the tests carried out on 750℃, 1000℃, and smouldered sands.

2.3.5. Summary and implications of soil changes

High temperature processes impact the dynamic properties of soils. The results outlined above highlight the sometimes contradictory responses to high temperature exposure, particularly water dynamics. The differences in void spaces do not fully explain the differences that are observed in the falling head infiltration profiles. The changes in mineralogy, especially on the grain surfaces in combination with a change in pH suggests a relationship that are visible in all treated samples through colour change do not correlate to the changes observed in dynamic behaviour as the sand is introduced to water. These results suggest that colour change alone cannot be used as an indicator of potential changes in soil behaviour.

Mobilisation of fines is a concern in all cases as a loss in soil mass can result in a loss of soil stability. Heat treatment above 500℃ has been shown to weaken and soften sandstones under loading, an effect that is linked to dehydroxylisation of kaolinite (Ranjith et al, 2012). No such effects were observed here, but samples were not subjected to load and all materials were allowed to cool prior to testing. Further testing would be beneficial to explore the effects on soils that are exposed to heat and subjected to loading, particularly in the context of remediation under existing infrastructure. Even though post-remediation soil is affected by reduced water holding capacity and capillary rise, it should still be amenable to stabilisation techniques. The cation exchange reactions of lime stabilisation may be impaired, but other aspects of the remediation process may aid stabilisation. Lime stabilisation has been shown to improve the compressive strength of quartz sand, increased

curing time has been shown to enhance this improvement, and elevated temperatures have been shown to enhance curing and ultimate strength achieved (Bell, 1996). Because of their thermal inertia, post-remediation soils are slow to cool. Reductions in lime uptake may be counterbalanced by strategic use of soil stabilisation techniques during the cooling process after remediation, particularly if the installation of new infrastructure after remediation is desired. Further work on the combination of aggressive remediation and soil stabilisation processes would be beneficial to determine if integration of these processes could optimise their benefits.

While further study into the links between changes in micro-scale properties and macro-scale behaviour is needed, this work illustrates the importance of understanding the effects of high temperature processes on fundamental soil properties. Further work can explore extended exposure times more reflective of thermal remediation techniques as well more complex soil compositions. This work suggests that the effects of elevated temperatures on soil properties should be considered as part of remediation planning and mitigation measures may be appropriate in the soil during or after exposure.

2.4. Conclusions

High temperature exposure in the form of thermal treatment and smouldering remediation result in changes to soil properties. Some links between grain-scale characteristics and dynamic behaviour have been established. After exposure of sand to elevated temperatures, particle size distribution increases and a related increase in capillary rise is observed as well. Water infiltration does not seem to be affected by elevated temperature, though this observation may be a function of

exposure duration. Sand exposed to smouldering remediation exhibits more rapid water infiltration from the surface. Changes in mineralogy are visible in all treated samples in the form of colour change as goethite is oxidised to hematite. Changes to the quartz crystal structures are observed at an exposure temperature of 1000℃. and maghemite. Colour change alone cannot be used as an indicator of potential changes in soil behaviour. Mass loss increases with increasing temperature and may be related to the mineralogical processes such as the dehydration of iron oxides, mobilisation of fines, and changes in quartz structure. Smouldering treatment has similar effects, perhaps more rapidly due to the higher temperatures achieved. In contrast to these results, thermal and smouldering treatment show minimal effects on silica sand particle and bulk densities. The changes in soil properties may result in altered dynamics between soil aggregates in the field. The effects of high temperature remediation on field soils are anticipated to be more complex as other soil fractions may be more susceptible to heating effects. Further investigation of the effects of high temperature exposure on soil fractions and whole soils, especially from field sites where aggressive remediation processes have been applied, is necessary to fully understand the impact of these processes on soils. After exposure to high temperature or smouldering remediation, soils should remain amenable to improvement with soil amendments. Follow-up investigation and monitoring after exposure is important to understand the extent of impacts and mitigation measures that may be necessary.

2.5. References

Are, K.S., Oluwatsin, G.A., Adeyolanu, O.D, Oke, A.O., (2009) Slash and burn effect on soil quality of an Alfisol: Soil physical properties. Soil and Tillage Research, 103(1), 4-10

Araruna Jr, J.T., Portes, V.L.O., Soares, A.P.L., Silva, M.G., Sthel, M.S., Schramm, D.U., Tibana, S. and Vargas, H., 2004. Oil spills debris clean up by thermal desorption. Journal of Hazardous Materials, 110(1-3): 161-171.

Are, K.S., Oluwatosin, G.A., Adeyolanu, O.D., and Oke, A.O., 2009. Slash and burn effect on soil quality of an Alfisol: Soil physical properties. Soil and Tillage Research, 103(1): 4-10.

Bell, F.G., 1996. Lime stabilization of clay minerals and soils. Engineering Geology, 42(4): 223-237.

Certini, G., 2005. Effects of fire on properties of forest soils: a review. Oecologia, 143(1): 1-10.

Chang, T.C., and Yen, J.H., 2006. On-site mercury-contaminated soils remediation by using thermal desorption technology. Journal of Hazardous Materials, 128(2-3): 208-217.

De Bruyn, D. and Thimus, J.F., 1996. The influence of temperature on mechanical characteristics of Boom clay: The results of an initial laboratory programme. Engineering Geology, 41(1–4): 117-126.

DeBano, L.F., 1981. Water Repellent Soils: a state-of-the-art. Pacific Southwest Forest and Range Experiment Station, General Technical Report PSW-46.

DeBano, L.F., 2000. The role of fire and soil heating on water repellency in wildland environments: a review. Journal of Hydrology, 231: 195-206.

Gan, S., Lau, E.V., and Ng, H.K., 2009. Remediation of soils contaminated with polycyclic aromatic hydrocarbons (PAHs). Journal of Hazardous Materials, 172(2-3): 532-549.

Goforth, B.R., Graham, R.C., Hubbert, K.R., Zanner, C.W., and Minnich, R.A., 2005. Spatial distribution and properties of ash and thermally altered soils after high-severity forest fire, southern California. International Journal of Wildland Fire, 14(4): 343-354.

Hand, R.J., Stevens, S.J., and Sharp, J.H., 1998. Characterisation of fired silicas. Thermochimica Acta, 318(1-2): 115-123.

Ketterings, Q.M., and Bigham, J.M., 2000. Soil color as an indicator of slash-and-burn fire severity and soil fertility in Sumatra, Indonesia. Soil Science Society of America Journal, 64(5): 1826-1833.

Komorida, Y. et al., 2010. Effects of pressure on maghemite nanoparticles with a core/shell structure. Journal of Magnetism and Magnetic Materials, 322(15): 2117-2126.

Khamehchiyan, M., Hossein Charkhabi, A. and Tajik, M., 2007. Effects of crude oil contamination on geotechnical properties of clayey and sandy soils. Engineering Geology, 89(3-4): 220-229.

Kronholm, J., Kalpala, J., Hartonen, K., and Riekkola, M.-L., 2002. Pressurized hot water extraction coupled with supercritical water oxidation in remediation of sand and soil containing PAHs. The Journal of Supercritical Fluids, 23(2): 123-134.

Lee, W.-J. et al., Shih, S.-I., Chang, C.-Y., Lai, Y.-C., Wang, L.-C. and Chang-Chien, G.-P., 2008. Thermal treatment of polychlorinated dibenzo-p-dioxins and dibenzofurans from contaminated soils. Journal of Hazardous Materials, 160(1): 220-227.

Mataix-Solera, J., and Doerr, S.H., 2004. Hydrophobicity and aggregate stability in calcareous topsoils from fire-affected pine forests in southeastern Spain. Geoderma, 118(1-2): 77-88.

McGowan, T.F., Greer, B.A., and Lawless, M., 1996. Thermal treatment and non-thermal technologies for remediation of manufactured gas plant sites. Waste Management, 16(8): 691-698.

Mollah, M.Y.A., Promreuk, S., Schennach, R., Cocke, D.L., and Güler, R., 1999. Cristobalite formation from thermal treatment of Texas lignite fly ash. Fuel, 78(11): 1277-1282.

North, P. F., 1976. Towards an absolute measurement of soil structural stability using ultrasound, Journal of Soil Science, 27(4): 451-459.

Pironi, P., Switzer, C., Gerhard, J.I., Rein, G., and Torero, J.L., 2011. Self-Sustaining Smoldering Combustion for NAPL Remediation: Laboratory Evaluation of Process Sensitivity to Key Parameters. Environmental Science & Technology, 45(7): 2980-2986.

Pironi, P. et al., Switzer, C., Rein, G., Fuentes, A., Gerhard, J.I. and Torero, J.L., 2009. Small-scale forward smouldering experiments for remediation of coal tar in inert media. Proceedings of the Combustion Institute, 32: 1957-1964.

Pomiès, M.P., Morin, G., and Vignaud, C., 1998. XRD study of the goethite-hematite transformation: Application to the identification of heated prehistoric pigments. European Journal of Solid State and Inorganic Chemistry, 35(1): 9-25.

Ranjith, P. G, Viete, D.R., Chen, B.J., Perera, M.S.A., 2012. Transformation plasticity and the effect of temperature on the mechanical behaviour of Hawkesbury sandstone at atmospheric pressure. Engineering Geology, 151(0): 120-127.

Rein, G., 2009. Smouldering Combustion Phenomena in Science and Technology. International Review of Chemical Engineering, 1: 3-18.

Rein, G., Cleaver, N., Ashton, C., Pironi, P., and Torero, J.L., 2008. The severity of smouldering peat fires and damage to the forest soil. CATENA, 74(3): 304-309.

Robichaud, P.R., and Hungerford, R.D., 2000. Water repellency by laboratory burning of four northern Rocky Mountain forest soils. Journal of Hydrology, 231: 207-219.

Switzer, C., Pironi, P., Gerhard, J.I., Rein, G., Torero, J.L., in review. Volumetric Scale-up of Smouldering Remediation of Contaminated Materials. Journal of Hazardous Materials.

Switzer, C., Pironi, P., Gerhard, J.I., Rein, G., and Torero, J.L., 2009. Self-Sustaining Smoldering Combustion: A Novel Remediation Process for Non-

Aqueous-Phase Liquids in Porous Media. Environmental Science & Technology, 43(15): 5871-5877.

Tan, Ö., Yilmaz, L., and Zaimoglu, A.S., 2004. Variation of some engineering properties of clays with heat treatment. Materials Letters, 58(7-8): 1176-1179.

Tang, C.-S., Cui, Y.-J., Tang, A.-M. and Shi, B., 2010. Experiment evidence on the temperature dependence of desiccation cracking behavior of clayey soils. Engineering Geology, 114(3–4): 261-266.

Terefe, T., Mariscal-Sancho, I., Peregrina, F., and Espejo, R., 2008. Influence of heating on various properties of six Mediterranean soils. A laboratory study. Geoderma, 143(3-4): 273-280.

Webb, S.W., and Phelan, J.M., 1997. Effect of soil layering on NAPL removal behavior in soil-heated vapor extraction. Journal of Contaminant Hydrology, 27(3-4): 285-308.

Wenk, H.-R., and Bulakh, A., 2004. Minerals Their Constitution and Origin. Cambridge University Press

3. Changes to Shear Strength of Thermally Treated Soils and its Consideration for Remediation strategy

3.1. Introduction

Shear strength of granular soils is one of the most important factors in civil engineering design and construction. Shear strength values are used in stability analysis for bearing capacity, slope stability, and the design of earth-retaining structures (Sarsby, 2000; Sezer, 2011). In soil, shear strength is a combination of particle cohesion and frictional resistance that can be determined by laboratory (direct shear or triaxial) or in-situ (e.g. CPT) testing as part of the site investigation.

The true cohesion of a soil is associated with the bond between particles or aggregates and it depends on its previous history such as overburden pressure or long-term loading. The bond strength between particles may disappear quickly under shear movements of the soil. In contrast, friction is solely based on the direct contact between individual soil particles (Sarsby, 2000). This interparticle friction controls the overall shear strength of the soil and any changes to the particle contacts will lead to a change in shear behaviour and strength of the soil. The aim of this study is to determine how thermal and smouldering remediation affect the particle contacts within a soil and if these treatments cause changes in interparticle friction and shear strength.

Smouldering and thermal remediation processes such as heated soil vapour extraction, thermal desorption, soil heating, microwave heating, and incineration are used to treat a wide range of organic contaminants (Webb and Phelan, 1997;

Kronholm et al., 2002; Chang and Yen, 2006; Lee et al., 2008; Gan et al., 2009; Switzer et al., 2009). The temperature range achieved by these processes varies based on heating method, soil type, and, in the case of smouldering, targeted contaminants. The temperature range lies between 105 and 1000℃ and the exposure duration can last from minutes to weeks or months. Research on wild fires shows that ground stability is affected as a result of the loss of surface layers, increasing risks of erosion, destruction of deeper soil layers, and ground collapse (Rein et al., 2008). Exposure to low and moderate fire temperatures can increase the structure stability of the soil, which is linked to aggregate stability as well as the formation of hydrophobic films on aggregate surfaces. Exposure to high temperatures destroys the organic material and this can lead to a decrease in the structural stability. However, the aggregates can be found to have an increased stability due to the formation of cementing oxides (Certini, 2005). In these studies, ground or structural stability are not defined in engineering terms and the stress conditions of the soil during testing are unclear. These discrepancies make it difficult to compare results from different research areas. In geotechnical engineering, soil shear strength is generally modelled with a linear relationship:

$$\tau = c' + \sigma' \tan \Phi' \qquad \text{(Eq. 3.1)}$$

where τ is the shear stress (kPa), σ' = normal effective stress (kPa), c' = effective cohesion, Φ' = angle of shearing resistance' (°). In direct shear strength testing, a constant normal stress is applied and shear stress to failure is measured. Knowing the applied normal stress and resulting shear stress allows prediction of shear strength of soil

Granular soils are assemblies of particles and the overall applied loads are carried through contact friction, also called interparticle friction (Oda et al., 1982; Mehrabadi and Nemat-Nasser, 1983; Sarsby, 2000; Sadrekarimi and Olson, 2011). These contacts vary depending on the soil matrix, particle size distribution, and angularity of the particles. In general, the shear strength increases with increasing mean particle size (Bagherzadeh-Khalkhali and Mirghasemi, 2009) and angularity of the grains. Angular particles interlock more easily when forced to move relative to each other compared to the rolling motions of rounder particles (Shinohara et al., 2000; Mair et al., 2002; Li and Aydin, 2010; Sadrekarimi and Olson, 2011). Interparticle friction also depends on the surface roughness of the particles. Research on glass ballotini with roughness created by milling and chemical etching shows that the interparticle friction and therefore the shear strength increases with increasing surface roughness (Skinner, 1969; Cavarretta et al., 2010). An increase of the interlocking behaviour hinders the grains from rotating. In soils, changes in roughness could happen through changes of the surface chemistry or mineralogical composition, which could, in turn, alter the hardness or texture of the particle and its surface (Frossard, 1979; Fannin et al., 2005). Increases in angularity and surface roughness lead to increases in dilatant behaviour (Collins and Muhunthan, 2003; Li and Aydin, 2010), leading to a larger displacement of soil during shearing.

For granular soils, the impact of fines is also important because naturally occurring granular soils contain significant amount of fines (Thevanayagam and Mohan, 2000; Monkul and Ozden, 2007; Chang and Yin, 2011). Chang et al (2011) shows that a fines content less than 25% does not affect the overall shear strength as the behaviour is still dominated by the coarse fraction. Monkul and Ozden (2007) also show that the addition of clay fractions less than 20% does not significantly reduce the shear strength of sand. However, this absence of influence is only true if the fine

particles solely occupy the available void space. If coarse fraction contacts are disrupted by fines, the overall behaviour is affected. With an increasing fines content, the overall shear strength decreases (Panayiotopoulos, 1989; Chang and Yin, 2011; Maleki et al., 2011). Particle shape is considered the most important factor impacting on soil shear strength compared to surface roughness or surface chemistry (Göktepe and Sezer, 2010).

Experiments on crude oil contaminated sandy soils shows that the shear strength decreases with increasing oil content. For clayey soils a decrease in liquid and plastic limits was also observed with increasing oil content. These decreases have been explained by the coating of the particles with the oil contaminant, which decreases the apparent cohesion and affects the shear strength. The oil coating also reduces the reaction of water with particles, which controls the plasticity of the soil (Khamehchiyan et al., 2007).

This study aims to systematically evaluate the impact of heat treatment temperature and smouldering remediation on soil stability using direct shear tests.

3.2. Materials and Methods

Simple soils were synthesised with silica sand (Leighton Buzzard 8/16, Sibelco, Sandbach, UK) and kaolin clay (Whitchem Ltd, UK). The sand and clay were accepted as received. A programmable muffle furnace (Nabertherm L9/11/SKM, Nabertherm GmbH, Lilienthal, Germany) was used for all heating experiments. The sands evaluated after smouldering remediation were prepared in a $3m^3$ experiment involving coal tar (Koppers, UK Ltd, Scunthorpe, UK) mixed with coarse silica. The initial concentration of this mixture was 31000 ± 14000 mg/kg total extractable petroleum hydrocarbons before treatment and the average concentration after

smouldering remediation across the majority of the vessel was 10 ± 4 mg/kg (Switzer et al., in review). In addition, sand and sand-kaolin samples were contaminated with coal tar and smouldered using a bench scale set up (0.003m^3 of sample) and following the procedure established in Switzer et al (2009) and Pironi et al (2011). In all smouldering experiments, one or more air injection devices were placed at the base of the vessel and covered in clean silica sand. One or more coiled cable heaters (Watlow Ltd, Linby, UK) were placed just above the air diffuser and covered with a thin layer of clean sand. The contaminated material was then placed on top of the clean layer and capped with another layer (5-15cm) of clean silica sand to absorb any expanding liquid and assist with emissions filtration. All systems were open to at the atmosphere at the top (Switzer et al., in review). The experiments are summarised in Table 3.1.

Table 3.1. Smouldering experiment summary for large and small scale set-up

		Smouldering set-up	
		Large scale	Small scale
Sample name		SM-1	SM-2 / SM-3
Sample volume	(m^3)	3	0.003
Test duration	(min)	1600	70-120
Average peak temperature	(°C)	900	1100

SM-2: silica sand; SM-3: silica sand +10% kaolin

3.2.1. Sample Preparation and Heat Treatment

The silica sand was soaked in a solution of hexametaphosphate and sodium carbonate for 24 hrs, washed over a 425µm sieve to eliminate any loose fines, and air dried for several days (BS1377-2:1990). After air drying, the sand was stored in

an air-tight container and used without further treatment. The sand-clay mixtures were prepared by dry-mixing 90% sand and 10% clay (by mass) and then adding distilled water to achieve 5% moisture content. Each sample was placed in a plastic bag, kneaded by hand for 10 minutes until the sample seemed thoroughly mixed by visual inspection, and allowed to rest for 2 hours before any heat treatment. For each test, the required amount of material (sand or sand-clay) was heated in the furnace at a temperature of 250, 500, 750, or 1000°C following the appropriate heat treatment programme listed in Table 3.2. After the heat treatment, the furnace cooled at a rate of 3.1°/min. The samples treated at 250°C and 500°C were removed from the muffle furnace immediately and placed in a desiccator to cool. Samples heated to temperatures above 500°C were allowed to cool in the furnace to 200°C before transfer to the desiccator.

Table 3.2. Heating patterns for silica sand and silica sand-kaolin samples

Sample	Pre-heating duration (min)	Peak temperature exposure (min)
Untreated	-	-
105	30	1440
250	30	60
500	30	60
750	60	60
1000	60	60

3.2.2. Laboratory Testing

The plastic and liquid limits for the clay were determined using the cone penetration and rolling methods (BS1377-2:1990). The clay was mixed with water to form a paste. This paste was placed into the penetrometer pot and the cone was dropped into the sample. After each test, a small sample was taken and placed in an oven at 105°C for 24hrs to determine the moisture content. A small sample was wetted with

a small amount of water so that when rolling it to 3mm, thin, small cracks were visible in the sample. The entire sample was also placed in the oven to determine the moisture content. The mineralogical composition of the kaolin clay was tested by BRUKER D8 ADVANCE with DAVINCI (2010) powder X-Ray Diffraction (XRD) on untreated and heat-treated powder samples.

3.2.3. Direct Shear Box Testing

The direct shear test is the simplest and most economical test for dry granular soils and widely used in geotechnical engineering because it is very quick and suitable for practical applications (Caruso and Tarantino, 2004; Cerato and Lutenegger, 2006). Like any test there are limitations. The sample is not allowed to fail along the weakest plane and the shear stress distribution over the shear surface is not uniform. For a comparative study, the results are suitable as these limitations can be reasonably assumed to affect all samples in the same way and differences in response can still be detected.

The samples were sheared using a Digital Direct/Residual Shear apparatus (ELE International, Sheffield, UK) with 100mm x 100mm shear box assembly. The assembly was designed for use with coarser samples as effects on the sample boundary were reduced (Lings and Dietz, 2004). A shear rate of 0.05mm/s and vertical stresses of 50, 100 and 150kPa were applied to reflect a stress regime associated with geotechnical engineering problems (Fannin et al., 2005; Cavarretta et al., 2010). All samples were tested in triplicate at room temperature and under dry conditions to simulate responses after exposure to heat treatments or smouldering. To minimise errors while placing the sample in the shear box and to ensure a consistent sample bulk density of 1.68 g/cm^3, a pluviator (Figure 3.1) was designed and built to fit the shear box. The design used in this set up contained two

parts that were connected by a 4mm mesh to disrupt the falling of the grains and reduce segregation of the grains by size. The top part also contained a set of fins spaced 1.5cm apart to disperse the sample on entry into the pluviator. The consistency of the pluviator was determined prior to testing by preparing 10 samples and determining the bulk densities. The standard error of these measurements was 0.02 g/cm^3.

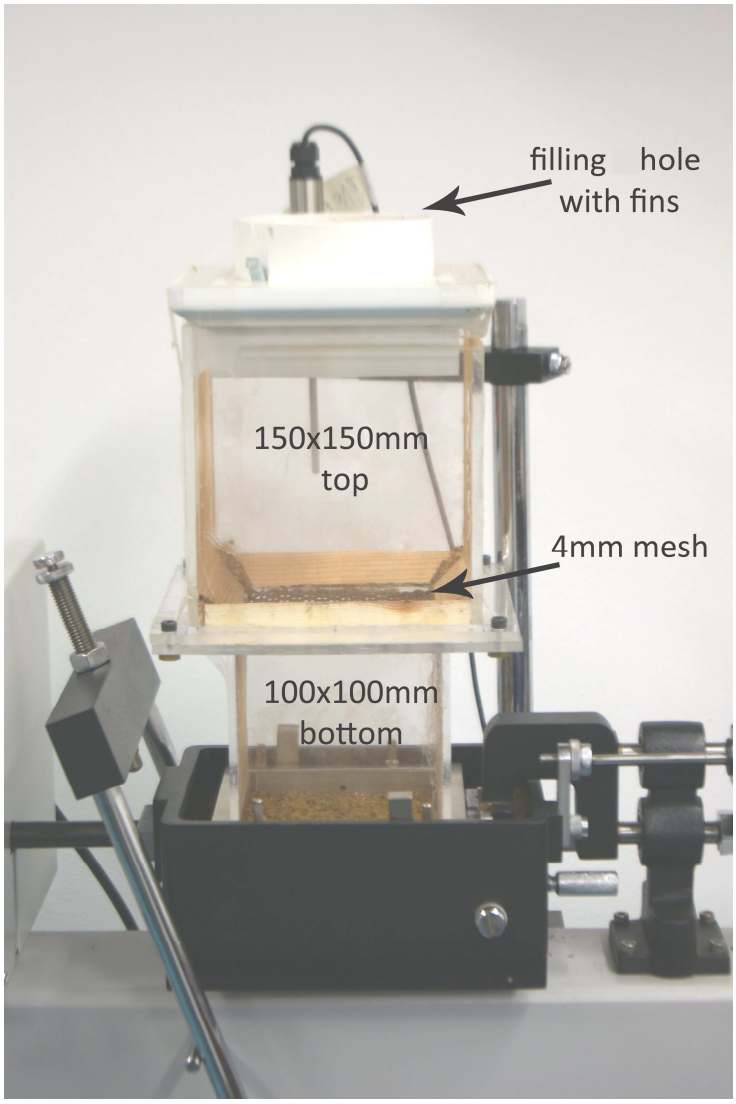

Figure 3.1 Pluviator design and shear box placement

The sample was placed into the shear box by pouring on half of the sample (200g) from the left side and the other half of the sample from the right side. The 4mm mesh in the pluviator dispersed the sample. After placing the sample into the shear box, the pluviator was removed and the loading plate was placed on top of the sample. Using the displacement screws, a 3mm gap was formed between the shearing plates to allow enough room for a shear band to form. The displacement transducers (ELE International, Sheffield, UK) were positioned and the support system for 5kN s-type load cell (ELE International, Sheffield, UK) was adjusted to make sure that the load cell was unloaded. The displacement transducers were reset to 0 and the shearing was started using the digital control system of the shear apparatus. When a maximum displacement of 70mm was achieved, the test was stopped and the shear box was returned to its starting position. The sample was removed and the mass retained was recorded. During shearing, the force at the load cell, horizontal and vertical displacements, and the test duration were recorded using the data acquisition program Labview (National Instruments, Newbury, UK). The calibration curves for the two displacement transducers and load cell are included in Figure 3.2 and Figure 3.3.

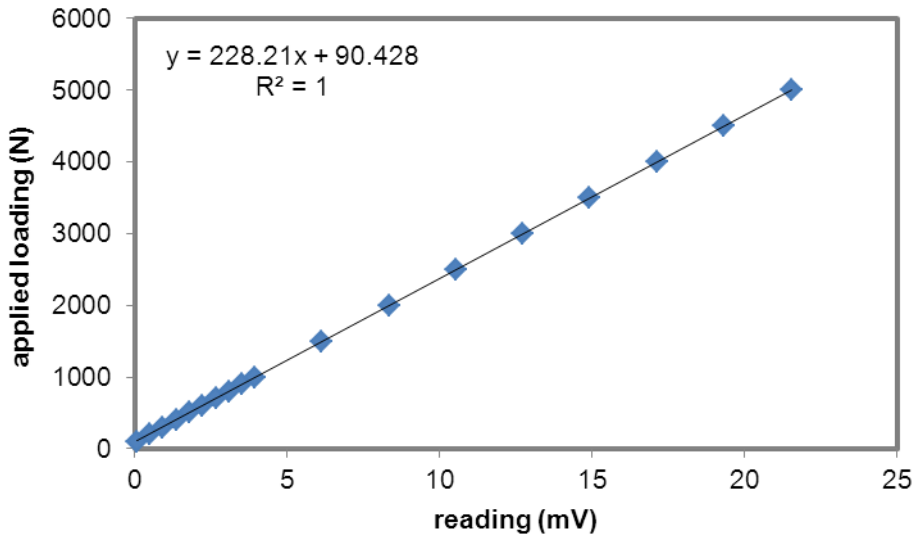

Figure 3.2 5kN s-type load cell calibration

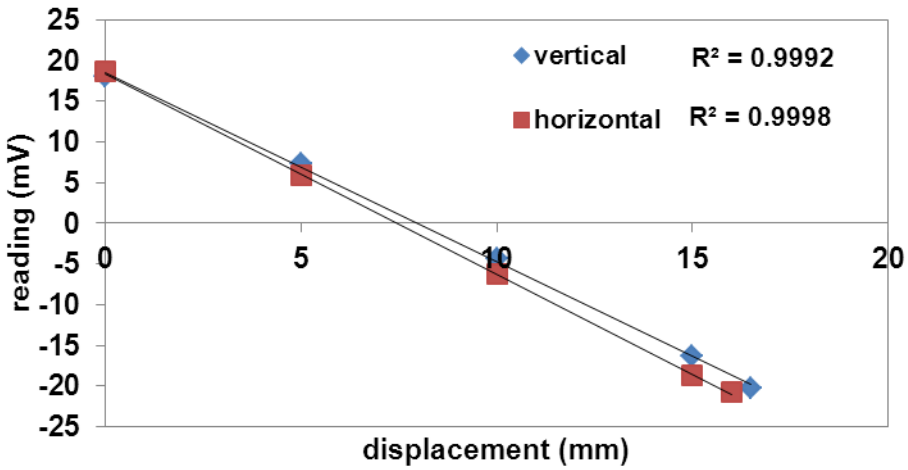

Figure 3.3. Calibration curves for vertical and horizontal displacement transducers

3.2.4. Image Analysis of Silica Sand Grain Photos and Thin Section Scans

Changes to grains surfaces were explored with 200 randomly-selected sand grains which were divided into four samples. For each sample, five rows of 10 silica sand grains were placed on a flat ceramic crucible (6cmx6cm). The grain arrangements

were photographed and then heat treated for 1 hour at each temperature up to 1000℃ (Table 3.2). After each temperature exposure the grains were allowed to cool and a photograph was taken before the next temperature treatment. The photographs were taken using a Sony DSLR A290L. Thin sections prepared from heat treated and smouldered sand were scanned with a high resolution EPSON photo scanner. In each scanned image, 50 grains were randomly selected and coloured by hand. The coloured scans were than rescanned and converted into binary images. Figure 3.4 shows the conversion from the grain images and Figure 3.5 shows the evolution from scan to binary image for the thin section analysis.

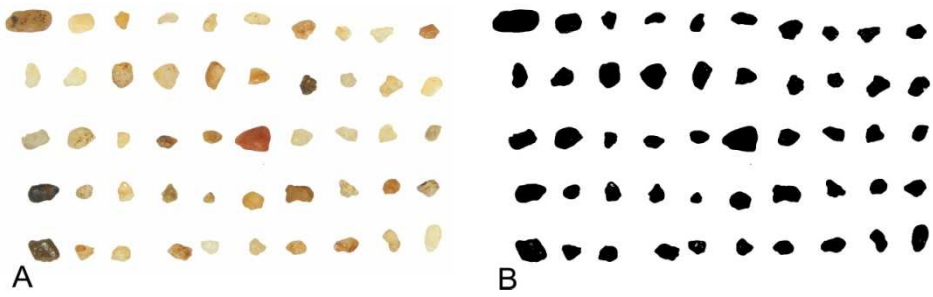

Figure 3.4. Grain photograph original (A) and binary image for analysis (B)

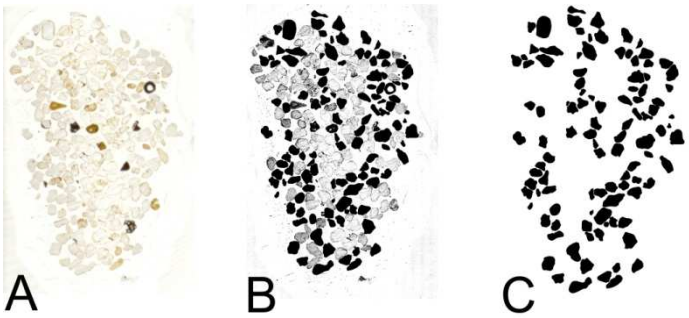

Figure 3.5. Thin section scan conversion to binary image for use with ImageJ software. A: original scan, B: scan after selected grains have been coloured in, C: binary image of selected grains

The photographs and scans were converted to binary images and analysed using the open source software ImageJ (Schneider et al., 2012) to determine the particle circularity and roundness. The circularity parameter gives the shape of the particle. A value of 1.0 describes a perfect circle and as the value approaches 0.0, the particle becomes more elongated. Circularity is defined as:

$$4\pi \times \frac{[Area]}{[Perimeter]^2} \qquad \text{(Eq. 3.2)}$$

Roundness reflects the relationship between the particle length, height and width, giving an indication of its eccentricity. Roundness is defined as:

$$4 \times \frac{[Area]}{\pi \times [Major\ axis]^2} \qquad \text{(Eq. 3.3)}$$

This is also the inverse of the particle aspect ratio.

3.3. Data Analysis and Friction Angle Determination

3.3.1. Silica Sand

For each sample, a set of nine direct shear test results was obtained, three for each vertical stress applied. The shear stress was determined from the recorded force and the area of the sample. Figure 3.6 shows two examples of silica sand data plotted for comparison. To check the tests for anomalies, the three data sets were

plotted as the calculated shear strength (Figure 3.6 A), normalised shear stress (shear stress to normal stress ratio) (Figure 3.6 B), and the vertical displacement (Figure 3.6 C) versus the horizontal displacement (x). For the data to be considered suitable for further analysis, the following criteria were assumed to be fulfilled:

(i) A decay in shear stress following peak is associated with dilatant behaviour

(ii) The inflection point of the displacement is associated with the peak shear stress

(iii) The calculated ultimate shear stress is smaller than peak shear stress

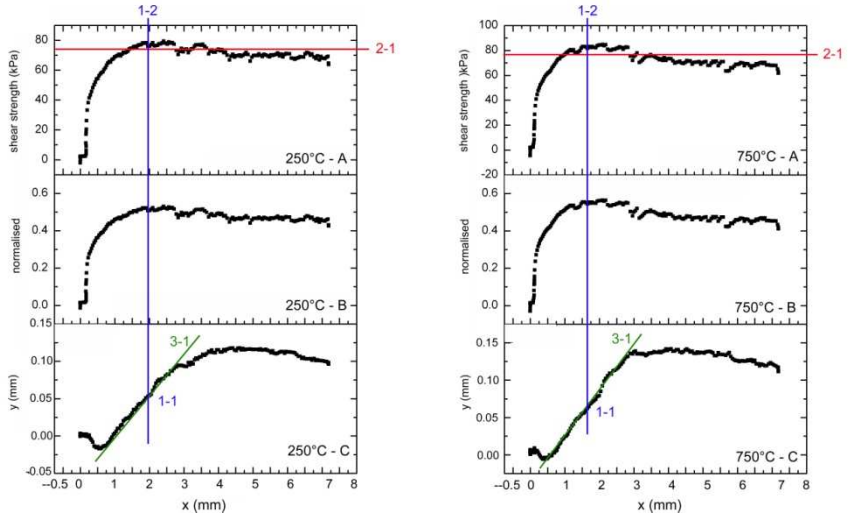

Figure 3.6. Example shear box data for silica sand treated at 250℃ and 750℃ sheared with a normal stress of 100kPa. 1-1: displacement inflection point, 1-2: peak shear stress, 2-1: ultimate shear stress, 3-1: slope of dilatancy

For the case of dilatant behaviour, the inflection point of the vertical versus horizontal displacement curve (Figure 3.6 1-1) was in line with the peak shear stress (Figure 3.6 1-2).The ultimate shear stress (Figure 3.6 2-1) was smaller than the peak shear stress.

Not all experimental data fulfilled the criteria described above. Data that failed these criteria were discarded after plotting, leaving at least 66% of data for each sample. Figure 3.7 below shows two examples where the collected data did not fulfil the criteria and were discarded. The inflection point of the displacement (Figure 3.7 1-1) did not line up with the peak shear stress for the sample treated at 250℃. In addition, no peak shear stress was apparent in this data set despite an overall dilatant behaviour and therefore, the ultimate shear stress (Figure 3.7 2-1) could not be calculated. For the sample treated at 750℃, the data were suitable to the peak shear stress but the displacement recorded after the point Figure 3.7 4-1 shows unexpected behaviour that seemed to lead to a fluctuation in the shear response (Figure 3.7 750℃ – 1 and 750℃ – 2). Based on the outlined criteria above, data sets like these have been eliminated from further analysis. In total, 42 of 117 data sets were not analysed further.

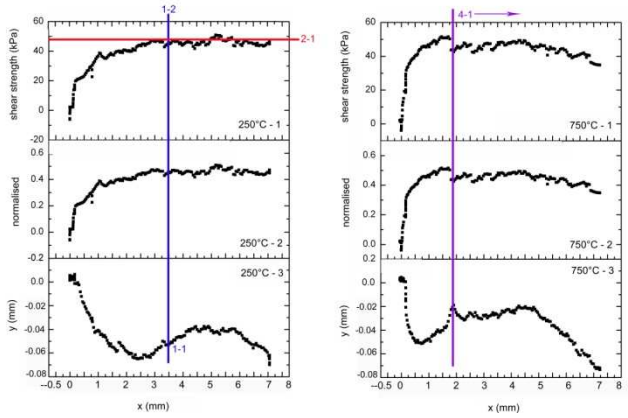

Figure 3.7. Example shear box data for silica sand treated at 250℃ and 750℃ sheared with a normal stress of 150kPa. 1-1: displacement inflection point, 1-2: peak shear stress, 2-1: ultimate shear stress, 4-1: start of non-typical test behaviour

Due to anomalous responses at large horizontal displacement, the ultimate shear stress was calculated using Equation 3.4 (Figure 3.6 2-1):

$$\left(\frac{\tau}{\sigma}\right)_{ult} = \left(\frac{\tau}{\sigma}\right)_{peak} - \frac{\delta y}{\delta x} \qquad \text{(Eq. 3.4)}$$

After determining the peak and ultimate shear stress values, the data were plotted in the normal effective stress-shear stress to characterise the shear strength behaviour. Figure 3.8 shows an example of ultimate shear strength for the silica sand data for the untreated sample.

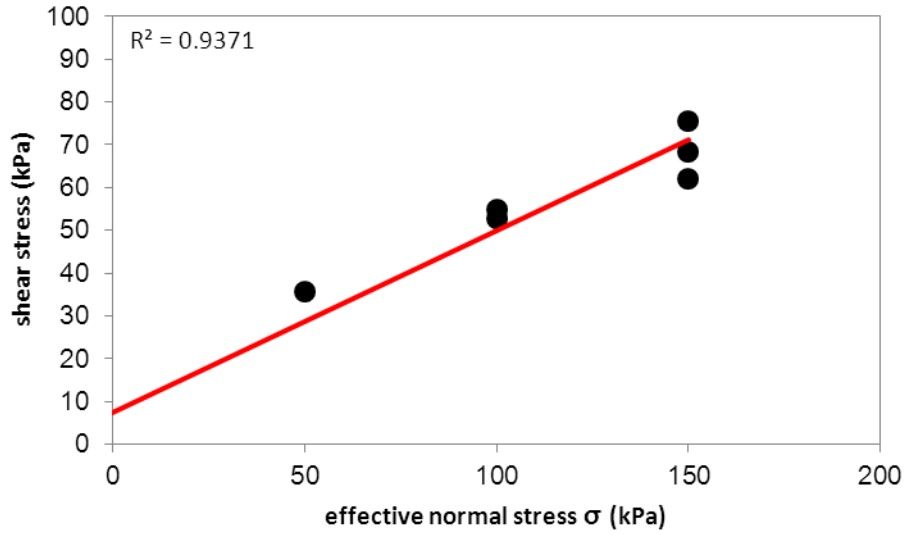

Figure 3.8. Ultimate shear stress vs normal stress graph for Untreated silica sand

The friction angle was determined by the slope (m) as shown below:

$$\Phi' = \tan^{-1} m \qquad \text{(Eq. 3.5)}$$

The slopes for the peak and ultimate shear strength of silica sand are included in Figure 3.9 and Figure 3.10.

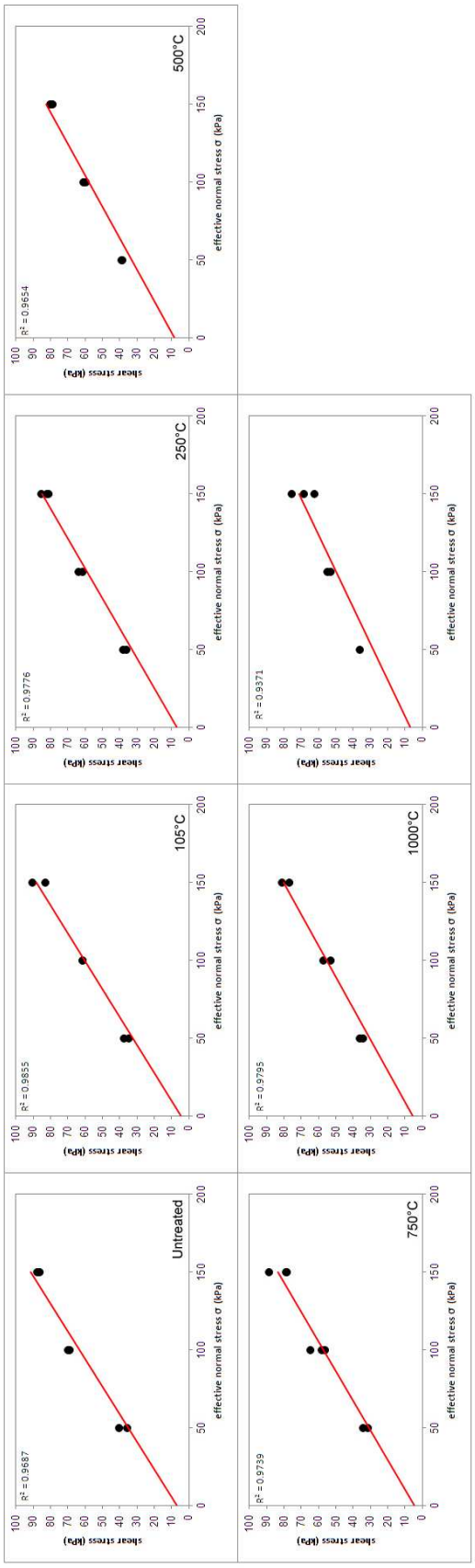

Figure 3.9. Peak shear stress vs effective normal stress for silica sand after different heat treatments

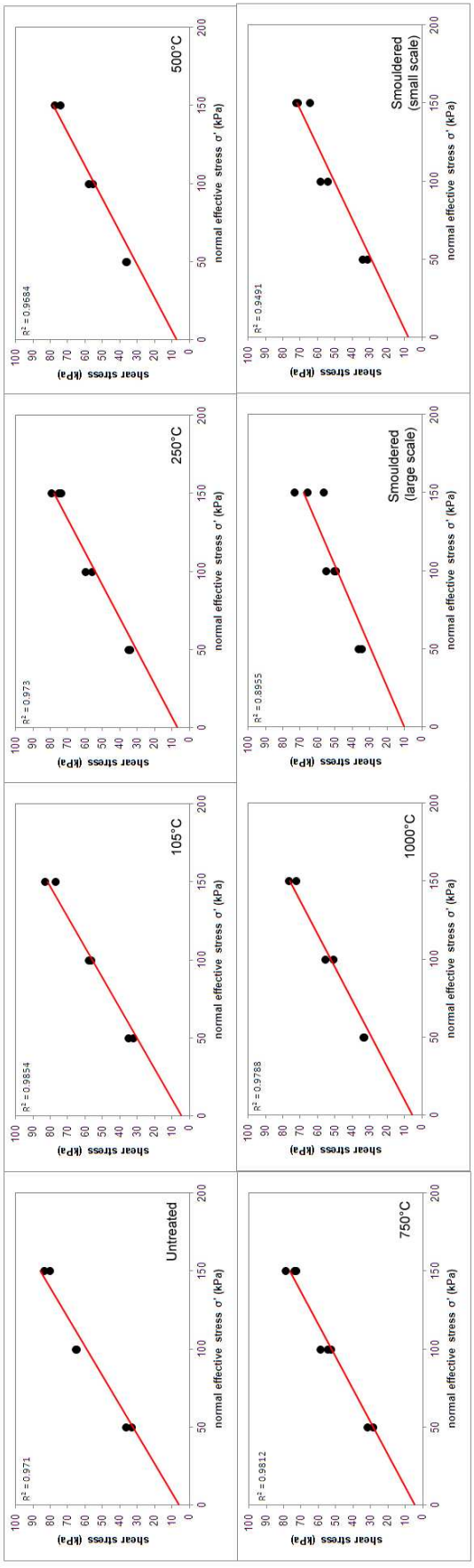

Figure 3.10. Ultimate shear stress vs effective normal stress for silica sand after different heat treatments

3.3.2. Silica Sand + 10% Kaolin

For the silica sand-kaolin mixtures, the contact angles were determined based on the normalised ultimate shear stress values and plotted individually for each temperature and normal stress. The value at 5.5mm displacement was taken where the dilatant behaviour was assumed to be stable. Figure 3.11 shows an example for the direct shear results and how the ultimate shear strength was determined. Only one data set for the silica sand + 10% kaolin was not analysed further.

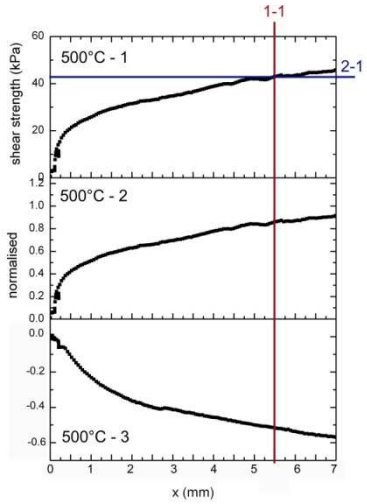

Figure 3.11. Example shear box data for silica sand + 10% kaolin treated at 500℃ sheared with a normal stress of 50kPa. 1-1: 55mm displacement, 2-1: ultimate shear stress

3.4. Results and Discussion

3.4.1. Friction Angle Changes from Heat Treatment in Silica Sand

Increasing temperature of heat treatment causes an overall friction angle decrease of 3° from untreated to 1000℃ treatment for the si lica sand for both peak and ultimate friction angle (Figure 3.12). This decrease may be due to changes in surface chemistry (Frossard, 1979; Cho et al., 2006), decreases in surface roughness (Cho et al., 2006; Cavarretta et al., 2010; Li and Aydin, 2010;

Sadrekarimi and Olson, 2011), rounding of the grain shapes (Oda et al., 1998; Mair et al., 2002; Collins and Muhunthan, 2003; Cho et al., 2006; Cavarretta et al., 2010; Göktepe and Sezer, 2010; Li and Aydin, 2010; Maleki et al., 2011; Sadrekarimi and Olson, 2011), or a combination of these three mechanisms.

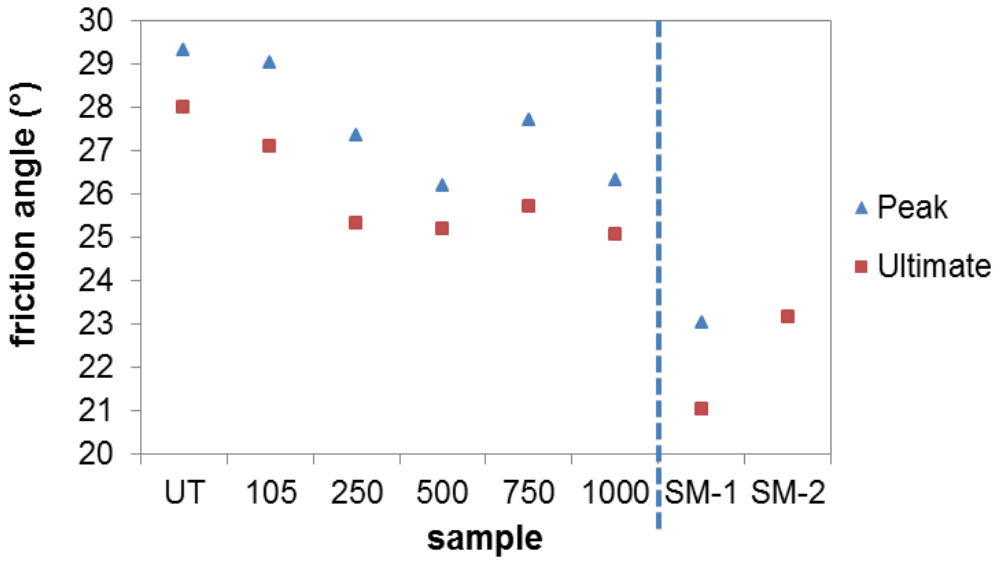

Figure 3.12. Peak and ultimate friction angle values of silica sand for various treatment temperatures

Due to behaviour of the small scale smouldered sand (SM-2) only an ultimate friction angle could be determined. An example of the direct shear data is shown in Figure 3.13.

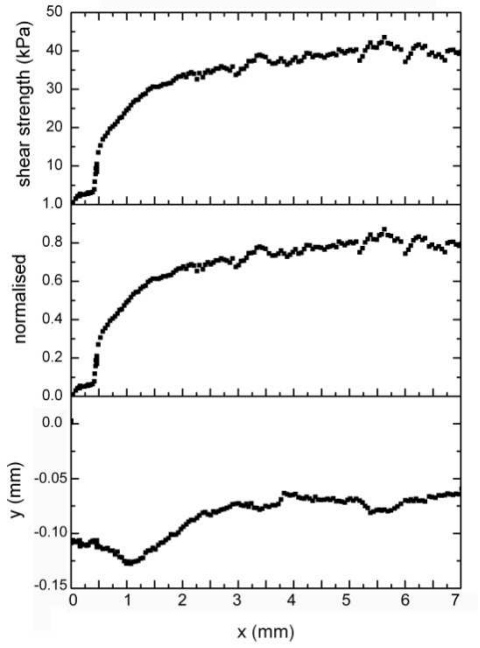

Figure 3.13. Example shear box data for silica sand treated with small scale smouldering (SM-2) sheared with a normal stress of 50kPa

Image analysis showed no significant changes to roundness or circularity of the grains with increasing temperature or between thermal and smouldering treatments (Table 3.3). The difference between full grains and thin section grains was likely due to hand colouring of the thin section grains and forcing of grains into position during preparation. The difference within each analysis (grains and thin section) showed no changes. Grain surface roughness did not seem to be affected by temperature or smouldering, but the resolution of the petrographic microscope may not have been high enough to detect small changes. In the thin section samples, exposure of 500℃ and above seemed to form a reddish reaction rim on the sand grains (Figure 3.14) as a result of iron oxidation (Chapter 2). Penetration of this rim seemed to increase with increasing temperature. In addition to goethite oxidation to hematite, exposure to 1000℃ and smouldering resulted in quartz transformation to tridymite and crystobalite polymorphs. Changes did occur at the grain surfaces, but the

effects on surface roughness were unclear. Further investigation using higher resolution microscopy and other techniques should be considered to fully investigate changes to the surface roughness.

Table 3.3. Image analysis results for full grains and thin section grains of silica sand

Sample	Grains			Thin section grains		
	analysed	roundness	circularity	analysed	roundness	circularity
Untreated	204	0.73 ± 0.009	0.79 ± 0.004	106	0.67 ± 0.015	0.53 ± 0.009
105	201	0.73 ± 0.009	0.78 ± 0.004	*untested*	*untested*	*untested*
250	125	0.75 ± 0.017	0.76 ± 0.009	148	0.67 ± 0.013	0.55 ± 0.007
500	204	0.72 ± 0.009	0.78 ± 0.006	158	0.68 ± 0.012	0.54 ± 0.006
750	198	0.73 ± 0.009	0.78 ± 0.005	*untested*	*untested*	*untested*
1000	194	0.74 ± 0.009	0.78 ± 0.004	127	0.67 ± 0.014	0.51 ± 0.009
SM-1 (large scale)	*untested*	*untested*	*untested*	234	0.65 ± 0.010	0.51 ± 0.007

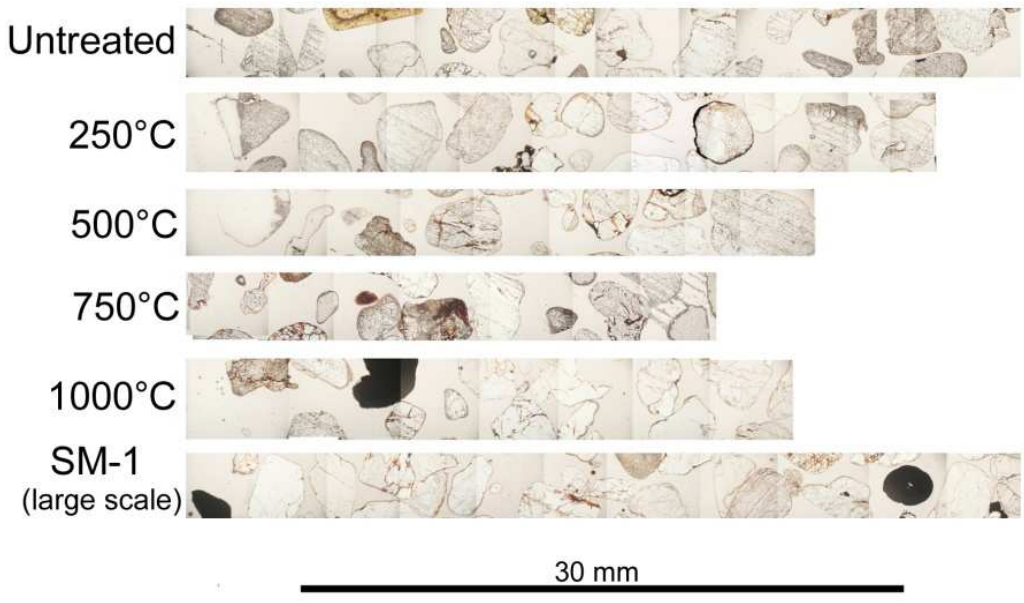

Figure 3.14. Thin section Images for different thermal treatment temperatures

3.4.2. Friction Angle Changes from Smouldering Remediation of Silica Sand

The smouldered samples were consistent with the heat treatment samples, showing a decreased friction angle compared to the untreated sand. The difference between the two friction angles was likely to be due to effects based on smouldering operating scale (Table 3.1). In both scales, the material was exposed to the similar peak temperatures (~1000℃) and the post-remediatio n conditions were very similar as well. However, due to the difference in scale and operating conditions, the smouldering front velocity in the large scale experiment (SM-1) was slower compared to the small scale experiments (SM-2 and SM-3) and the duration of exposure to elevated temperatures was significantly longer in the large scale experiment as well. Exposure duration included attainment of the peak temperature as the smouldering front moved through the material and cooling of the post-remediation material to ambient conditions. Since the ultimate friction angle is lower for the small scale experiment (SM-2) compared to the large scale experiment (SM-1), high temperature exposure may not account for all of the change. It is possible that the shorter exposure duration in the small scale experiment did not remove all contaminants and that the additional increase was due to residual contamination. Experiments on crude oil contaminated sandy soils showed a decrease in contact angle with increase of oil content (Khamehchiyan et al., 2007), so residual contamination may account for the further reduction of the ultimate friction angle.

3.4.3. Friction Angle Changes in Silica Sand-Kaolin

The samples containing 10% kaolin clay showed an increase in friction angle of 5° with increasing treatment temperature from 105℃ to 1000℃ (Figure 3.15). This increase can be explained with two effects, bonding and mineral changes. Increased bonding of the kaolin was observed with increasing temperature. The kaolin coated

the sand grains after mixing and with increasing temperature, this coating appeared to become stronger. The bonding effect can be two-fold. The clay coating may increase the effective grain size, which may in turn cause an increase in shear strength or by creating bonds between sand grains through clay bridges. The mineral change of the kaolin, for example the emergence of mullite after exposure above 500℃ is also going to affect the overall res ponse of the sample (Figure 3.16).

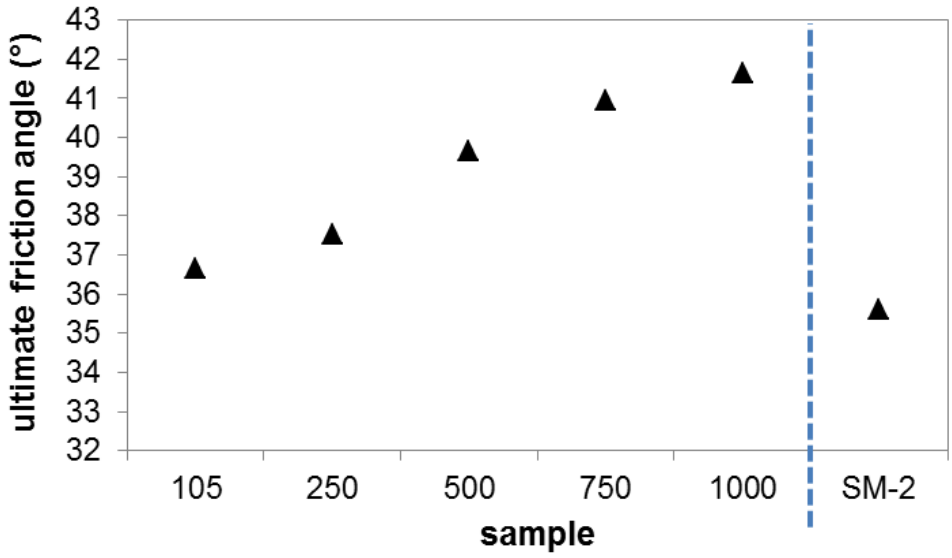

Figure 3.15. Ultimate Friction Angle values (standard error) for sand-kaolin (10%) for different thermal treatment temperatures

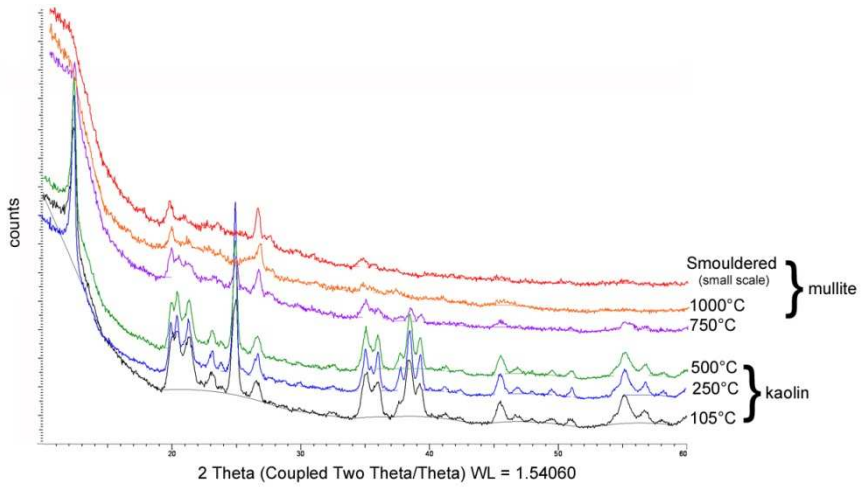

Figure 3.16. XRD results for kaolin clay powder for different heat treatments

Increases in the friction angle likely resulted from a combination of both phenomena. In contrast, the smouldered sample showed a small decrease in friction angle compared to the 105℃ treated samples. This was pro bably due to a combination of the exposure temperature, exposure duration, residual contamination, clay faction separation, and chemistry changes. There were several significant handling steps between remediation of the contaminated material and shear box testing. Mobilisation of fines was apparent visually during this process and may have affected the results.

Table 3.4. Liquid and plastic limits for dry powder kaolin after different heat treatment temperatures

Sample	Liquid Limit	Plastic Limit	Plasticity Index	Plasticity Chart Classification
	w_L	w_P	I_p	
		%		
105	64.4	35.9	28.5	MH: silt, high plasticity
250	63.7	30.8	32.9	CH: clay, high plasticity
500	65.2	42.7	22.6	MH: silt, high plasticity
750	81.6	57.4	24.1	MV: silt, very high plasticity
1000	*ND*[1]	*ND*	*ND*	*ND*

[1]Plastic and liquid limit for the sample treated at 1000℃ could not be determined due to non-newtonian like behaviour

Further testing is required to understand if these changes to friction angle are permanent or temporary and the extent to which they are linked to operating conditions. Based on significant differences in exposure duration and residual contamination, testing of samples obtained from large-scale experiments or field sites after remediation would be highly beneficial. In addition, testing after initial wetting would allow for investigation of the soil response and if there are additional changes to the soil strength and friction behaviour.

3.4.4. Discussion

A lower friction angle for post-remediation sandy soils could cause stability problems during earth works on site. Stability analysis should be carried out using the post-remediation friction angle values. Expanding the test regime to materials with different mineralogical compositions and particle ranges (e.g. silty sands) could help determine if a 3° friction angle decrease is common across many soils and site materials and can be predicted based on site parameters such as contaminant or operating conditions.

In all cases in this study, the friction angle and therefore soil strength was affected by thermal and smouldering treatments. Thermal and smouldering remediation process are used in ex situ (excavated) and in situ (non-excavated) settings. Changes to soil properties can be managed easily in the ex situ setting, but may be more difficult to detect in the in situ setting. If the load that a soil can safely support has been calculated using friction angle values from tests on untreated soil, the calculations may not reflect site conditions after remediation. Site engineers should carry out stability analysis using more accurate data from tests on post-remediation materials. Soils may require preventive or stabilising measures after remediation as part of the redevelopment strategy. Ground investigation after remediation is essential to determine the extent of changes to soil conditions as a result of remediation so that safety issues related to ground stability can be detected and resolved. To ensure safe use of the post-remediation material, tests like the direct shear test should be implemented to better understand the post-remediation material uses and limitations.

3.5. Conclusions

This study shows that the friction angle for sand and sand-clay mixtures are affected by thermal and smouldering treatments. The decrease of 3° for the tested sand is very important for granular and sandy soils that are being treated by remediation techniques using high temperatures. Decrease of shear strength during and after remediation may impact the suitability of post-remediation soil for re-use and limit future uses of the site after remediation. Predicting possible changes to soils before remediating the site is highly recommended and should be considered as part of the site investigation protocol. This will allow additional loading calculations and relevant precautions to be implemented into the remediation strategy. Follow-up ground

investigation after remediation is essential to characterise the full extent of changes to soil properties and design appropriate rehabilitation measures.

The increase of friction angle for the mixture containing 10% clay shows that thermal treatment can improve the shear strength but this improvement should be treated with caution since sites can be heterogeneous with a range of clay contents and types. The presence of residual contamination, common after any remediation activity, may have significant influence on the shear strength. In addition, this study did not assess whether this increase in shear strength persists after soil saturation. To better understand the effects on soils containing clay fractions, broadening the research to include clay types commonly found in natural soils, such as smectite and illite, is highly recommended. This study shows that shear strength of sand and sand-clay mixtures are affected by heat and smouldering treatments. The remediated medium itself should be considered different after treatment and appropriate testing regimes should be implemented prior to site redevelopment.

3.6. References

Bagherzadeh-Khalkhali, A., Mirghasemi, A.A., 2009. Numerical and experimental direct shear tests for coarse-grained soils. Particuology, 7(1): 83-91.

Caruso, M., Tarantino, A., 2004. A shearbox for testing unsaturated soils at medium to high degrees of saturation. Géotechnique, 54(4): 281-284.

Cavarretta, I., Coop, M., O'Sullivan, C., 2010. The influence of particle characteristics on the behaviour of coarse grained soils. Géotechnique, 60(6): 413-423.

Cerato, A.B., Lutenegger, A.J., 2006. Specimen Size and Scale Effects of Direct Shear Box tests of Sands. Geotechnical Testing Journal, 29(6).

Certini, G., 2005. Effects of fire on properties of forest soils: a review. Oecologia, 143(1): 1-10.

Chang, C.S., Yin, Z.-Y., 2011. Micromechanical modeling for behavior of silty sand with influence of fine content. International Journal of Solids and Structures, 48(19): 2655-2667.

Chang, T.C., Yen, J.H., 2006. On-site mercury-contaminated soils remediation by using thermal desorption technology. Journal of Hazardous Materials, 128(2-3): 208-217.

Cho, G.C., Dodds, J., Santamarina, J.C., 2006. Particle Shape Effects on Packing Density, Stiffness and Strength: Natural and Crushed Sands. Journal of Geotechnical and Geoenvironmental Engineering, 132(5): 591-602.

Collins, I.F., Muhunthan, B., 2003. On the relationship between stress-dilatancy, anisotropy, and plastic dissipation for granular materials. Géotechnique, 53(7): 611-618.

Fannin, R.J., Eliadorani, A., Wilkinson, J.M.T., 2005. Shear strength of cohesionless soils at low stress. Geotechnique, 55(6): 467-478.

Frossard, E., 1979. Effect of sand grain shape on interparticle friction; indirect measurements by Rowe's stress dilatancy theory. Géotechnique, 29(3): 341-350.

Gan, S., Lau, E.V., Ng, H.K., 2009. Remediation of soils contaminated with polycyclic aromatic hydrocarbons (PAHs). Journal of Hazardous Materials, 172(2-3): 532-549.

Göktepe, A.B., Sezer, A., 2010. Effect of particle shape on density and permeability of sands. Proceedings of the Institution of Civil Engineers-Geotechnical Engineering, 163(6): 307-320.

Khamehchiyan, M., Hossein Charkhabi, A., Tajik, M., 2007. Effects of crude oil contamination on geotechnical properties of clayey and sandy soils. Engineering Geology, 89(3-4): 220-229.

Kronholm, J., Kalpala, J., Hartonen, K., Riekkola, M.-L., 2002. Pressurized hot water extraction coupled with supercritical water oxidation in remediation of sand and soil containing PAHs. The Journal of Supercritical Fluids, 23(2): 123-134.

Lee, W.-J. et al., 2008. Thermal treatment of polychlorinated dibenzo-p-dioxins and dibenzofurans from contaminated soils. Journal of Hazardous Materials, 160(1): 220-227.

Li, Y.R., Aydin, A., 2010. Behavior of rounded granular materials in direct shear: Mechanisms and quantification of fluctuations. Engineering Geology, 115(1-2): 96-104.

Lings, M.L., Dietz, M.S., 2004. An improved direct shear apparatus for sand, Geotechnique, pp. 245-256.

Mair, K., Frye, K.M., Marone, C., 2002. Influence of grain characteristics on the friction of granular shear zones. Journal of Geophysical Research, 107(B10, 2219): EVC 4-1 - EVC 4-9.

Maleki, M., Ezzatkhah, A., Bayat, M., Mousivand, M., 2011. Effect of physical parameters on static undrained resistance of sandy soil with low silt content. Soil Dynamics and Earthquake Engineering, 31(10): 1324-1331.

Mehrabadi, M.M., Nemat-Nasser, S., 1983. Stress, dilatancy and fabric in granular materials. Mechanics of Materials, 2(2): 155-161.

Monkul, M.M., Ozden, G., 2007. Compressional behavior of clayey sand and transition fines content. Engineering Geology, 89(3–4): 195-205.

Oda, M., Kazama, H., Konishi, J., 1998. Effects of induced anisotropy on the development of shear bands in granular materials. Mechanics of Materials, 28(1-4): 103-111.

Oda, M., Konishi, J., Nemat-Nasser, S., 1982. Experimental micromechanical evaluation of strength of granular materials: Effects of particle rolling. Mechanics of Materials, 1(4): 269-283.

Panayiotopoulos, K.P., 1989. Packing of sands--A review. Soil and Tillage Research, 13(2): 101-121.

Rein, G., Cleaver, N., Ashton, C., Pironi, P., Torero, J.L., 2008. The severity of smouldering peat fires and damage to the forest soil. CATENA, 74(3): 304-309.

Sadrekarimi, A., Olson, S.M., 2011. Critical state friction angle of sands, Geotechnique, pp. 771-783.

Sarsby, R.W., 2000. Shear Strength. Environmental Geotechnics, Chapter 6.

Schneider, C.A., Rasband, W.S., Eliceiri, K.W., 2012. NIH Image to ImageJ: 25 years of image analysis. Nat Meth, 9(7): 671-675.

Sezer, A., 2011. Prediction of shear development in clean sands by use of particle shape information and artificial neural networks. Expert Systems with Applications, 38(5): 5603-5613.

Shinohara, K., Oida, M., Golman, B., 2000. Effect of particle shape on angle of internal friction by triaxial compression test. Powder Technology, 107(1-2): 131-136.

Skinner, A.E., 1969. A note on the influence of interparticle friction on the shearing strength of a random assembly of spherical particles. Géotechnique, 19(1): 150-157.

Switzer, C., Pironi, P., Gerhard, J.I., Rein, G., Torero, J.L., 2009. Self-Sustaining Smoldering Combustion: A Novel Remediation Process for Non-Aqueous-Phase Liquids in Porous Media. Environmental Science & Technology, 43(15): 5871-5877.

Switzer, C., Pironi, P., Gerhard, J.I., Rein, G., Torero, J.L., in review. Volumetric Scale-up of Smouldering Remediation of Contaminated Materials. Journal of Hazardous Materials.

Thevanayagam, S., Mohan, S., 2000. Intergranular state variables and stress-strain behaviour of silty sands. Géotechnique, 50(1): 1-23.

Webb, S.W., Phelan, J.M., 1997. Effect of soil layering on NAPL removal behavior in soil-heated vapor extraction. Journal of Contaminant Hydrology, 27(3-4): 285-308.

4. Unsaturated and Saturated Hydraulic Response of Silica Sand and Silica Sand-Kaolin after Thermal and Smouldering Treatments

4.1. Introduction

A wide range of thermal treatments are used to treat particularly recalcitrant organic contaminants, including hot water extraction (<300°C), thermal desorption (low T <112℃, high T <750℃), heated soil extraction (<30 0℃), incineration (<850℃) and smouldering remediation (600-1100℃, depending on c ontaminant) (Webb and Phelan, 1997; Kronholm et al., 2002; Chang and Yen, 2006; Lee et al., 2008; Gan et al., 2009; Switzer et al., 2009). Wild fire and heat treatment research shows that exposure to elevated temperatures alters soil erosion rate and infiltration behaviour (Hatten et al., 2005; Rein et al., 2008; Terefe et al., 2008; Are et al., 2009). Temperatures reached during thermal and smouldering remediation are likely to affect the hydraulic response of the soil. The properties, including physical, chemical and mechanical affected by high temperatures and smouldering, based on results presented in Chapters 2 and 3, are summarised in Table 4.1. Investigating the hydraulic response of post-remediation soils is important to better understand changes to infiltration, run-off, and transport of residual or co-contaminants.

The hydraulic conductivity describes how easily porous media such as rocks or soils can transmit a fluid. It is a complex phenomenon influenced by the scale of the medium (Fallico et al., 2010). Porous media have hydraulic conductivities in saturated and unsaturated ranges and changes to both are of interest in post-remediation soils.

Table 4.1. Summary of silica sand properties after different thermal treatments

Sample	Sieve Analysis		Mass loss	Friction angle	
	> 1.18mm	< 1.18mm	Sample mass loss	Peak	Ultimate
	% retained		%	°	
Untreated	94.6 ± 0.7	5.3 ± 0.6	0	31.5	29.9
105	*untested*	*untested*	4.21	30.4	28.5
250	95.8 ± 1.2	4.1 ± 1.2	4.74	29.6	27.5
500	94.3 ± 0.4	5.6 ± 1.2	5.1	28.8	27.6
750	*untested*	*untested*	5.37	29.2	27.2
1000	93.5 ± 0.9	6.5 ± 0.8	5.63	28	26.8
Smouldered (large scale)	*untested*	*untested*	*untested*	27.4	26.7

Smouldering and thermal remediation processes displace water during operation. During smouldering, this displacement occurs mainly within the treatment zone but also at a rim surrounding the target area. During thermal remediation, where operating time is on the order of weeks to months, water displacement in the subsurface may be more extensive. With removal of soil water, the treatment zone becomes unsaturated. The unsaturated hydraulic conductivity describes how a fluid flows in an unsaturated soil. The saturated hydraulic conductivity describes water flow through the soil once it is fully saturated. It is important to understand how thermal and smouldering remediation processes impact water movement through the soil following exposure to elevated temperatures during remediation or other high temperature processes.

Hydraulic conductivity values are used to simulate migration of water in unsaturated or partially-saturated, compacted geomaterials e.g. (Chiu and Shackelford, 1998). Aggressive, high temperature remediation processes change soil surfaces (Chapter 3). Modelling water migration in post-remediation soils will be an essential part of the

reuse of this soil. Significant decreases in hydraulic conductivity may lead to increased surface run-off, increased soil erosion, and flooding, which may lead to rapid transport of co-contaminants present in the surface material (Bagarello et al., 2006; Gonçalves et al., 2007). An increase in hydraulic conductivity can lead to preferential flow along the path of increased conductivity. Preferential flow allows contaminants to bypass large areas of soil, decreasing filtration of contaminants and, in turn, allowing them to be transported either to a different area within the soil or reaching the ground water (Šimůnek et al., 2003; Lipsius and Mooney, 2006; Allaire et al., 2009; Hamlett et al., 2011).

A range of properties and characteristics affect the hydraulic conductivity of a porous medium. Pore size, particle size distribution and to a lesser extent bulk density, void ratio, shape and continuity of the pores affect the flow of water through the medium. Void ratios (Volume voids divided by the volume of solids) can be used to characterise soil structure or fabric but soils with the same void ratios can have different pore networks that lead to different flows. A high number of small pores will have a lower hydraulic conductivity than a soil with fewer larger pores even though the void ratios will be similar. The behaviour also depends on the arrangement of the particles and therefore pore size, shape, and network (Juang and Holtz, 1986; Gonçalves et al., 2007). The proportion and nature of the fine fraction (silts and clays) also control the conductivity (Shafiee, 2008) partly by filling the available pore space lowering the pore volume. Experiments show that addition of 10% of kaolin can decrease the conductivity of a sandy soil by a factor of 5 (Al-Shayea, 2001). Sieve analysis on sand and clay mixtures shows that with increasing temperature the fine fraction can be mobilised by detachment from sand grains (Table 4.1). Thermal and smouldering remediation processes are likely to affect one or more of these controlling factors in soil and in turn, alter the hydraulic conductivity. The aim

of this study is to investigate how these thermal and smouldering remediation processes affect the conductivity of soil using silica sand and silica sand-kaolin mixtures as simple soils.

4.2. Materials and Methods

4.2.1. Sample Preparation and Heat Treatment

The silica sand was soaked in a solution of sodium hexametaphosphate and sodium carbonate for 24 hrs, washed over a 425μm sieve to eliminate any loose fines, and air dried for several days (BS1377-2:1990). After air drying, the sand was stored in a container and used without further treatment. For the silica sand samples, only untreated and smouldered samples were tested. Previous work on sands exposed to 250, 500, 750, and 1000℃ showed no differences in hydraulic conductivities, so these experiments were not repeated (Skordou, 2012).

Table 4.2. Heating and cooling programme for silica sand + 10% kaolin samples

Sample	Heating rate (℃/min)	Peak temperature (°C)	Cooling duration in furnace (min)
Untreated	-	-	-
105	3.5	105	0
250	8.3	250	0
500	16.6	500	~60
750	12.5	750	~180
1000	16.6	1000	~240

The sand-kaolin mixtures were prepared by dry-mixing 90% silica sand and 10% kaolin clay (by mass) and then adding distilled water to achieve 5% moisture content. The mixture was placed in a plastic bag and thoroughly kneaded by hand

for 10 minutes and allowed to rest for 2 hours before any heat treatment. In addition, one sample of silica sand (90%) and kaolin clay (10%) was prepared without the addition of any water. For each test, the sand-kaolin sample with 5% moisture content was heated in the furnace following the heat treatment programmes listed in Table 4.2. The silica sand-kaolin sample prepared dry was only tested without high temperature treatment. After the required exposure duration, the samples were removed from the muffle furnace and placed in a desiccator to cool. Samples heated to temperatures above 500℃ were allowed to cool in the furnace to 200℃ before transfer to the desiccator.

4.2.2. pH Testing

The pH for silica sand, kaolin clay and silica sand-kaolin clay mixtures was determined by preparing a solution with distilled water and 30g of sample as outlined in BS1377-3:1990. The mixture was placed in a glass beaker, covered and left to rest for 24hrs in a room at 20℃. After 24hrs, the sample was stirred for 5 minutes before taking three pH readings with a pH meter (Mettler Toledo Ltd, Leicester, UK) with an accuracy of ± 0.004.

4.2.3. Hydraulic Conductivity Testing

The experimental set up was based on a well-established constant head test method involving infiltration into the soil from the bottom of the permeability column (Head, 1980).

A permeability column of diameter 0.077m and height 0.238m (Wykeham Farrance Engineering Ltd, Slough, UK) was used for all experiments. A fine mesh (<1mm) was placed at the bottom of the permeability column to avoid any particles blocking the column infiltration holes. A cup fitted with a 3mm mesh was placed into the column and 200g of the sample was poured on top of the cup. The cup was lifted

slowly, disturbing the sample layer in an effort to minimise gravitational affects when pouring the sample. The layer was then compacted three times by dropping a mass of 472.75g from 0.213m above the layer. This procedure was repeated for a total of 6 layers. After the last layer was compacted the sample height was measured and another fine mesh (<1mm) placed on top of the sample. The lid stencil was placed on top of the column and the lid was fastened. The mass (column + sand or sand/kaolin) was recorded. The valve at the bottom inlet of the column was opened and the sample was purged with carbon dioxide (CO_2) for 3 hours at a flow rate of 10ml/s. After purging, the valve was closed and the CO_2 disconnected, the column was carefully moved to the test bench.

A 5L water tank was filled with distilled water and placed on a top loading balance (Denver Instruments SI-6002) and connected to the inlet used for purging the sample. Ensuring that the valve was closed, the tank was filled with 3L of distilled water and all air bubbles were removed from the tubing. The data acquisition programme Labview (National Instruments, Newbury, UK) was used to record water mass loss from the balance. Once the system was set to a mass of 0, the valve was opened to start the test. The water was allowed to infiltrate the sample from the bottom, through the outflow in the lid, and collected in a glass beaker. The experimental set up is shown in Figure 4.1.

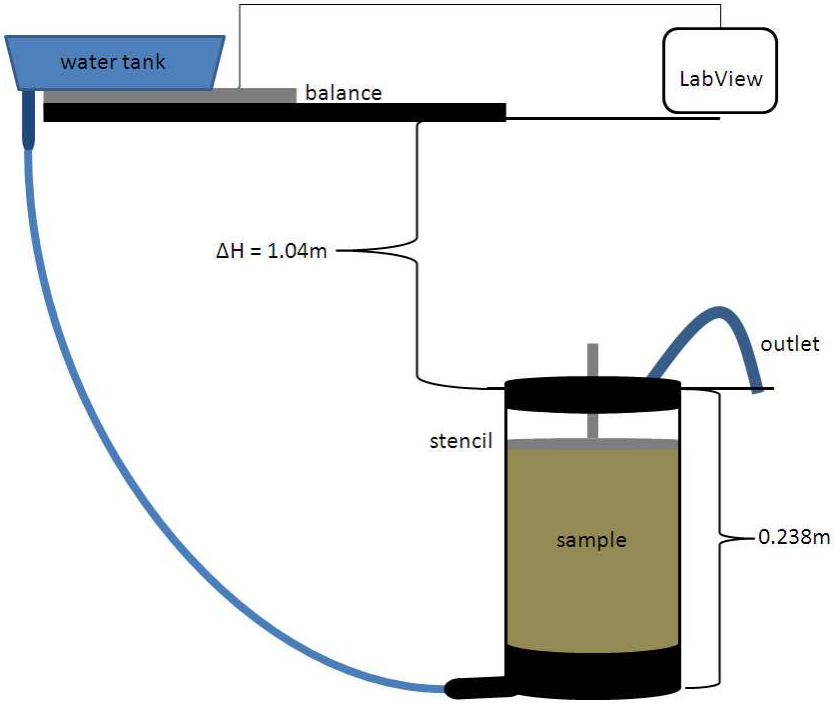

Figure 4.1. Hydraulic conductivity test – experimental set-up

The loss of mass from the water tank was recorded for the duration of the test. After the 3L of water infiltrated the sample, the bottom valve was closed to disconnect the sample from the system. The sample was drained and the mass after draining (column + wet sample) was recorded. The sample was removed from the permeability column and placed into a tray for oven drying.

4.2.4. Limitations and Assumptions

The overall head loss in the water tank (5cm) was relatively small compared to the overall hydraulic head (104cm) and was therefore neglected in the calculations for the saturated hydraulic conductivity. In addition the samples were assumed to represent the same network of pores. The sample preparation method results in the same sample porosities of 0.383 ± 0.009 (9 measurements) for the silica sand and 0.218 ± 0.008 (21 measurements) for the silica sand + 10% kaolin samples. For the

tests using the sand + 10% kaolin, a steady-state flow was not achieved for the duration of the test. However, the sample was fully saturated allowing the determination of the unsaturated conductivity and investigation of the initial stage of saturation. To validate that Darcy's Law was applicable for this experimental set up, the Reynolds numbers were calculated using Equation 4.1 for the different samples.

$$Re = \frac{q\,d}{\nu} \qquad \text{(Eq. 4.1)}$$

where q is the specific discharge (m/s), d is the mean particle diameter (m) and ν is the kinematic viscosity of the fluid (m^2/s) (Bear, 1973). For water at 20℃, ν is 1.004 x 10^{-6} m^2/s. The specific discharge was calculated using Equation 4.2

$$q = \frac{Q}{n \times A} \qquad \text{(Eq. 4.2)}$$

where Q is the volumetric flow (m^3/s), n is the porosity and A is the cross-sectional area of the sample (m^2).

The range of Reynolds numbers was between 1.73 and 2.60 for silica sand + 10% kaolin and 1.89 and 2.01 for the silica sand (Table 4.3). According to Bear (1979), Darcy's Law is valid for flow in porous media if the Reynolds number value lies between 1 and 10. This criterion was met, so Darcy's Law was considered to be valid in all cases.

Table 4.3. Reynolds number (Re) for silica sand and silica sand + 10% kaolin for different treatment temperatures

Silica Sand	Reynolds number (Re)	Silica Sand + 10% kaolin	Reynolds number (Re)
Untreated	2.01 ± 0.004	105℃	3.22 ± 0.01
Smouldered (large scale)	2.05 ± 0.02	250℃	2.58 ± 0.04
Smouldered (small scale)	1.89 ± 0.004	500℃	2.31 ± 0.04
		750℃	2.20 ± 0.02
		1000℃	2.60 ± 0.02
		Smouldered (small scale)	1.73 ± 0.01

4.2.5. Calculations

The porosity n was calculated using the total and void volumes

$$n = \frac{V_v}{V_t} \quad \text{(Eq. 4.3)}$$

where V_v was volume of voids (m^3) and V_t was the total volume (m^3). The relationship between V_v and V_t was

$$V_v = V_t \times \left(1 - \frac{W_s}{\rho_p}\right) \quad \text{(Eq. 4.4)}$$

where W_s was the unit mass of soilds (g/cm^3) which for a dry sample was equal to the total mass divided by the total volume and ρ_p was the particle density (g/cm^3).

The hydraulic conductivity was calculated using the Darcy's Law equation:

$$q = kA \frac{\Delta H}{Lw} \quad \text{(Eq. 4.5)}$$

where q was the volumetric flow (m^3/s), A was the cross sectional area (m^2) of the column, L was the sample height (m), ΔH was the hydraulic head (m), and k was the coefficient of hydraulic conductivity (m/s), a constant of proportionality and characteristic for porous media. To determine k, the equation was solved as:

$$k = \frac{q}{A} \times \frac{Lw}{\Delta H} \quad \text{(Eq. 4.6)}$$

For the saturated hydraulic conductivity, the values used for ΔH, Lw, and A are constant using the following values: ΔH = 1.04m, L = 0.238m and A = $0.0047m^3$ reflecting the experimental conditions. The value for q was based on the flow once the sample became fully saturated and steady state conditions were achieved. To calculate hydraulic conductivity during transient stage the assumption was made that, the values were time dependent and therefore vary during the filling of the sample. This transient stage represents the unsaturated conditions in the sample. Equation 4.6 needed to be amended to allow for this time dependency. Variable values for L, ΔH, and q were calculated as.

$$Lw = \frac{Mw}{A \times n \times \rho_w} \quad \text{(Eq. 4.7)}$$

where Mw was the mass of water (g), A was the sample area (m^2), n was the porosity and ρ_w was the density of water (g/cm^3), and

$$\Delta H_u = \Delta H\infty + L - Lw\ (t) \quad \text{(Eq. 4.8)}$$

where ΔHu is the hydraulic gradient (m), ΔH∞ is the difference between the hydraulic head in the tank and the wetting front (m), L is the length of the sample and Lw is the saturated sample behind the wetting front (Figure 4.2).

The volumetric flow q was based on the difference in flow between any two time points used to calculate Lw. This now gives the equation to calculate the transient hydraulic conductivity, which represents the hydraulic conductivity during the filling of the column before the sample becomes fully saturated.

$$k = \frac{q}{A} \times \frac{L_w}{\Delta H_u} \qquad \text{(Eq. 4.9)}$$

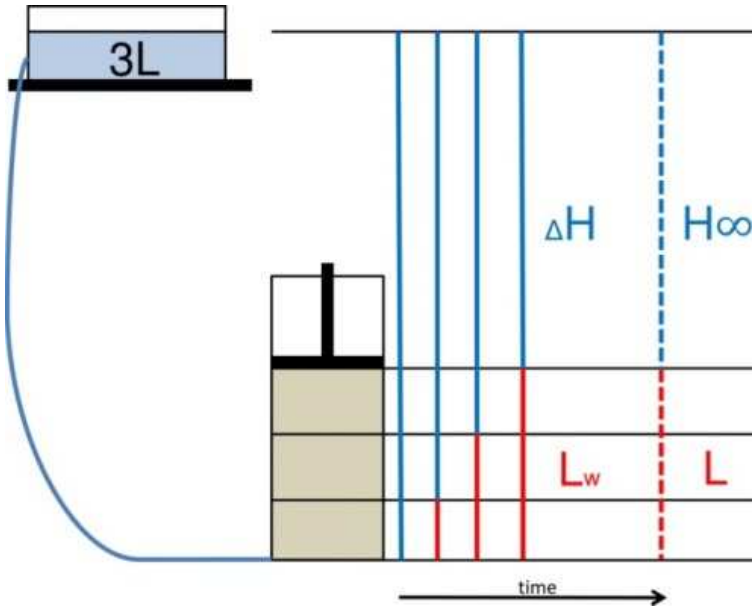

Figure 4.2. Experimental set-up and value definition for unsaturated hydraulic conductivity determination

4.3. Results and Discussion

Experimental data was collected for the duration of the experiment and the change in mass over time was plotted to determine when the column had become fully saturated (Figure 4.3).

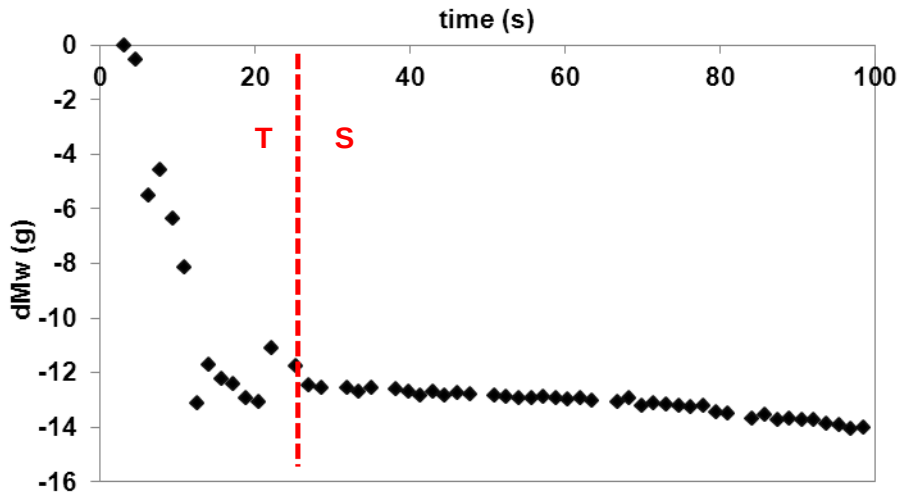

Figure 4.3. Mass of water entering the column over the duration of the experiment

In Figure 4.3, T represents the transient stage of the test where the sample is partially saturated and S represents the fully-saturated stage. As the wetting front moves through the sample, the rate of mass loss from the water tank approaches a constant value. Data to point T were analysed for unsaturated hydraulic conductivity and data from point S were analysed for saturated hydraulic conductivity. The slight slope in the change in mass could be due to lag in balance readings when the change in mass becomes very small or effects during infiltration.

4.3.1. Saturated Hydraulic Conductivity

The average (95% confidence interval) coefficients of hydraulic conductivity for the saturated phase of the untreated and smouldered (large scale) silica sand were 0.0018m/s (Figure 4.4), which was consistent with previous work (Skordou, 2012). For the saturated hydraulic conductivity effects of the solid water interface friction may be negligible. Slight changes to these characteristics may not be evident in hydraulic conductivity measurements. Once fully saturated, silica sand does not behave differently after smouldering treatment compared to no treatment. A similar response after saturation, however, does not mean that the unsaturated conductivities are the same.

Figure 4.5 shows the average hydraulic conductivities for silica sand + 10% kaolin mixtures for untreated dry, untreated wet (5% moisture content added) and smouldered (small scale, SM-3) sample. The coefficients of hydraulic conductivity for the smouldered and untreated dry samples were very similar with k_{sm}=0.0007m/s and with k_{dry}=0.0008m/s. However, the samples prepared with a moisture content of 5% showed a coefficient of k_{mc}=0.0015m/s, which was very similar to the value of silica sand (k=0.0018m/s). This may have been due to the coating effect observed during mixing and represented by the particle size distribution analysis (Table 4.1). The added moisture may have allowed the kaolin to form a bond with the sand particles (Zihms et al., 2013a), likely to result in behaviour similar to that of silica sand. Due to the coating bond the clay was no longer available to fill the pore space between sand particles thus minimising its effect on the overall hydraulic conductivity.

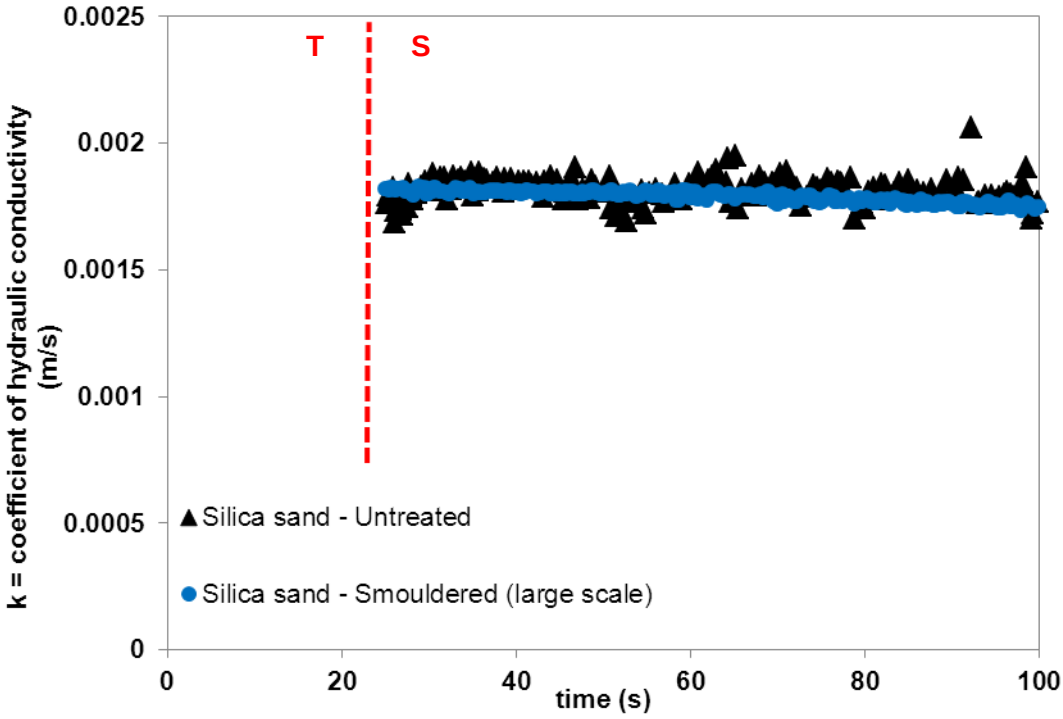

Figure 4.4. Average coefficient of hydraulic conductivity for silica sand

The differences may reflect the changes in microstructure and hydraulic history of the samples in terms of degree of saturation. The samples due not reach full saturation along the same saturation path. The sample mixed without the addition of water experienced an increase of degree of saturation from 0 to100%, whereas the sample prepared with the added moisture content had a hydraulic history of degree of saturation from 0 to 5% during preparation, 2 hours at 5%, and finally, a rapid increase to 100% during the experiment. The samples prepared for the smouldering experiment (SM-3) were also prepared with an added moisture content of 5% but were additionally mixed with coal tar prior to testing. The presence of coal tar, a dense organic liquid, affected the moisture distribution in the bulk sample as well as its microstructure. Smouldering treatment seems to destroy the effect of initial moisture content and related hydraulic history. During particle size distribution analysis, detachment and mobilisation of fines was observed (Table 4.1) and

mobilisation of fines was evident in the column effluent. The nature of the fines fraction may have affected the hydraulic behaviour, a phenomenon observed in other soils (Shafiee, 2008). These phenomena need further investigation using a range of moisture content and soil conditions for heat and smouldering treatments to fully understand the impact. Based on these results, the hydraulic history should be considered when preparing samples for laboratory testing.

Table 4.4. Bulk densities and void ratios silica sand and silica sand + 10% kaolin samples

Silica sand	Bulk density g/cm^3	Void ratio	Silica sand + 10% kaolin	Bulk density g/cm^3	Void ratio
Untreated	1.64 ± 0.03	0.62 ± 0.002	105°C	2.04 ± 0.001	0.29 ± 0.001
Smouldered (large scale)	1.67 ± 0.02	0.59 ± 0.003	250°C	2.09 ± 0.01	0.27 ± 0.007
Smouldered (small scale)	1.69 ± 0.02	0.60 ± 0.002	500°C	2.08 ± 0.01	0.29 ± 0.005
			750°C	2.10 ± 0.01	0.29 ± 0.007
			1000°C	2.09 ± 0.003	0.29 ± 0.002
			Smouldered (small scale)	2.22 ± 0.02	0.28 ± 0.01

Figure 4.5 shows the average (95% confidence interval) saturated hydraulic conductivity for silica sand + 10% kaolin samples after heat treatment and smouldering. These samples were prepared with the addition of water to reflect natural conditions of soils. Based on the results, the samples can be divided into three categories: low temperature treatment (~105℃), medium to high temperature treatment (250-1000℃), and smouldering treatment. The highest hydraulic

conductivity was observed after the low temperature treatment; this value was slightly higher than the hydraulic conductivity measured in the untreated material. High temperature treatment (250-1000℃) resulted in slightly lower hydraulic conductivity values, at or below the hydraulic conductivity of the untreated material. The hydraulic conductivity after contamination and smouldering remediation was the lowest measured, approximately 1/3 of the hydraulic conductivity of the untreated material. Mobilised fines were evident in the air during transfer and in the initial column effluent during testing, but the hydraulic conductivity calculation did not seem to be affected (Figure 4.6). Further tests in a system that does not require handling between smouldering and hydraulic conductivity testing may be helpful to eliminate this effect.

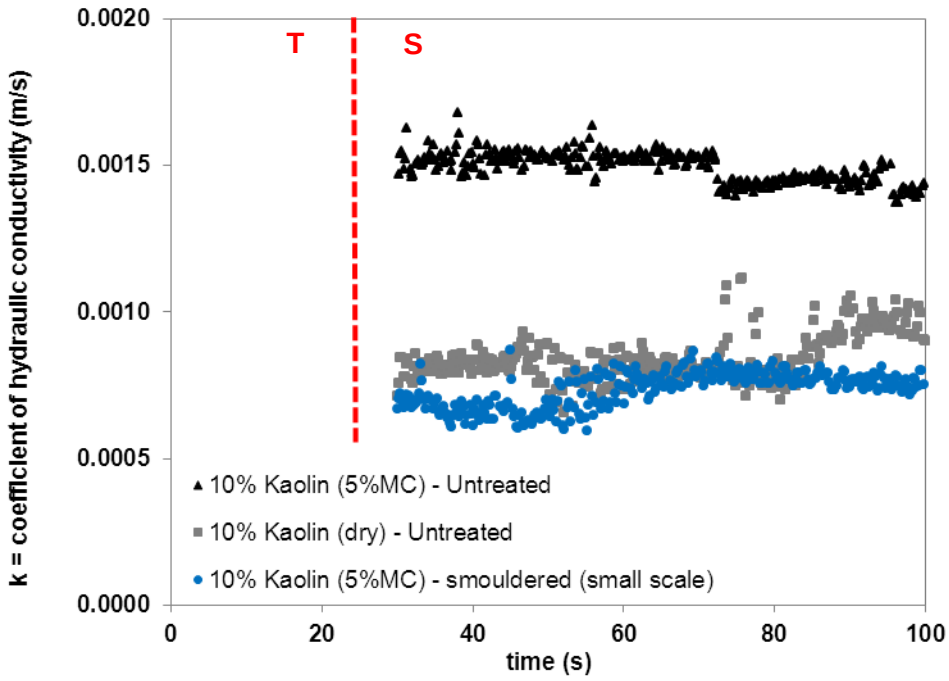

Figure 4.5. Saturated hydraulic conductivity for silica sand + 10% kaolin (5%MC) after different heat treatments

As shown in Table 4.4 the bulk densities and void ratios for the different samples tested are very similar and therefore the results for hydraulic conductivities can be compared for the different thermal treatments. Observed changes are not due to differences in the sample porosity or bulk density.

4.3.2. Influence of Mineralogy on Saturated Hydraulic Conductivity

The higher hydraulic conductivity for the sample treated at 105℃ is probably linked to the coating of clay particles. With increasing temperature, kaolin transforms into metakaolin and mullite (Vaughan, 1954; Fabbri et al., 2013). This change is associated with a change in crystal structure and increase in particle size through sintering of particles. These processes may lead to an increase of coating around the sand particles and therefore decrease the available pore space for water flow. Temperatures in the region of 1000℃ are capable of destroying the mullite and forming amorphous quartz and alumina (Vaughan, 1954). This decomposition may destroy the bond between sand and clay particles and allow the clay particles to move into the pore space.

While heat treatment effects on silica sand pH are small to negligible, the effects on kaolin pH are more significant (Table 4.5). The effects of contamination and smouldering remediation are more substantial. The kaolin powder pH is acidic (4.8 to 5.2) and increases to 6.5 for treatment with exposure to 1000℃ or 6.3 after smouldering. The pH of silica sand is slightly alkaline (7.8 to 8.2) and shifts more acidic after smouldering treatment. This change in pH for the kaolin clay is likely due to the change of mineralogical composition and related dehydroxilation. For the silica sand, the change in pH may be caused by the initial coal tar contamination, smouldering reactions during remediation, or residual contamination remaining after remediation. For the binary mixture of silica sand and kaolin clay, both reactions

seem to counter balance each other and the range is relatively constant with values between 6.0 and 6.8. Smouldering treatment does not seem to affect the mixture. Changes in pH may alter the chemistry and reactivity of the particle surfaces which could lead to a change in wettability.

Table 4.5. pH values for kaolin, silica sand and silica sand + 10% kaolin after different thermal treaments

Sample	pH		
	kaolin	silica sand	silica sand + 10% kaolin
Untreated	5.1 ± 0.01	8.2 ± 0.07	6.3 ± 0.04
105	4.8 ± 0.03		6.5 ± 0.13
250	5.0 ± 0.01	8.0 ± 0.02	6.3 ± 0.07
500	4.8 ± 0.01	7.8 ± 0.02	6.8 ± 0.03
750	5.2 ± 0.01	7.9 ± 0.11	6.0 ± 0.04
1000	6.5 ± 0.02	7.8 ± 0.17	6.7 ± 0.05
Smouldered (large scale)		6.1 ± 0.05	
Smouldered (small scale)		6.5 ± 0.04	6.3 ± 0.03

After smouldering, significant mobilisation of fines is observed. The particles are easily detached from the sand grains. After transport and the additional handling steps the sample appears to be separated into the two original particle fractions. Smouldering may therefore have two effects on the hydraulic conductivity. Firstly, it destroys the bond between clay and sand fraction and this allows clay particles to occupy the available pore space, which is intensified by the additional handling steps included in the sample preparation method. Secondly, the clay minerals may undergo transformations similar to the sample treated at 1000℃ and therefore behave differently to the original kaolin when in contact with water. Liquid and plastic limit tests (Chapter 3) show that the clay changes to non-Newtonian behaviour at

this temperature. Clay mineral transformations and decomposition may add to the changes in hydraulic conductivity with increasing temperature and smouldering.

4.3.3. Links between Changes in Particle Size to Changes in Pore Size

To investigate if the change in particle size can be linked to a change in overall pore size, the Navier-Stokes equation used to calculate actual velocity v_{act} of the liquid can be used to calculate an equivalent diameter. This equivalent diameter represents the sample as a single tube without any grains. A change of representative tube diameter can be used to interpret a change in pore size within the sample.

$$v_{act} = \left(\frac{g}{2\eta} R_H^2\right) i \qquad \text{(Eq. 4.10)}$$

where g is the acceleration of gravity (m/s^2), η is the kinematic viscosity of the liquid (m^2/s), R_H is the hydraulic radius (m), and i is the hydraulic gradient (m) (Tarantino, 2010). R_H is d/4 for the tube in Figure 4.2.,Solving for R_H, the value for the equivalent hydraulic radius and actual velocity can be calculated as

$$R_H^2 = \frac{v_{act} \times 2\eta}{i\, g} \qquad \text{(Eq. 4.11)}$$

$$v_{act} = \frac{Q}{A\, n} \qquad \text{(Eq. 4.12)}$$

where Q is the volumetric flow (m^3/s), A is the cross-sectional area of the smaple (m^2) and n is the porosity.

$$i = \frac{\Delta H}{L} \qquad \text{(Eq. 4.13)}$$

where ΔH is the difference in hydraulic head (m) and L is the length of the sample (m).

$$d = \sqrt{R_H^2} \times 4 \quad \text{(Eq. 4.13)}$$

Table 4.6 shows the results for the different treatments and a decrease in equivalent diameter with increasing temperature up to 750℃ fr om 45.0 ± 0.2µm to 36.2 ± 0.3µm, followed by a slight increase to 40.5 ± 0.4µm for a treatment temperature of 1000℃. These changes in equivalent diameter may be linked to the changes observed in kaolin with increasing temperature. To better understand how the clay coating and the hydraulic conductivity are connected, further investigations are necessary. As mentioned before, the smouldering process mobilises the fine fraction and the calculated equivalent radius of 30.9 ± 0.2µm represents a smaller pore compared to the heat treated samples, suggesting that more clay particles are in the pore space. Since the overall porosities are very similar, porosity may not be the best value to represent the pore network.

Table 4.6. Equivalent diameter for silica sand + 10% kaolin after different treatment temperatures

Sample	Equivalent pore diameter µm
105	45.0 ± 0.2
250	40.0 ± 0.6
500	37.5 ± 0.2
750	36.2 ± 0.3
1000	40.5 ± 0.3
Smouldered (small scale)	30.9 ± 0.2

Smouldering appears to not affect the saturated hydraulic conductivity of silica sand but the addition of 10% kaolin shows a temperature and smouldering effect. This may be related to hydraulic history as well as mobilisation of fine particles. Even though the materials used in this study are simple compared to real soils the indications are very useful for the investigation of more complex materials. Samples prepared in the laboratory for hydraulic conductivity testing should be representative of the natural environment, especially in regards to hydraulic history.

4.3.4. Transient Hydraulic Conductivity

To investigate the transient hydraulic conductivity, the data were corrected using Equation 4.9 with values to represent the saturated layer the time interval investigated and the corresponding hydraulic head (Figure 4.6). This correction for the transition stages (T) of the sample during infiltration required some assumptions about the flow conditions. The porosity is assumed to be equal for all samples and the wetting front is assumed to be laminar moving equally through the sample. The results for untreated and smouldered silica sand samples are shown in Figure 4.6.

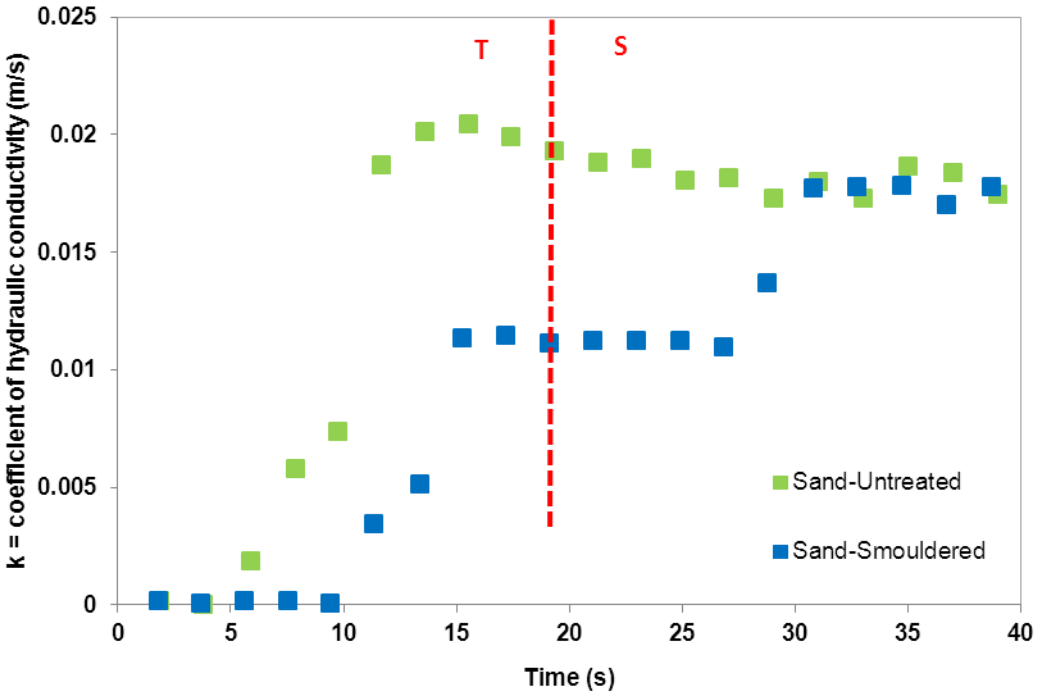

Figure 4.6. Transient hydraulic conductivity of silica sand (corrected for the change of saturated sample length and hydraulic head)

Based on Equation 4.9 a higher coefficient of hydraulic conductivity (k) reflects a higher flow through the apparatus and therefore filling a larger sample volume in the time interval (δt) and decreasing the hydraulic head (H_u).

Flow in the untreated sand is faster than flow in the smouldered sand and the corresponding values for k in the transient stage are higher for the untreated sample (Figure 4.7). Calculating the wetting front height for both sands shows that in the untreated sample, the wetting front progresses faster to the total sample length of ~130mm (Table 4.7). This behaviour could be due to an increased wettability of the particle surfaces for the smouldered sample. If the wettability of the smouldered sand increases after smouldering treatment, then the infiltration flow from the bottom to the top could be decreased because the liquid can spread more easily across the

particle surfaces, wetting a larger surface area relative to particle surfaces with less wettability.

Table 4.7. Wetting front height for untreated and smouldered silica sand

Time (s)	Wetting front height (mm)	
	Untreated	Smouldered (large scale)
5.74	38.2 ± 2.3	10.8 ± 0.92
7.67	54.00 ± 3.5	29.00 ± 2.9
9.58	65.67 ± 3.5	41.00 ± 2.1
11.5	78.00 ± 3.5	75.33 ± 3.2
13.47	91.00 ± 1.0	92.67 ± 2.9
15.38	105.67 ± 3.7	102.33 ± 3.3
17.3	116.33 ± 3.4	113.00 ± 4.4

This would also explain the increased surface infiltration rate observed for smouldered samples (Chapter 2). Changes on the particle surface control wettability (Wenzel, 1936). An increase in wettability may lead to an increase in infiltration from the top of the sample as the grains wet more easily and gravitational effects are more apparent. The differences observed in the experimental setups are linked to the flow direction used in the experiments.

The transient phase (T) for the silica sand + 10% kaolin samples (Figure 4.7) appears to be more complex than the silica sand samples. The samples treated at 105 and 1000℃ show a similar coefficient for the u nsaturated (T) and saturated (S) stage, in comparison the samples treated at 250, 500 and 750℃, and smouldering experience higher unsaturated hydraulic conductivity before reaching the saturated values around 20s. These differences may be linked to a difference in wetting front establishment before the sample is fully saturated.

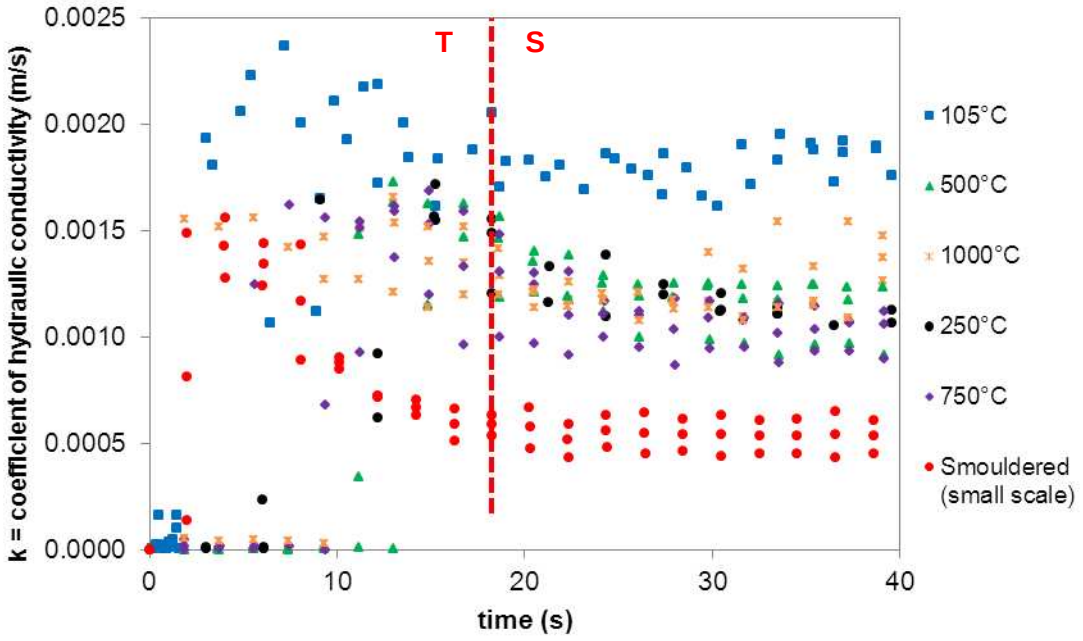

Figure 4.7. Transient hydraulic conductivity of silica sand + 10% kaolin (corrected for the change of saturated sample length and hydraulic head)

In addition, the samples at 105 and 1000℃ have the largest equivalent diameters (Table 4.6). The differences in transient hydraulic conductivities may be linked to the initial flows through the samples. The results for the saturated stage show the flow through the sample is likely linked to the kaolin coating and the changes of its structure and chemistry with increasing treatment temperatures. To better understand what changes influence the transient behaviour, further investigation should be considered using slower flow values by either increasing the sample size, decreasing the hydraulic head or both. To better understand the effects of the kaolin during the unsaturated phase, samples with higher clay content should also be considered.

4.3.5. Mobilisation of Fines

During the testing of the silica sand +10% kaolin treated at 105 and 250℃, mobilisation of fines led to the formation of a gap (~2cm) in the lower third of the sample. Figure 4.8 shows the formation of the gap in the sample near the base of the column and the discolouration of the effluent water with the fines; both phenomena are most apparent in frames D and E of Figure 4.8. The gap was stable during water infiltration; however, once flow ceased the sample collapsed. Comparing the sample height before and after testing, the collapse comprised 4.7-10.0% of the overall sample height.

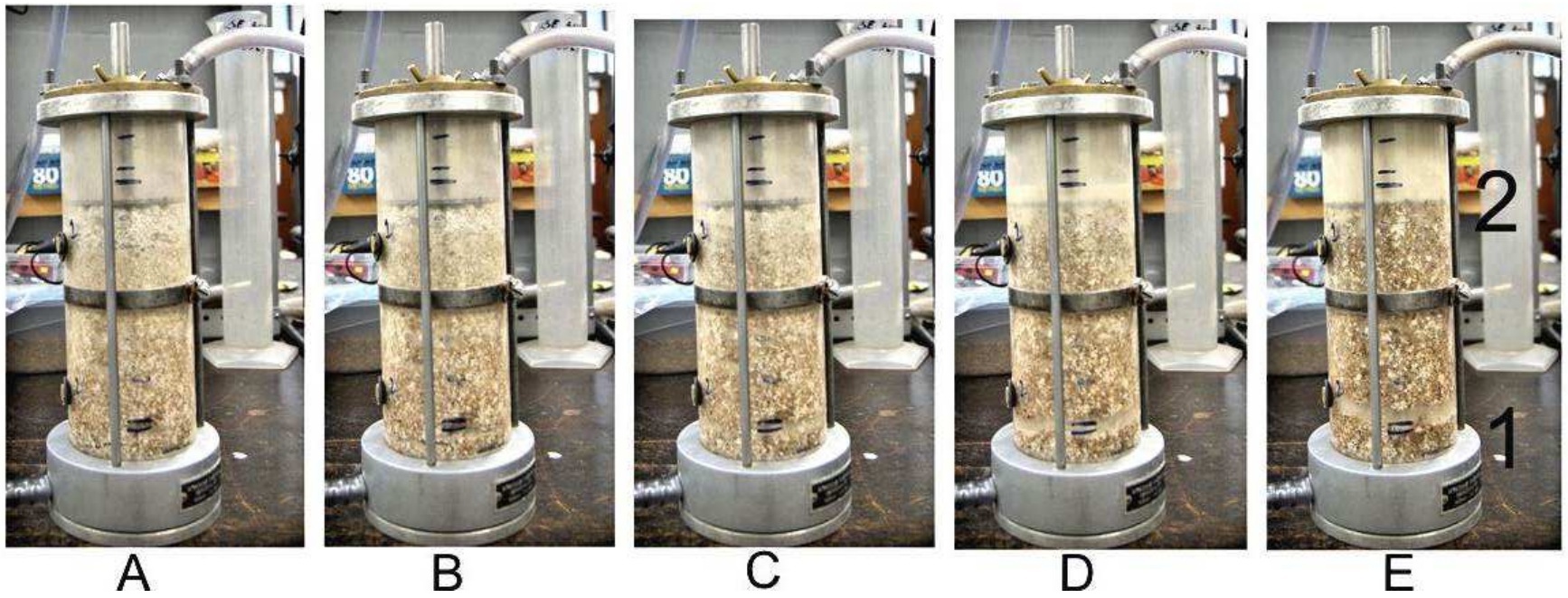

Figure 4.8. Time lapse photographs during infiltration of silica sand + 10% kaolin sample (105-2). Showing the formation of a gap in the sample (1 A-E) and the removal of fines (2 A-E)

Table 4.8 summarises the height loss (%) of the overall sample height for the different heat treatments. This collapse was not observed for samples treated at temperatures above 250℃ or the smouldered sample.

Table 4.8. Sample height loss after infiltration for silica sand + 10% kaolin samples after heat treatment of 105 and 250℃

Sample	Sample height (m)	% loss
105-1	0.13	4.9
105-2	0.14	7.9
105-3	0.12	8.1
250-1	0.14	4.7
250-2	0.14	5.2
250-3	0.11	10.0

As described for the saturated and unsaturated hydraulic conductivities, this effect is likely linked to the kaolin coating. The treatment temperatures of 105 and 250℃ are probably too low to permanently sinter the kaolin particles together to form a stronger bond. Upon wetting, this bond is lost and the kaolin particles can be transported by the water. For higher treatment temperatures, the sintering effect probably forms a stronger bond between kaolin particles. This bond is likely to be permanent and therefore wetting cannot remove the kaolin coating. For treatment at 1000℃, the liquid and plastic limit tests cannot b e determined because the kaolin does not mix with the water (Zihms et al., 2013b). This behaviour could also explain why for higher temperatures, the removal of kaolin particles is hindered as kaolin is less likely to be transported out of the pore space during infiltration. The overall loss is too small to cause a sample collapse. Due to the observation of the fines mobilisation after smouldering treatment, it is highly likely that a sample tested

directly after smouldering and without any additional handling steps will behave more like the 105 and 250℃ treated samples. The fines may be removed by the water since smouldering seems to destroy the bonds between sand and clay fraction. This requires further investigation testing a smouldered sample directly after remediation without any handling or other disturbance of the material.

4.4. Conclusions

This study shows that smouldering treatment does not affect the saturated hydraulic conductivity of silica sand but affects silica sand samples containing 10% kaolin. Differences in saturated conductivity appear to be linked to the hydraulic history of the sample and its preparation as well as changes to the kaolin chemistry and structure with increasing temperature. The saturated response for the silica sand + 10% kaolin can be related to treatment temperature, where the saturated conductivity decreases for temperatures >105℃. There may be differences for the higher treatment temperatures but these cannot be identified by this study.

The unsaturated hydraulic conductivity is affected in all cases, showing that even similar saturated conductivities not necessarily correlate to similar unsaturated behaviour. For the silica sand, the unsaturated conductivity may be linked to surface alterations of the sand particles occurring during thermal and smouldering treatment, which may change the wetting behaviour. Increased wetting appears to slow down the unsaturated flow in the smouldered sample. This could mean that a remediated site recovers its water balance slower, which could lead to increased run-off or erosion rates on the surface. For the sample containing 10% kaolin, the surface effects are probably more complex since kaolin changes structure and chemistry with increasing exposure temperature. Unsaturated response for samples containing 10% kaolin can be separated into three categories of 105 and 1000℃; 250, 500 and

750℃; and smouldering. The behaviour observed seem s to correlate to equivalent diameter and Reynolds number, which suggest that the unsaturated conductivity is controlled by the flow behaviour and probably linked to the kaolin characteristics. Further investigation may be beneficial, but the results indicate that changes at the particle scale influence bulk response.

Detachment and mobilisation of the kaolin clay fraction lead to changes in sample texture and height loss up to 10% overall height. This was not observed for samples treated at temperatures above 250℃. Further tests examining the impact of smouldering remediation is essential to determine if this observed mobilisation could be of concern for post-smouldered samples.

The results show that understanding the history of a real sample is important as changes to the hydraulic history can affect the hydraulic conductivity. It also shows the bond between particles is affected and that the mobilisation of this fraction and increased mobility and removal could lead to an increased risk of subsidence on a site. To better understand how these effects impact real soils, the study needs to be broadened to investigate other soil components such as silts and different mineralogical compositions of particles as well.

4.5. References

Al-Shayea, N.A., 2001. The combined effect of clay and moisture content on the behavior of remolded unsaturated soils. Engineering Geology, 62(4): 319-342.

Allaire, S.E., Roulier, S., Cessna, A.J., 2009. Quantifying preferential flow in soils: A review of different techniques. Journal of Hydrology, 378(1-2): 179-204.

Are, K.S., Oluwatosin, G.A., Adeyolanu, O.D., Oke, A.O., 2009. Slash and burn effect on soil quality of an Alfisol: Soil physical properties. Soil and Tillage Research, 103(1): 4-10.

Bagarello, V., Elrick, D.E., Iovino, M., Sgroi, A., 2006. A laboratory analysis of falling head infiltration procedures for estimating the hydraulic conductivity of soils. Geoderma, 135(0): 322-334.

Bear, J., 1973. Dynamics of fluid flow in porous media. Environmental Science. American Elsevier Publishing Company, New York.

Chang, T.C., Yen, J.H., 2006. On-site mercury-contaminated soils remediation by using thermal desorption technology. Journal of Hazardous Materials, 128(2-3): 208-217.

Chiu, Shackelford, 1998. Unsaturated Hydraulic Conductivity of Compacted Sand-Kaolin Mixtures. Journal of Geotechnical and Geoenvironmental Engineering, 124(2): 160-170.

Fabbri, B., Gualtieri, S., Leonardi, C., 2013. Modifications induced by the thermal treatment of kaolin and determination of reactivity of metakaolin. Applied Clay Science, 73: 2-10.

Fallico, C., De Bartolo, S., Troisi, S., Veltri, M., 2010. Scaling analysis of hydraulic conductivity and porosity on a sandy medium of an unconfined aquifer reproduced in the laboratory. Geoderma, 160(1): 3-12.

Gan, S., Lau, E.V., Ng, H.K., 2009. Remediation of soils contaminated with polycyclic aromatic hydrocarbons (PAHs). Journal of Hazardous Materials, 172(2-3): 532-549.

Gonçalves, R.A.B. et al., 2007. Hydraulic conductivity of a soil irrigated with treated sewage effluent. Geoderma, 139(1–2): 241-248.

Hamlett, C.A.E. et al., 2011. Effect of Particle Size on Droplet Infiltration into Hydrophobic Porous Media As a Model of Water Repellent Soil. Environmental Science & Technology, 45(22): 9666-9670.

Hatten, J., Zabowski, D., Scherer, G., Dolan, E., 2005. A comparison of soil properties after contemporary wildfire and fire suppression. Forest Ecology and Management, 220(1-3): 227-241.

Head, K.H., 1980. Manual of Laboratory Soil Testing Volume 2: Permeability, Shear Strength and Compressibility Tests.

Juang, C., Holtz, R., 1986. Fabric, Pore Size Distribution, and Permeability of Sandy Soils. Journal of Geotechnical Engineering, 112(9): 855-868.

Kronholm, J., Kalpala, J., Hartonen, K., Riekkola, M.-L., 2002. Pressurized hot water extraction coupled with supercritical water oxidation in remediation of sand and soil containing PAHs. The Journal of Supercritical Fluids, 23(2): 123-134.

Lee, W.-J. et al., 2008. Thermal treatment of polychlorinated dibenzo-p-dioxins and dibenzofurans from contaminated soils. Journal of Hazardous Materials, 160(1): 220-227.

Lipsius, K., Mooney, S.J., 2006. Using image analysis of tracer staining to examine the infiltration patterns in a water repellent contaminated sandy soil. Geoderma, 136(3–4): 865-875.

Rein, G., Cleaver, N., Ashton, C., Pironi, P., Torero, J.L., 2008. The severity of smouldering peat fires and damage to the forest soil. CATENA, 74(3): 304-309.

Shafiee, A., 2008. Permeability of compacted granule–clay mixtures. Engineering Geology, 97(3–4): 199-208.

Šimůnek, J., Jarvis, N.J., van Genuchten, M.T., Gärdenäs, A., 2003. Review and comparison of models for describing non-equilibrium and preferential flow and transport in the vadose zone. Journal of Hydrology, 272(1–4): 14-35.

Skordou, U.A., 2012. An Investigation into the Effects of High Temperatures and STAR Treatment has on Sand Properties, University of Strathclyde, United Kingdom.

Switzer, C., Pironi, P., Gerhard, J.I., Rein, G., Torero, J.L., 2009. Self-Sustaining Smoldering Combustion: A Novel Remediation Process for Non-Aqueous-Phase Liquids in Porous Media. Environmental Science & Technology, 43(15): 5871-5877.

Tarantino, A., 2010. Basic concepts in the mechanics and hydraulics of unsaturated geomaterials. New Trends in the Mechanics of unsaturated Geomaterials(3-28).

Terefe, T., Mariscal-Sancho, I., Peregrina, F., Espejo, R., 2008. Influence of heating on various properties of six Mediterranean soils. A laboratory study. Geoderma, 143(3-4): 273-280.

Vaughan, F., 1954. Energy Changes when Kaolin Minerals are heated. British Ceramic Research Association.

Webb, S.W., Phelan, J.M., 1997. Effect of soil layering on NAPL removal behavior in soil-heated vapor extraction. Journal of Contaminant Hydrology, 27(3-4): 285-308.

Wenzel, R.N., 1936. RESISTANCE OF SOLID SURFACES TO WETTING BY WATER. Industrial & Engineering Chemistry, 28(8): 988-994.

Zihms, S.G., Switzer, C., Irvine, J., Karstunen, M., 2013a. Effects of high temperature processes on physical properties of silica sand. Engineering Geology.

Zihms, S.G., Switzer, C., Karstunen, M., Tarantino, A., 2013b. Understanding the effects of high temperature processes on the engineering properties of soils. Proceedings of the 18th International Conference on Soil Mechanics and Geotechnical Engineering, Paris 2013.

5. Analysis of Wettability of Heat Treated and Smouldered Silica Sands and Silica Sand-Kaolin

5.1. Introduction

Wettability reflects how easily a porous medium such as soil or rock can be wetted by a liquid. It is a surface phenomenon and describes the intimate contact between liquid and solid. The degree of wetting describes the extent of this contact and is generally given by the contact angle (Kumar and Prabhu, 2007). It is important in a range of applications in agriculture, oil recovery, chemical processes and geotechnical engineering (DeBano, 2000b; Kumar and Prabhu, 2007). Wettability affects the precipitation of minerals, infiltration, evapotranspiration, seepage, water retention, and imbibition of water into soil (Kowalik, 2006; Schembre et al., 2006; Beatty and Smith, 2010; Lourenço et al., 2012). Due to the complexity of the processes and their links, it is important to understand how thermal and smouldering treatments affect wettability. Wild fire research shows that soils after forest and wild fires can become water repellent (DeBano, 2000a; Doerr et al., 2000; Mataix-Solera and Doerr, 2004; Mataix-Solera et al., 2008). Research on oil contaminated sands shows that contamination such as oily substances decrease wettability (Lourenço et al., 2012). However, the effects of temperatures reached during smouldering remediation have not been investigated.

Wettability impacts agglomeration of particles and aggregate stability through liquid bridges between the particles. The strength of liquid bridges and wettability of the solid are related and the bridges weaken with decreasing wettability (Iveson et al., 2004; Ramírez-Flores et al., 2008). The agglomeration bond affects the fate and transport of colloids within a porous media system as these can be mobilised during

infiltration or drainage of the system and then transported through the media. Wettability determines the rate of these processes (Chatterjee et al., 2012). Physical and chemical properties of the porous media such as pore size and distribution, particle surface roughness and chemistry affect wettability and overall water balance (Rodríguez-Caballero et al.; Wenzel, 1936; Bikerman, 1950; Tamai and Aratani, 1972; Hong et al., 1994; Siebold et al., 1997; Dang-Vu et al., 2006; Kumar and Prabhu, 2007; Goebel et al., 2008; Chau et al., 2009; Shang et al., 2010; Chatterjee et al., 2012).

Wettability of porous media can defined by the contact angle, which represents the angle between a droplet of liquid, the surface it is placed on, and the atmosphere (Lourenço et al., 2012). It is a result of cohesion within the liquid and adhesion between the liquid droplet and solid surface. For a perfect system where the solid is smooth, homogeneous, and non-deformable, only one stable contact angle exists (Marinho et al., 2008). However, this is not the case for porous media where particles are heterogeneous and not smooth. In this case, the contact angle exhibits hysteresis so more than one stable contact angle exists (Marinho et al., 2008). A difference in surface characteristics along a particle can alter the contact angle and affect how a pore is filled or emptied. Figure 5.1 shows the relationship between wetting conditions, droplet shape, and contact angle. For a non-wetting (hydrophobic) surface, the droplet is almost perfectly round (contact angle $\theta = 90°$ or $>90°$) and if the surface is completely wetting the droplet lies flat across the surface (contact angle $\theta = 0°$). These contact angles can also be achieved based on properties of the liquid.

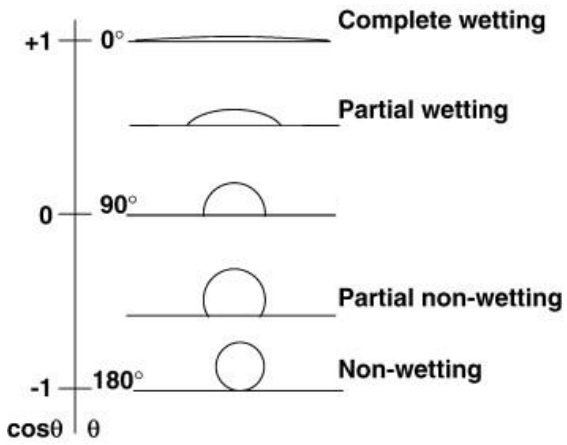

Figure 5.1. Representation of a liquid droplet on a surface under different wetting conditions. Relationship between wettability and contact angle (modified after Kumar and Prabhu (2007)

Soils are naturally wetting and have a contact angle between 0 and 90°. Contact angles greater than 90° are typical for hydrophobic surfaces (Kumar and Prabhu, 2007), which include sands coated with oil contamination (Lourenço et al., 2012) and soils after wild and forest fires (Doerr et al., 2000; Robichaud and Hungerford, 2000; Mataix-Solera and Doerr, 2004; Mataix-Solera et al., 2008). Contact angles are widely used in soil science, chemical process engineering, geotechnical and civil engineering to describe and compare wetting behaviour of porous media.

Particle surface roughness has a high influence on wettability of porous media. In some studies, increasing surface roughness of the particles seems to magnify the wetting properties of the medium due to increasing the surface area while maintaining the same wetting properties (Wenzel, 1936; Chau et al., 2009). This means that an already wetting surface becomes even more wetting and a non-wetting surface becomes, less wetting, or hydrophobic, with increasing surface roughness. Other researchers suggest that surface roughness only affects the wetting kinetics but not the overall contact angle (Marmur and Cohen, 1997; Dang-Vu et al., 2006) and an increase in roughness leads to a decrease in wettability

(Bikerman, 1950; Tamai and Aratani, 1972; Hong et al., 1994). These differences are likely to be caused by the different materials tested such as glass beads and field-obtained soils.

On the mineral surfaces oxidation of copper and aluminium increases the wettability (Hong et al., 1994). For iron ores, higher hematite content correlates to a higher contact angle, illustrating a relationship between wettability and iron oxide content (Iveson et al., 2004). This range of changes shows that the wetting properties of porous media can be influenced by chemistry and heterogeneity of the starting material as well as a range of physical and chemical changes. An investigation into the behaviour is necessary to gain a better understanding how processes are affected and linked. Results from Chapters 2, 3, and 4 show that exposure to elevated temperatures affect some silica sand and kaolin clay properties, including mechanical, physical and chemical (Table 5.1 and Table 5.2), and these changes are expected to affect the wettability. The aim of this research is to investigate if these changes of silica sand and silica sand-kaolin after thermal and smouldering treatment affect their wettability.

Table 5.1. Summary of properties of silica sand + 10% kaolin clay after different thermal treatments

Sample	Sieve analysis	Mass loss	pH	Coefficient of saturated hydraulic conductivity
	> 1.18mm	Sample mass loss		k
	% retained	%		m/s
Untreated (dry)	61.4 ± 1.2	0.00	*untested*	*untested*
Untreated (5% mc)	*untested*	*untested*	6.3	*untested*
105	81.2 ± 1.9	0.13	6.5	0.0016 ± 0.00007
250	82.5 ± 0.8	0.26	6.3	0.0012 ± 0.00003
500	74.3 ± 3.2	0.88	6.8	0.0013 ± 0.00011
750	65.5 ± 3.6		6.0	0.0011 ± 0.00006
1000	67.6 ± 0.8		6.7	0.0014 ± 0.00006
Smouldered (small scale)	*untested*	*untested*	6.3	0.0007 ± 0.00015

Table 5.2. Summary of pH and plastic and liquid limits of kaolin clay after different thermal treatment

Sample	pH	Liquid Limit	Plastic Limit	Plasticity Index	Plasticity Chart Classification
		w_L	w_P	I_p	
		%			
105	4.8	64.4	35.9	28.5	MH: silt, high plasticity
250	4.8	63.7	30.8	32.9	CH: clay, high plasticity
500	5.2	65.2	42.7	22.6	MH: silt, high plasticity
750	6.5	81.6	57.4	24.1	MV: silt, very high plasticity
1000*					

*the sample after 1000℃ treatment could not be tes ted due to non-newtonian like behaviour

5.1.1. Relationship between Wettability and Hydraulic Behaviour

Wettability affects the hydraulic behaviour of soils in the unsaturated states. The relationship of contact angle and capillary rise height is shown in Figure 5.2. The liquid rise height (h_c) depends on the contact angle of the meniscus (θ), the surface tension of the liquid (σ), and on the capillary radius (r) (Figure 5.2).

Assuming the atmospheric pressure at the concave side of the meniscus equal to 0, the vertical force associated with the water pressure ($u\ \pi\ r^2$) is balanced by the vertical force associated with the surface tension ($\sigma\ 2\pi\ r\ \cos\theta$):

$$\sigma\ 2\pi\ r\ cos\theta + u\ \pi\ r^2 = 0 \qquad \text{(Eq. 5.1)}$$

The pore water pressure (u) at the back of the meniscus is therefore given by

$$u = \frac{-2\sigma\ cos\theta}{r} \qquad \text{(Eq. 5.2)}$$

In this situation, the pore water pressure is negative and the water within the column is in a state of suction (Figure 5.2 B). The maximum value for this negative pressure is $\gamma_w h_c$ at the top of the column. Substituting the pore pressure (u) we can rewrite Equation 5.2 as

$$h_c = \frac{2\sigma\ cos\theta}{\gamma_w\ r} \qquad \text{(Eq. 5.3)}$$

where γ_w is the specific weight of water (kN/m^3) (Smith, 2009).

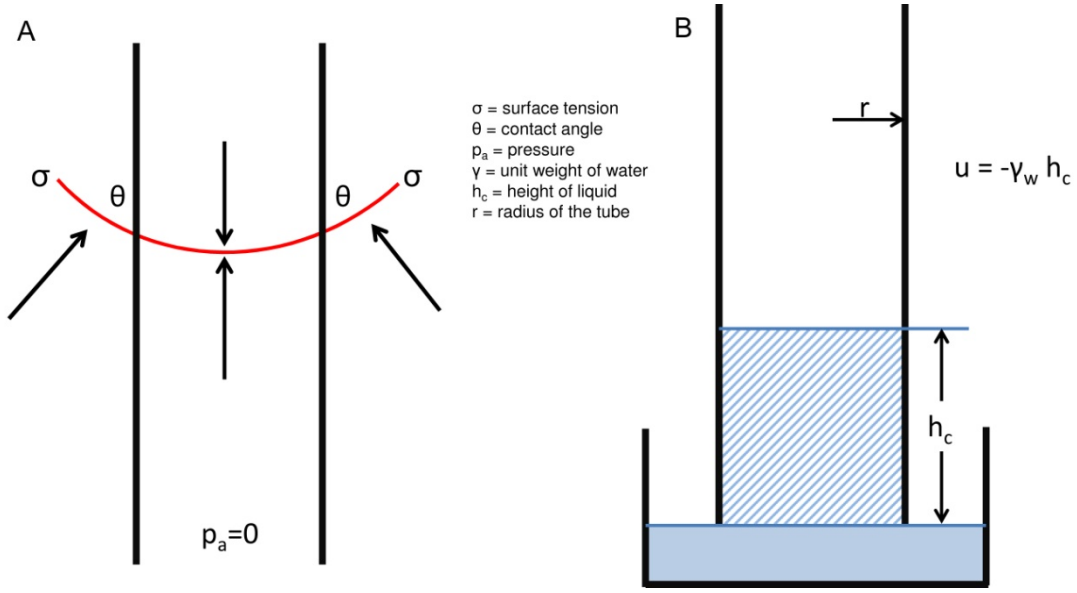

Figure 5.2. Rise of a liquid into a capillary; modified after (Smith, 2009)

Wettability also affects water flow. Washburn (1921) expressed the rate of rise of the wetting front in a powder-filled glass tube (dh/dt) by means of Poiseuille's law, i.e. as

$$\frac{dh}{dt} = \frac{R_d^2}{8\eta}\frac{\Delta P}{h} \qquad \text{(Eq. 5.4)}$$

where R_d is the mean hydrodynamic pore radius (m), η is the dynamic viscosity of the fluid (kg/ms), ΔP is the pressure difference (Pa) across the meniscus and h is the rise height (m). By equating the pressure differential ΔP to Equation 5.3, the Washburn equation can be integrated as follows:

$$h^2 = \frac{r\,\sigma_l\,cos\theta}{2\eta}\,t \qquad \text{(Eq. 5.5)}$$

where h is the rise height (m), r is the effective capillary radius (m), σ_l is the surface tension of the liquid (mJ/m^2), θ is the contact angle (°) and η is the dynamic viscosity of the liquid (kg/ms) (Bachmann et al., 2003).

Table 5.3. Summary of properties for n-hexane and water

		Water	Hexane	
dynamic viscosity	η	0.001003	0.000294	kg/(ms)
surface tension	σ_l	0.0728	0.0184	mJ/m^2
density	ρ	1	0.6548	Mg/m^3
$\eta / (\sigma_l \times \rho^2)$	Fw[1]	0.0138		Mg/(ms)
	Fh[1]	0.0373		

[1] Bachmann et al (2003)

5.2. Contact Angle Determination

There are a range of direct and indirect methods to establish the contact angle of a porous medium including the Wilhelmy plate method, sessile drop method, wicking method, and capillary rise method. For the Wilhelmy plate method, the sample is placed as a thin layer onto double-sided adhesive tape and placed on a glass plate. The glass plate is immersed in a liquid and the immersion velocity and depth are

measured to calculate the contact angle (Goebel et al., 2008; Ramírez-Flores et al., 2010). The sessile drop method uses a droplet of water placed on the surface of the bulk media or on a single particle. For the sessile drop method, the tangent between the droplet, air and solid is measured and this gives the contact angle (Ramírez-Flores et al., 2010). Both Wilhelmy plate and sessile drop method are suited for fine soils where the pores are much smaller compared to the liquid droplet. This ensures best contact between liquid and soil. The sessile drop method can also be used on single grains if the grain is large compared to the liquid droplet. The wicking method and capillary rise method are based on similar principles. For the wicking method, a column containing a bulk sample is placed horizontally and connected to the wetting liquid through a cellulose wick immersed in the bulk liquid. The time and distance of the penetration front are recorded to calculate the contact angle (Hajnos et al., 2013). The capillary rise method uses also bulk material in a column, but the set up is vertical and the bottom of the column surface is placed in contact with the liquid surface to achieve capillary rise.

The material used in this study is a coarse material (silica sand and silica sand+10% kaolin) and therefore most methods are not suitable. In case of the Wilhelmy plate and sessile drop methods, the coarse nature of the material makes these tests unsuitable because placement of the material onto adhesive tape would leave large pore space between particles. Placement of a droplet onto the bulk surface is not appropriate because the pore size leads to immediate penetration of any droplet independent of wettability. Therefore, the indirect capillary rise method is favoured for coarse material. The method is based on the relationship between the penetration rise height of a liquid into a cylindrical capillary. The rise height is indirectly proportional to the capillary radius. The same liquid rises higher in a smaller capillary (under the same conditions) (Washburn, 1921). The capillary rise

method in this work is modified from Bachman et al (2003), Ramírez-Flores et al (2008), and Ramírez-Flores et al (2010).

5.2.1. Capillary Rise Method after Bachmann et al (2003)

The approach described by Bachmann et al (2003) was followed for analysis of capillary rise data. The method is based on the Washburn equation (Eq. 5.5). Because the rise height is difficult to measure in a porous medium, it is more accurate to measure the mass gain (w) of the sample. In the set up used in this study, w is equal to the mass loss of wetting liquid from the container (Bachmann et al., 2003; Ramírez-Flores et al., 2008; Ramírez-Flores et al., 2010). The Washburn equation can now be written as:

$$w^2 = c\frac{\rho^2 \sigma_l \cos\theta}{\eta} t = mt \qquad \text{(Eq. 5.6)}$$

where ρ is the liquid density (Mg/m^3) and c is a specific soil factor depending on pore characteristics resulting in a linear relationship between w^2 and t. The slope being denoted by m (Bachmann et al., 2003). The specific soil factor c is determined mathematically based on the wetting using n-hexane.

$$c = m_{hex} \times \frac{\eta_{hex}}{\sigma_{hex}\rho_{hex}^2} = m_{hex} \times F_{hex}(T) \qquad \text{(Eq. 5.7)}$$

where F is the value based on the liquid properties, viscosity, density and surface tension (Table 5.3)

Using the results for n-hexane to solve for c, this value can then be used to calculate the contact angle for water.

$$cos\theta_w = \frac{m_w}{c} \times \frac{\eta_w}{\sigma_w \rho_w{}^2} = \frac{m_w}{c} \times F_w(T) \qquad \text{(Eq. 5.8)}$$

Alternatively, by rewriting Equation 5.7, the contact angle can be determined using only the slopes of the capillary rise experiments for both wetting liquids and their dynamic viscosities and surface tensions (Figure 5.3 and Figure 5.4).

$$cos\theta_w = \frac{m_w}{m_{hex}} \frac{F_w(T)}{F_{hex}(T)} \qquad \text{(Eq. 5.9)}$$

Based on the relationship defined in Equation 5.6, the data is plotted using the square value for the mass gain (w^2) versus duration of the test (Figure 5.3).

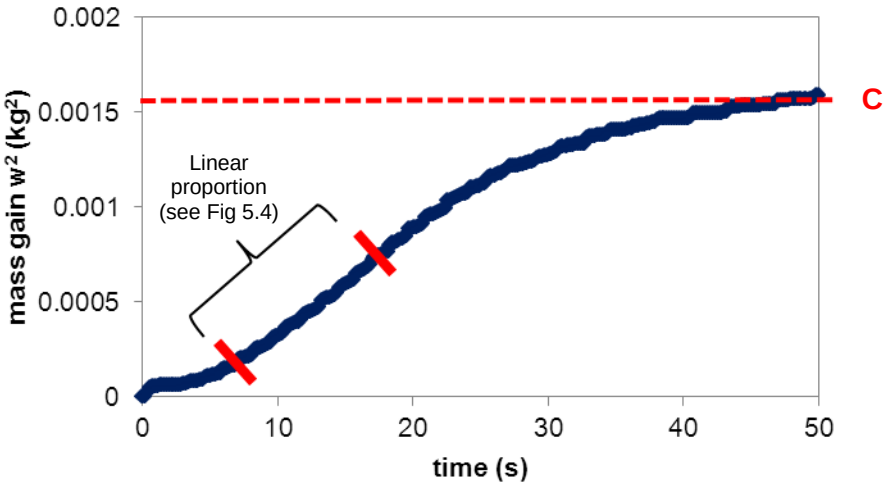

Figure 5.3. Data for Silica Sand Untreated (2) showing the mass gain w^2 for the test duration

Based on the linear relationship between w^2 and the test time, the linear proportion is plotted to determine m for each experiment (Figure 5.4).

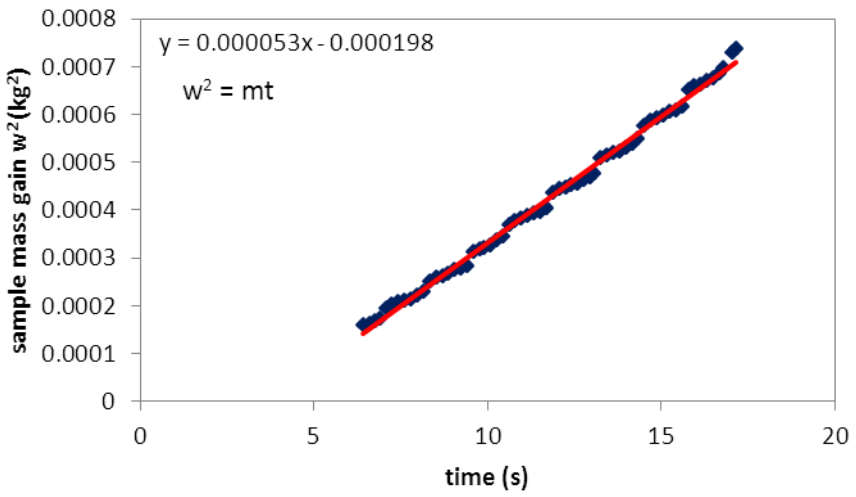

Figure 5.4. Linear proportion of the capillary rise experiment for Silica sand Untreated (2)

5.2.2. Effective Radius Method

Because of the difficulties encountered in applying the method proposed by Bachmann et al (2003), an alternative approach was developed based on static and transient and capillary rise to determine the static and dynamic contact angle. The approach is based on the Washburn equation is used to compare wettability behaviour of samples prepared to the same porosity.

5.2.2.1. Static Contact Angle

Using the equation for capillary rise and assuming

$$h_c = \frac{2\sigma \cos\theta}{\rho_w g r} \qquad \text{(Eq. 5.10)}$$

The capillary height can be inferred from the mass M_w gain of the sample,

$$h_c = \frac{M_w}{A \cdot n \cdot \rho_w} \qquad \text{(Eq. 5.11)}$$

where A is the sample area (m^2), $\rho_w$is the water density and n is the sample porosity. By combining the above equations, we obtain

$$cos\theta_w = \frac{g}{2} \frac{r}{\sigma} \frac{M_w}{A \cdot n} \quad \text{(Eq. 5.12)}$$

5.2.2.2. Dynamic Contact Angle

This method is using the same approach as Bachman et al (2003) based on the relationship between velocity of capillary rise and contact angle.

$$h^2 = \frac{r\,\sigma_l\,cos\theta}{2\eta}\,t \quad \text{(Eq. 5.5)}$$

Assuming a sharp wetting front and the soil is fully saturated behind this wetting front, the mass of water gain in the sample is expressed as

$$M_w = h\,A\,n\,\rho_w \quad \text{(Eq. 5.13)}$$

where n is the porosity, A is the cross-sectional area (m), ρ_w is the density of water (kg/m^3). This relationship becomes

$$M_w^2 \left[= (A\,n\,\rho_w)^2 \left(\frac{r\,\sigma_l \cos\theta}{2\eta}\right)\right] t = m\,t \quad \text{(Eq. 5.14)}$$

which can be solved to determine cosθ as

$$cos\theta = \frac{m}{(A\,n\,\rho_w)^2\,\sigma_l\,r}\,2\,\eta \quad \text{(Eq. 5.15)}$$

5.2.3. Effective Radius Determination

Using the equations for the static and dynamic contact angle, a radius range is used rather than determined using the Bachmann et al (2003) method with the hexane results and assumption of a contact angle of 0°. Based on the relationship between particle and pore diameters (Smith, 2009), the order of magnitude of effective radius can be determined based on the particle size of the material

For both samples, 10% of particles pass 0.63mm. Assuming the relationship between d_{pore} is 0.4 times the d_{10} grain size. This gives an effective pore radius of 0.26mm for silica sand and silica sand-kaolin mixture. This radius is considered large for the material. By decreasing the radius value in Equation 5.12, the static contact angle reaches 90°, which suggests no wetting. Since capillary rise has been observed for all experiments, this radius (0.006mm) is considered to represent the lower range. To estimate a change in contact angle, a radius within this range has been estimated as 0.1mm. All contact angles presented were determined using a effective radius of 0.1mm.

5.3. Materials and Methods

Silica sand (Leighton Buzzard 8/16, Sibelco, Sandbach, UK) and kaolin clay (Whitchem Ltd, UK) were accepted as received and the sand was subjected to the same pre-treatment. A programmable muffle furnace (Nabertherm L9/11/SKM, Nabertherm GmbH, Lilienthal, Germany) was used for all heating experiments. The sands evaluated after smouldering remediation were prepared in a $3m^3$ experiment involving coal tar mixed with coarse sand. The initial concentration of this mixture was 31000 ± 14000 mg/kg total extractable petroleum hydrocarbons before treatment and the average concentration after smouldering remediation across the majority of the vessel was 10 ± 4 mg/kg (Pironi et al., 2009). In addition sand and

sand-kaolin samples where smouldered using the bench scale set up (0.003m^3 of sample) and following the procedure for the large scale experiments.

5.3.1. Sample Preparation and Heat Treatment

Loose fines were removed from the sand by soaking it in a solution of sodium hexametaphosphate and sodium carbonate for 24 hrs before being washed over a 425µm screen to eliminate any loose fines and air dried for several days (BS1377-2:1990). After air drying, the sand was stored in an airtight container until its use. The sand-clay mixtures were prepared by dry-mixing 90% sand and 10% clay (by mass) in a 1L plastic bag and distilled water was added at a rate of to achieve 5% moisture content. The sample was placed in a plastic bag and thoroughly kneaded by hand for 10 minutes and allowed to rest for 2 hours before any heat treatment. The required amount of sample (sand and sand-clay) was heated in the furnace to 250, 500, 750 and 1000℃ and kept at the maximum te mperature for 60min. In addition, one sample was heated to 105℃ and kept a t the maximum temperature for 24hrs to simulate the heating duration for moisture content testing. After the required exposure duration, the samples were removed from the muffle furnace and placed in a desiccator to cool. Samples heated to temperatures above 500℃ were allowed to cool in the furnace to 200℃ before tran sfer to the desiccator. The samples cooled in the furnace at a rate of 3.1℃/min .

5.3.2. Modified Capillary Rise Experimental Set up and Method

A permeability column set was fitted with a silica glass column (radius= 3.85cm, height = 24.00cm) below a wooden table (w and l = 30cm, h = 40cm) and secured with 4 screws (Figure 5.5). The table has an opening to allow filling of the column. A fine mesh (1mm) was placed at the bottom of the glass column to avoid any particles blocking the column infiltration hole. Above the mesh a layer of 200g of

3mm glass ballotini was placed and compacted once by dropping a mass of 472.75g from 0.213m above the layer. Another fine mesh was placed on top of the glass ballotini to avoid any material penetration of the layer. A cup fitted with a 3mm mesh was placed into the column and 200g of the sample were poured on top of the cup. The cup was slowly lifted, disturbing the sample layer and minimising any gravitational affects when pouring the sample. The layer was then compacted three times by dropping a mass of 472.75g from 0.213m above the layer. This procedure was repeated for a total of 3 layers. After the last layer was compacted, the sample height was measured. This compaction method led to a sample porosity of 0.436 ± 0.003 and 0.440 ± 0.008 for the silica sand and silica sand-kaolin sample, respectively.

The table including the glass column was carefully moved into a fume cupboard and purged for 3 hours with CO_2 using a flow rate of 10ml/s. After purging the CO_2 was disconnected. A glass container (20cm OD) was placed on a top loading balance (Denver Instruments SI-6002) connected to an acquisition program (LabView, National Instruments, Newbury, UK). The table including the glass column was placed above the glass container ensuring no contact was made with the rim or bottom and the table legs were not in contact with the balance. This was important to ensure the mass recorded is of the glass container and the wetting liquid. The acquisition program was started and the container was slowly filled with the wetting liquid until it is level with the top of the glass ballotini layer in the glass column. The acquisition program recorded the mass to the glass container and the wetting liquid for the test duration. The experiment was repeated in triplicate using distilled water and n-hexane as wetting liquids.

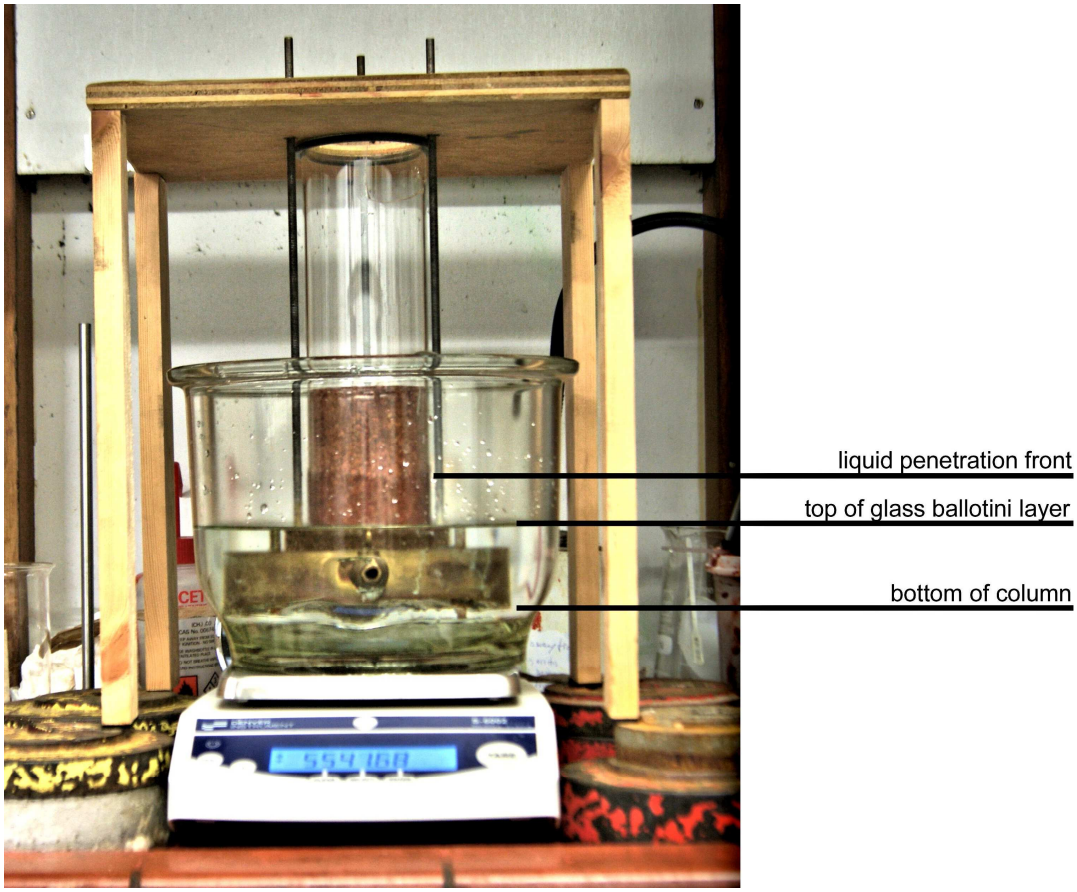

Figure 5.5. Capillary rise method – experimental set up

Based on the set up, the column in the water had a small effect through buoyancy. As the water enters the sample through capillary forces the overall effect is a mass decrease as the water level drops in relation to the column. The water level decreases by 1.6mm in the container, which relates to a mass decrease of 0.74g of water. The buoyancy effect was therefore neglected.

5.3.3. Data processing

The data recorded had to be processed as described here using the results for the second untreated silica sand test as an example. The point of capillary flow was

determined as the point where the mass increase to the balance stops (Figure 5.6, point A).

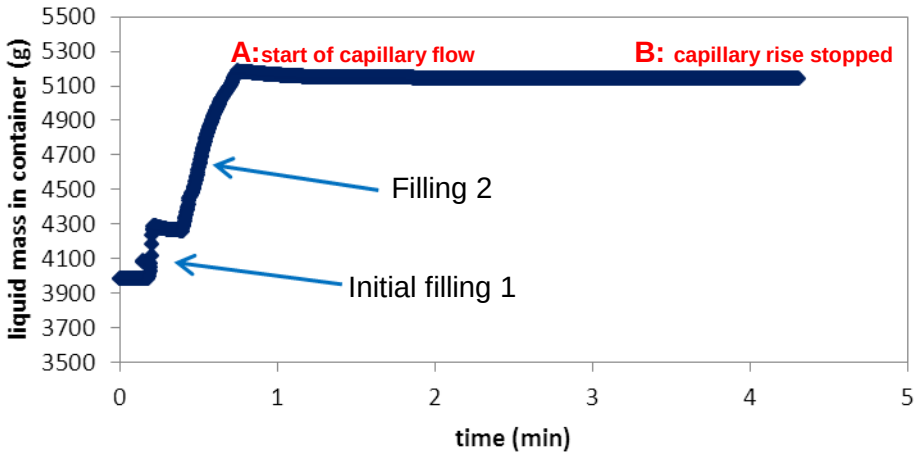

Figure 5.6. Data for Silica Sand Untreated (2) experiment

The data before point A (Figure 5.6) represented the filling of the container to reach the required height of the liquid front and was therefore discarded and the results plotted again (Figure 5.7). The test was considered finished when the recorded mass loss was stable for at least 20s (Figure 5.7 B).

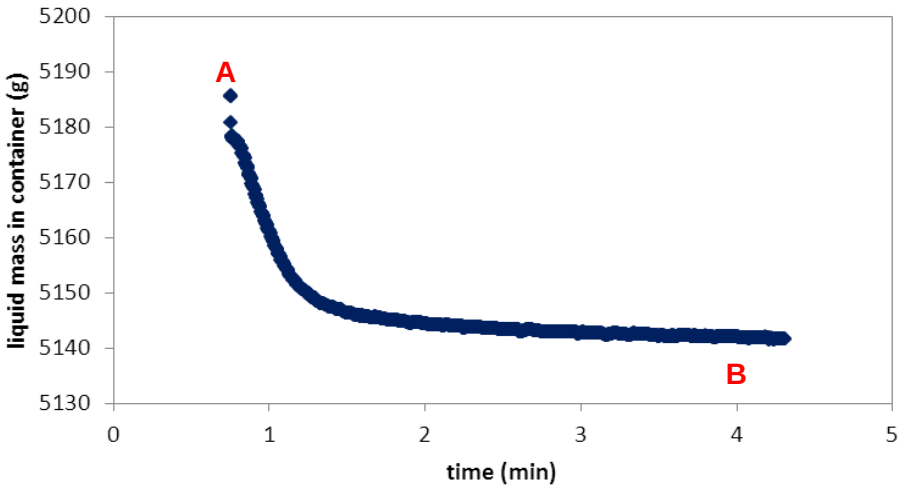

Figure 5.7. Data for Silica sand Untreated (2) experiment after discarding the filling data

The data between Figure 5.7 A and B are used for the analysis of the capillary rise and calculation of the contact angles. For the analysis method used in this study, the mass gain of the sample is needed and the set up used for this study (Figure 5.5) the mass gain of the sample is equal to the recorded mass loss of wetting liquid from the glass container. Figure 5.8 shows the normalised data presented as mass gain of the sample (w) for the test duration.

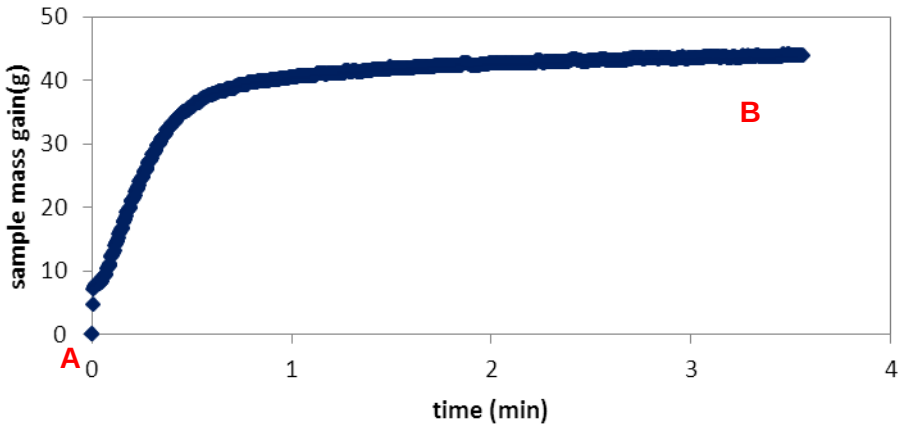

Figure 5.8. Data for Silica Sand Untreated (2) after calculating mass gain of the sample for the experiment duration

5.4. Validation of Contact Angle Determination Methods

5.4.1. Method after Bachman et al (2003)

During data analysis some anomalies were observed and the Bachman et al approach using the capillary rise velocity was re-examined to understand if the assumptions were correct and if this approach is suitable for the material tested in this study. There should be no relationship between the slope m and the capillary rise height for an all wetting liquid. All experiments should reach the same final rise height. Figure 5.9 shows the values for silica sand and Figure 5.10 for silica sand + 10% kaolin.

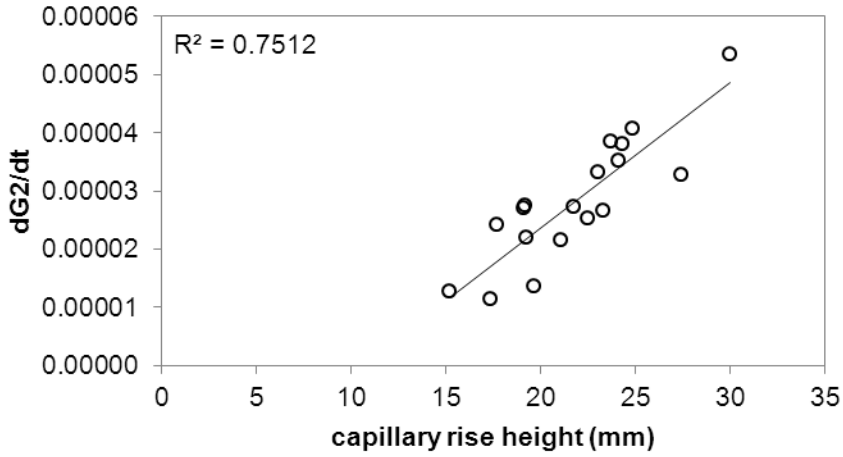

Figure 5.9. Relationship of final capillary rise height and capillary rise velocity for silica sand

For the silica sand, there is a linear relationship between capillary rise velocity and final rise height for n-hexane. This suggests that for the material used (n-hexane) cannot be assumed to be an all wetting liquid. It is likely that thermal and smouldering treatments affect the particles and therefore alter the contact angle for

n-hexane. A similar observation can be made for the sample containing 10% kaolin. Figure 5.10 shows that there are two distinct groups reaching a similar final capillary rise height. These appear to be dependent on temperature, where the samples treated at 105, 250 and 500℃ reach a similar rise height of 18-19mm and samples treated at 750 and 1000℃, and smouldering treatmen t reach a rise height of 24-25mm. This also suggests that the contact angle is not 0°for all material tested and it is highly likely that thermal and smouldering treatments are the reason for this alteration in wetting behaviour.

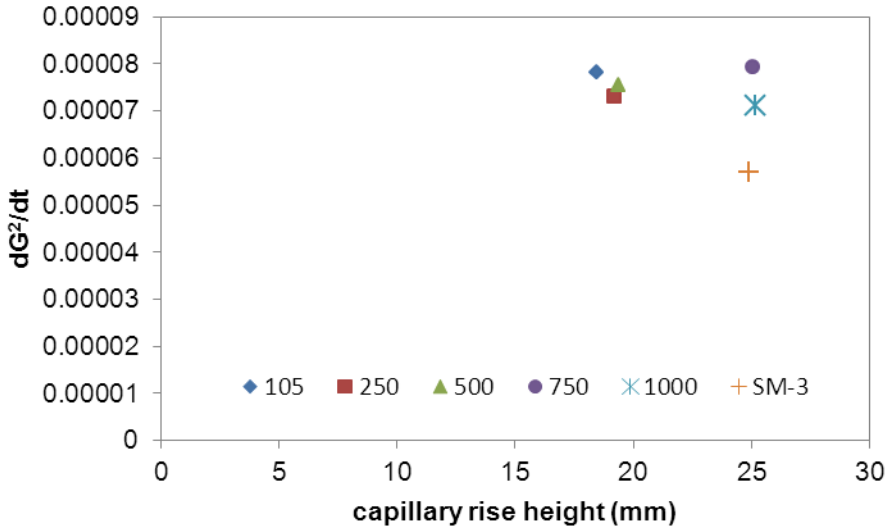

Figure 5.10. Relationship of final capillary rise height and capillary rise velocity for silica sand + 10% kaolin

It is likely that the assumption that the soil only has one unique contact angle and that hexane is all wetting are not suitable for the silica sand and silica sand-kaolin.

5.4.2. Effective Radius Method

The effective radius method is used to compare changes to the wettability in regards to thermal and smouldering treatment by investigating changes in the contact angle

as they can be used to interpret wetting behaviour of the material. If the assumptions behind Equation 5.10 are correct, the static capillary rise height (h) should be linear to cosθ as calculated from the dynamic approach. The method of combining the static and dynamic contact angle equations (Eq. 5.10 and Eq. 5.5) and determining a range of pore radii appears more suitable for the material tested in this study than the previous calculations with the Bachmann et al (2003) method. Therefore, the data discussed below has been determined using the effective radius method.

5.5. Results and Discussion

The contact angles were estimated using a pore radius of 0.1mm, which is an acceptable radius for sand and sand-kaolin. This radius was within the range of pore radii for which the method was validated. Therefore, the values presented are not the only possible contact angles for the material but the trends will be same with the pore range.

5.5.1. Silica Sand

Figure 5.11 shows the results for the silica sand samples. The contact angle decreases from 78° to 73° from untreated to 1000℃ treatment. A decrease in contact angle means that a liquid can wet the material more easily. Using the static contact angle values based on the median effective radius and calculating the capillary rise velocity (Eq. 5.5), a contact angle decrease of 5° can be related to an increase in capillary rise velocity by 50% from untreated to 1000℃ and smouldering. The increasing temperature alters the mineralogical iron composition of the silica sand from goethite to hematite and the structure of the quartz (Chapter 2). Research shows that an increase in hematite is linked to an increase in contact angle (Iveson et al., 2004).

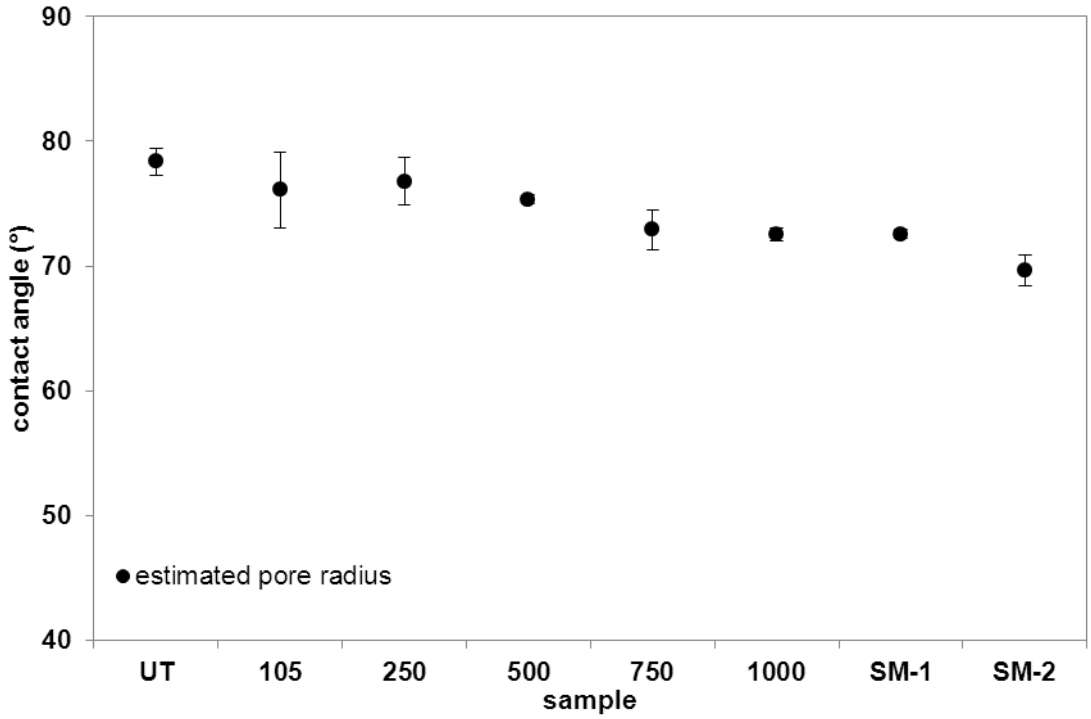

Figure 5.11. Contact angle values for silica sand based on maximum (0.26mm) and minimum (0.06mm) effective capillary radius after different thermal treatments

It is likely that the amount of iron oxides present in the silica sand is too small to have an effect the overall contact angle. However, it is possible that the oxidation from goethite to hematite decreases the contact angle reduction and that for silica sand containing less iron oxides the decrease in contact angle values would be greater. The quartz itself forms polymorphs such as cristobalite and trydimite, which have the same chemical composition (SiO_2) but a different crystal structure (Kubicki and Lasaga, 1988; Hand et al., 1998; Wenk and Bulakh, 2004; Zihms et al., 2013). This change in crystal structure is observed in heated quartz and is an indicator that the surfaces of the sand particles are close to melting or have partly melted to form these new crystal structures. In addition, this exposure to elevated temperatures could cause a grain ripening whereby the grains surfaces are smoothed and imperfections are reduced. This leads to a decrease in surface roughness, which

leads to an increase in wettability (Bikerman, 1950; Tamai and Aratani, 1972). The samples treated by the large scale smouldering technique (SM-1) show the same contact angle (73°) as the sample treated at 1000℃ , which may suggest that the temperature experienced by the material during smouldering is in the region of 1000℃ and that the post-treatment effects are similar to that of heat treatment of a clean sample. This similarity also suggests that the material after smouldering contains no or very small amounts of residual contaminants since contaminants would be expected to affect the wettability. In contrast, the sample treated using the small scale smouldering set-up (SM-2) shows a lower contact angle than the high temperature heat or large scale smouldering treatment. The small scale set up shows a contact angle reduction of 9° compared to the untreated sample and 3° compared to the 1000℃ and large scale smouldered samples. Since the heat losses in the small scale set-up (SM-2) are higher than the large scale set-up (SM-1), the average temperature across the small-scale setup is lower. The exposure duration to the peak temperature is smaller as well. The observed additional reduction in contact angle may be related to another process than temperature. It is likely that this is linked to reactions between contamination and kaolin and could affect the in the post-remediation material wettability of the sample. It is very likely that this is a scale effect and further investigation is needed by comparing a range of different scale set ups to better understand the effect of smouldering scale on the results. The decreases in contact angle and related wettability are probably not of concern in regards to remediation and post-remediation wetting behaviour as the contact angles are still in the range considered as partly wetting (Kumar and Prabhu, 2007).

5.5.2. Silica sand – kaolin

To understand the effect of the fines fraction on wettability the contact angles for the silica sand-kaolin mixtures are shown in Figure 5.12.

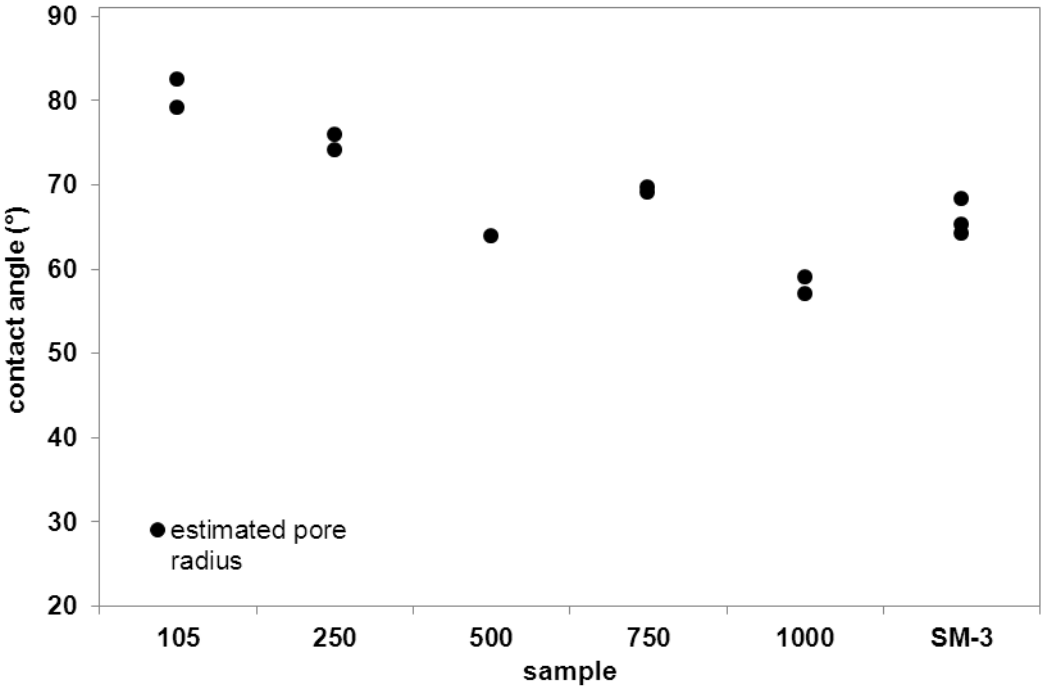

Figure 5.12. Contact angle values for silica sand-kaolin mixtures based on maximum (0.26mm) and minimum (0.06) effective capillary radius after different thermal treatments

Overall, the trend is the same as for the silica sand and the contact angle decreases with increasing treatment temperature. The contact angle for the 105℃ is in the range of that for the silica sand only sample, 79 to 83. However the added kaolin increases the reduction in contact angle more than 2-fold compared to the silica sand sample. The contact angle decreases to 57 to 59° after treatment of 1000℃. Using the static contact angle values based on the median effective radius and calculating the capillary rise velocity (Eq. 5.5) a contact angle decrease of 20° can be related to a 4-fold increase in capillary rise velocity 105℃ to 1000℃ and 3-fold increase after small scale smouldering (SM-3). This is likely due to the clay

chemistry and structure as it changes from kaolinite to mullite after exposure to temperatures above 500℃ (Chen et al., 2004). The liquid and plastic limits for the temperature treatment up to 500℃ are similar, with liquid limits of 64±2%. For treatment temperatures of 750℃ the liquid limit in creases to 81% (Table 5.2) and this sample has a very high plasticity range compared to the lower temperatures. This is likely due to the increased dehydration of the clay at this temperature. The liquid limit test for the sample treated at 1000℃ was not possible due to the clay not mixing properly with the water and behaving slightly non-newtonian, which means as the mixing motion stopped the sample liquefied and it was impossible to create a testable sample. It is likely that the temperature of 1000℃ causes de-hydroxylation of the clay minerals, followed by aggregation of the particles and sintering (Fabbri et al., 2013). It is very likely that these mineralogical changes affect the wetting behaviour of the mixture.

In addition to the changes of the clay fraction, the quartz is partly protected by the clay layer and effects on the particle surfaces e.g. polymorph formation are likely to be reduced. This shows that the addition of 10% kaolin has a severe impact on the contact angle of the overall sample. The reduction of contact angle and therefore the increase in wettability of the silica sand-kaolin sample is within the range of partial wettability but it is moving closer to the completely wetting contact angle range of 0 to 45° (Kumar and Prabhu, 2007). Since the values o btained using the effective capillary radius method do not give real contact angle values a decrease in contact angle of 20° could be significant if the starting c ontact angle is close to a boundary between wetting conditions (Figure 5.1). The observed increase in wettability with increasing treatment temperature and after smouldering treatment could be of concern for the initial wetting response of soils containing kaolin clay and requires

further investigation to understand the impact on more complex materials such as real soils.

The effective radius method is limited due to the pore radius being selected based on material properties but it might not reflect the true pore radius of the sample. This is especially the case for non-uniform soils that have a range of pore radii. The effective radius method would not be suitable to represent such as sample. Contact angle measurements should also be validated by a second method such as the ones described in Section 5.1. However, due to the coarse material these methods were not suitable and a comparison and validation of the contact angle results was therefore not possible as part of this study.

5.5.3. Discussion

By combining the static and dynamic contact angles and using an estimated pore radius to estimated contact angle trends, changes to the wetting behaviour of hexane are not affecting the results. Thermal and smouldering appear to change the wetting of silica sand and silica sand by hexane and a contact angle of 0° should not be assumed.

By back calculating capillary rise velocities (Equation 5.6) an increase by 50% was determined for the silica sand after high temperature thermal and smouldering treatment and an increase 3 to 4 times the original velocity for silica sand + 10% kaolin. These increases in capillary rise velocity suggest that the area treated with high temperature thermal or smouldering treatments wets faster compared to the surrounding soil. This could lead to a change in the water balance and create preferential flow paths in the treatment zone. This increase in recharge to the treated area could lead to increased contaminant transport, increased mobilisation of fine soil fractions. This could lead to changes in stability within the treatment zone

as well as surrounding area by mobilising fines and changing the soil structure. Results presented in Chapter 4 show that heat treatment can affect the bond between clay and sand fractions. Increased mobilisation can result in height losses of up to 10% were observed. Monitoring of ground water movement during these treatments may help to predict how these changes affect a site during and after remediation.

5.6. Conclusion

Increasing treatment temperature leads to increasing in wettability of sand and sand-kaolin. In the case of sand-kaolin, this change may affect the overall water balance of the bulk material and to increased preferential flow and infiltration. The results show effects due to the coarse (sand) fraction and the fine (clay) fraction. Further, increase in kaolin content may lead to further increases in wettability in similar exposure conditions. To allow prediction of changes of wettability of natural soils, the study of thermal effects needs to be broadened to include other clay minerals commonly found in natural soils, as clay minerals such as smectite and illite are likely to behave differently to kaolin after exposure to elevated temperatures. Their mineralogical composition is different and this may lead to a different response compared to kaolin.

This research shows that the capillary rise method can be used to determine changes in wettability of porous samples. The approach by Bachmann et al (2003) is not suitable and the contact angle of n-hexane should not be assumed as 0°. The effective radius method is suitable for the comparison of changes but cannot be used to determined real contact angle values.

The contact angles of silica sand and silica sand-kaolin mixtures decrease with increasing treatment temperatures, likely due to processes at the particle surface that effect the overall wettability of the soil. In addition to the changes in wetting response after thermal and smouldering treatment, this study also shows that contact angle values can be used as indicators for particle roughness.

5.7. References

Bachmann, J., Woche, S.K., Goebel, M.O., Kirkham, M.B., Horton, R., 2003. Extended methodology for determining wetting properties of porous media. Water Resources Research, 39(12).

Beatty, S.M., Smith, J.E., 2010. Fractional wettability and contact angle dynamics in burned water repellent soils. Journal of Hydrology, 391(1–2): 97-108.

Bikerman, J.J., 1950. The Surface Roughness and Contact Angle. The Journal of Physical and Colloid Chemistry, 54(5): 653-658.

Chatterjee, N., Lapin, S., Flury, M., 2012. Capillary Forces between Sediment Particles and an Air–Water Interface. Environmental Science & Technology, 46(8): 4411-4418.

Chau, T.T., Bruckard, W.J., Koh, P.T.L., Nguyen, A.V., 2009. A review of factors that affect contact angle and implications for flotation practice. Advances in Colloid and Interface Science, 150(2): 106-115.

Chen, Y.-F., Wang, M.-C., Hon, M.-H., 2004. Phase transformation and growth of mullite in kaolin ceramics. Journal of the European Ceramic Society, 24(8): 2389-2397.

Dang-Vu, T., Hupka, J., Drzymala, J., 2006. Impact of roughness on hydrophobicity of particles measured by the Washburn method. Physicochemical Problems of Mineral Processing, 40: 45-52.

DeBano, L.F., 2000a. The role of fire and soil heating on water repellency in wildland environments: a review. Journal of Hydrology, 231: 195-206.

DeBano, L.F., 2000b. Water repellency in soils: a historical overview. Journal of Hydrology, 231: 4-32.

Doerr, S.H., Shakesby, R.A., Walsh, R.P.D., 2000. Soil water repellency: its causes, characteristics and hydro-geomorphological significance. Earth-Science Reviews, 51(1-4): 33-65.

Fabbri, B., Gualtieri, S., Leonardi, C., 2013. Modifications induced by the thermal treatment of kaolin and determination of reactivity of metakaolin. Applied Clay Science, 73: 2-10.

Goebel, M.O., Bachmann, J., Woche, S.K., 2008. Modified technique to assess the wettability of soil aggregates: comparison with contact angles measured on crushed aggregates and bulk soil. European Journal of Soil Science, 59(6): 1241-1252.

Hajnos, M., Calka, A., Jozefaciuk, G., 2013. Wettability of mineral soils. Geoderma, 206(0): 63-69.

Hand, R.J., Stevens, S.J., Sharp, J.H., 1998. Characterisation of fired silicas. Thermochimica Acta, 318(1-2): 115-123.

Hong, K.T., Imadojemu, H., Webb, R.L., 1994. Effects of oxidation and surface roughness on contact angle. Experimental Thermal and Fluid Science, 8(4): 279-285.

Iveson, S.M., Holt, S., Biggs, S., 2004. Advancing contact angle of iron ores as a function of their hematite and goethite content: implications for pelletising and sintering. International Journal of Mineral Processing, 74(1-4): 281-287.

Kowalik, P.J., 2006. Drainage and capillary rise components in water balance of alluvial soils. Agricultural Water Management, 86(1-2): 206-211.

Kubicki, J.D., Lasaga, A.C., 1988. Molecular dynamics simulations of SiO2 melt and glass: Ionic and covalent models. American Mineralogist, 73: 941-955.

Kumar, G., Prabhu, K.N., 2007. Review of non-reactive and reactive wetting of liquids on surfaces. Advances in Colloid and Interface Science, 133(2): 61-89.

Lourenço, S., Wakefield, C., Bryant, R., Doerr, S.H., MORLEY, C., 2012. Wettability Assessment of an Oil coated soil. Proceedings of the 2nd European Conference on Unsaturated Soils.

Marinho, F.A.M., Take, W.A., Tarantino, A., 2008. Measurement of Matric Suction Using Tensiometric and Axis Translation Techniques. Geotechnical and Geological Engineering, 26(6): 615-631.

Marmur, A., Cohen, R.D., 1997. Characterization of Porous Media by the Kinetics of Liquid Penetration: The Vertical Capillaries Model. Journal of Colloid and Interface Science, 189(2): 299-304.

Mataix-Solera, J. et al., 2008. Can terra rossa become water repellent by burning? A laboratory approach. Geoderma, 147(3-4): 178-184.

Mataix-Solera, J., Doerr, S.H., 2004. Hydrophobicity and aggregate stability in calcareous topsoils from fire-affected pine forests in southeastern Spain. Geoderma, 118(1-2): 77-88.

Pironi, P. et al., 2009. Small-scale forward smouldering experiments for remediation of coal tar in inert media. Proceedings of the Combustion Institute, 32: 1957-1964.

Ramírez-Flores, J.C., Bachmann, J., Marmur, A., 2010. Direct determination of contact angles of model soils in comparison with wettability characterization by capillary rise. Journal of Hydrology, 382(1–4): 10-19.

Ramírez-Flores, J.C., Woche, S.K., Bachmann, J., Goebel, M.-O., Hallett, P.D., 2008. Comparing capillary rise contact angles of soil aggregates and homogenized soil. Geoderma, 146(1-2): 336-343.

Robichaud, P.R., Hungerford, R.D., 2000. Water repellency by laboratory burning of four northern Rocky Mountain forest soils. Journal of Hydrology, 231: 207-219.

Rodríguez-Caballero, E., Cantón, Y., Chamizo, S., Afana, A., Solé-Benet, A., Effects of biological soil crusts on surface roughness and implications for runoff and erosion. Geomorphology(0).

Schembre, J.M., Tang, G.Q., Kovscek, A.R., 2006. Wettability alteration and oil recovery by water imbibition at elevated temperatures. Journal of Petroleum Science and Engineering, 52(1–4): 131-148.

Shang, J., Flury, M., Harsh, J.B., Zollars, R.L., 2010. Contact angles of aluminosilicate clays as affected by relative humidity and exchangeable cations. Colloids and Surfaces A: Physicochemical and Engineering Aspects, 353(1): 1-9.

Siebold, A., Walliser, A., Nardin, M., Oppliger, M., Schultz, J., 1997. Capillary Rise for Thermodynamic Characterization of Solid Particle Surface. Journal of Colloid and Interface Science, 186(1): 60-70.

Smith, I., 2009. Smith's Elements of Soil Mechanics 8th Edition. Blackwell Publishing, Oxford.

Tamai, Y., Aratani, K., 1972. Experimental study of the relation between contact angle and surface roughness. The Journal of Physical Chemistry, 76(22): 3267-3271.

Washburn, E.W., 1921. The Dynamics of Capillary Flow. Physical Review, 17(3): 273-283.

Wenk, H.-R., Bulakh, A., 2004. Minerals Their Constitution and Origin. Cambridge University Press.

Wenzel, R.N., 1936. RESISTANCE OF SOLID SURFACES TO WETTING BY WATER. Industrial & Engineering Chemistry, 28(8): 988-994.

Zihms, S.G., Switzer, C., Irvine, J., Karstunen, M., 2013. Effects of high temperature processes on physical properties of silica sand. Engineering Geology.

6. Conclusions & Future Work

6.1. Conclusions

Exposure to high temperatures and smouldering remediation affect silica sand, kaolin clay, and binary mixtures of the two materials. Some properties are affected by exposure to temperature independent of treatment type and some changes are dependent on treatment type, which is likely linked to reactions due to the coal tar addition for the smouldering treatment. Figure 6.1 shows the effects on sand and sand +10% kaolin with thermal treatment.

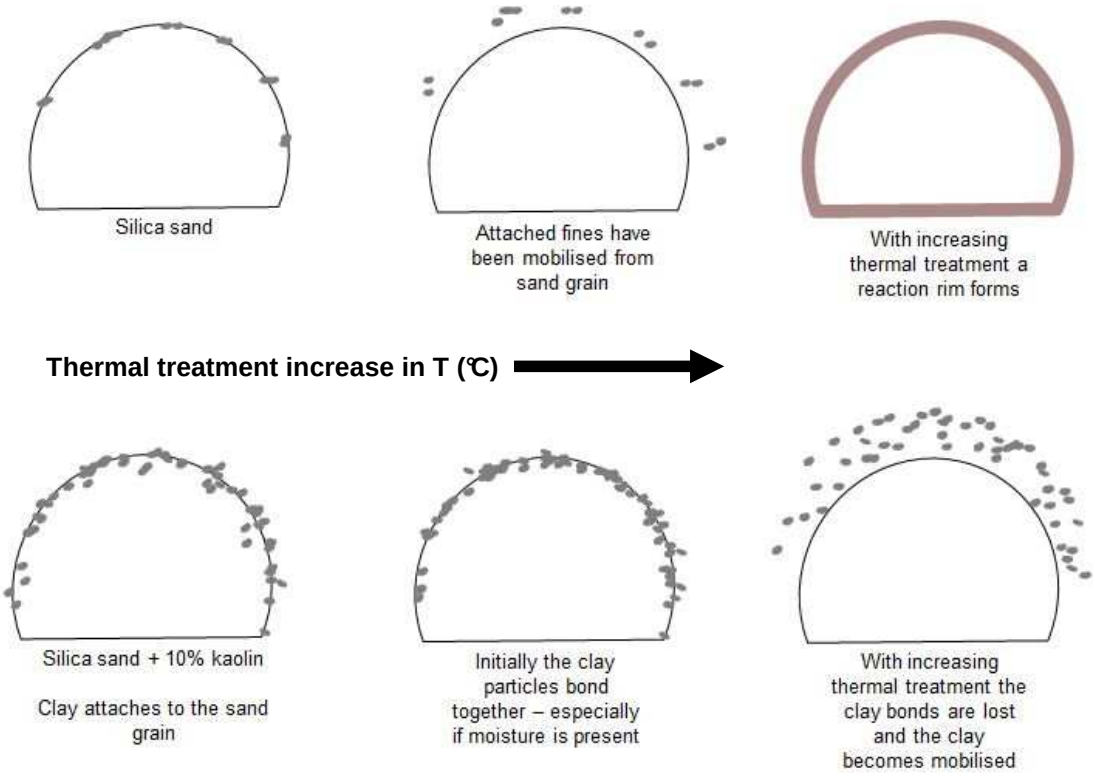

Figure 6.1. Sketch of silica sand grain and silica sand grain + 10% kaolin with increasing thermal treatment (not to scale)

Physical and chemical properties of the silica sand and kaolin appear to be affected in three ways (Table 6.1):

i) Not affected (N)

ii) High temperature exposure – independent of treatment type (T)

iii) Effects of thermal treatment are different to smouldering treatment – high temperature exposure but further changes as a result of smouldering (T < S)

Table 6.1. Summary of physical and chemical properties tested and how they are affected (T: temperature exposure independent of treatment; T<S: treatment dependent; N: not affected)

Property	Kaolin clay	Silica sand	Silica sand + 10% kaolin clay
Particle size distribution		**T**	**T**
Mobilisation of fines		**T**	**T**
Densities		**N**	
Mass loss	**N**	**T**	
Plasticity	**T**		
Particle shape		**N**	
Mineralogy	**T**	**T < S**	
pH	**T**	**T < S**	**N**

These observed particle scale changes can be linked to the dynamic response of the material. For shear strength and wettability, a link to treatment temperature and smouldering remediation has been found. Both responses are linear with increasing temperature for thermal treatment; however the response after smouldering is different. During smouldering, additional processes related to the combustion or residual contamination remaining after remediation alter the particles, which ,may lead to the changes in response.

Shear strength for silica sand decreases with increasing treatment temperature compared to an increase for the sample containing 10% kaolin. A similar link is observed for the hydraulic conductivity, where effects due to exposure to elevated temperature are magnified by the presence of kaolin. The kaolin bonds with the sand grains causing a coating effect on the sand grains and protecting them from the temperature. Also, clays have larger surface areas than sand and therefore are more affected by the high temperatures.

In hydraulic conductivity experiments with samples containing kaolin, the response is not only dependent on the microstructure of the bulk material but also the hydraulic history. This shows that samples tested in a laboratory need to be prepared to the specific environmental conditions of the site to allow an accurate prediction of bulk response. The microstructure of the sample is also linked to the kaolin and its changes in mineralogy and chemistry with increasing treatment temperature.

This study shows that particle scale changes to silica sand and kaolin clay can be linked to overall bulk behaviour and a better understanding of these links can help improve predictions of changes to soil behaviour following exposure to elevated temperatures. Figure 6.2 shows how the particle scale changes and bulk behaviour can be linked.

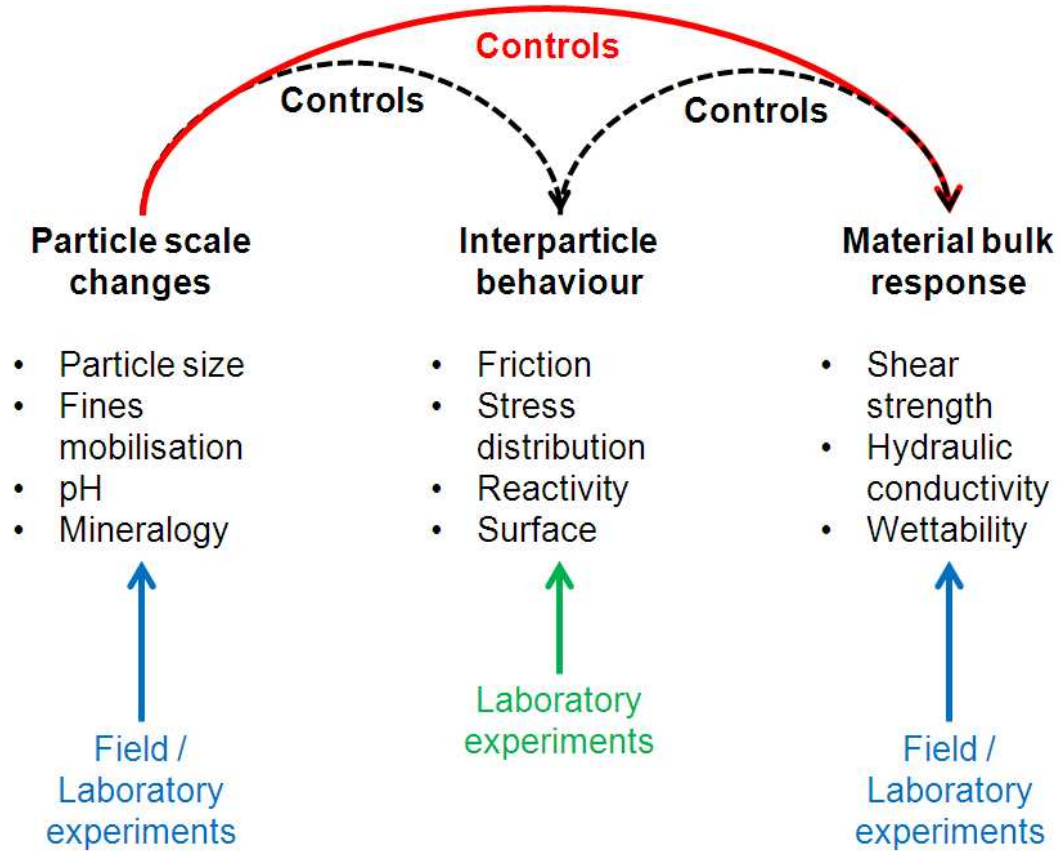

Figure 6.2. Links between particle scale changes and sample bulk response for silica sand and silica sand + 10% kaolin investigated in this study

The determination of properties such as particle size, mineralogy, and bulk responses such as shear strength can be determined through laboratory and field experiments. However, changes to the interparticle behaviour are more difficult to analyse. The complexity of the relationships makes it difficult to correlate how individual changes on particle or interparticle level control the bulk behaviour and which processes dominate. However, overall links between characteristic properties and bulk behaviour can be used to predict certain behaviour after exposure to elevated temperatures and aid in the design of preventive measures that may be necessary during redevelopment of the site.

This study shows that silica sand, kaolin clay and binary mixtures of the two materials are different after exposure to elevated temperatures either through heat or smouldering treatment. Based on differences between high temperature and smouldering remediation, temperature testing alone cannot be used to simulate the effects of smouldering on soil properties. In remediation practice, soil property and behaviour testing after remediation should be incorporated into the remediation plans that involve thermal and smouldering processes to ensure appropriate material characterisation prior to site redevelopment.

6.2. Future Work

Considering the observed changes for silica sand and kaolin clay with exposure to elevated temperatures through heat and smouldering treatment shows that soil properties as well as behaviour are affected. To better understand the links and controlling factors, further investigation of the interparticle behaviour is recommended. Characterisation of changes to the surface roughness of the particles is particularly important. Based on changes to shear strength and wettability observed in this work, changes in roughness are possible. No changes were apparent under petrographic microscope, but the resolution may not have been high enough. Further investigation of surface roughness with Scanning Electron Microscopy, 3D-scanning techniques, or Micro-Computed Tomography (CT) would capture the surfaces of the particles and allow investigation of changes at much smaller scales.

Smouldering remediation leads to an increased detachment of fines which increases their mobility. This is additionally affected by handling steps required to test and

analyse the post-smouldering material. Wettability tests should therefore be conducted with no handling steps after remediation. Adaptation of a smouldering column for subsequent use in testing hydraulic conductivity or capillary rise would allow for a more accurate analysis of material behaviour after smouldering.

Comparison of small and large scale smouldering experiments shows a difference in post-smouldering properties and behaviour. Future experiments should examine the effects of smouldering at different operating scales to better understand the effects of scale, improve interpretation from small scale laboratory experiments to contaminated sites, and allow for better predictions of changes to soil properties at sites remediated by this technique. The temperature achieved during smouldering depends on the contaminant. To understand links between contaminant and changes to soil properties and bulk response, other contaminants such as crude oil and its derivatives should be investigated.

To improve understanding on how exposure to elevated temperatures affect real soils, further tests should build upon this work and expand to other particle fractions like silts as well as field-derived soils. Based on the observations in regards to mineralogy and the effect of its changes to bulk behaviour, materials with different mineralogical compositions should also be tested. Broadening the materials tested and analysed will improve understanding of high temperature and smouldering effects on real soils. This, in turn, will improve predictions of behaviour during and after remediation as well the post-remediation development of contaminated sites.

6.3. Recommendations for Practice

When using smouldering or thermal remediation techniques in the field, practitioners should not assume that soil properties after remediation will be equivalent to soil

properties in uncontaminated and untreated soils. As part of the initial site investigation, samples are taken for classification and other laboratory testing. Further site characterisation should be conducted after remediation. In addition to the standard requirements the following test should be included after heat or smouldering remediation

a) particle size distribution
b) pH
c) mineralogical composition

To minimise laboratory testing, samples could only be heat treated at the maximum expected temperature achieved during the remediation process. In the case of smouldering, soil tested in treatability tests may be suitable for this testing. In addition to classification testing, some dynamic testing should be included to investigate the shear strength and the wettability.

The shear strength can be determined by direct shear testing or triaxial cell and should be compared for untreated and heat treated samples. Any change in soil strength can be used to recalculate the bearing capacity of the soil and if necessary alter the footing design. If the difference in strength is larger than can be compensated by footing design changes, additional reinforcements may be necessary. Considering the change in wettability, it might be feasible to re-wet the soil artificially after remediation and add stabilising clays or grouts via the water. Further investigation into stabilisation methods after remediation is necessary to determine how these methods could be applied and what benefits can be achieved.

In regards to hydraulic response of a site after thermal or smouldering remediation, the relationship of small scale changes to field sites needs to be further investigated.

It is possible to implement data determined by small scale hydraulic experiments and their changes in hydraulic models to explore these effects. Further modelling should help to identify any changes beyond anisotropic behaviour of a site.

The main recommendation based on the results from this work is that a site remediated by thermal or smouldering processes should never be assumed to have the same characteristics or behaviour as the site prior to contamination or remediation.

APPENDIX A

A.1 Engineering Geology Journal Paper

A.2 Conference paper accepted for the 18th International Conference on Soil Mechanics and Geotechnical Engineering, Paris 2013

Engineering Geology 164 (2013) 139–145

Contents lists available at ScienceDirect

Engineering Geology

journal homepage: www.elsevier.com/locate/enggeo

Effects of high temperature processes on physical properties of silica sand

S.G. Zihms, C. Switzer *, J. Irvine, M. Karstunen [1]

Department of Civil and Environmental Engineering, University of Strathclyde, Glasgow G4 0NG, United Kingdom

ARTICLE INFO

Article history:
Received 30 December 2012
Received in revised form 5 June 2013
Accepted 12 June 2013
Available online 20 June 2013

Keywords:
Soil engineering properties
High temperature
Thermal remediation
Smouldering remediation
Fire

ABSTRACT

High temperature processes may alter soil properties, creating potential risks of subsidence, erosion and other hazards. Soils may be exposed to high temperatures during some aggressive contaminant remediation processes as well as natural events such as fires. Characterising the effects of high temperatures on soil properties is essential to understanding the potential hazards that may arise after exposure. Thermal treatment and smouldering remediation were carried out on silica sand used here as a simple soil. Changes observed in physical properties were associated with the treatment type and exposure temperature. Particle, minimum and maximum densities were independent of heat treatment type and temperature. In contrast, particle size distribution, mineralogy, capillary rise, and hydraulic conductivity were linked to treatment type and exposure temperature with the most substantial changes associated with smouldering remediation. Changes in colour and mass loss with increasing temperature suggest changes within the crystal structure of the silica sand beyond loss of moisture content within the pore space and dehydration of iron deposits from goethite to hematite. Based on these observations, exposure to high temperature processes and the complex geo-chemical reactions during smouldering remediation can have significant effects on soil properties. Monitoring after exposure is advisable to determine the severity of exposure and any mitigation measures that may be necessary.

1. Introduction

Soils can be exposed to elevated temperatures naturally through wild, forest or peat fires or through thermal remediation processes designed to mitigate high concentrations of hazardous organic contaminants. Most research on soil properties and their heat dependency is based on forest fires and therefore concentrates on erosion rates, ground stability and nutrients affected by fire severity. The effects of exposure to temperatures up to 500 °C have been studied widely (De Bruyn and Thimus, 1996; Certini, 2005; Rein et al., 2008; Are et al., 2009; Rein, 2009). Literature published on heat treatments of clay evaluates the effects of temperatures up to 1000 °C (Tan et al., 2004). Exposures of 200–850 °C have been observed in soils during wildfires (DeBano, 2000; Mataix-Solera and Doerr, 2004; Certini, 2005; Rein et al., 2008). Moderate (300–400 °C) and high (>450 °C) temperature processes, such as hot water extraction, thermal desorption, soil heated vapour extraction, incineration or smouldering are widely used to treat contaminated soils (McGowan et al., 1996; Webb and Phelan, 1997; Kronholm et al., 2002; Araruna et al., 2004; Chang and Yen, 2006; Lee et al., 2008; Gan et al., 2009; Pironi et al., 2009, 2011; Switzer et al., 2009). Previous studies on the effects of non-aqueous phase liquid (NAPL) contamination on soil properties shows a net reduction in soil stability as NAPL content increases (Khamehchiyan et al., 2007). NAPLs displace soil moisture and thus change the interactions between soil particles. Most research on soil remediation techniques focuses on the remediation result and less on the effects the technique has on the soil properties. In some cases, the effects on soil properties may be a criterion for selection of the remediation technique (Chang and Yen, 2006; Pironi et al., 2011) or the soil properties may influence the results (Webb and Phelan, 1997). There is little research on the effects of thermal remediation processes on soil physical properties. High temperature remediation displaces soil moisture and removes or destroys NAPL content. In order to establish whether the soil can recover strength and stability after remediation, it is important to establish the changes these remediation processes have on fundamental soil properties.

The maximum temperatures observed in contaminant remediation vary by the process that is used (Table 1). Thermal desorption and soil heated vapour extraction use electric resistant heating either on the soil surface or through steel walls. The current transforms the groundwater and soil water into steam which in turn evaporates any harmful chemicals. The vapours are collected and treated or disposed (Araruna et al., 2004; Chang and Yen, 2006). Hot water extraction uses pre-heated and pressurised water, which is injected into the soil, to extract and react with the targeted chemicals (Kronholm et al., 2002). In practice, maximum temperature is related to the soil

* Corresponding author. Tel.: +44 1415484671.
E-mail address: christine.switzer@strath.ac.uk (C. Switzer).
[1] Now at: Department of Civil and Environmental Engineering, Chalmers University of Technology, SE-412 96 Gothenburg, Sweden.

0013-7952/$ – see front matter © 2013 Elsevier B.V. All rights reserved.
http://dx.doi.org/10.1016/j.enggeo.2013.06.004

Table 1
Possible maximum temperatures of exemplar moderate to high remediation techniques.

Remediation process	Maximum observed temperature (°C)	Reference
Hot water extraction	300	Kronholm et al. (2002)
(Low temperature) Thermal desorption	112	Webb and Phelan (1997)
(High temperature) Thermal desorption	750	Chang and Yen (2006)
Heated soil extraction	300	Gan et al. (2009)
Incineration	850	Lee et al. (2008)
Smouldering remediation	600–1100[a]	Switzer et al. (2009)

[a] Maximum temperature is associated with contaminant type and treatment conditions.

conditions, process operating conditions and in some cases, the contaminant that is being treated.

With the exception of smouldering remediation, all of these remediation techniques use heat or heated water to volatilise the contaminant within the soil to enable its extraction. Maximum temperatures for these technologies are typically adjacent to the heat source with more moderate target temperatures of 80–100 °C achieved within the wider treatment zone. The contaminant must be collected and treated (McGowan et al., 1996; Webb and Phelan, 1997; Kronholm et al., 2002; Chang and Yen, 2006; Lee et al., 2008; Gan et al., 2009). These processes maintain high temperatures in the soil for weeks to months or longer. In contrast, smouldering remediation uses the contaminant itself as fuel for the combustion reaction (Pironi et al., 2009, 2011; Switzer et al., 2009). In laboratory studies, the soil particles are exposed to high temperatures on the order of 1000 °C for coal tars and 600–800 °C for oils for up to 60 min. Field scale efforts may result in exposure durations on the order of hours or longer.

Elevated temperatures have been shown to alter the mineralogical composition of soil. These effects have been studied extensively in relation to the effects of wildfires on soil properties. Colour change in soils has been observed after wildfire and after smouldering remediation. In most cases it changes from yellowish brown to reddish brown. This is due to the oxidation of soil iron content from goethite to maghemite or hematite (Ketterings and Bigham, 2000; Goforth et al., 2005). Decomposition of soil particles, especially clay minerals, starts at temperatures above 550 °C (Certini, 2005). These temperatures are rarely reported for wild and forest fire, but temperatures up to 1200 °C can be achieved during smouldering remediation (Pironi et al., 2009; Switzer et al., 2009).

In previous work, soil stability has been observed to increase with exposure to low and moderate temperatures as cementation of the clay particles occurs (Certini, 2005; Rein et al., 2008). This coincides with a measured increase of sand particle size with increasing temperatures in this range (Terefe et al., 2008). In clay-rich soils, bulk density and compressive strength were observed to increase as temperature was increased above ambient conditions whereas shear strength, liquid limit, and plasticity were observed to decrease (De Bruyn and Thimus, 1996). As exposure duration increases, clay cracking is observed as moisture is lost. This drying process has two distinct stages: constant evaporation as moisture is lost from the surface followed by decreasing evaporation as the drying front propagates inward (Tang et al., 2010). Cracks form as a result of tensile stresses at the surface and can grow rapidly as moisture depletes.

At temperatures of 500 °C or higher, the soil stability has been observed to decrease dramatically. This reduced stability is linked to the loss of organic cements (Certini, 2005). Wild fire temperatures can reach temperatures up to 850 °C at the soil–litter interface but temperatures at 0.05 m depth are unlikely to exceed 150 °C (DeBano, 2000). Therefore, wild fire temperatures do not cover the temperature range encountered by thermal and smouldering remediation processes. It is necessary to understand possible impacts to soil from exposure to the whole temperature range of thermal remediation treatments.

This study aims to characterise the effects of moderate and high temperatures as well as smouldering on physical soil properties to determine the impact any changes will have to the soil and therefore predict possible complications during or after remediation treatment. Silica sand is used as a simple soil with relatively homogenous mineralogy and minimal internal pore structure. These aims are achieved by comparing clean, heat-treated and smouldered silica sands with untreated and oven-dried sands. After each treatment, fundamental properties of the sand are tested and compared to determine the impacts of the treatment conditions.

2. Materials and methods

Coarse silica sand (Leighton Buzzard 8/16, Sibelco, Sandbach, UK) was used as the base soil for all of the experiments. The sand contains 99% silicon-dioxide, has a mean grain size of 1.34 mm and a bulk density of 1.7 g/cm^3 (Switzer et al., 2009). All sand was accepted as received and subjected to the same pre-treatment. A programmable muffle furnace (Nabertherm L9/11/SKM, Nabertherm GmbH, Lilienthal, Germany) was used for all heating experiments. The sands evaluated after smouldering remediation were prepared in a 3 m^3 experiment involving coal tar mixed with coarse sand. The concentration of this mixture was 31,000 ± 14,000 mg/kg total extractable petroleum hydrocarbons before treatment and the average concentration after smouldering remediation across the majority of the vessel was 10 ± 4 mg/kg. A 25 L sample of the post-treatment material was collected and set aside for characterisation. Kaolin (Whitchem Ltd, UK) was used as an exemplar, non-swelling clay in a limited number of experiments.

2.1. Sample preparation and heat treatment

The silica sand was washed and wet sieved using a 0.63 μm sieve to eliminate any loose fines and then air dried for several days. For each test the required amount of samples were placed in a ceramic crucible heated in the muffle furnace, following the heat treatment profiles listed in Table 2. Maximum temperatures of 105, 250, 500, 750, and 1000 °C were investigated. Each sample was subjected to a rapid increase in temperature, held at the peak temperature for 1 h, cooled, and transferred for testing. After the heating period the samples were removed from the muffle furnace and placed in a desiccator to cool. Samples heated to temperatures above 500 °C were allowed to cool in the furnace to 200 °C before transfer to the desiccator. The necessary pre-treatment meant that all samples were disturbed by handling steps. Therefore, only characteristics unrelated to soil structure were investigated in this study.

2.2. Laboratory testing

Particle density was measured using the gas-jar method suitable for coarse soils (BS1377-2:1990). A sample of 1000 g mass was placed in a

Table 2
Heat treatment conditions for silica sand.

Maximum exposure temperature (°C)	Heating pattern		
	Pre-heating duration (min)	Peak temperature exposure duration (min)	Cooling period duration (min)
Untreated	–	–	–
105	30	1440	0
250	30	60	0
500	30	60	~60[a]
750	60	60	~180
1000	60	60	~240

[a] Cooling period varied for each batch so approximate duration is shown.

1 L gas jar with approximately 500 mL of water. The sample was set aside for 4 h and then shaken end-over-end for 30 min. The gas jar was filled with water fully. The average particle density was determined based on the mass of the sand, mass of the water and volume of water displaced by the sand.

Minimum density was measured using 1000 g of sand in a 1 L glass measuring cylinder with 20 mL graduation (BS1377-4:1990). The cylinder was shaken to loosen the sand and inverted four times. The cylinder was then inverted until all of the sand was at rest, returned to the initial position and carefully placed on a flat surface. The volume was recorded at the mean level of the surface to the nearest 10 mL. The test was repeated 10 times with the same sample. The minimum density was calculated using the greatest volume reading in the cylinder (BS1377-4:1990).

Maximum density was determined using the vibrating hammer method (BS1377-4:199). Approximately 3000 g of sand was placed in a bucket with warm water and thoroughly stirred to remove any air bubbles. The sand was left to cool overnight. A 1 L compaction mould was used for all density measurements. The mould was placed in a water tight container on a solid base. Water was poured into the mould to 50 mm depth in the mould body and the surrounding container. A portion of the sand–water mixture was carefully added to the mould, approximately filling a third of the mould after compaction. Water was added to the surrounding container to match the water level in the mould. The vibrating hammer used a circular tamper to compact the sand for at least 2 min using a force between 300 N and 400 N on the sample. This process was repeated for the other 2 layers to fill the mould. The masses of sand and water in the mould were used to determine the maximum density.

Particle size distribution for the sand was determined using a dry sieving method (BS1377-2:1990). Approximately 200 g of each sample was placed into the top of set of sieves that included 1.18 mm, 600 μm, 425 μm, 300 μm and 212 μm sieve sizes. The set of sieves was shaken for 10 min. The mass of sand retained on each sieve was used to determine the particle size distribution. Particle size distribution was carried out in triplicate for each material.

The silica sand pH was tested using 30 g of silica sand and 75 mL of distilled water in 100 mL glass beaker. The mixture was agitated, covered and left overnight at 19 °C room temperature. The mixture was agitated again right before the measurement of pH.

A modified falling head test was used to measure infiltration profile and falling head rate. A cylindrical tube (50 cm H × 6 cm OD) was filled with sand to height of 30 cm. Using a funnel and diffuser system, a volume of 170 mL of distilled water, which corresponded to a head of water of 60 mm, was added to the top of the cylinder and allowed to flow into the sand. Falling head was measured as the time of this 60 mm head of water reaching fixed increments on the column as it infiltrated into the sand column. The set-up for this experiment is shown in Fig. 1.

Capillary rise was tested using a cylindrical tube (9.3 cm H × 2 cm OD) with a fine mesh fitted over the bottom. The cylinder was filled with approximately 50 g of sand, placed above a reservoir filled with water and slowly lowered until it made contact with the water surface. To ensure a stable setup, the tube was held in place with a clamp system. The water was drawn into the sand through capillary forces and the final height was measured once the water level in the tube was observed to remain constant for 2 min. Capillary rise measurements were carried out in triplicate for each material.

The mineralogical composition of the silica sands was tested by BRUKER D8 ADVANCE with DAVINCI (2010) powder X-ray Diffraction (XRD) on crushed samples. Vibrational spectroscopy using Raman measurements were taken on individual silica sand grains. The Raman spectra were measured using a Renishaw inVia Raman Microscope running from 240 to 2000 cm^{-1} argon beam of 514 nm, 2400 l mm^{-1} (vis) grating, 10 exposure times, 1 accumulation and 10% power (cross-polar) was used for excitation.

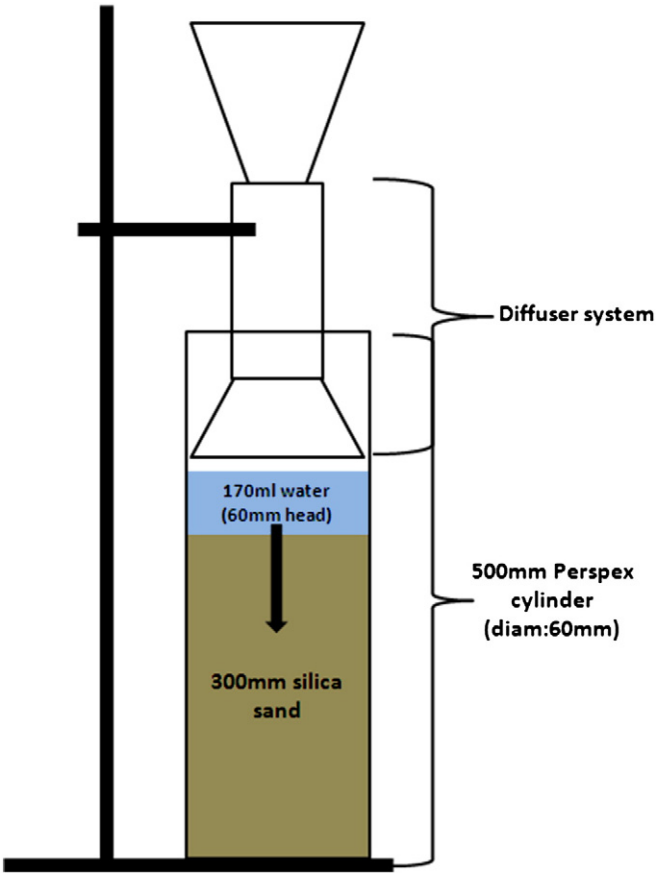

Fig. 1. Schematic diagram of the modified falling head test apparatus.

3. Results and discussion

3.1. Mineralogy

During the heat treatment testing and after smouldering remediation, a colour change of the silica sand was observed (Figure 2). Exposure of this material to high temperatures results in colour change from yellowish brown to reddish brown with increasing temperature for the silica sand grains and a change from yellow to pinkish red for the crushed silica sand. This colour change is associated with the dehydration reaction of goethite with increasing temperatures to form hematite or maghemite.

During the dehydration reaction of goethite, the density of the iron-hydroxide increases from 4.3 mg/m^3 for goethite to 5.2 mg/m^3 for hematite (Wenk and Bulakh, 2004). The sand is comprised primarily of silicon dioxide; iron oxides make up a small fraction of its composition. High temperatures may cause additional changes in mineralogy that may be less likely to be detected by visual examination (Pomiès et al., 1998; Goforth et al., 2005). Similar effects may occur within the silicon dioxide, which becomes unstable with high temperatures and forms silica polymorphs such as trydimite or cristobalite (Hand et al., 1998; Wenk and Bulakh, 2004). Thermal treatments (100–1200 °C) on fly ash showed that cristobalite becomes present in the samples and that smaller particles had a more glassy composition due their faster cooling time (Mollah et al., 1999).

Analysis of the silica sands by X-ray diffraction showed that both, iron oxide and quartz minerals are affected by heat treatment and smouldering remediation (Figure 3). Due to the high quartz content, the signal of the iron-oxides is small, but shifts are apparent. Shifts in quartz are apparent in the smouldered samples. For example, the quartz peaks from $2\theta = 36$ to 46 are very low for the smouldered

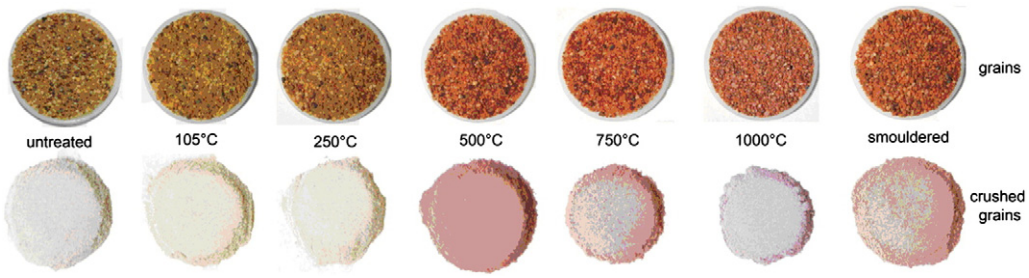

Fig. 2. Colour change observed in silica sand grains after heat treatment.

samples. Glass is amorphous and cannot be excited by XRD analysis. The quartz in the sand grains exposed to smouldering remediation may be losing its crystal structure.

Due to the nature of the excitement in XRD analysis, XRD cannot distinguish between quartz and its polymorphs as they have the same composition with a different structure. The formation of polymorphs was examined by Raman spectroscopy, a technique that allows a more targeted analysis of the grain surfaces (Komorida et al., 2010). After exposure to 1000 °C, trydimite and hematite were observed and after smouldering remediation, trydimite, crystobalite, dumortierite, and hematite were observed (Table 3). Trydimite and cristobalite have flatter structures than α-quartz. Mineralogy changes were not observed in Raman measurements at lower temperatures, though small shifts were apparent in X-ray diffraction spectra. Raman analysis on thin sections prepared of sand grains showed no polymorphs, suggesting that the effect remains at the surface.

Use of the Bruker XRD instrument required crushing of the sand grains, effectively diluting any surface changes. Raman spectroscopy was carried out under microscope and limited by the selection of single points for analysis. The extent of changes seems to be increasing with increasing temperature, as expected. More analysis is necessary to fully understand the exposure conditions that trigger these changes to the grain surfaces and how these changes may affect the grain–grain and grain–water interactions, particularly in more complex soils.

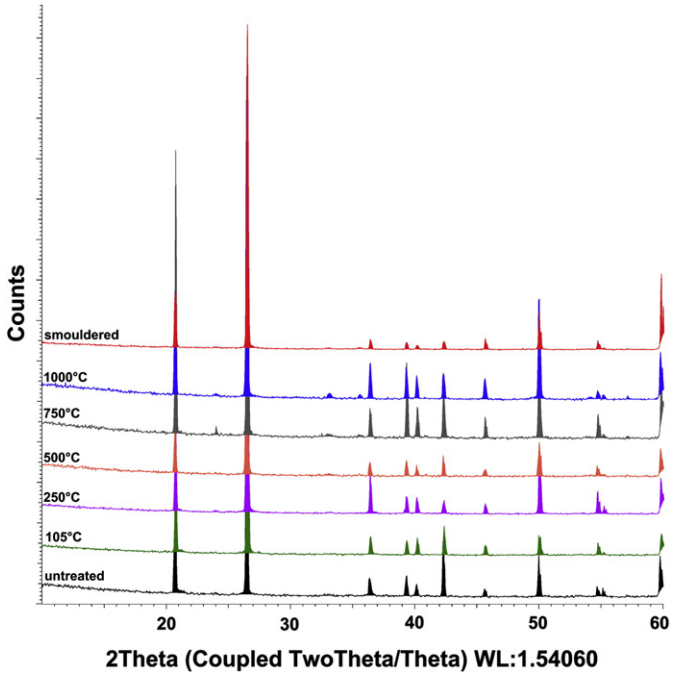

Fig. 3. X-ray diffraction spectra for silica sand after thermal and smouldering treatments.

3.2. Particle and bulk densities

In contrast to mineralogy, elevated temperatures did not seem to affect the particle density or minimum/maximum bulk densities of the silica sand (Table 4). No real relationship was apparent between treatment temperature and density. For the particle density, the values are consistently near 2.65 mg/m^3, which is a value that is widely used in geotechnical engineering calculations. The maximum and minimum densities are equally unaffected by heat treatment or smouldering. These observations are not consistent with the literature on wild and forest fire effects on soil properties, which suggests that bulk density would increase with temperature (Certini, 2005; Are et al., 2009). The lack of organic matter may explain the contrast. Organic matter is highly-affected by elevated temperature and thus organic-rich soils may exhibit density changes after exposure. Temperatures in the range of 260–370 °C are linked with melting and decomposition of organic matter and temperatures in excess of 370 °C are linked with complete or near-complete destruction (DeBano, 1981, 2000; Robichaud and Hungerford, 2000). The results in this study, which show no significant change in density, suggest that the changes in soil density that are observed after wildfires are associated primarily with effects on organic matter and potentially the smaller silt and clay-sized particles.

3.3. Particle size distribution

Particle size analyses suggest that heat treatment has a small but appreciable effect on grain distribution (Table 4). The sieve analyses show that the sample retained on the 1.18 mm sieve increases from 94.4% ± 0.7% for the untreated sample to 95.5% ± 1.2% for treatment at 250°. After this initial increase, the sample retained on the 1.18 mm sieve decreases to 94.0% ± 0.4% and 93.3% ± 0.9%, as exposure temperature is increased to 500 °C and 1000 °C, respectively. Corresponding measurements on sieves <1.18 mm show an initial decrease from 5.3% ± 0.6% to 4.1% ± 1.2% for the untreated sample to 250 °C heat treatment, followed by an increase to 5.6% ± 0.4% and 6.2% ± 0.8%, for 500 °C and 1000 °C, respectively. Fig. 4 shows the impact of temperature on the fines' fraction <600 μm, which increases with increasing temperature. Collection of the sand samples after smouldering remediation involved multiple handling steps, all of which resulted in visually-apparent mobilisation of fines. Thus, these sands were not tested for particle size distribution.

The variation in particle size distribution may be linked to the loss of mass beyond the initial moisture content (Table 4). In the mass loss tests, samples were prepared to 5% moisture content and then treated according to the temperature specified. As temperature increases, mass loss increases, exceeding the initial 5% added moisture for temperatures above 500 °C. Although there is a dehydration reaction

Table 3
Exemplary mineralogy of points on sand grain surfaces after selected heat treatments.

Treatment	Grains	Analysis points	Number of detections of each mineral					
			Quartz	Tridymite	Cristobalite	Dumortierite	Geothite	Hematite
Untreated	5	9	9					
500 °C	3	5	3				2	
1000 °C	3	9	5	2				2
Smouldered	12	37	12	6	3	8	5	2

from goethite to hematite, the fraction of iron oxide relative to the total composition of the sand is too small for this reaction alone to account for the whole additional mass loss. Other mineralogical reactions are likely to contribute to this loss in sample mass. Further investigation is necessary to identify and quantify the mineral changes that are occurring. The changes in particle size distribution can affect larger-scale behaviour of soil such as compaction.

Further fractionation of the sand after heat treatment shows that as temperature increases, fines are recovered across a wider range of size fractions (Table 3). These results show that with increasing temperature the particle size distribution of the sand is extended, which is in accordance with results from thermal desorption tests on sands (Araruna et al., 2004). Based on the same mineralogical composition of fines after the thermal desorption, Araruna et al. (2004) argue that the fines are the product of grains breaking with exposure to higher temperatures. This is a possibility, but not the only explanation that should be considered here. Mobilisation of clay deposits on the sand grains, which would lose their bonds with the sand particles during thermal treatment, may affect the particle size distribution. The potential for clay mobilisation was explored with a set of experiments involving sand–clay mixtures. With moisture, clay was observed to coat the sand grains for temperatures up to 500 °C and that this coating is lost for temperatures above 750 °C (Figure 5). This supports the theory that the bond between the fines and sand grains is lost and that this causes the extension in particle size distribution. This bond appears to be driven by the presence or loss of moisture. It is therefore likely that this effect can occur during thermal and smouldering treatment. At this point, the data are inconclusive to eliminate the potential for breaking of the grains under high temperature, particularly as handling steps release fines into the air as dust, but the clay experiments illustrate the potential that increased fines can result from clay mobilisation.

3.4. Water dynamics

Water dynamics in the sand was measured with two separate but interrelated tests: falling head and capillary rise. These tests were conducted to show how temperature and smouldering affect interaction of silica sand and water. The falling head test results show that heat treatment has a minimal effect on the sand permeability. For the untreated and heat treated samples, the change in head over time follows approximately the same profile. In contrast, the smouldered sample shows a much steeper profile (Figure 6). Water moves much more rapidly through the smouldered sand. The entire column of water disappears into the sand in 7 s and drainage from the column is observed after less than 20s. The delay in the first measurement of head height for the smouldered sand is due to this rapid infiltration. Approximately 50% of the total volume of water infiltrates into the sand as the total volume is delivered to the top of the sand column. In contrast, 17–22% of the total volume of water infiltrates during initial delivery to the other treated and untreated sand columns. In addition, drainage from the smouldered sand is noticeably discoloured with particulates. Channelling is observed in the column and lateral propagation is not evident, though some water is retained in the pore space after infiltration and excavation. These differences in falling head behaviour are not represented in the correlating hydraulic conductivity values, which are on the order of 10^{-4} m/s for all samples (Table 5).

Differences are observed in the capillary rise test when comparing the heat-treated and smouldered sand samples (Table 5). While capillary rise is present in all samples, the capillary rise is lower in the smouldered sample. As the temperature of thermal treatment is increased, the resulting capillary rise after cooling and exposure to the water bath increases as well. Capillary rise is consistent or greater in compacted samples, which may reflect the presence of small clay aggregates in the pore space, which is consistent with the changes observed in particle size distribution. The voids between the grains may have decreased to some extent and therefore caused the capillary forces to increase. In the smouldered sample, the capillary rise in both uncompacted and compacted states is below than that observed in all other samples. This difference suggests greater void spaces between the grains, potentially changed contact angles, and less capillary forces, all of which may be influenced by the mobilisation of fines and other potential changes to the grain surfaces.

Heat treatment showed slight influence on the silica sand pH, which remained slightly alkaline between 7.8 and 8.2 (Table 5). The pH of the sand after smouldering remediation had shifted to slightly acidic. This change in pH is likely to be caused by the coal tar contamination present before smouldering and the chemical reactions that take place during smouldering. Decreased pH is associated with decreased cation exchange capacity in the soil, which is, in turn, linked

Table 4
Particle density, minimum and maximum bulk density, particle size distribution, and mass loss observed in silica sand after exposure to elevated temperatures or smouldering remediation.

Sample	Densities			Sieve analysis							Mass loss
	Particle	Minimum	Maximum	2.36 mm	1.18 mm	600 μm	425 μm	300 μm	212 μm	<212 μm	Sample mass loss
	mg/m³			% retained							%
Untreated	2.68	1.45	1.65	0.2 ± 0.5	94.4 ± 0.7	5.3 ± 0.6	0.00	0.00	0.00	0.00	0.00
105 °C	2.62	1.44	*ND*[a]	*ND*	*ND*	*ND*	*ND*	*ND*	*ND*	*ND*	4.21
250 °C	2.66	1.43	1.67	0.3 ± 0.06	95.5 ± 1.2	4.1 ± 1.2	0.00	0.00	0.00	0.00	4.74
500 °C	2.69	1.45	1.68	0.3 ± 0.04	94.4 ± 0.4	5.6 ± 0.4	0.02 ± 0.001	0.01 ± 0.004	0.00	0.00	5.10
750 °C	2.7	1.44	1.65	*ND*	*ND*	*ND*	*ND*	*ND*	*ND*	*ND*	5.37
1000 °C	2.71	1.45	1.69	0.2 ± 0.03	93.3 ± 0.9	6.2 ± 0.8	0.09 ± 0.0003	0.07 ± 0.004	0.03 ± 0.002	0.06 ± 0.005	5.63
Smouldered	2.68	1.46	1.68	*ND*	*ND*	*ND*	*ND*	*ND*	*ND*	*ND*	*ND*

[a] Not determined (ND).

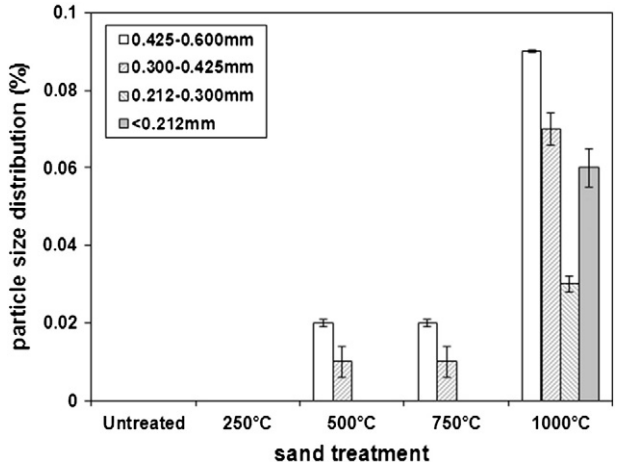

Fig. 4. Mobilisation of particles smaller than 0.600 mm from sand exposed to heat at 250, 500, 750, and 1000 °C. Particles between 0.600 and 2.36 mm make up 99.7–99.9% of the particle size distribution in all cases.

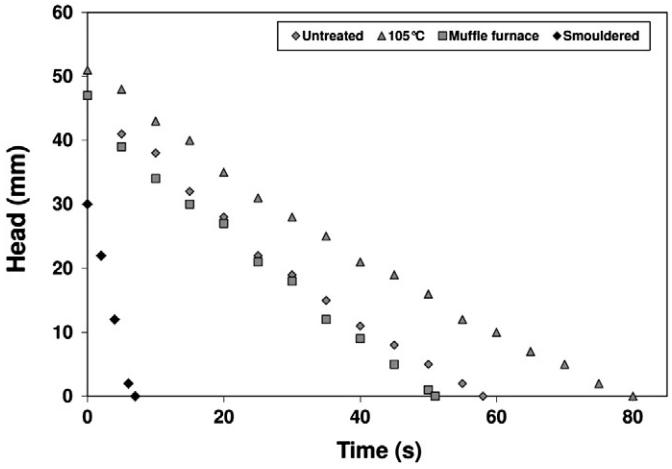

Fig. 6. Head loss (mm) observed over time in untreated sand, heat-treated sand, and sand after contamination with coal tar and smouldering remediation.

to water holding capacity. Based on the heat treatment results, similar effects are expected in soil treated by smouldering remediation, though the presence of organic matter in the soil and its potential melting or destruction during remediation will affect pH as well. Though soil pH affects grain–water interactions, the changes in infiltration cannot be explained by pH change alone, particularly as saturated hydraulic conductivity is not observed to change as a result of high temperature exposure or smouldering remediation (Table 5). Sand after smouldering has small amounts of chemical residue, typically below detection limits (Switzer et al., 2009). The nature and extent of the residue are unknown, which challenges the decoupling of physical and chemical influences on water infiltration. Although hydraulic conductivity was not observed to be affected by heat treatment or smouldering, the mobilisation of fines was apparent in the effluent water of the tests carried out on 750 °C, 1000 °C, and smouldered sands.

3.5. Summary and implications of soil changes

High temperature processes impact the dynamic properties of soils. The results outlined above highlight the sometimes contradictory responses to high temperature exposure, particularly water dynamics. The differences in void spaces do not fully explain the differences that are observed in the falling head infiltration profiles. The changes in mineralogy that are visible in all treated samples through colour change do not correlate to the changes observed in dynamic behaviour as the sand is introduced to water. These results suggest that colour change alone cannot be used as an indicator of potential changes in soil behaviour.

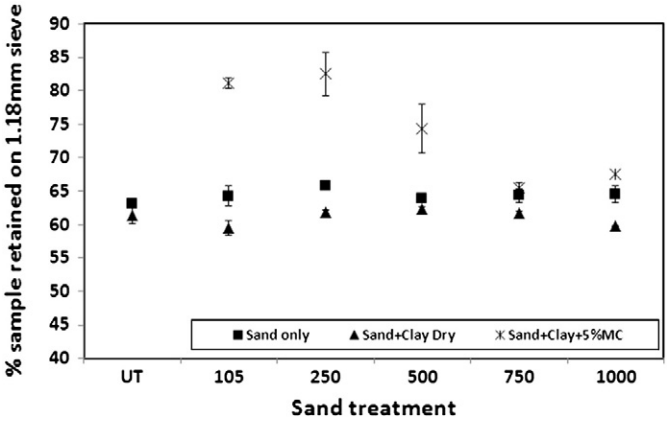

Fig. 5. Percentage of sand and sand/clay sample masses retained on the 1.18 mm sieve after heat treatment and dry sieving.

Mobilisation of fines is a concern in all cases as a loss in soil mass can result in a loss of soil stability. Heat treatment above 500 °C has been shown to weaken and soften sandstones under loading, an effect that is linked to dehydroxylisation of kaolinite (Ranjith et al., 2012). No such effects were observed here, but samples were not subjected to load and all materials were allowed to cool prior to testing. Further testing would be beneficial to explore the effects on soils that are exposed to heat and subjected to loading, particularly in the context of remediation under existing infrastructure. Even though post-remediation soil is affected by reduced water holding capacity and capillary rise, it should still be amenable to stabilisation techniques. The cation exchange reactions of lime stabilisation may be impaired, but other aspects of the remediation process may aid stabilisation. Lime stabilisation has been shown to improve the compressive strength of quartz sand, increased curing time has been shown to enhance this improvement, and elevated temperatures have been shown to enhance curing and ultimate strength achieved (Bell, 1996). Because of their thermal inertia, post-remediation soils are slow to cool. Reductions in lime uptake may be counterbalanced by strategic use of soil stabilisation techniques during the cooling process after remediation, particularly if the installation of new infrastructure after remediation is desired. Further work on the combination of aggressive remediation and soil stabilisation processes would be beneficial to determine if integration of these processes could optimise their benefits.

While further study into the links between changes in micro-scale properties and macro-scale behaviour is needed, this work illustrates the importance of understanding the effects of high temperature processes on fundamental soil properties. Further work can explore extended exposure times more reflective of thermal remediation techniques as well more complex soil compositions. This work suggests that the effects of elevated temperatures on soil properties should be considered as part of remediation planning and mitigation measures may be appropriate in the soil during or after exposure.

4. Conclusions

High temperature exposure in the form of thermal treatment and smouldering remediation results in changes to soil properties. Some links between grain-scale characteristics and dynamic behaviour have been established. After exposure of sand to elevated temperatures, particle size distribution increases and a related increase in capillary rise is observed as well. Water infiltration does not seem to be

Table 5
Capillary rise height, void ratio, saturated hydraulic conductivity, and pH values for silica sand retained on the 1.18 mm sieve.

Sample	Capillary rise height (mm)		Void ratio		Hydraulic conductivity K (m/s)	pH
	Uncompacted	Compacted	Uncompacted	Compacted		
Untreated	20.63 ± 4.13	20.63 ± 1.38	0.67	0.63	$9.6 \pm 0.6 \times 10^{-4}$	8.2
105 °C	20.63 ± 4.13	20.63 ± 1.38	0.66	0.63	$7.0 \pm 0.5 \times 10^{-4}$	8.1
250 °C	22.00 ± 0.00	23.38 ± 2.37	0.67	0.64	$5.2 \pm 0.7 \times 10^{-4}$	8.0
500 °C	22.00 ± 2.75	23.38 ± 1.59	0.67	0.68	$5.5 \pm 0.7 \times 10^{-4}$	7.8
750 °C	23.38 ± 1.27	23.38 ± 1.59	0.67	0.64	$5.0 \pm 0.6 \times 10^{-4}$	7.9
1000 °C	22.63 ± 0.00	26.13 ± 1.38	0.67	0.61	$5.0 \pm 1.0 \times 10^{-4}$	7.8
Smouldered	16.50 ± 3.50	19.25 ± 0.00	0.70	0.63	$7.3 \pm 0.4 \times 10^{-4}$	6.1

affected by elevated temperature, though this observation may be a function of exposure duration. Sand exposed to smouldering remediation exhibits more rapid water infiltration from the surface. Changes in mineralogy are visible in all treated samples in the form of colour change as goethite is oxidised to hematite. Changes to the quartz crystal structures are observed at an exposure temperature of 1000 °C. Colour change alone cannot be used as an indicator of potential changes in soil behaviour. Mass loss increases with increasing temperature and may be related to the mineralogical processes such as the dehydration of iron oxides, mobilisation of fines, and changes in quartz structure. Smouldering treatment has similar effects, perhaps more rapidly due to the higher temperatures achieved. In contrast to these results, thermal and smouldering treatments show minimal effects on silica sand particle and bulk densities. The changes in soil properties may result in altered dynamics between soil aggregates in the field. The effects of high temperature remediation on field soils are anticipated to be more complex as other soil fractions may be more susceptible to heating effects. Further investigation of the effects of high temperature exposure on soil fractions and whole soils, especially from field sites where aggressive remediation processes have been applied, is necessary to fully understand the impact of these processes on soils. After exposure to high temperature or smouldering remediation, soils should remain amenable to improvement with soil amendments. Follow-up investigation and monitoring after exposure is important to understand the extent of impacts and mitigation measures that may be necessary.

Acknowledgements

The authors gratefully acknowledge financial support of the University of Strathclyde in the form of a Faculty Scholarship for Ms Zihms as well as the valuable assistance from colleagues at the Universities of Strathclyde, Glasgow, Edinburgh, and Western Ontario as well as SiREM. In particular, we wish to thank Peter Chung for his assistance with the Raman analysis and Ross Blake and Ursula Skordou for their help with some of the physical characterisation tests. Smouldering combustion of liquids is a patented remediation process (PCT Application PCT/GB2006/004591 priority date 10 December 2005 (awarded in the USA as US/8132987) and PCT/US2012/035248—priority date 29 April 2011).

References

Araruna Jr., J.T., Portes, V.L.O., Soares, A.P.L., Silva, M.G., Sthel, M.S., Schramm, D.U., Tibana, S., Vargas, H., 2004. Oil spills debris clean up by thermal desorption. Journal of Hazardous Materials 110 (1–3), 161–171.

Are, K.S., Oluwatsin, G.A., Adeyolanu, O.D., Oke, A.O., 2009. Slash and burn effect on soil quality of an Alfisol: soil physical properties. Soil and Tillage Research 103 (1), 4–10.

Bell, F.G., 1996. Lime stabilization of clay minerals and soils. Engineering Geology 42 (4), 223–237.

Certini, G., 2005. Effects of fire on properties of forest soils: a review. Oecologia 143 (1), 1–10.

Chang, T.C., Yen, J.H., 2006. On-site mercury-contaminated soils remediation by using thermal desorption technology. Journal of Hazardous Materials 128 (2–3), 208–217.

De Bruyn, D., Thimus, J.F., 1996. The influence of temperature on mechanical characteristics of Boom clay: the results of an initial laboratory programme. Engineering Geology 41 (1–4), 117–126.

DeBano, L.F., 1981. Water repellent soils: a state-of-the-art. Pacific Southwest Forest and Range Experiment Station. General Technical Report PSW-46.

DeBano, L.F., 2000. The role of fire and soil heating on water repellency in wildland environments: a review. Journal of Hydrology 231, 195–206.

Gan, S., Lau, E.V., Ng, H.K., 2009. Remediation of soils contaminated with polycyclic aromatic hydrocarbons (PAHs). Journal of Hazardous Materials 172 (2–3), 532–549.

Goforth, B.R., Graham, R.C., Hubbert, K.R., Zanner, C.W., Minnich, R.A., 2005. Spatial distribution and properties of ash and thermally altered soils after high-severity forest fire, southern California. International Journal of Wildland Fire 14 (4), 343–354.

Hand, R.J., Stevens, S.J., Sharp, J.H., 1998. Characterisation of fired silicas. Thermochimica Acta 318 (1–2), 115–123.

Ketterings, Q.M., Bigham, J.M., 2000. Soil color as an indicator of slash-and-burn fire severity and soil fertility in Sumatra, Indonesia. Soil Science Society of America Journal 64 (5), 1826–1833.

Khamehchiyan, M., Hossein Charkhabi, A., Tajik, M., 2007. Effects of crude oil contamination on geotechnical properties of clayey and sandy soils. Engineering Geology 89 (3–4), 220–229.

Komorida, Y., et al., 2010. Effects of pressure on maghemite nanoparticles with a core/shell structure. Journal of Magnetism and Magnetic Materials 322 (15), 2117–2126.

Kronholm, J., Kalpala, J., Hartonen, K., Riekkola, M.-L., 2002. Pressurized hot water extraction coupled with supercritical water oxidation in remediation of sand and soil containing PAHs. Journal of Supercritical Fluids 23 (2), 123–134.

Lee, W.-J., et al., Shih, S.-I., Chang, C.-Y., Lai, Y.-C., Wang, L.-C., Chang-Chien, G.-P., 2008. Thermal treatment of polychlorinated dibenzo-p-dioxins and dibenzofurans from contaminated soils. Journal of Hazardous Materials 160 (1), 220–227.

Mataix-Solera, J., Doerr, S.H., 2004. Hydrophobicity and aggregate stability in calcareous topsoils from fire-affected pine forests in southeastern Spain. Geoderma 118 (1–2), 77–88.

McGowan, T.F., Greer, B.A., Lawless, M., 1996. Thermal treatment and non-thermal technologies for remediation of manufactured gas plant sites. Waste Management 16 (8), 691–698.

Mollah, M.Y.A., Promreuk, S., Schennach, R., Cocke, D.L., Güler, R., 1999. Cristobalite formation from thermal treatment of Texas lignite fly ash. Fuel 78 (11), 1277–1282.

Pironi, P., et al., Switzer, C., Rein, G., Fuentes, A., Gerhard, J.I., Torero, J.L., 2009. Small-scale forward smouldering experiments for remediation of coal tar in inert media. Proceedings of the Combustion Institute 32, 1957–1964.

Pironi, P., Switzer, C., Gerhard, J.I., Rein, G., Torero, J.L., 2011. Self-sustaining smoldering combustion for NAPL remediation: laboratory evaluation of process sensitivity to key parameters. Environmental Science & Technology 45 (7), 2980–2986.

Pomiès, M.P., Morin, G., Vignaud, C., 1998. XRD study of the goethite–hematite transformation: application to the identification of heated prehistoric pigments. European Journal of Solid State and Inorganic Chemistry 35 (1), 9–25.

Ranjith, P.G., Viete, D.R., Chen, B.J., Perera, M.S.A., 2012. Transformation plasticity and the effect of temperature on the mechanical behaviour of Hawkesbury sandstone at atmospheric pressure. Engineering Geology 151, 120–127.

Rein, G., 2009. Smouldering combustion phenomena in science and technology. International Review of Chemical Engineering 1, 3–18.

Rein, G., Cleaver, N., Ashton, C., Pironi, P., Torero, J.L., 2008. The severity of smouldering peat fires and damage to the forest soil. Catena 74 (3), 304–309.

Robichaud, P.R., Hungerford, R.D., 2000. Water repellency by laboratory burning of four northern Rocky Mountain forest soils. Journal of Hydrology 231, 207–219.

Switzer, C., Pironi, P., Gerhard, J.I., Rein, G., Torero, J.L., 2009. Self-sustaining smoldering combustion: a novel remediation process for non-aqueous-phase liquids in porous media. Environmental Science & Technology 43 (15), 5871–5877.

Tan, Ö., Yilmaz, L., Zaimoglu, A.S., 2004. Variation of some engineering properties of clays with heat treatment. Materials Letters 58 (7–8), 1176–1179.

Tang, C.-S., Cui, Y.-J., Tang, A.-M., Shi, B., 2010. Experiment evidence on the temperature dependence of desiccation cracking behavior of clayey soils. Engineering Geology 114 (3–4), 261–266.

Terefe, T., Mariscal-Sancho, I., Peregrina, F., Espejo, R., 2008. Influence of heating on various properties of six Mediterranean soils. A laboratory study. Geoderma 143 (3–4), 273–280.

Webb, S.W., Phelan, J.M., 1997. Effect of soil layering on NAPL removal behavior in soil-heated vapor extraction. Journal of Contaminant Hydrology 27 (3–4), 285–308.

Wenk, H.-R., Bulakh, A., 2004. Minerals Their Constitution and Origin. Cambridge University Press.

Understanding the Effects of High Temperature Processes on the Engineering Properties of Soils

Comprendre les effets des procédés a haute température sur les propriétés des sols

S.G. Zihms, C. Switzer, M. Karstunen and A. Tarantino
University of Strathclyde, Glasgow, United Kingdom

ABSTRACT: High temperature processes such as in situ smouldering and thermal remediation techniques can achieve rapid removal of organic contaminants from soils in much shorter time periods than traditional remediation technologies. Thermal remediation processes use heat or heated water to volatilise the contaminant within the soil to enable its extraction. High temperatures affect the particle size distribution, mass loss, mineralogy and permeability of the soil. In sandy soils, the particle size decreases with increasing temperature due to a mobilisation of fines, which is likely due to the bond of fines to the sand grains being affected by temperature. In clayey soils, the overall particle size increases with increasing temperature due to aggregation and cementation of the clay fraction. Permeability seems to be affected by treatment type rather than temperature alone, comparing heat treated and smouldered samples showed an increase of sand permeability by approximately two magnitudes. This study illustrates the effects of high temperature and smouldering processes on soil characteristics and dynamic behaviour. Monitoring during and after aggressive remediation is advisable so that rehabilitation measures can be implemented before site redevelopment.

RÉSUMÉ : Des procédés a haute température tels que la combustion lente in situ et des techniques de traitement thermique peuvent achever une élimination rapide des contaminants organiques des sols en beaucoup moins de temps que les technologies de traitement traditionnelles. Les procédés de traitement thermique utilisent la chaleur ou de l'eau chauffée pour vaporiser les contaminants dans le sol pour permettre leur extraction. Des températures élevées affectent la distribution granulométrique, la perte de masse, la minéralogie et la perméabilité du sol. Dans les sols sablonneux, la taille des particules décroît avec l'augmentation de température due à une mobilisation des particules les plus fines, probablement dû à la liaison de ces particules aux grains de sable, affectée par la température. Dans les sols argileux, la taille des particules augmente avec l'augmentation de température due à l'agrégation et la cimentation de la fraction argileuse. La perméabilité semble être affectée par le type de traitement plutôt que par la température uniquement, des échantillons traités par la chaleur ont montré une augmentation de la perméabilité du sable d'environ deux ordres de grandeur par rapport à ceux traités par combustion lente.Cette étude montre les effets des températures élevées et des procédés de combustion lente sur les caractéristiques du sol et sur son comportement dynamique. Il est conseillé d'utiliser un système de surveillance pendant et après traitement agressif afin que les mesures de réhabilitation puissent être appliquées avant le réaménagement du site.

KEYWORDS: Thermal behaviour of soils, smouldering remediation, high temperature

1. INTRODUCTION

Soils can be exposed to elevated temperatures naturally through wild, forest or peat fires or through thermal remediation processes designed to mitigate contamination by hazardous organic chemicals. Most research on soil properties and their heat dependency is based on forest fires and therefore concentrates on erosion rates, ground stability and nutrients affected by fire severity. The effects of exposure to temperatures up to 500°C have been studied widely (*1-4*). Literature published on heat treatments of clay evaluates the effects of temperatures up to 1000°C (*5*). Exposures of 200 – 850°C have been observed in soils during wildfires (*2, 3, 6, 7*). Moderate (300-400°C) and high (>450°C) temperature processes, such as hot water extraction, thermal desorption, soil heated vapour extraction, incineration or smouldering are used widely to treat contaminated soils (*8-17*). Most research on soil remediation techniques focuses on the remediation result and less on the effects the process has on the soil properties itself. In some cases, the effects on soil properties may be a criterion for selection of the remediation technique (*13, 15*) or the soil properties may influence the results (*10*). There is little research on the effects of thermal remediation processes on soil properties (*9, 17*). Based on the observations of soil erosion and subsidence after wildfires, further understanding of the effects of high temperature remediation processes must be developed.

The maximum temperatures observed in contaminant remediation vary by the process that is used. With the exception of smouldering remediation, all of these remediation techniques use heat or heated water to volatilise the contaminant within the soil to enable its extraction. Maximum temperatures for these technologies are typically adjacent to the heat source with more moderate target temperatures of 80-100°C achieved within the wider treatment zone. The contaminant must be collected and treated (*10-12, 14-16*). These processes maintain high temperatures in the soil for weeks to months or longer. In contrast, smouldering remediation uses the contaminant itself as fuel for the combustion reaction (*8, 9, 13*). In laboratory studies, the soil particles are exposed to high temperatures on the order of 1000°C for coal tars and 600-800°C for oils for up to 60 minutes. Field scale efforts may result in exposure durations on the order of hours or longer.

Elevated temperatures have been shown to alter the mineralogical composition of soil. These effects have been studied extensively in relation to the effects of wildfires on soil properties. Colour change in soils has been observed after wildfire and after smouldering remediation. In most cases it

changes from yellowish brown to reddish brown. This is due to the oxidation of soil iron content from goethite to maghemite or hematite (*18, 19*). Decomposition of soil particles, especially clay minerals, starts at temperatures above 550°C (*2*). These temperatures are rarely reported for wild and forest fire, but temperatures up to 1200°C can be achieved during smouldering remediation (*8, 9*).

This study aims to characterise the effects of moderate and high temperatures as well as smouldering on soil properties to determine the impact changes will have to the soil and predict possible complications that may arise during or after remediation treatment. Silica sand and kaolin clay are used as constituents of a synthesised simple soil. Clean untreated, heat-treated and contaminated/smouldered materials are evaluated to determine the impacts of the treatment conditions on soil properties.

2. MATERIALS AND METHODS

Coarse silica sand (Leighton Buzzard 8/16, Sibelco, Sandbach, UK) and kaolin clay (Whitchem Ltd, UK) were used as the base soil for all of the experiments. The sand contains 99% silicon-dioxide, has a mean grain size of 1.34 and a bulk density of 1.7g/cm^3 (*8*). The sand and clay were accepted as received and the sand was subjected to the same pre-treatment. A programmable muffle furnace (Nabertherm L9/11/SKM, Nabertherm GmbH, Lilienthal, Germany) was used for all heating experiments. The sands evaluated after smouldering remediation were prepared in a 3m^3 experiment involving coal tar mixed with coarse sand. The initial concentration of this mixture was 31000 ± 14000 mg/kg total extractable petroleum hydrocarbons before treatment and the average concentration after smouldering remediation across the majority of the vessel was 10 ± 4 mg/kg (*9*).

2.1 Sample Preparation and Heat Treatment

The silica sand was washed and wet sieved using a 425µm screen to eliminate any loose fines and air dried for several days. In case of mixed samples the dried silica sand was mixed with 10% mass kaolin clay and 5% moisture content before being heat treated. For each test, the required amount of samples was heated in the furnace following the heat treatment programmes listed in Table 2.

Table 1. Heat treatment programs

Sample Name	Pre-heating time (min)	Peak temperature for 60min	cooling down time (min)
Untreated			
105	**30**	**105°C (24h)**	**0**
250	**30**	**250°C**	**0**
500	**30**	**500°C**	**~ 60**
750	**60**	**750°C**	**~ 180**
1000	**60**	**1000°C**	**~ 240**

After the required exposure duration, the samples were removed from the muffle furnace and placed in a desiccator to cool. Samples heated to temperatures above 500°C were allowed to cool in the furnace to 200°C before transfer to the desiccator.

2.2 Laboratory Testing

Particle density was measured using the gas-jar method suitable for coarse soils. Minimum density was measured using 1000g of sand in a 1Ll glass measuring cylinder with 20mL graduation BS1377-2:1990 and BS1377-4:1990). Maximum density was determined using the vibrating hammer method (BS1377-4:199). Particle size distribution for the sand was determined using a sieving method (BS1377-2:1990) using1.18mm, 600µm, 425µm, 300µm and 212µm sieve sizes. The Atterberg Limits for the clay were determined using the cone penetration and rolling methods as outlined in BS1377-2:1990.

The sand-clay mixtures were prepared by dry-mixing 90% sand and 10% clay (by mass) and then adding distilled water to achieve a 5% moisture content. The sample was the thoroughly kneaded in a plastic bag by hand for 10 minutes and allowed to rest for 2 hours before any heat treatment.

3. RESULTS AND DISCUSSION

3.1. Mineralogy

During the heat treatment testing and after smouldering remediation, a colour change of the silica sand was observed (Figure 1). Exposure of this material to high temperatures results in colour change from yellowish brown to reddish brown with increasing temperature for the silica sand grains and a change from yellow to pinkish red for the crushed silica sand. This colour change is associated with the dehydration reaction of goethite with increasing temperatures to form hematite or maghemite. During the dehydration, the density of the iron-hydroxide increases from 4.3 mg/m^3 for goethite to 5.2 mg/m^3 for hematite (*20*). The sand is comprised primarily of silicon dioxide; iron oxides make up a small fraction of its composition. High temperatures may cause additional changes in mineralogy that may be less likely to be detected by visual examination (*18, 21*). For example, silicon dioxide becomes unstable with high temperatures and forms silica polymorphs such as trydimite or cristobalite (*20, 22*). Thermal treatments (100-1200°C) on fly ash have transformed quartz minerals to cristobalite and smaller particles exhibit a characteristic glassy composition due their faster cooling time (*23*).

Figure 1. Silica Sand grains and crushes grains after heat treatment

During testing that required the addition of distilled water, the clay was observed to discolour in the mixed samples, but the distilled water stayed clear (Figure 2). This is very likely associated with the iron oxidation reaction described above. It is possible that this surface reaction enables some of the iron oxides to become mobile and attach themselves onto the clay particles causing this discolouration (*24*). In the clay-only samples, slight colour changes from white to greyish white were observed. In the smouldered samples for 10% clay and 20% clay mixtures with sand, the colour change was to a darker grey than the heat-only samples. This colour change was likely influenced by staining from the coal tar as well as the inherent colour change of the kaolin.

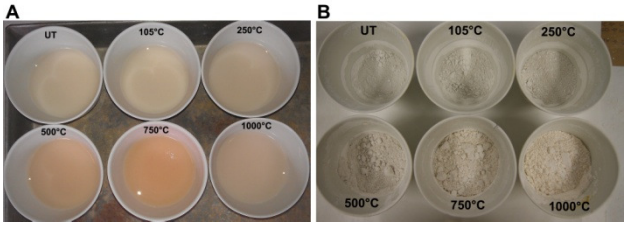

Figure 2. A:Kaolin clay (sand-clay mixture) fraction after heat treatment; B: Kaolin only after heat treatment

3.2. Particle Size Distribution and Densities

In contrast to mineralogy, elevated temperatures did not seem to affect the particle density or minimum/maximum bulk densities of the silica sand. No real relationship was apparent between treatment temperature and density. For the particle density, the values are consistently near 2.65mg/m^3, which is a value that is widely used in geotechnical engineering calculations. The maximum and minimum densities are equally unaffected by heat treatment or smouldering. These observations are not consistent with the literature on wild and forest fire effects on soil properties, which suggests that bulk density would increase with temperature (*1, 2*). The lack of organic matter may explain the contrast. The results in this study, which show no significant change in density, suggest that the changes in soil density that are observed after wildfires are associated primarily with effects on organic matter and potentially the smaller silt and clay–sized particles.

Heat treatment has a small but appreciable effect on particle size distribution. As exposure temperature increases from 250 to 1000°C, the sample retained on the 1.18mm sieve increases. The variation in particle size distribution may be linked to the loss of mass beyond the initial moisture content. As temperature increases, mass loss increases. Although there is a dehydration reaction from goethite to hematite in the sand, the fraction of iron oxide relative to the total composition of the sand is too small for this reaction alone to account for the whole additional mass loss. For the silica sand kaolin clay mixture the trend is slightly different (Table 3). The sample retained on the 1.18mm sieve increases very slightly for 250°C, followed by an overall decrease for 250, 500, 750 and 1000°C. For 105 and 250°C the clay coats the sand grains allowing them to be retained on the 1.18mm sieve, for temperatures above 500°C this coating is destroyed resulting in less sample being retained. The coating effect increases the sand fraction >1.18mm by 7 to 16% compared to the higher temperature samples. This is not an increase in the sand fraction but an increase in grains the size of this fraction due to the additional clay coating. This coating could have an impact on the permeability and shear behaviour of these lower temperature samples after heat treatment depending on how easily it can be destroyed or removed by grain interaction or interaction with water.

Table 2. Sieve analysis results for silica sand – 10% kaolin clay mixtures (5% MC) for different heat treatments

Sample	SIEVE ANALYSIS	
	1.18mm	<1.18mm
	% retained	
105	81.8 ± 1.9	18.2 ± 2.1
250	82.7 ± 0.8	17.3 ± 1.0
500	74.5 ± 3.2	25.5 ± 3.6
750	65.6 ± 3.6	34.4 ± 3.7
1000	67.7 ± 0.8	32.3 ± 1.5

3.3. Atterberg Limits for kaolin clay

High temperature processes impact the dynamic properties of soils, particularly liquid and plastic limits at the highest temperatures. This impact on the clay fraction can lead to changes in dynamic behaviour for the clay – sand mixtures. The Atterberg limits for the temperature treatment up to 500°C are similar, especially the liquid limits are all within 64±2%, where the liquid limit for 750°C increases to 81% (Table 3) and this clay has a very high plasticity range compared to the lower temperatures. This is likely due to the increased dehydration of the clay at this temperature. These results are in contrast to Tan et al (2004) (*5*) who recorded an decrease in both liquid and plastic limits with increasing temperature treatment, including non-plastic behaviour for the clays above 400°C. This difference in behaviour can be two-fold. Firstly it can an affect based on the state of the tested sample, especially in regards to initial moisture content. Tan et al (5) uses over consolidated natural clays from Turkey, where this study investigated commercial loose kaolin powder with no moisture content. Secondly, the behaviour can be based on the main mineral contained in the sample, montmorillonite (2:1 clay) for the natural clays from Turkey compared to kaolinite (1:1 clay) for the commercial powder samples. Kaolininte does not swell in the presence of water whereas montmorillonite does swell. Based on this distinction, the responses of montmorillonite and other swelling clays to heat treatment may be different from the responses of kaolinite. Further work is necessary to explore the responses of montmorillonite and other clay minerals during thermal and smouldering remediation processes. The liquid limit test for the sample treated at 1000°C was not possible due to the clay not mixing properly with the water and behaving slightly non-newtonian, which means as the mixing motion stopped the sample liquefied and it was impossible to create a testable sample. Initially, the clay mixed well with the water and it was possible to produce a paste but with increasing water content the behaviour changed and the sample only stayed solid under a constant mixing motion, after stopping the mixing the sample quickly liquefied and dispersed. Storage in a sealed container did not yield different results. In contrast to the other samples (105-750°C treatments), no clay paste was formed. Instead, a stiff clay layer formed at the bottom of the bag with an overlying layer of clean water (Figure 3). This is an unexpected behaviour of the clay and no explanation has been found in the literature. It is likely that the temperature of 1000°C causes de-hydroxylation of the clay minerals, followed by aggregation of the particles and sintering (*25*). The net result is that the kaolin particles seem to become hydrophobic. The induced hydrophobicity will affect dynamic properties of the soil such as grain-grain and grain-water interactions.

Table 3. Atterberg Limits and BSCS for kaolin clay for different treatment temperatures

Sample	Liquid Limit w_L	Plastic Limit w_P	Plasticity Index I_p	Plasticity Chart Classification
	%			
105°C	64.4	35.9	28.5	MH: silt, high plasticity
250°C	63.7	30.8	32.9	CH: clay, high plasticity
500°C	65.2	42.7	22.6	MH: silt, high plasticity
750°C	81.6	57.4	24.1	MV: silt, very high plasticity
1000°C	*ND*[1]	*ND*	*ND*	*ND*

[1]: Not determined

In swelling clays, the effects are expected to be similar to those observed in kaolinite, though based on previous work (5), the shift toward hydrophobic particles may occur at lower temperatures. Because other clays are swelling, the effects of the dehydration and melting reactions are expected to have more substantial effects on clay volume as well as grain-grain and grain-water interactions. This work has demonstrated that high temperature remediation processes may have significant, long-term effects on soil properties and these effects must be taken into account as part of a holistic approach to aggressive, high-temperature soil remediation.

Figure 3. Kaolin clay after 1000°C treatment

4. CONCLUSIONS

High temperature exposure in the form of thermal treatment and smouldering remediation result in changes to soil properties. These changes are very likely to affect dynamic behaviour such as infiltration, permeability and shear behaviour. The impact appears to be different depending on the sample composition, sand only or sand-clay mixtures. This is due to the mineralogical composition and grain size of these two soil components. This study shows that some results are in contrasts to similar tests (kaolin compared to natural clays from Turkey) and this highlights the complexity of soils and their behaviour. This study gives a good insight into possible changes due to thermal or smouldering treatment. It shows that even lower temperatures (<500°C) can have an impact on the soil, especially on the clay-sand mixture samples. The observed coating of sand particles by clay can impact the infiltration and shear behaviour of the sample. If the coating can be easily removed than this can affect the structure of the sample and in turn weaken the sample or cause collapse after infiltration. This coating can also protect the sand grains from further impact by heat treatment and stabilise the sample. Further analysis is required to fully understand the effect of the clay coating and its stability. The change of Atterberg limits for the kaolin clay with increasing temperature shows that very high temperatures (1000°C) can severely change the behaviour of the soil. Further testing with other clays is necessary to fully understand the relationship between mineralogy and Atterberg Limits.

References

1. K. S. Are, G. A. Oluwatosin, O. D. Adeyolanu, A. O. Oke, *Soil and Tillage Research* **103**, 4 (2009).
2. G. Certini, *Oecologia* **143**, 1 (2005).
3. G. Rein, N. Cleaver, C. Ashton, P. Pironi, J. L. Torero, *CATENA* **74**, 304 (2008).
4. G. Rein, *International Review of Chemical Engineering* **1**, 3 (January 2009, 2009).
5. Ö. Tan, L. Yilmaz, A. S. Zaimoglu, *Materials Letters* **58**, 1176 (2004).
6. J. Mataix-Solera, S. H. Doerr, *Geoderma* **118**, 77 (2004).
7. L. F. DeBano, *Journal of Hydrology* **231**, 195 (2000).
8. C. Switzer, P. Pironi, J. I. Gerhard, G. Rein, J. L. Torero, *Environmental Science & Technology* **43**, 5871 (2009).
9. P. Pironi *et al.*, *Proceedings of the Combustion Institute* **32**, 1957 (2009).
10. S. W. Webb, J. M. Phelan, *Journal of Contaminant Hydrology* **27**, 285 (1997).
11. S. Gan, E. V. Lau, H. K. Ng, *Journal of Hazardous Materials* **172**, 532 (2009).
12. J. Kronholm, J. Kalpala, K. Hartonen, M.-L. Riekkola, *The Journal of Supercritical Fluids* **23**, 123 (2002).
13. P. Pironi, C. Switzer, J. I. Gerhard, G. Rein, J. L. Torero, *Environmental Science & Technology* **45**, 2980 (2011/04/01, 2011).
14. W.-J. Lee *et al.*, *Journal of Hazardous Materials* **160**, 220 (2008).
15. T. C. Chang, J. H. Yen, *Journal of Hazardous Materials* **128**, 208 (2006).
16. T. F. McGowan, B. A. Greer, M. Lawless, *Waste Management* **16**, 691 (1996).
17. J. T. Araruna Jr *et al.*, *Journal of Hazardous Materials* **110**, 161 (2004).
18. B. R. Goforth, R. C. Graham, K. R. Hubbert, C. W. Zanner, R. A. Minnich, *International Journal of Wildland Fire* **14**, 343 (2005).
19. Q. M. Ketterings, J. M. Bigham, *Soil Science Society of America Journal* **64**, 1826 (2000).
20. H.-R. Wenk, A. Bulakh, *Cambridge University Press*, (2004).
21. M. P. Pomiès, G. Morin, C. Vignaud, *European Journal of Solid State and Inorganic Chemistry* **35**, 9 (1998).
22. R. J. Hand, S. J. Stevens, J. H. Sharp, *Thermochimica Acta* **318**, 115 (1998).
23. M. Y. A. Mollah, S. Promreuk, R. Schennach, D. L. Cocke, R. Güler, *Fuel* **78**, 1277 (1999).
24. S. Zhang *et al.*, *Journal of Contaminant Hydrology* **124**, 57 (2011).
25. B. Fabbri, S. Gualtieri, C. Leonardi, *Applied Clay Science*.

APPENDIX B

B.1 Shear box data sets used in analysis for silica sand and silica sand + 10% kaolin

B.2 Discarded Shear box data sets for silica sand and silica sand + 10% kaolin

SILICA SAND

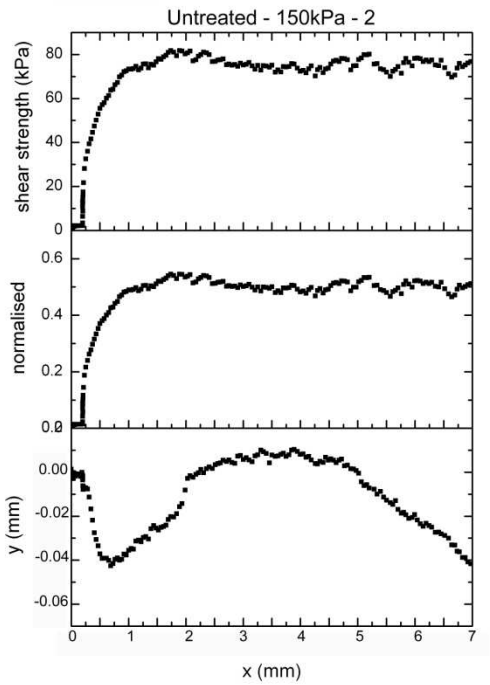
Untreated - 150kPa - 2
shear strength (kPa)
normalised
y (mm)
x (mm)

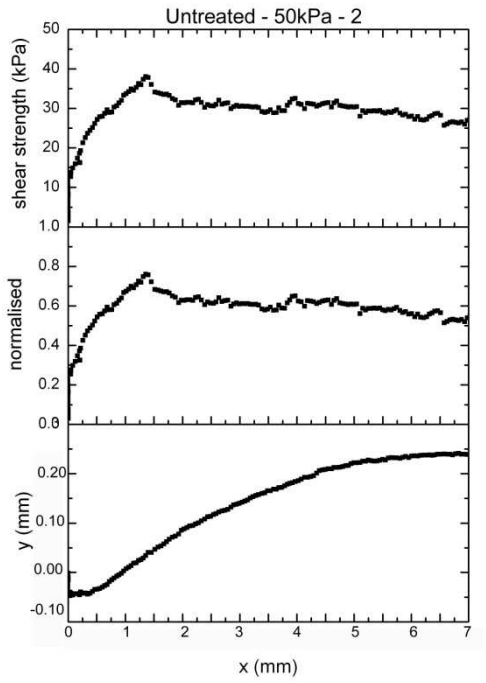
Untreated - 50kPa - 2
shear strength (kPa)
normalised
y (mm)
x (mm)

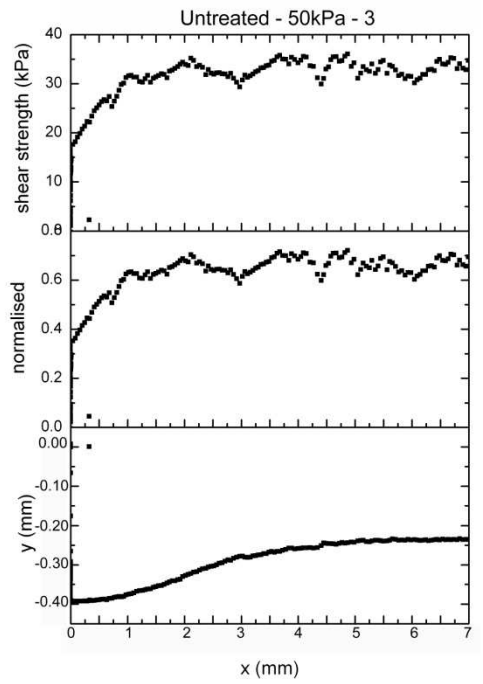
Untreated - 50kPa - 3
shear strength (kPa)
normalised
y (mm)
x (mm)

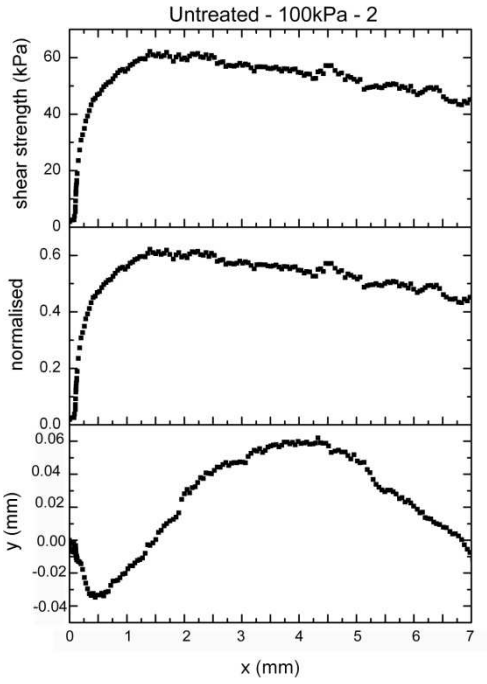
Untreated - 100kPa - 2
shear strength (kPa)
normalised
y (mm)
x (mm)

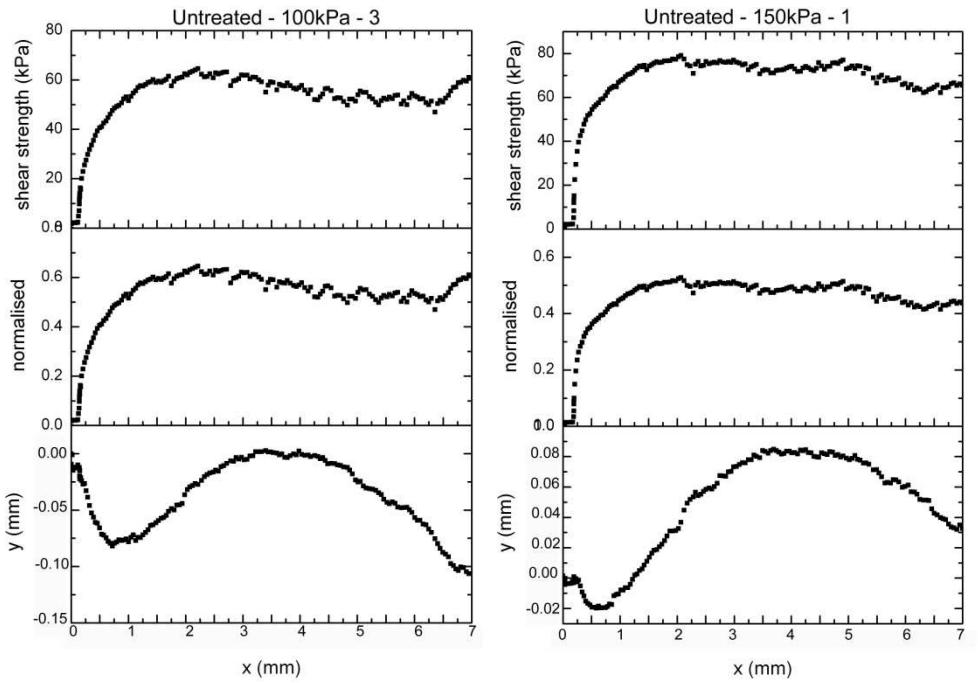
Untreated - 100kPa - 3
Untreated - 150kPa - 1
shear strength (kPa)
normalised
y (mm)
x (mm)

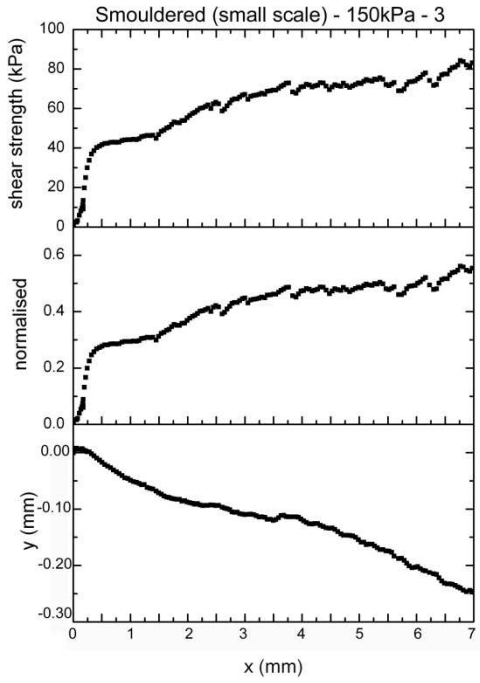
Smouldered (small scale) - 150kPa - 3
shear strength (kPa)
normalised
y (mm)
x (mm)

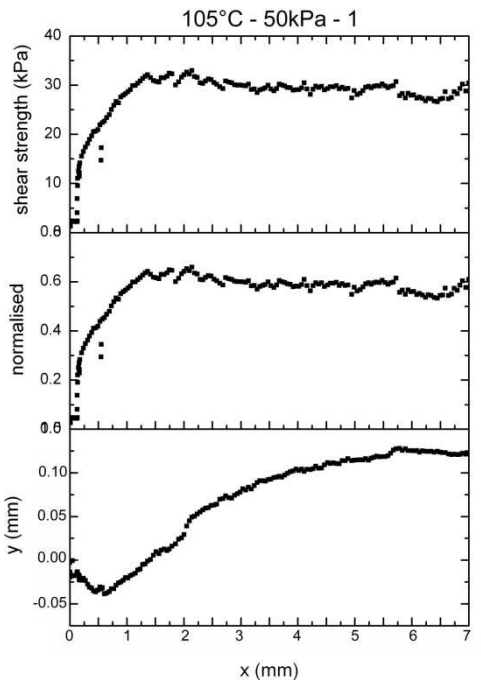
105°C - 50kPa - 1
shear strength (kPa)
normalised
y (mm)
x (mm)

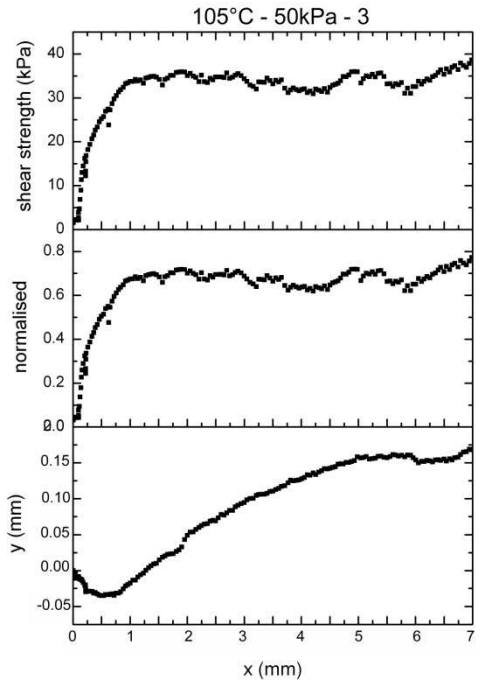
105°C - 50kPa - 3
shear strength (kPa)
normalised
y (mm)
x (mm)

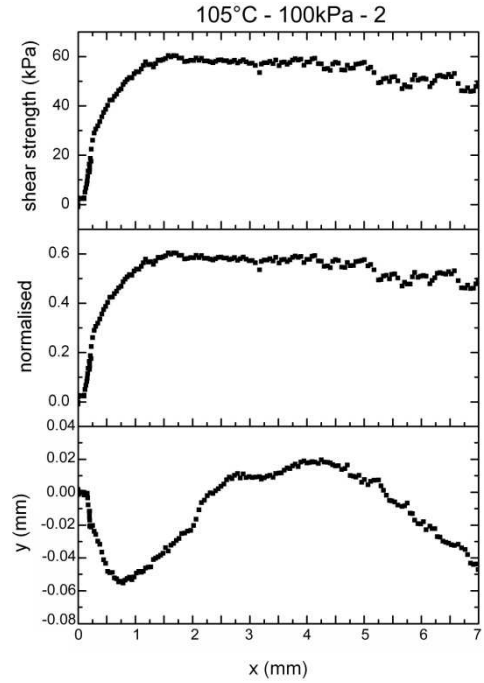
105°C - 100kPa - 2
shear strength (kPa)
normalised
y (mm)
x (mm)

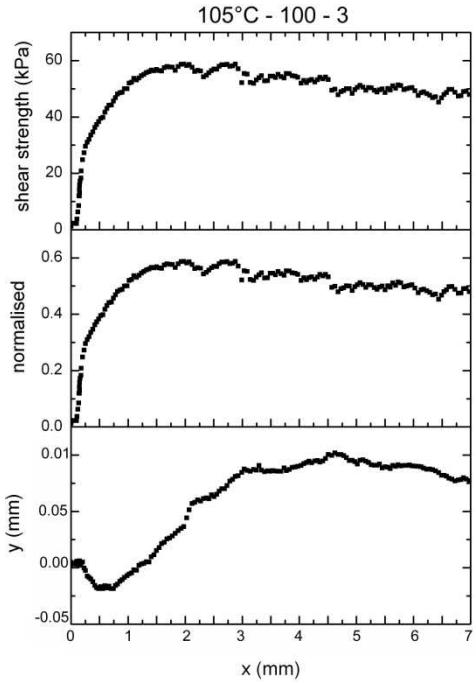
105°C - 100 - 3
shear strength (kPa)
normalised
y (mm)
x (mm)

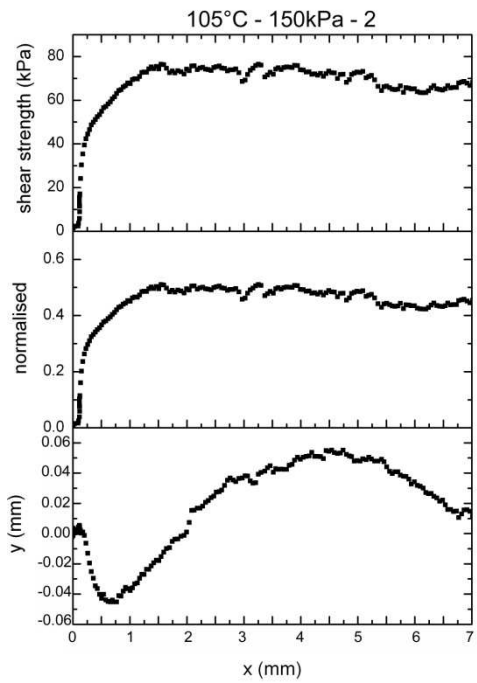
105°C - 150kPa - 2
shear strength (kPa)
normalised
y (mm)
x (mm)

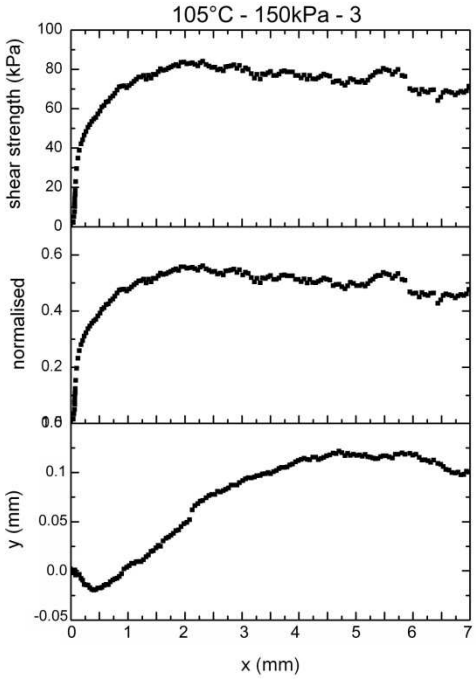
105°C - 150kPa - 3
shear strength (kPa)
normalised
y (mm)
x (mm)

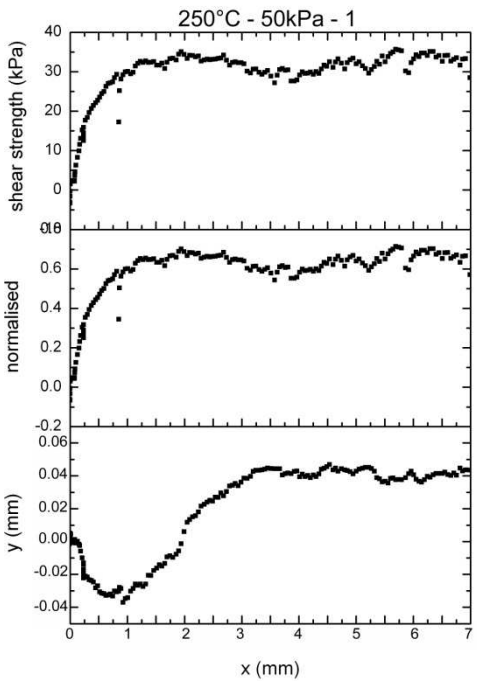
250°C - 50kPa - 1
shear strength (kPa)
normalised
y (mm)
x (mm)

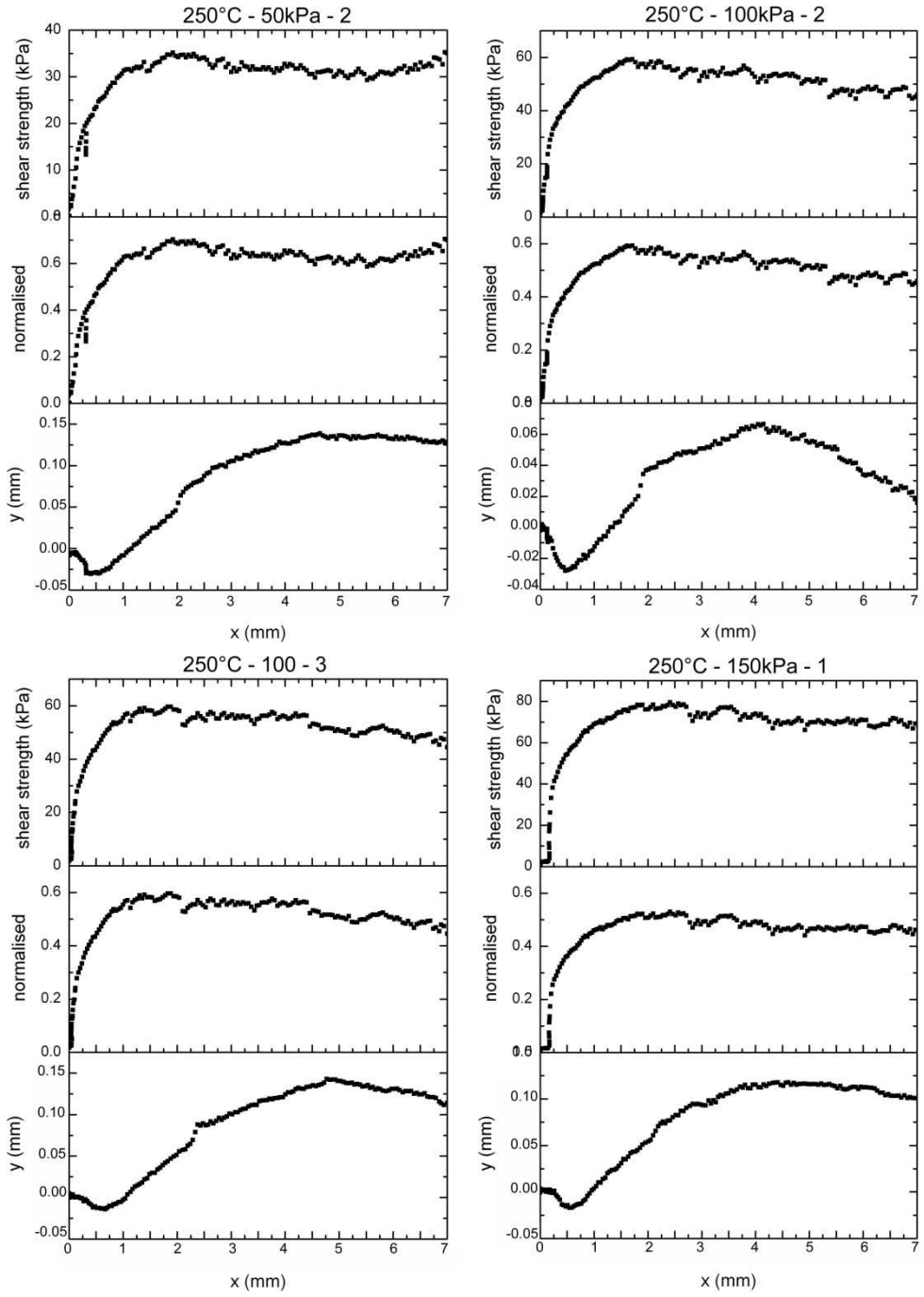
250°C - 50kPa - 2
250°C - 100kPa - 2
250°C - 100 - 3
250°C - 150kPa - 1
shear strength (kPa)
normalised
y (mm)
x (mm)

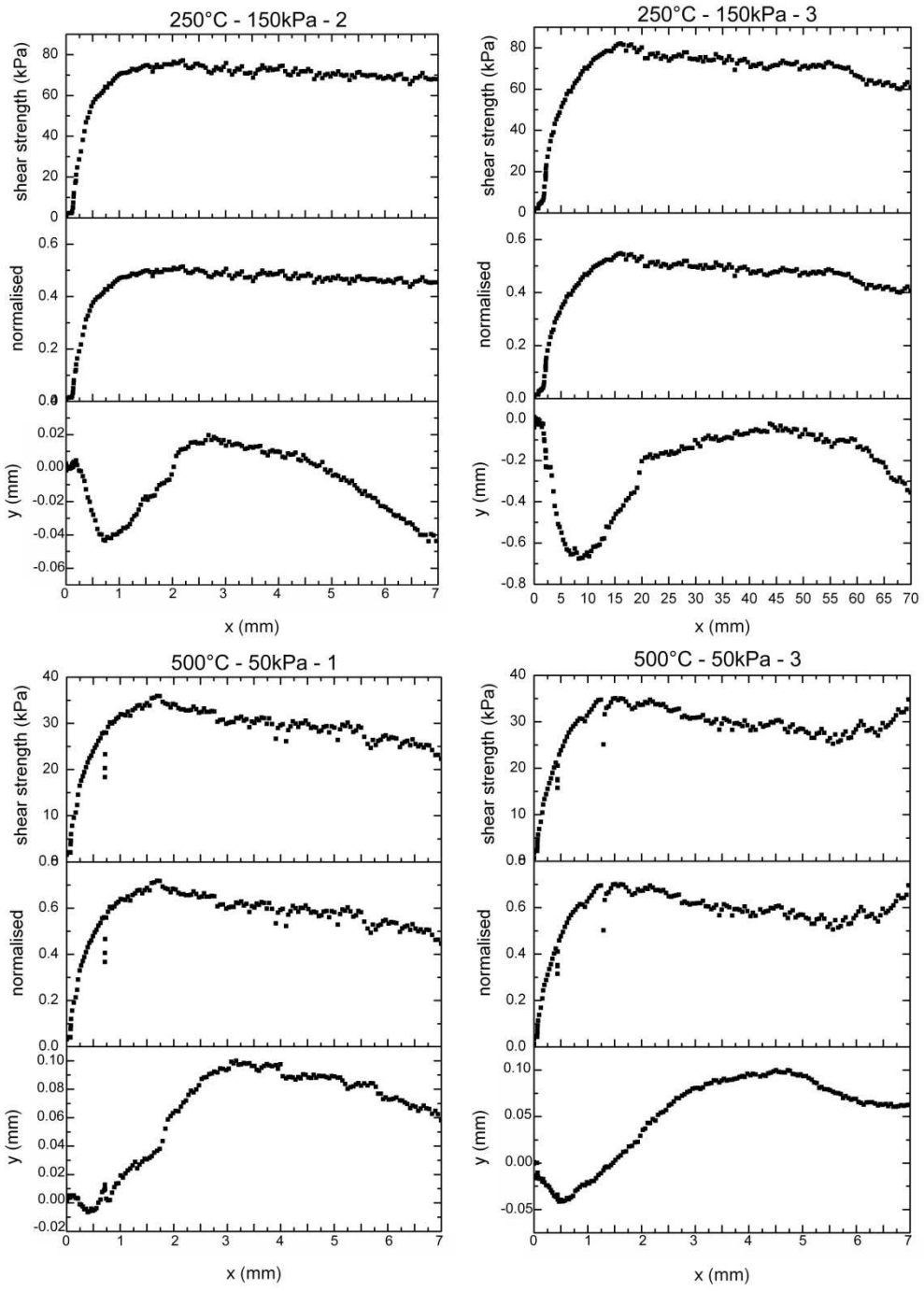
250°C - 150kPa - 2
250°C - 150kPa - 3
500°C - 50kPa - 1
500°C - 50kPa - 3
shear strength (kPa)
normalised
y (mm)
x (mm)

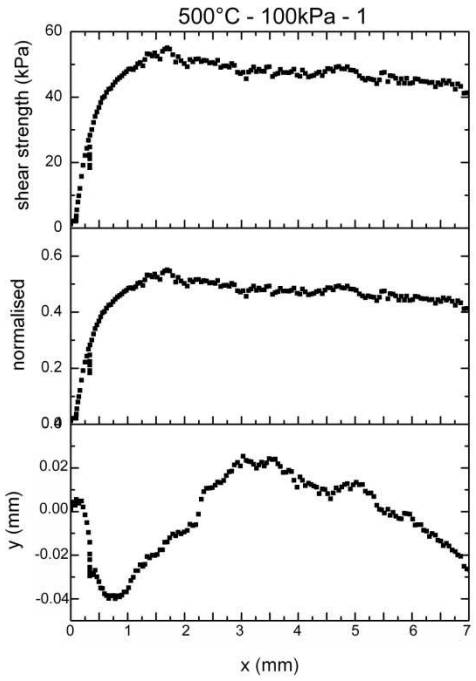
500°C - 100kPa - 1
shear strength (kPa)
normalised
y (mm)
x (mm)

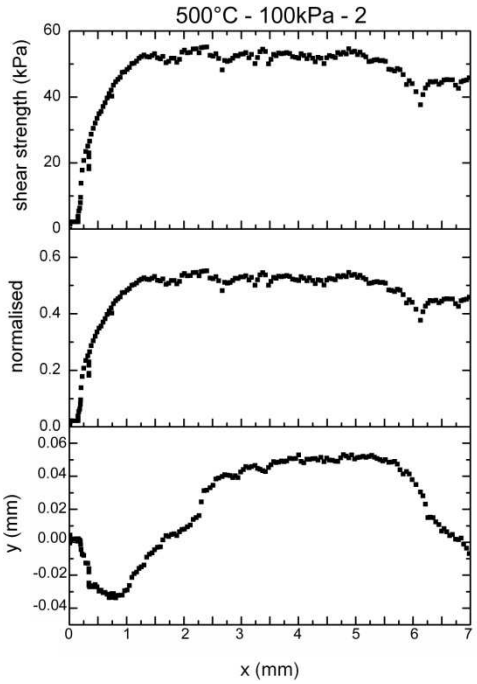
500°C - 100kPa - 2
shear strength (kPa)
normalised
y (mm)
x (mm)

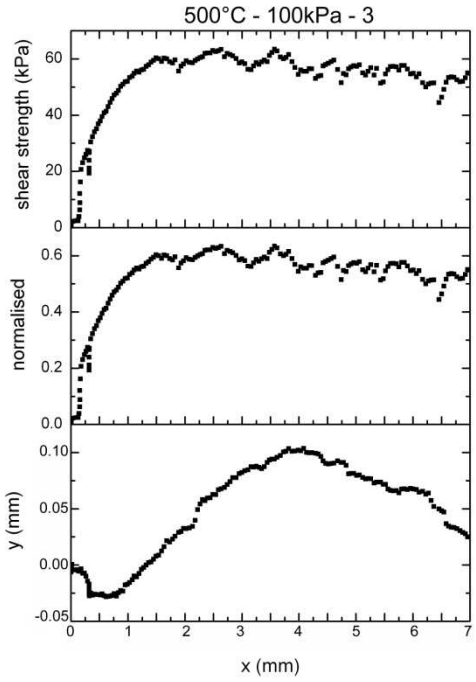
500°C - 100kPa - 3
shear strength (kPa)
normalised
y (mm)
x (mm)

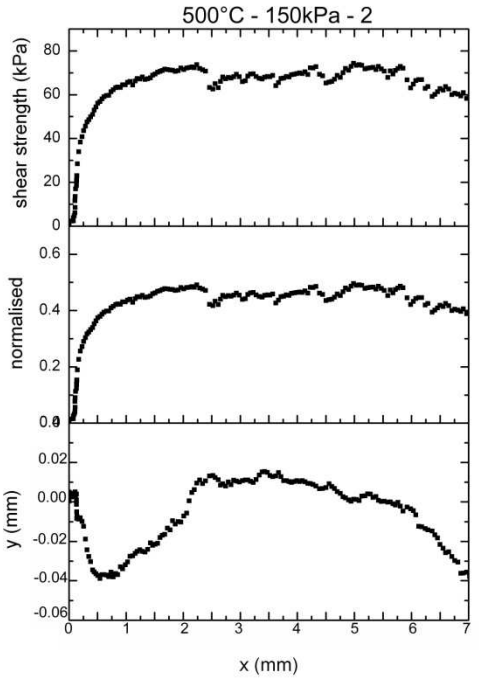
500°C - 150kPa - 2
shear strength (kPa)
normalised
y (mm)
x (mm)

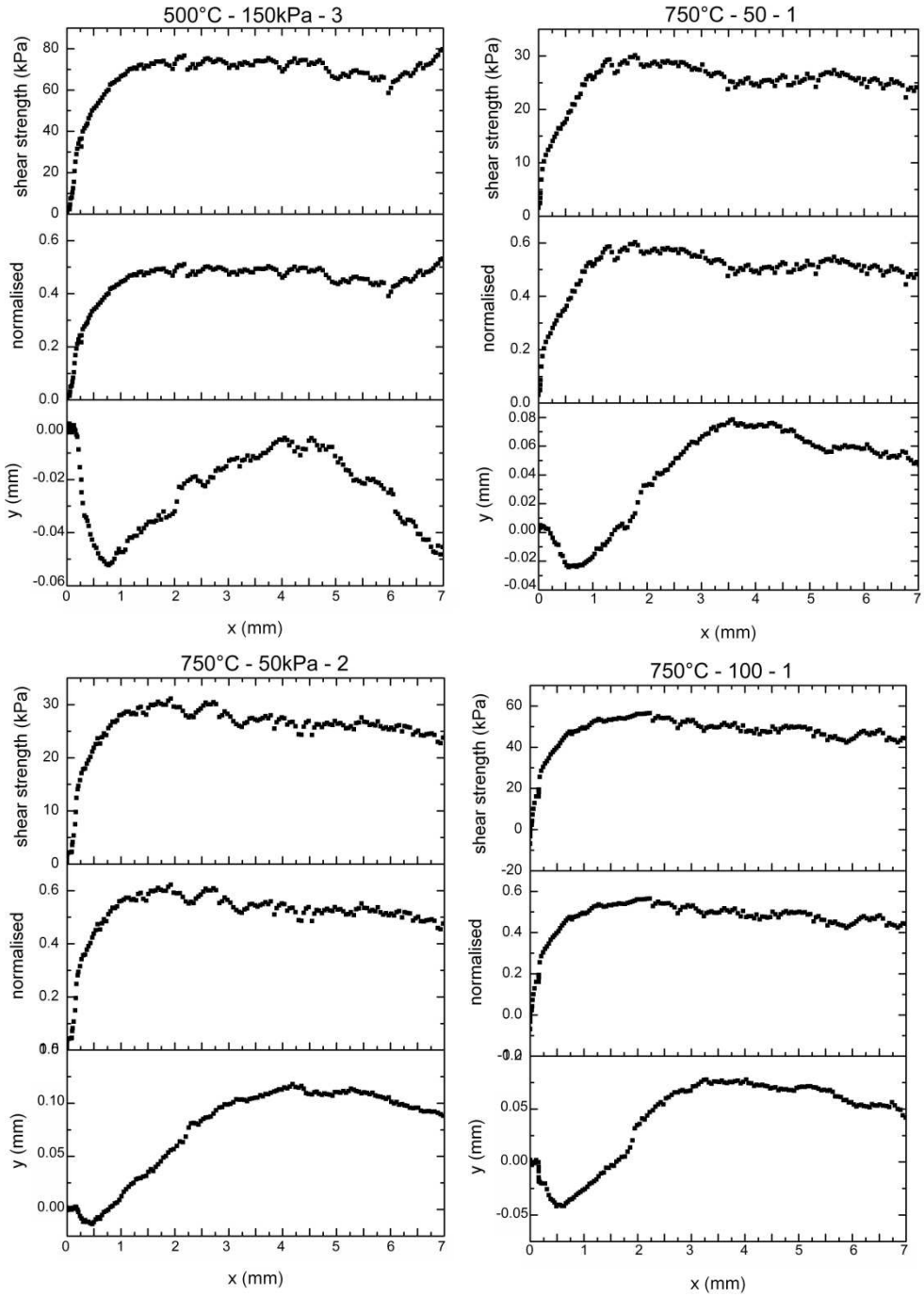
500°C - 150kPa - 3
750°C - 50 - 1
750°C - 50kPa - 2
750°C - 100 - 1
shear strength (kPa)
normalised
y (mm)
x (mm)

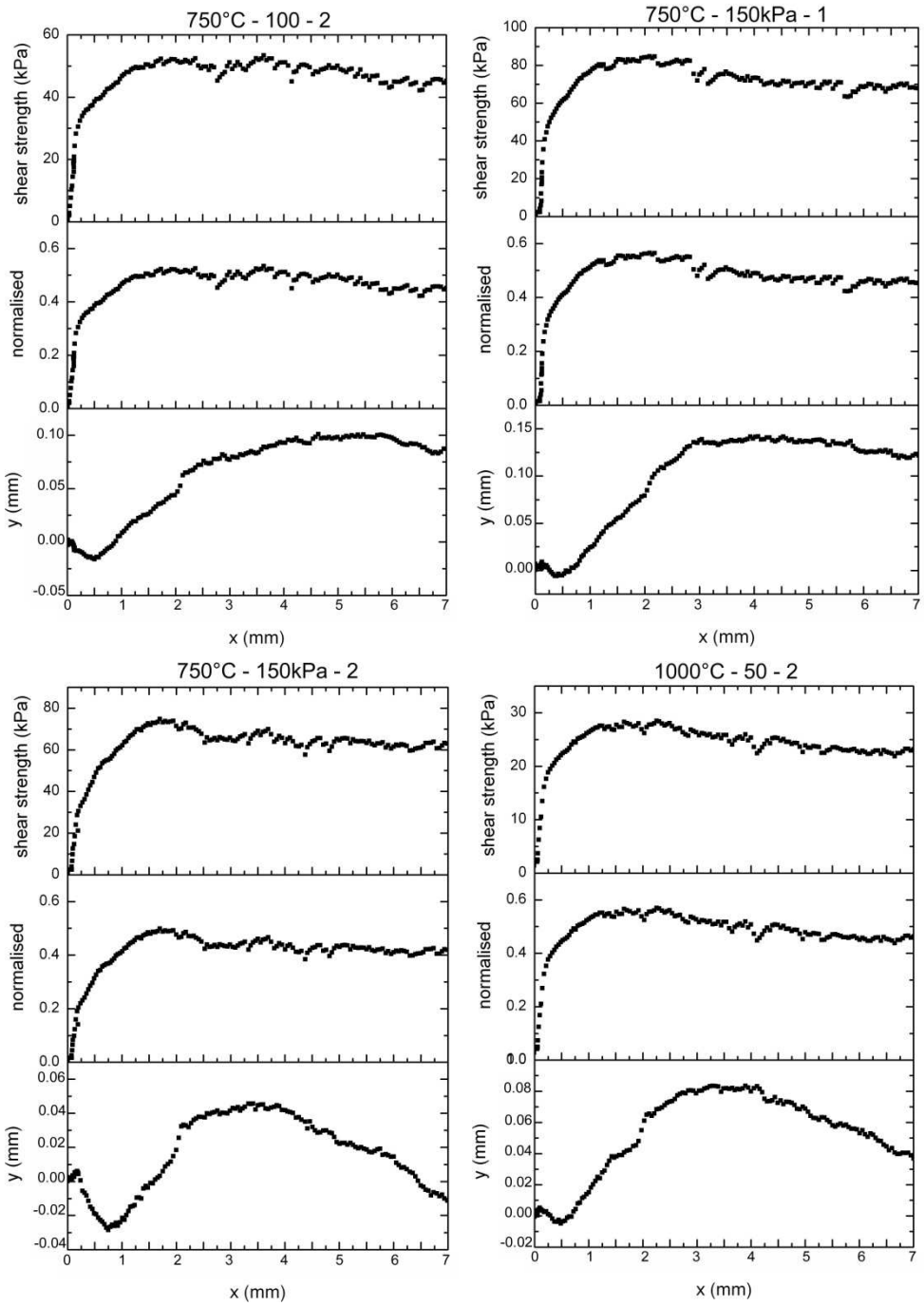
750°C - 100 - 2
750°C - 150kPa - 1
750°C - 150kPa - 2
1000°C - 50 - 2
shear strength (kPa)
normalised
y (mm)
x (mm)

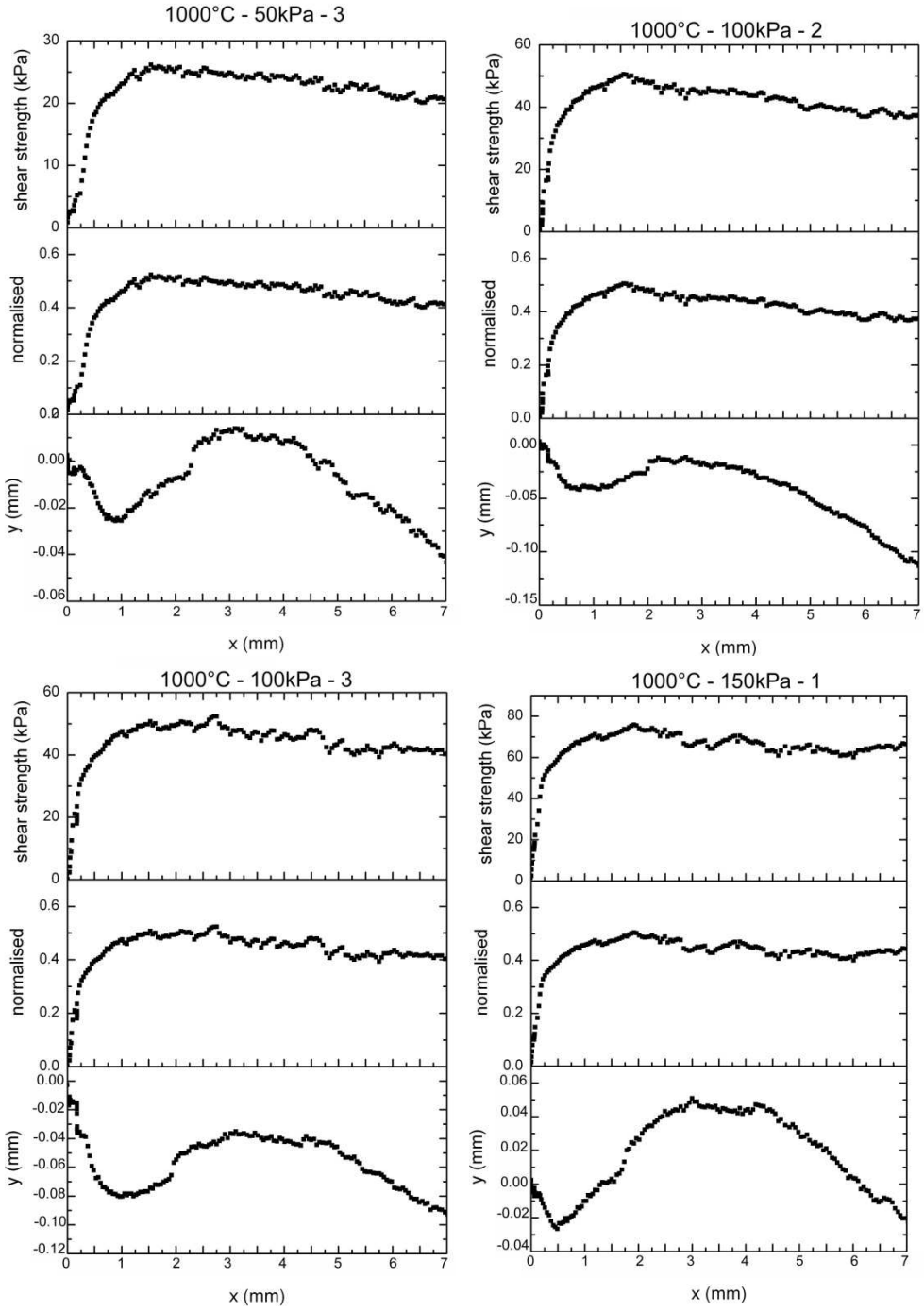
1000°C - 50kPa - 3
shear strength (kPa)
normalised
y (mm)
x (mm)
1000°C - 100kPa - 2
shear strength (kPa)
normalised
y (mm)
x (mm)
1000°C - 100kPa - 3
shear strength (kPa)
normalised
y (mm)
x (mm)
1000°C - 150kPa - 1
shear strength (kPa)
normalised
y (mm)
x (mm)

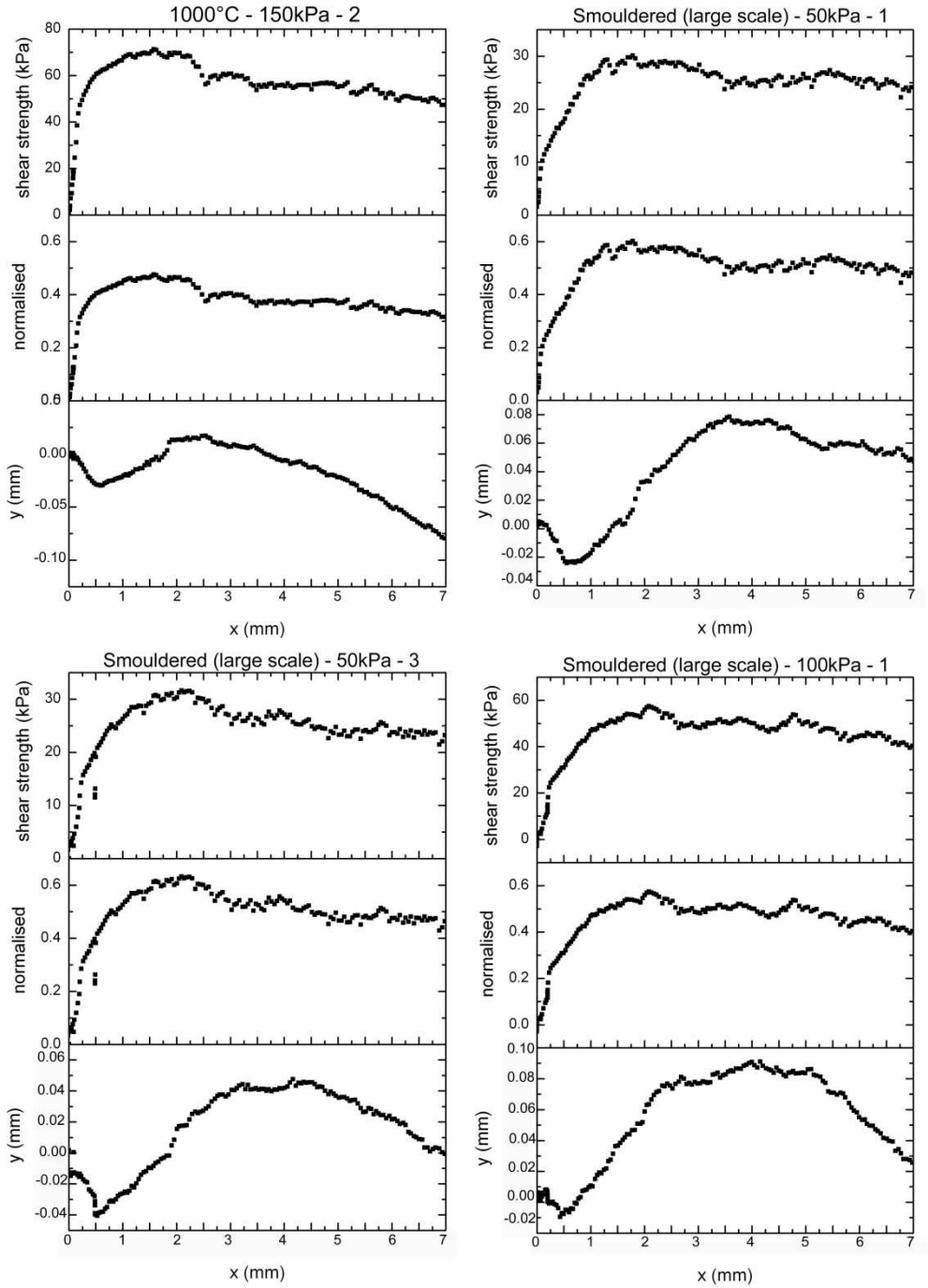
1000°C - 150kPa - 2
shear strength (kPa)
normalised
y (mm)
x (mm)
Smouldered (large scale) - 50kPa - 1
shear strength (kPa)
normalised
y (mm)
x (mm)
Smouldered (large scale) - 50kPa - 3
shear strength (kPa)
normalised
y (mm)
x (mm)
Smouldered (large scale) - 100kPa - 1
shear strength (kPa)
normalised
y (mm)
x (mm)

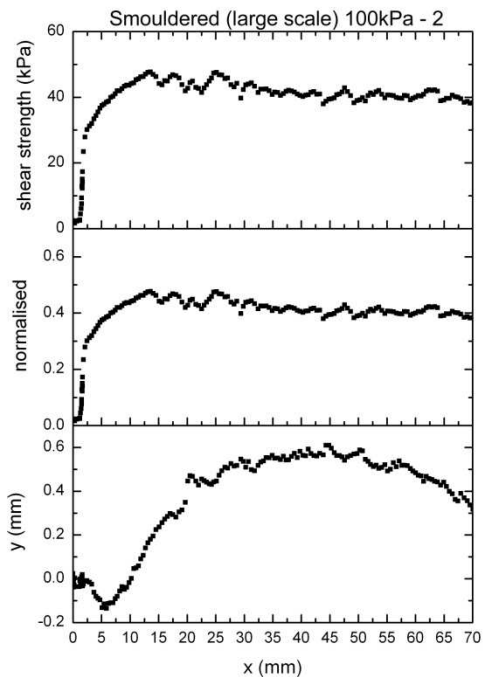
Smouldered (large scale) 100kPa - 2
shear strength (kPa)
normalised
y (mm)
x (mm)

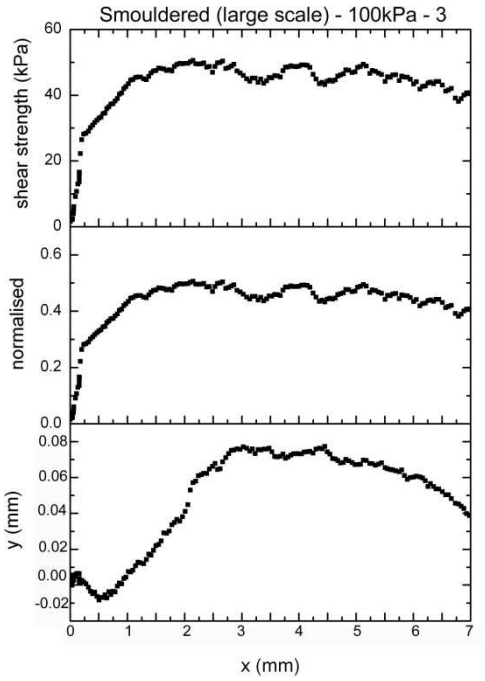
Smouldered (large scale) - 100kPa - 3
shear strength (kPa)
normalised
y (mm)
x (mm)

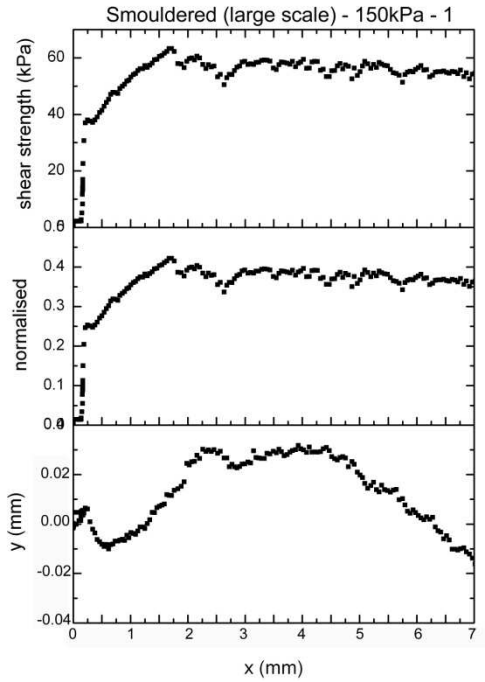
Smouldered (large scale) - 150kPa - 1
shear strength (kPa)
normalised
y (mm)
x (mm)

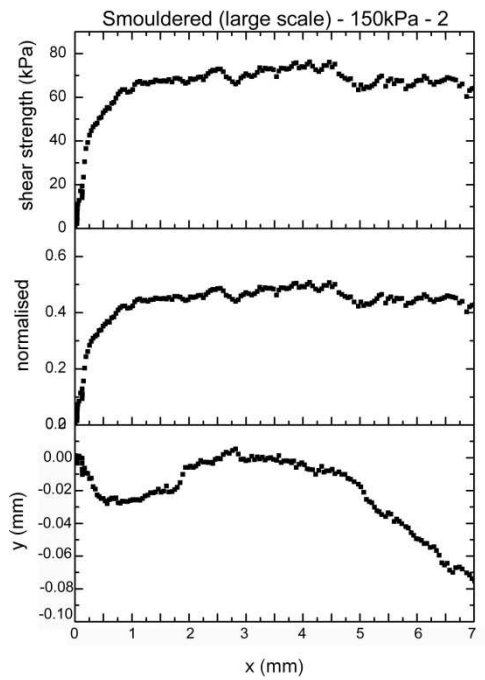
Smouldered (large scale) - 150kPa - 2
shear strength (kPa)
normalised
y (mm)
x (mm)

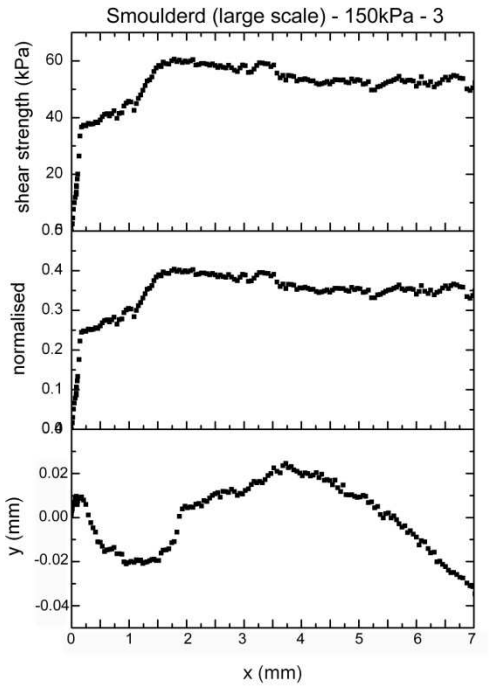
Smoulderd (large scale) - 150kPa - 3
shear strength (kPa)
normalised
y (mm)
x (mm)

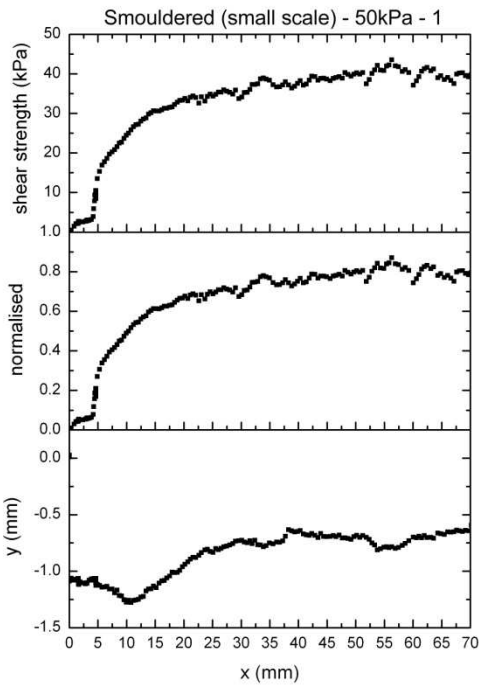
Smouldered (small scale) - 50kPa - 1
shear strength (kPa)
normalised
y (mm)
x (mm)

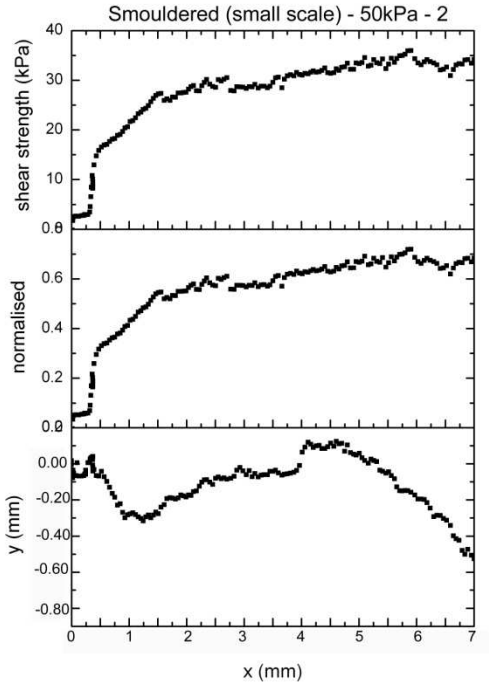
Smouldered (small scale) - 50kPa - 2
shear strength (kPa)
normalised
y (mm)
x (mm)

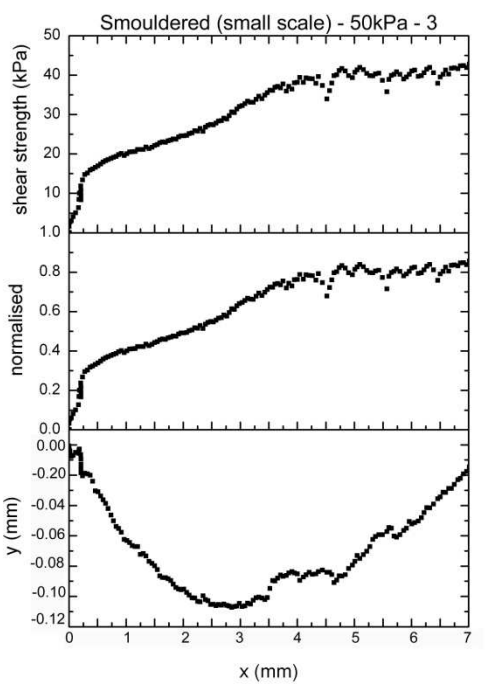
Smouldered (small scale) - 50kPa - 3
shear strength (kPa)
normalised
y (mm)
x (mm)

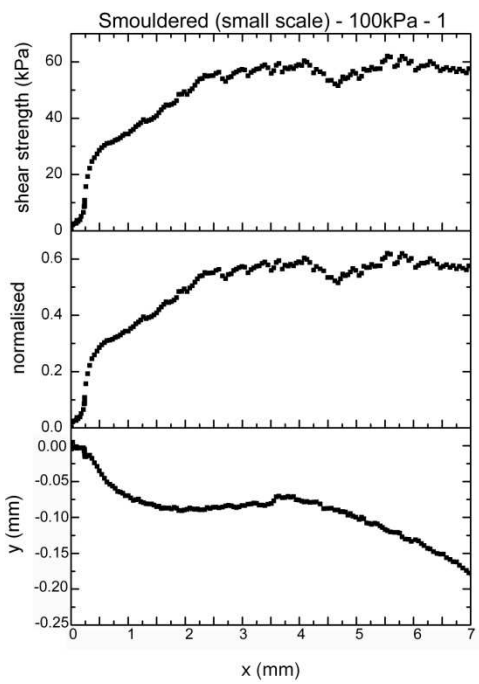
Smouldered (small scale) - 100kPa - 1
shear strength (kPa)
normalised
y (mm)
x (mm)

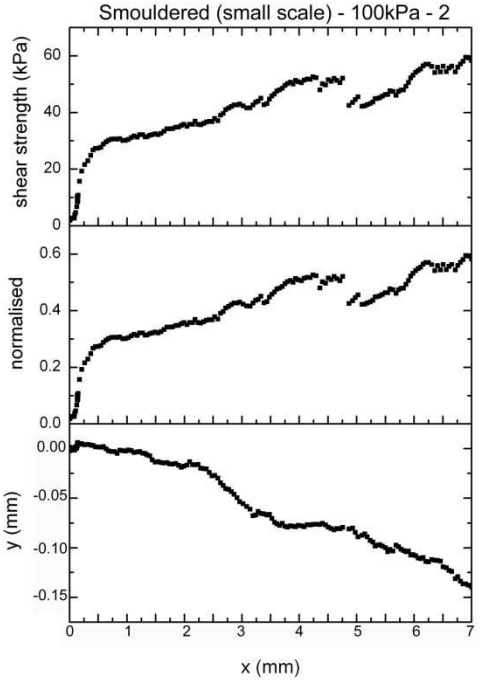
Smouldered (small scale) - 100kPa - 2
shear strength (kPa)
normalised
y (mm)
x (mm)

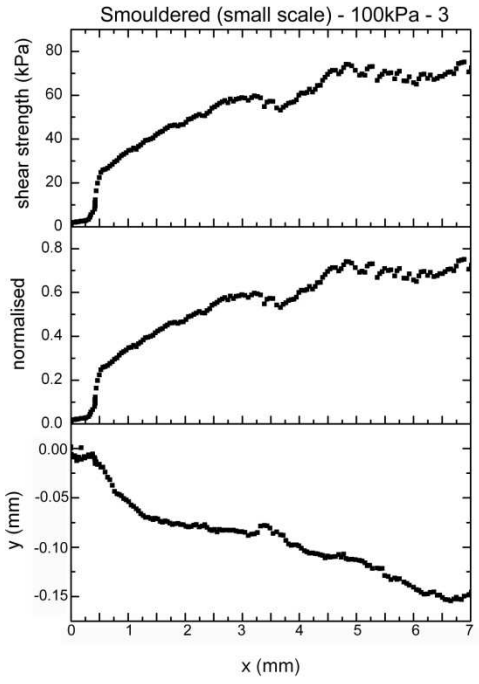
Smouldered (small scale) - 100kPa - 3
shear strength (kPa)
normalised
y (mm)
x (mm)

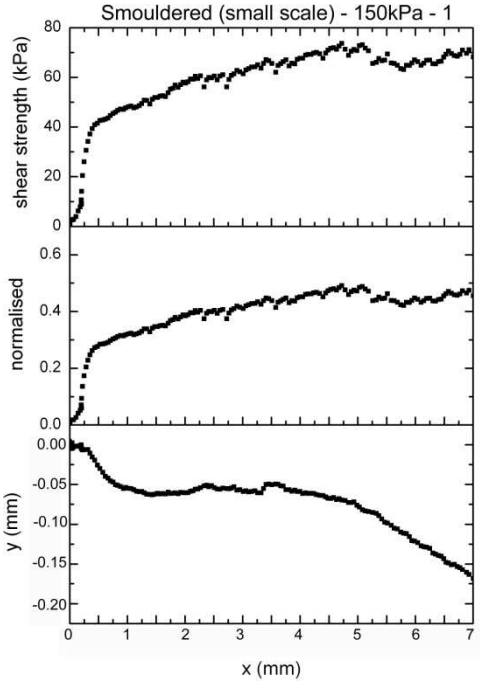
Smouldered (small scale) - 150kPa - 1
shear strength (kPa)
normalised
y (mm)
x (mm)

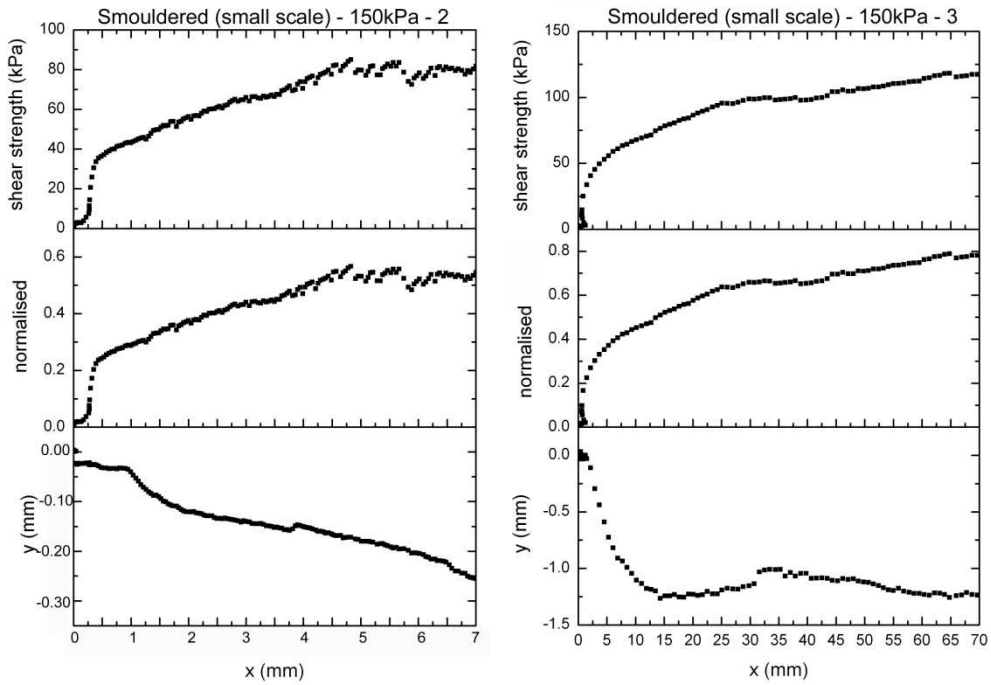
Smouldered (small scale) - 150kPa - 2
shear strength (kPa)
normalised
y (mm)
x (mm)
Smouldered (small scale) - 150kPa - 3
shear strength (kPa)
normalised
y (mm)
x (mm)

SILICA SAND + 10% KAOLIN

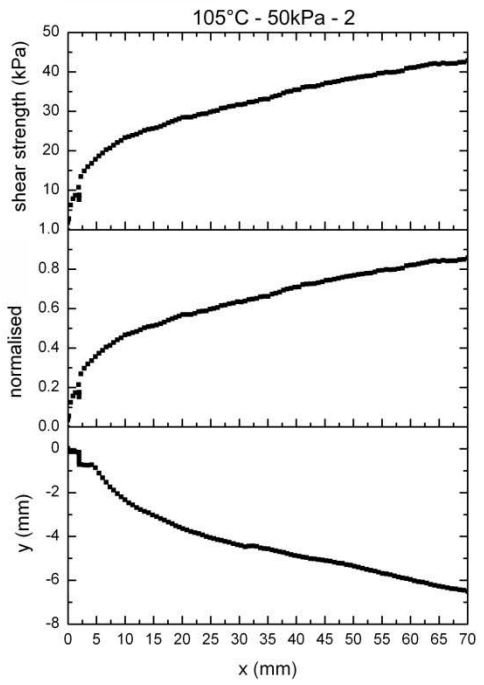

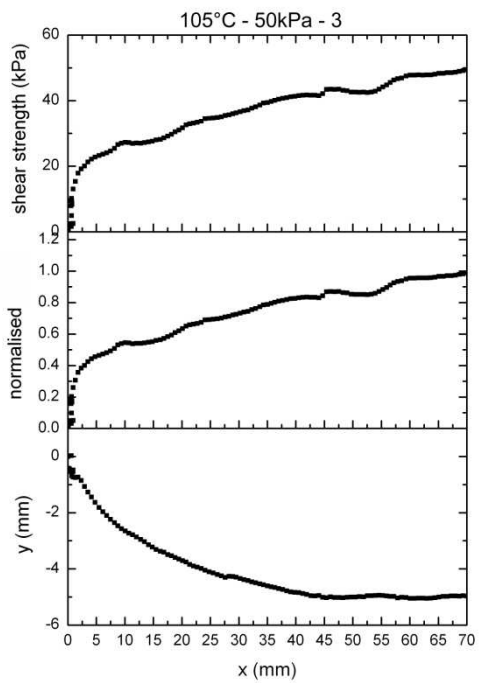

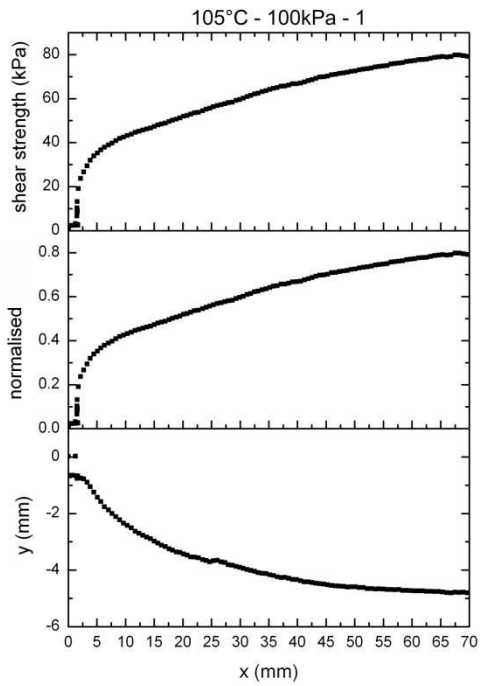

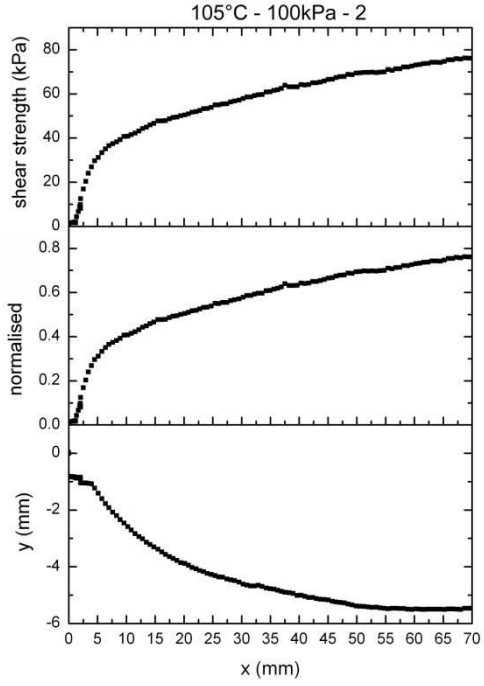

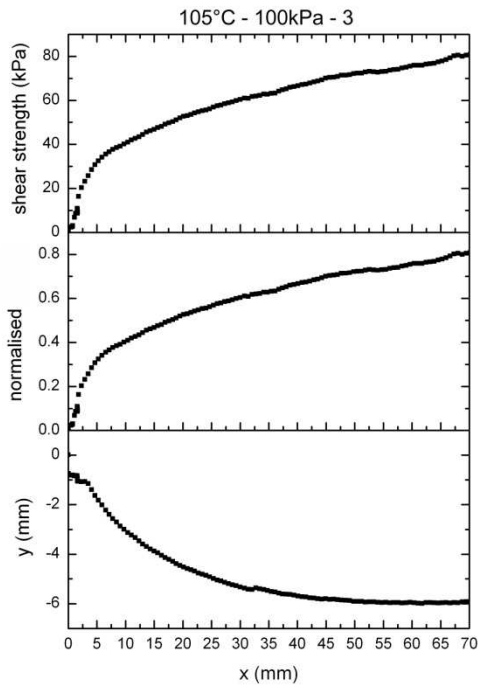
105°C - 100kPa - 3
shear strength (kPa)
normalised
y (mm)
x (mm)

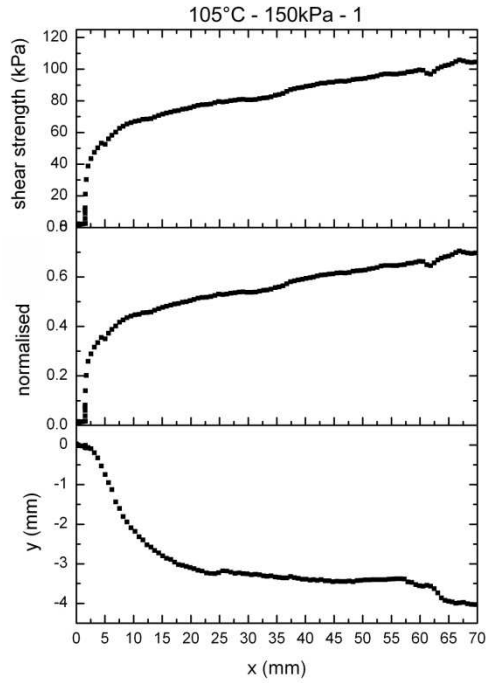
105°C - 150kPa - 1
shear strength (kPa)
normalised
y (mm)
x (mm)

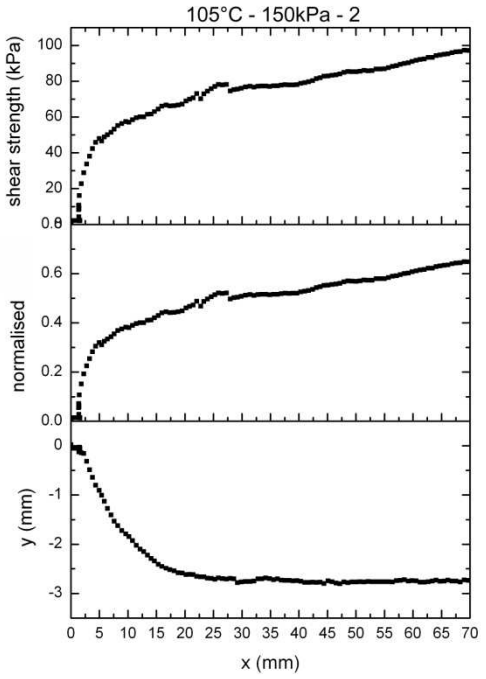
105°C - 150kPa - 2
shear strength (kPa)
normalised
y (mm)
x (mm)

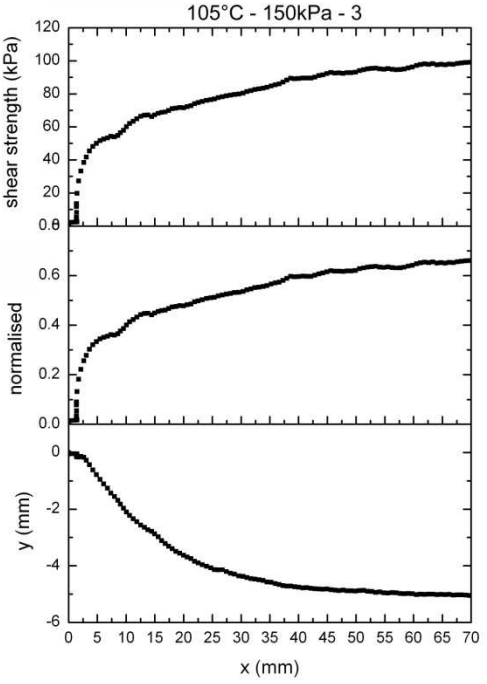
105°C - 150kPa - 3
shear strength (kPa)
normalised
y (mm)
x (mm)

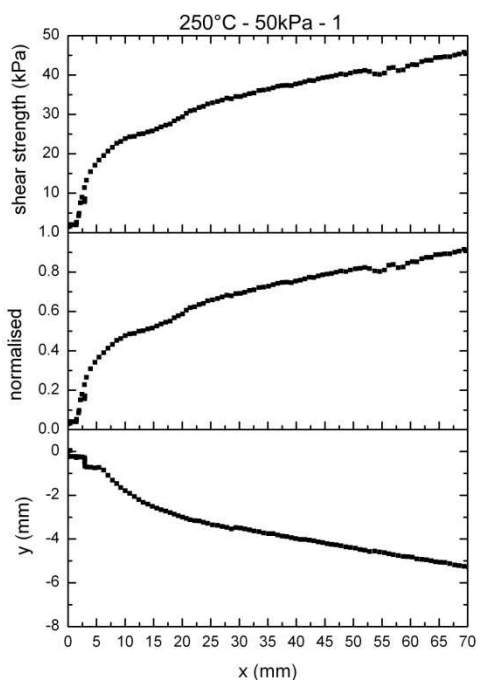
250°C - 50kPa - 1
shear strength (kPa)
normalised
y (mm)
x (mm)

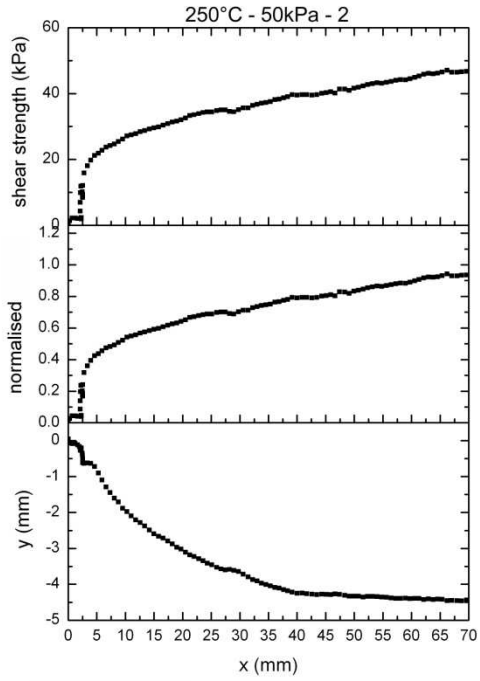
250°C - 50kPa - 2
shear strength (kPa)
normalised
y (mm)
x (mm)

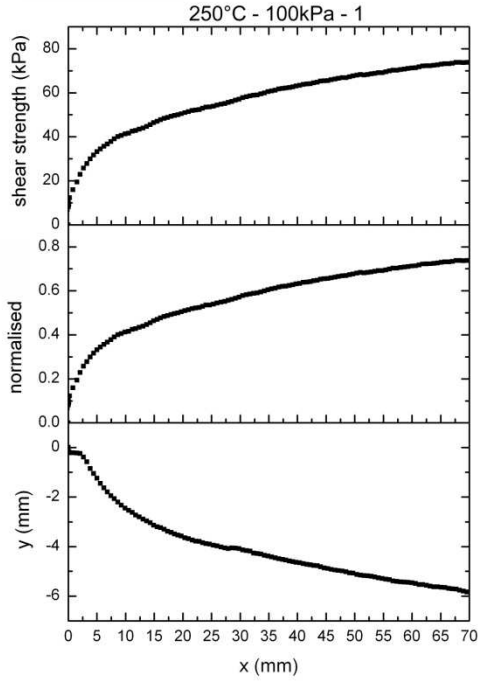
250°C - 100kPa - 1
shear strength (kPa)
normalised
y (mm)
x (mm)

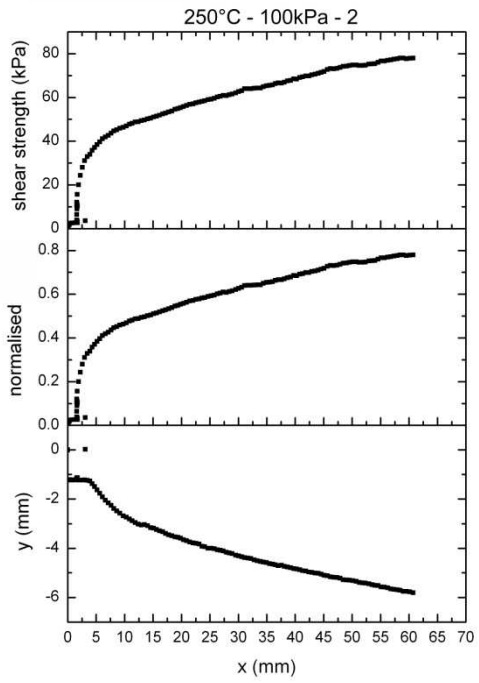
250°C - 100kPa - 2
shear strength (kPa)
normalised
y (mm)
x (mm)

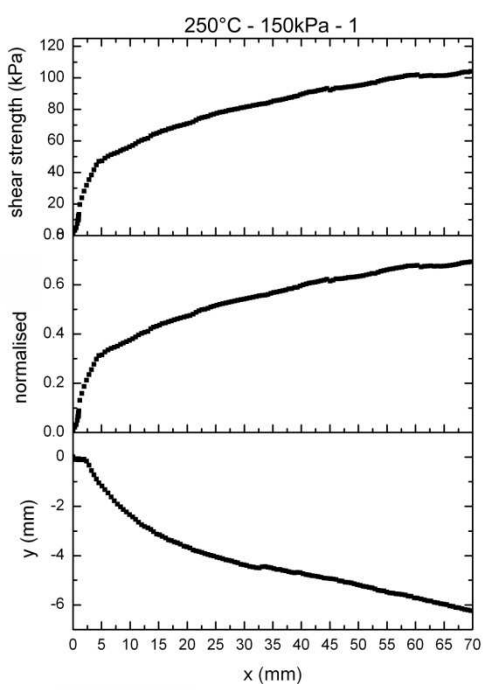
250°C - 150kPa - 1
shear strength (kPa)
normalised
y (mm)
x (mm)

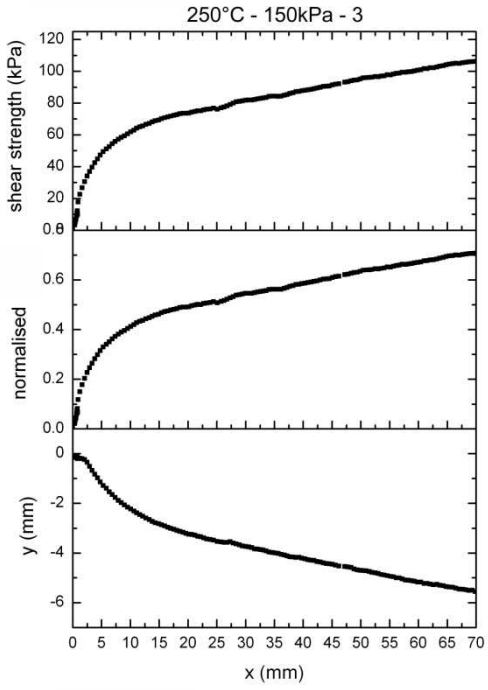
250°C - 150kPa - 3
shear strength (kPa)
normalised
y (mm)
x (mm)

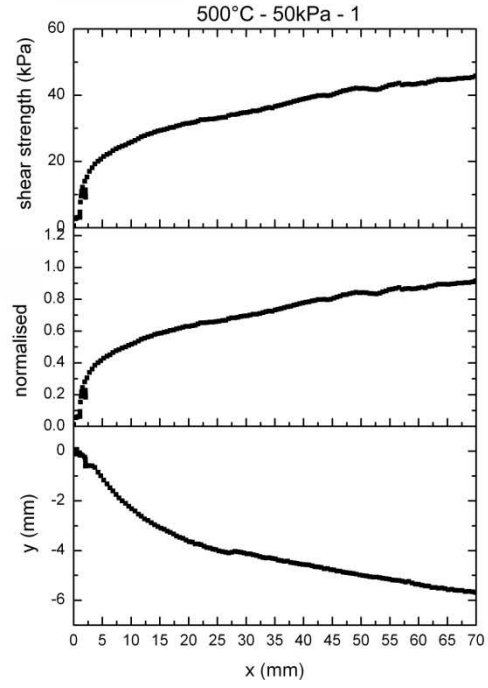
500°C - 50kPa - 1
shear strength (kPa)
normalised
y (mm)
x (mm)

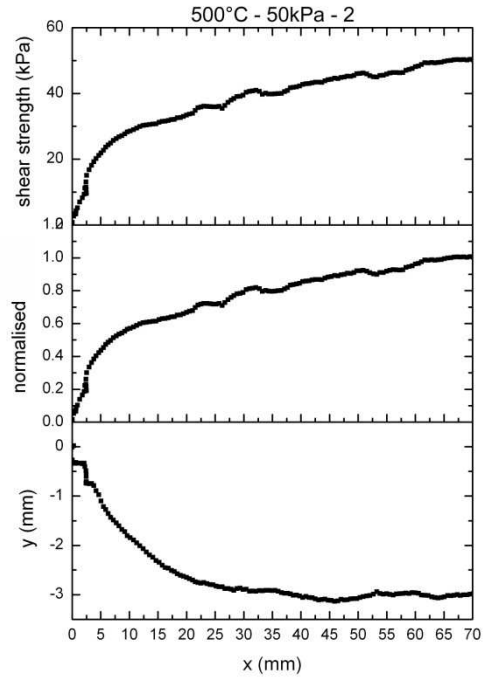
500°C - 50kPa - 2
shear strength (kPa)
normalised
y (mm)
x (mm)

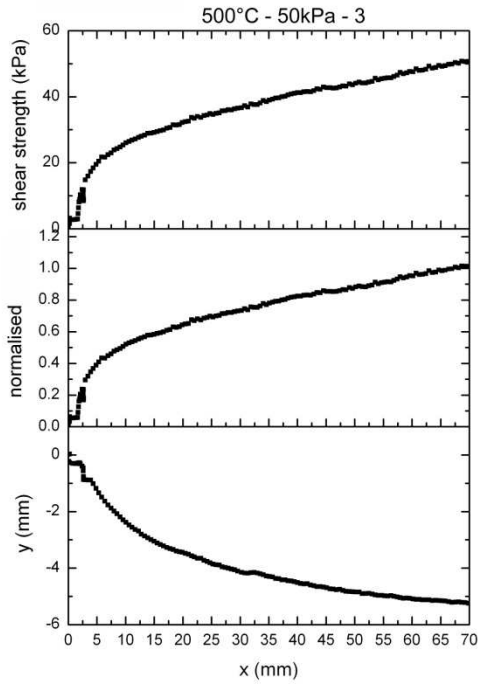
500°C - 50kPa - 3
shear strength (kPa)
normalised
y (mm)
x (mm)

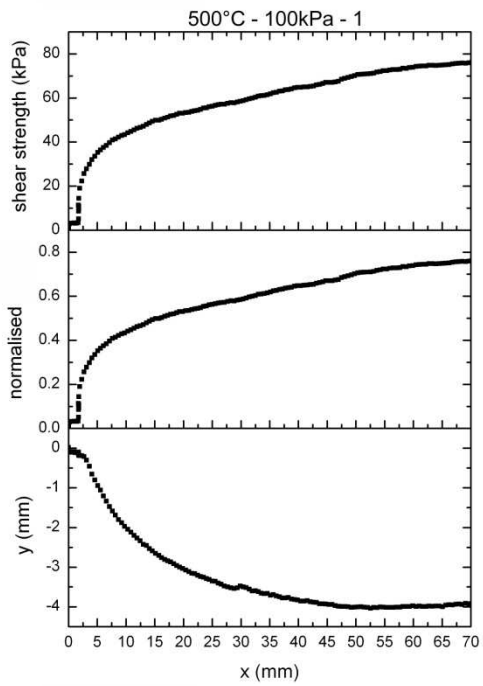
500°C - 100kPa - 1
shear strength (kPa)
normalised
y (mm)
x (mm)

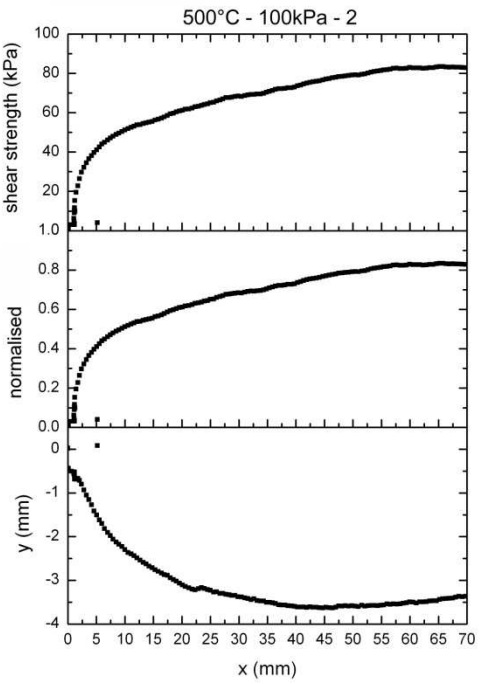
500°C - 100kPa - 2
shear strength (kPa)
normalised
y (mm)
x (mm)

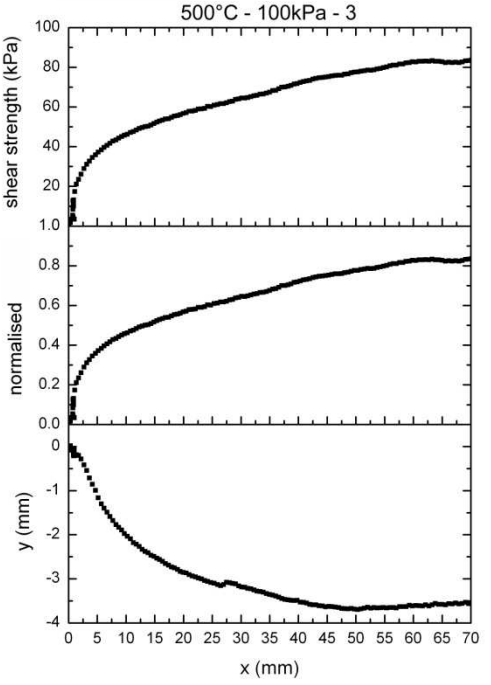
500°C - 100kPa - 3
shear strength (kPa)
normalised
y (mm)
x (mm)

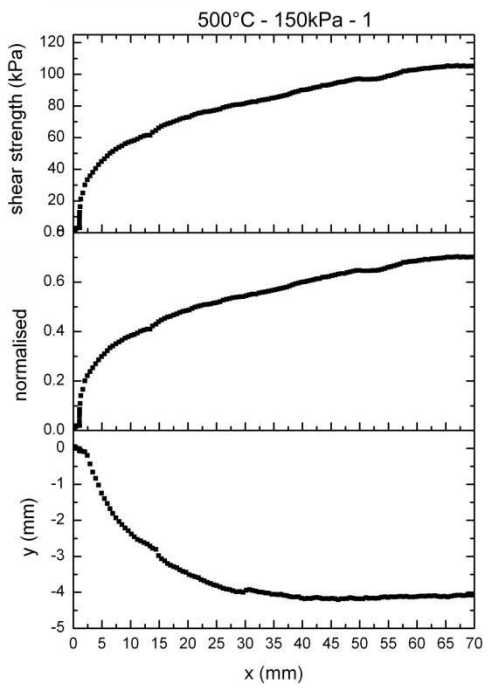
500°C - 150kPa - 1
shear strength (kPa)
normalised
y (mm)
x (mm)

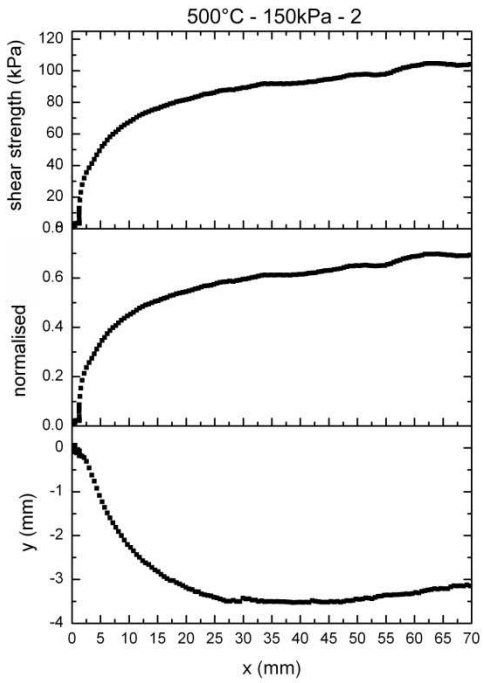
500°C - 150kPa - 2
shear strength (kPa)
normalised
y (mm)
x (mm)

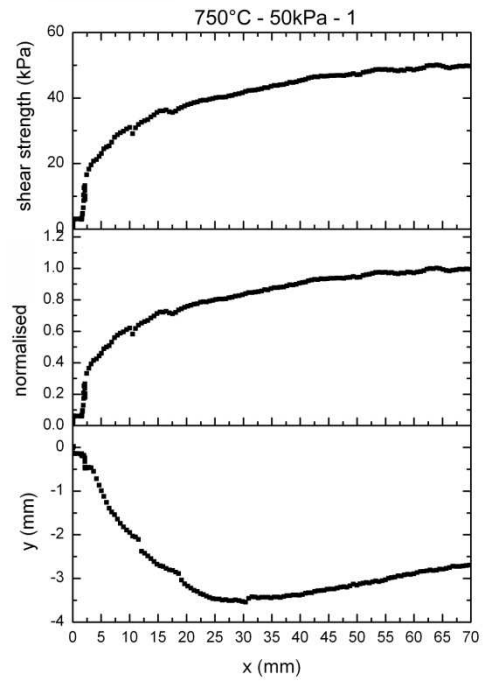
750°C - 50kPa - 1
shear strength (kPa)
normalised
y (mm)
x (mm)

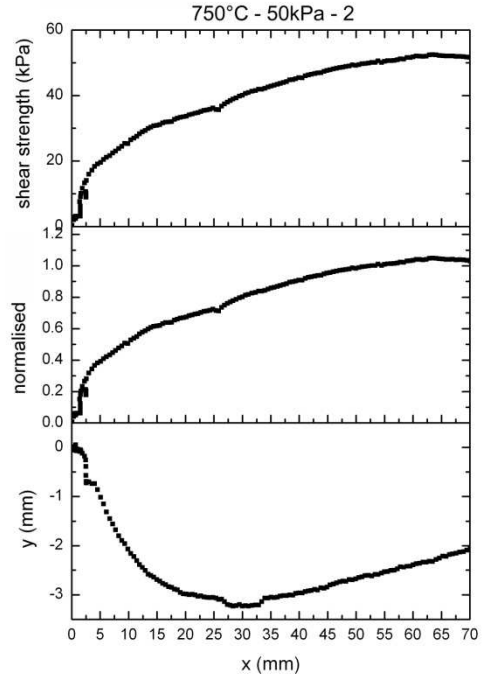
750°C - 50kPa - 2
shear strength (kPa)
normalised
y (mm)
x (mm)

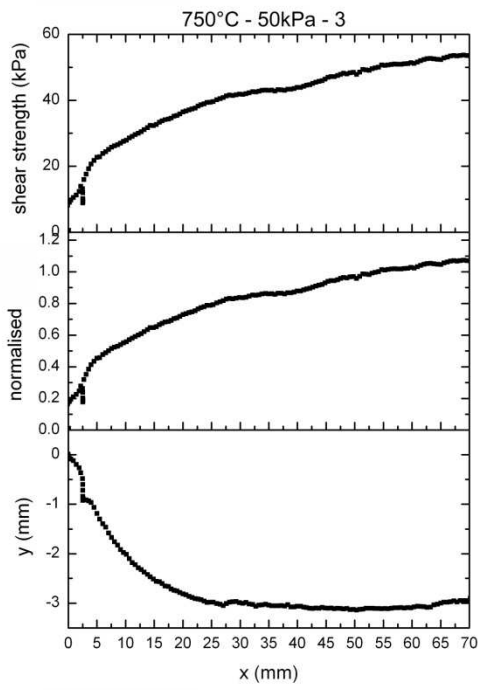
750°C - 50kPa - 3
shear strength (kPa)
normalised
y (mm)
x (mm)

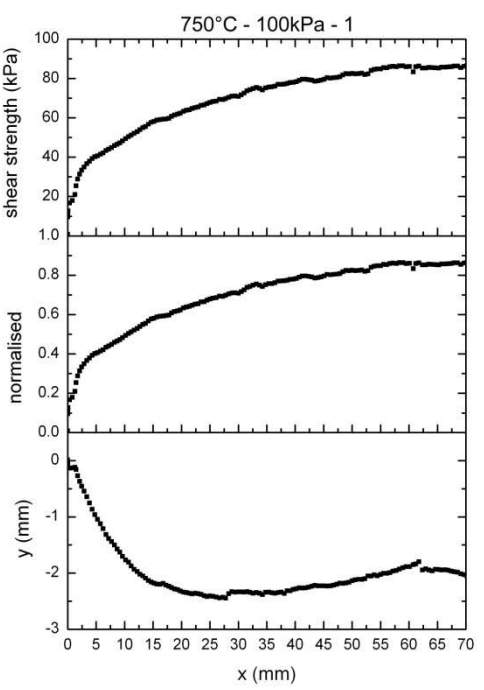
750°C - 100kPa - 1
shear strength (kPa)
normalised
y (mm)
x (mm)

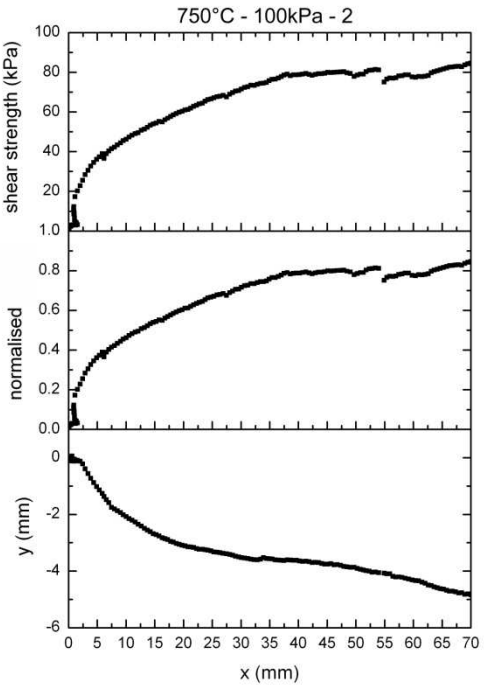
750°C - 100kPa - 2
shear strength (kPa)
normalised
y (mm)
x (mm)

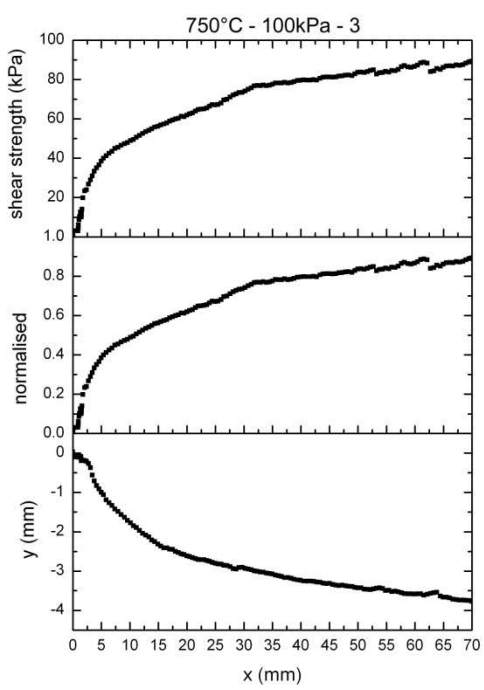
750°C - 100kPa - 3
shear strength (kPa)
normalised
y (mm)
x (mm)

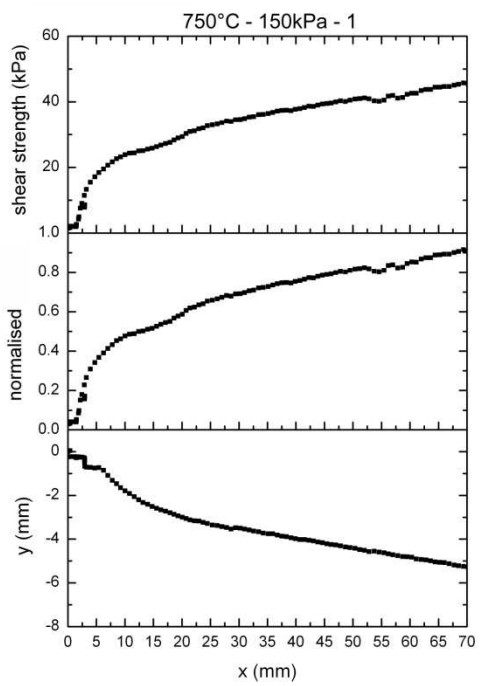
750°C - 150kPa - 1
shear strength (kPa)
normalised
y (mm)
x (mm)

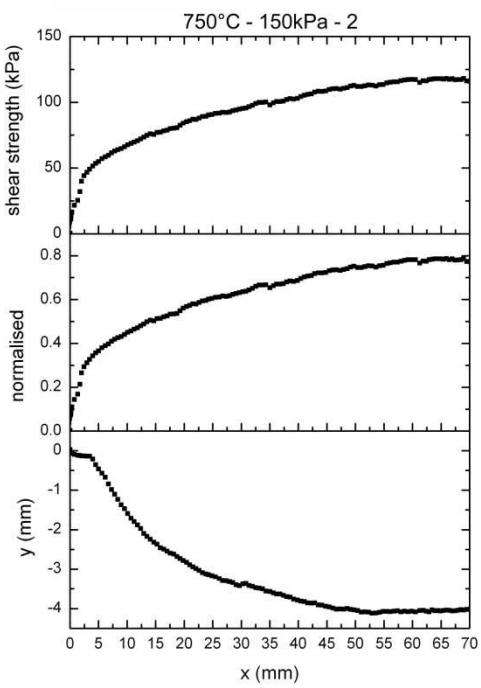
750°C - 150kPa - 2
shear strength (kPa)
normalised
y (mm)
x (mm)

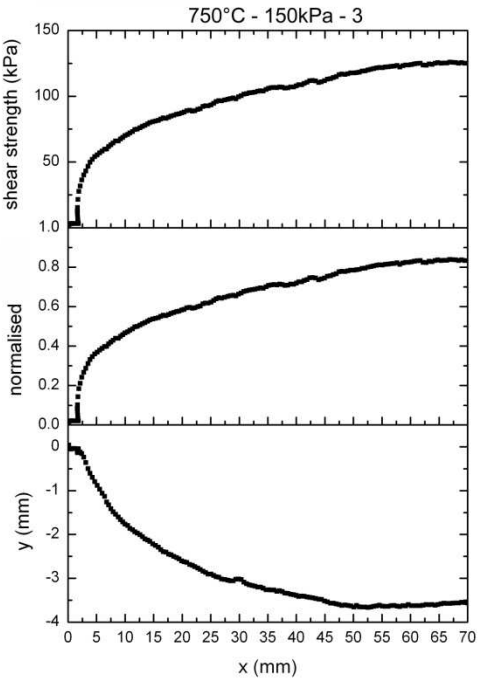
750°C - 150kPa - 3
shear strength (kPa)
normalised
y (mm)
x (mm)

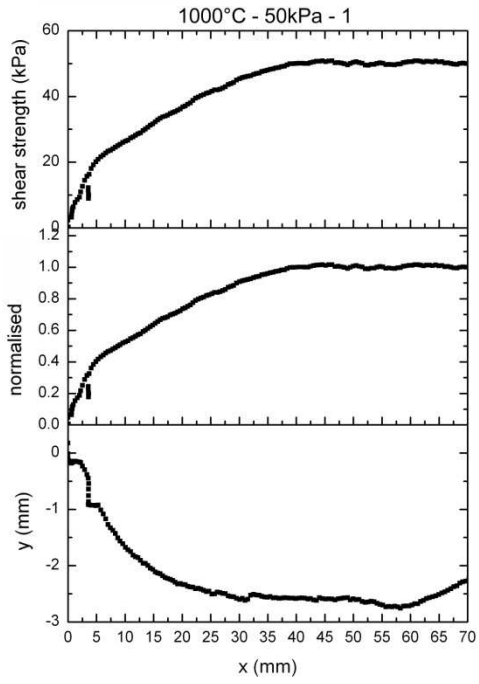
1000°C - 50kPa - 1
shear strength (kPa)
normalised
y (mm)
x (mm)

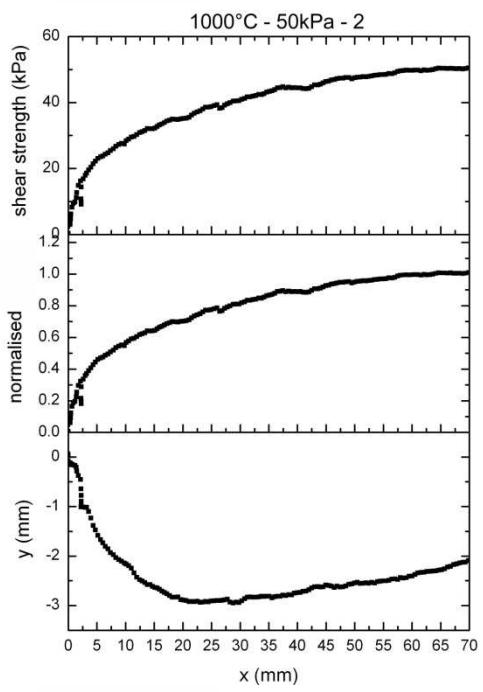
1000°C - 50kPa - 2
shear strength (kPa)
normalised
y (mm)
x (mm)

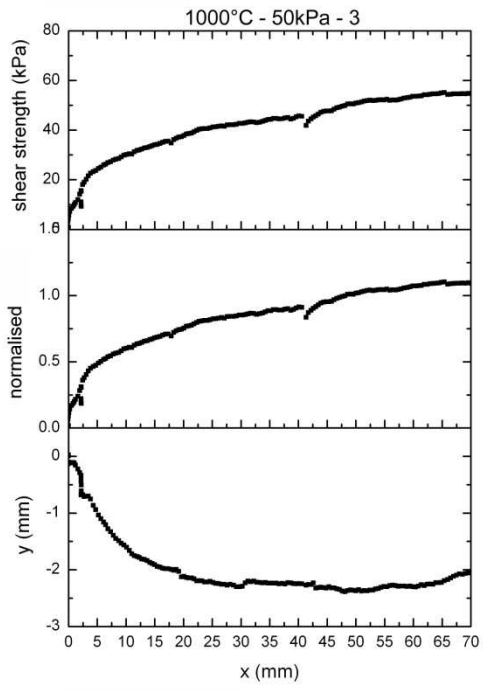
1000°C - 50kPa - 3
shear strength (kPa)
normalised
y (mm)
x (mm)

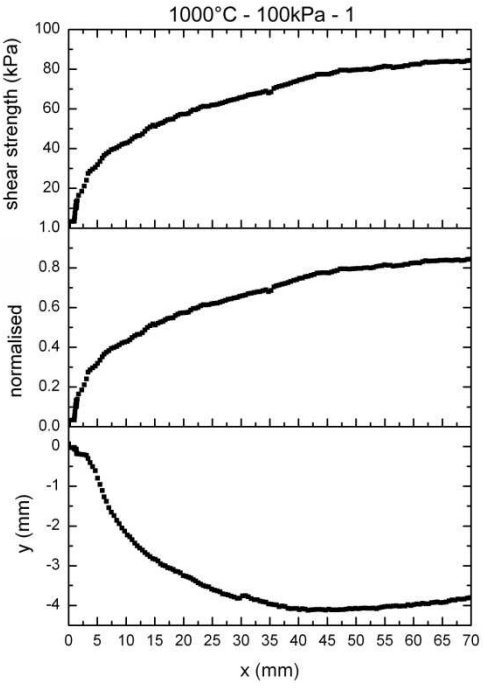
1000°C - 100kPa - 1
shear strength (kPa)
normalised
y (mm)
x (mm)

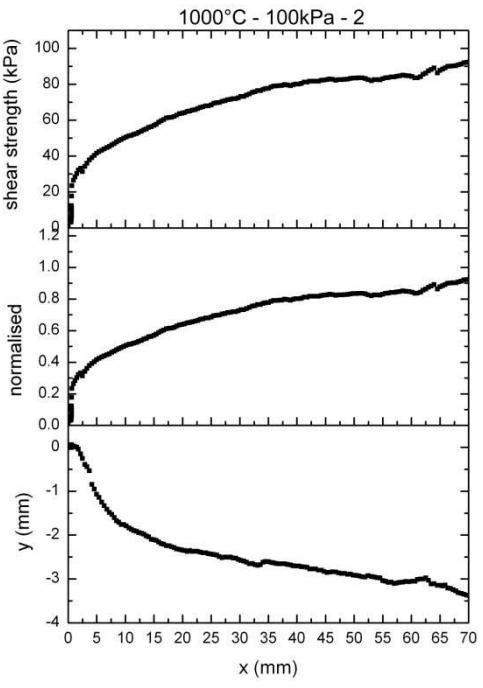
1000°C - 100kPa - 2
shear strength (kPa)
normalised
y (mm)
x (mm)

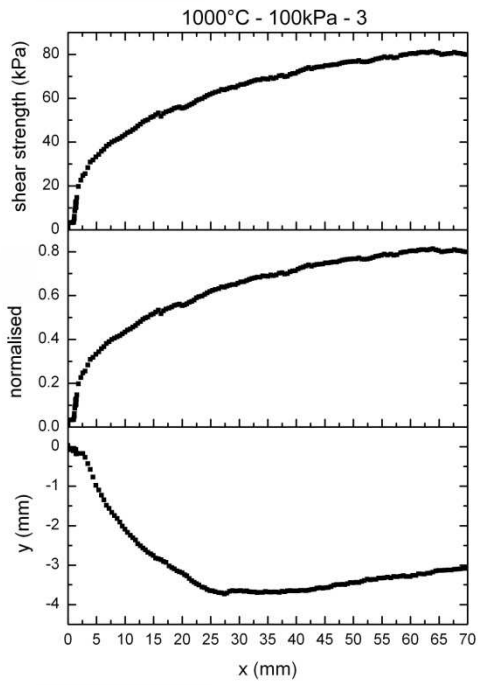
1000°C - 100kPa - 3
shear strength (kPa)
normalised
y (mm)
x (mm)

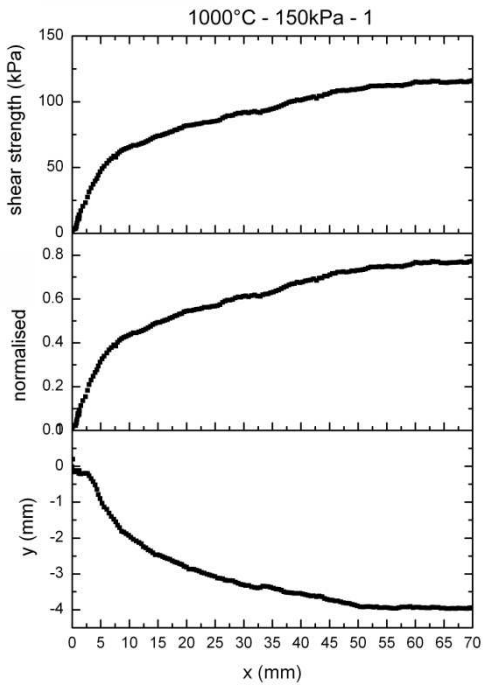
1000°C - 150kPa - 1
shear strength (kPa)
normalised
y (mm)
x (mm)

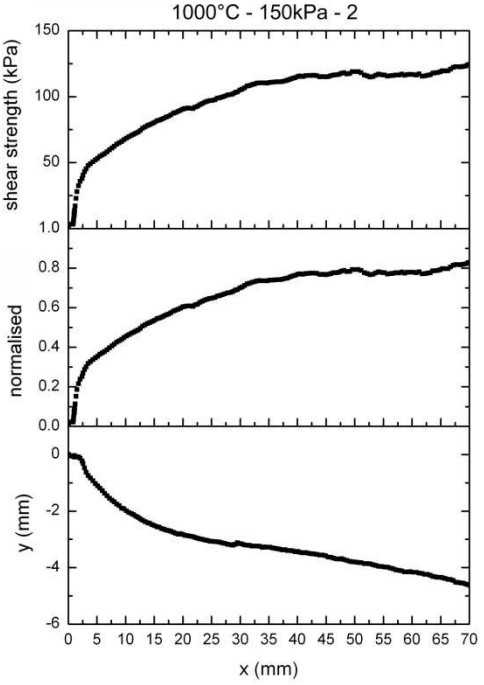
1000°C - 150kPa - 2
shear strength (kPa)
normalised
y (mm)
x (mm)

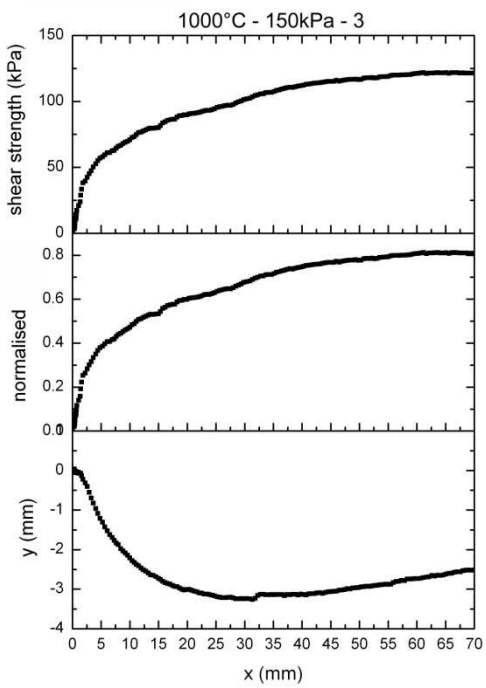
1000°C - 150kPa - 3
shear strength (kPa)
normalised
y (mm)
x (mm)

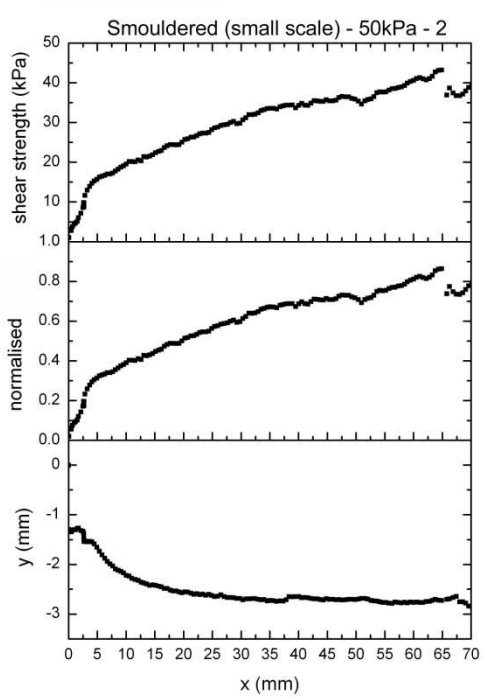
Smouldered (small scale) - 50kPa - 2
shear strength (kPa)
normalised
y (mm)
x (mm)

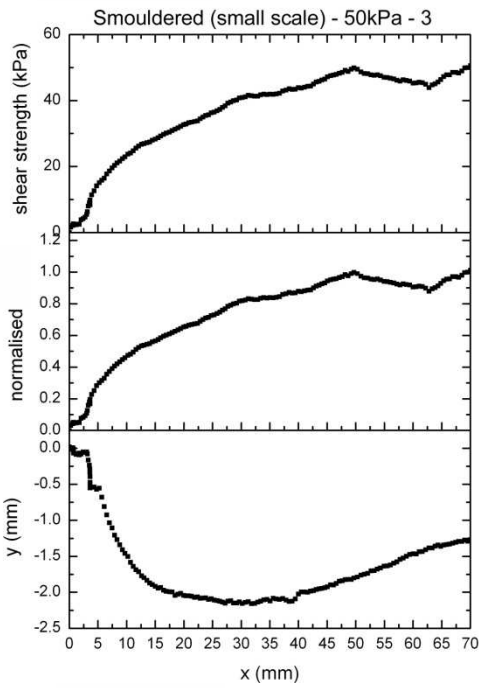
Smouldered (small scale) - 50kPa - 3
shear strength (kPa)
normalised
y (mm)
x (mm)

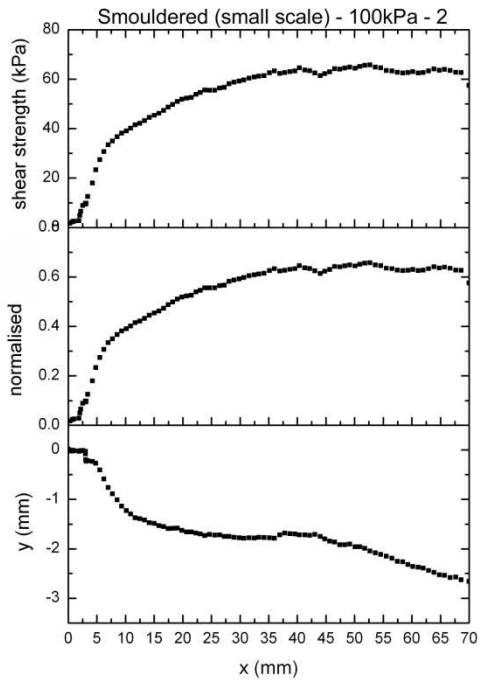
Smouldered (small scale) - 100kPa - 2
shear strength (kPa)
normalised
y (mm)
x (mm)

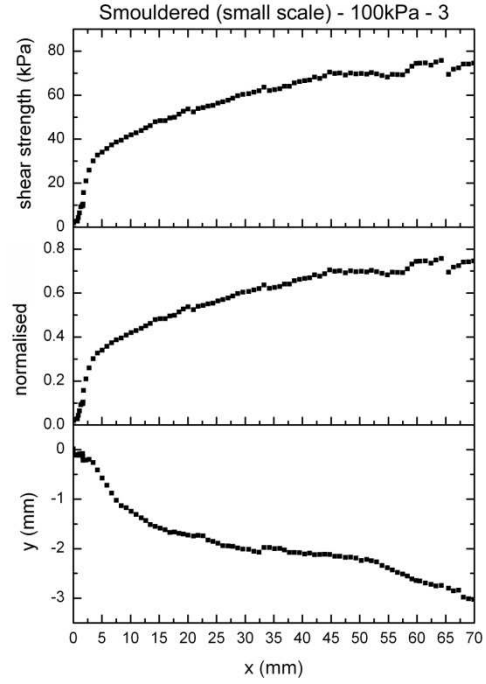
Smouldered (small scale) - 100kPa - 3
shear strength (kPa)
normalised
y (mm)
x (mm)

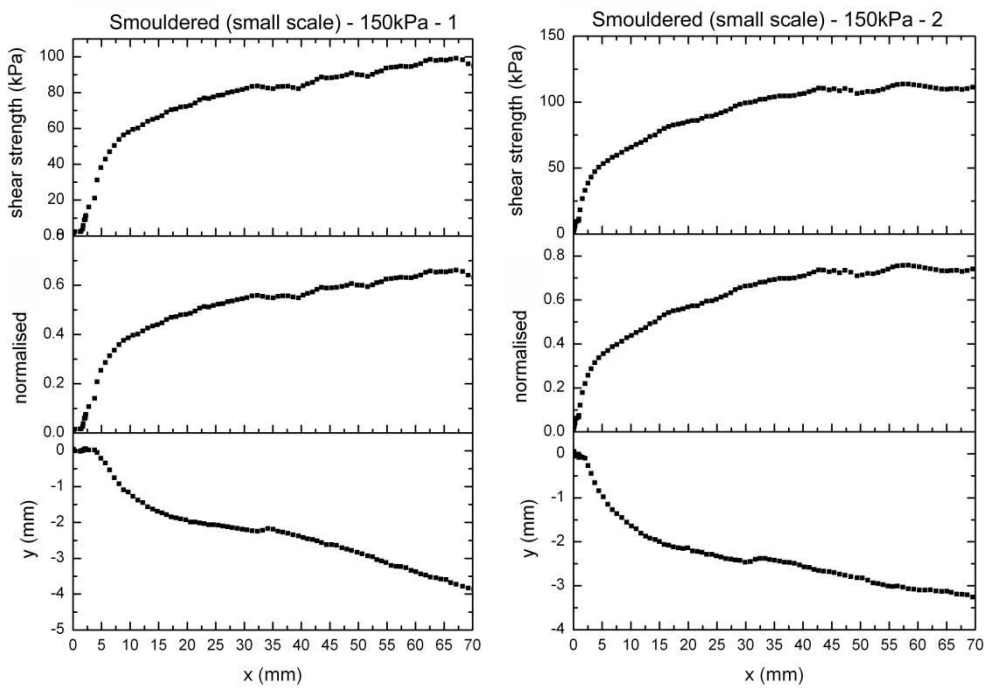
Smouldered (small scale) - 150kPa - 1
shear strength (kPa)
normalised
y (mm)
x (mm)
Smouldered (small scale) - 150kPa - 2
shear strength (kPa)
normalised
y (mm)
x (mm)

APPENDIX B.2

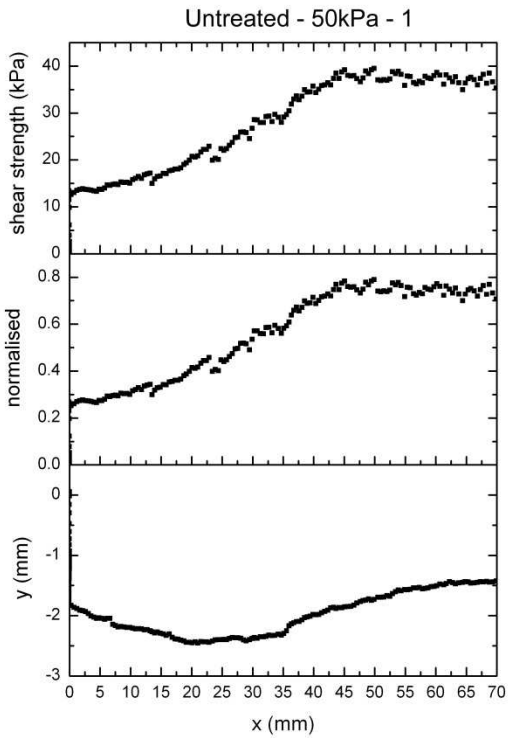

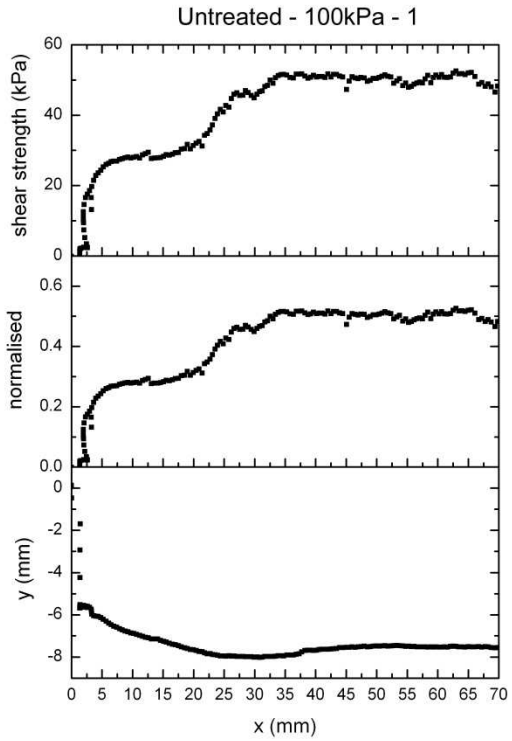

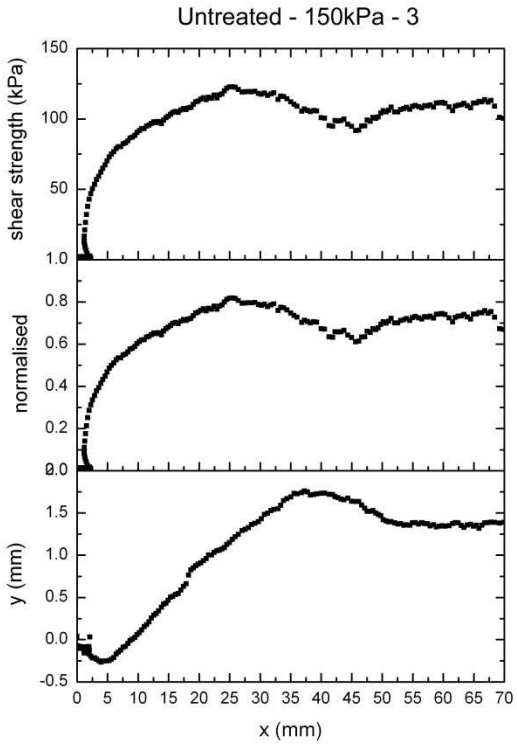

Untreated 50kPa 1: no peak developed

Untreated 100kPa 1: no peak developed

Untreated 150kPa 3: dip in shear strength after 25mm displacement

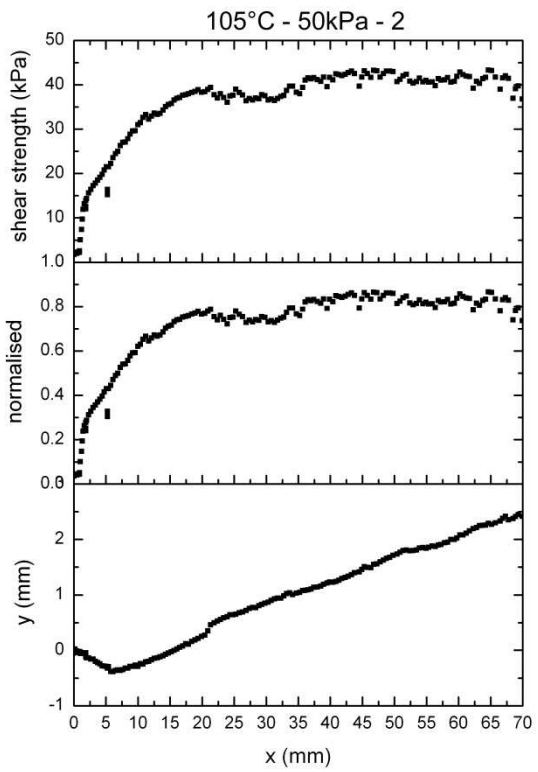

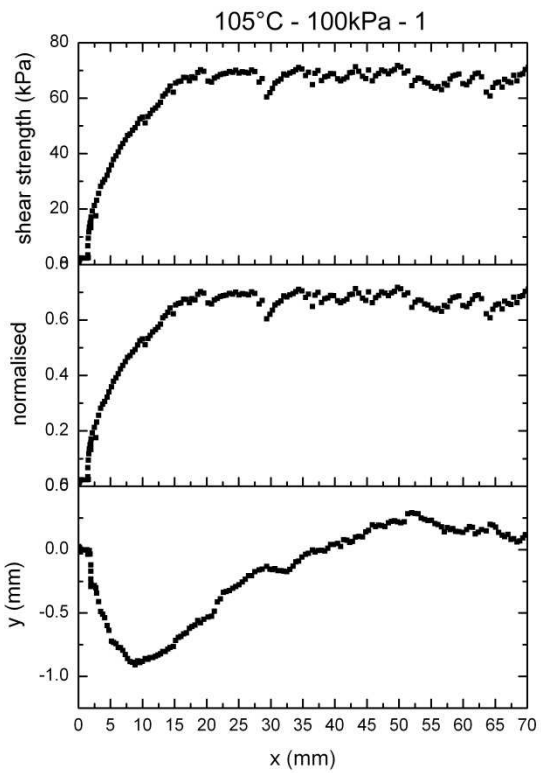

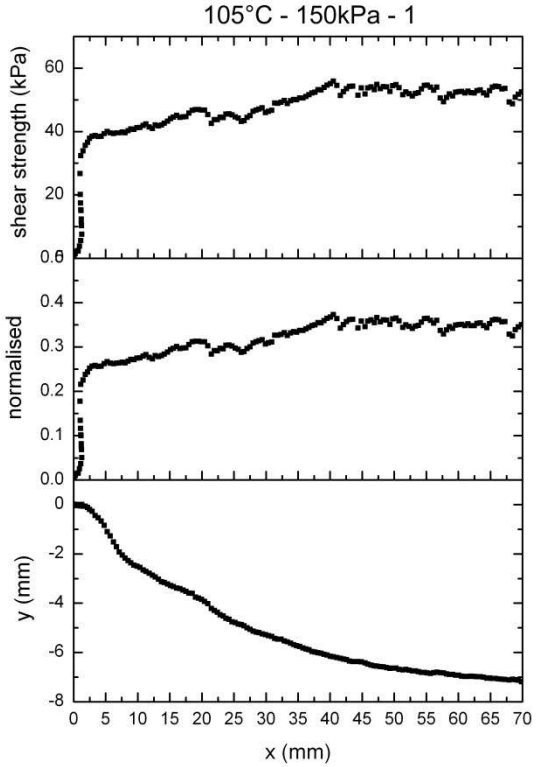

105°C 50kPa 2: no peak developed

105°C 100kPa 1: fluctuations after 25mm displacement, no peak developed

105°C 150kPa 1: no peak developed

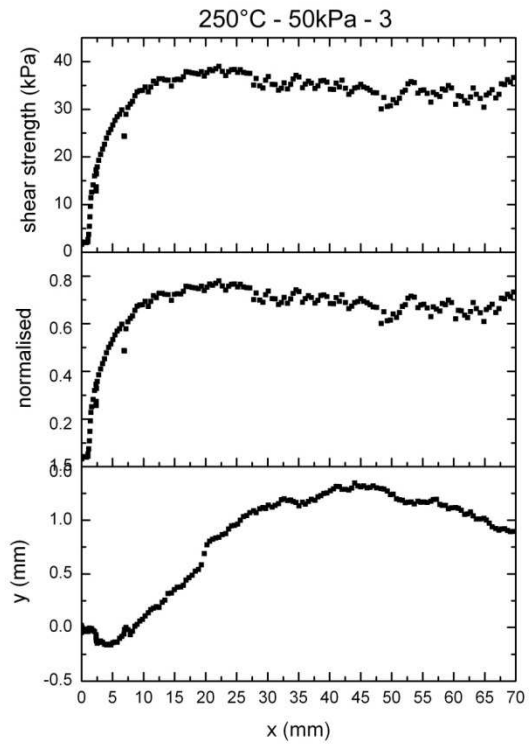

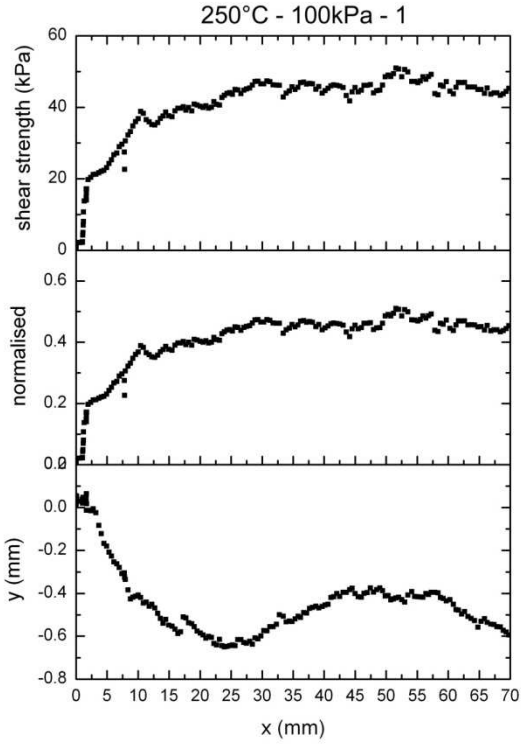

250°C 50kPa 3: fluctuations after 30mm displacement

250°C 100kPa 1: no peak developed

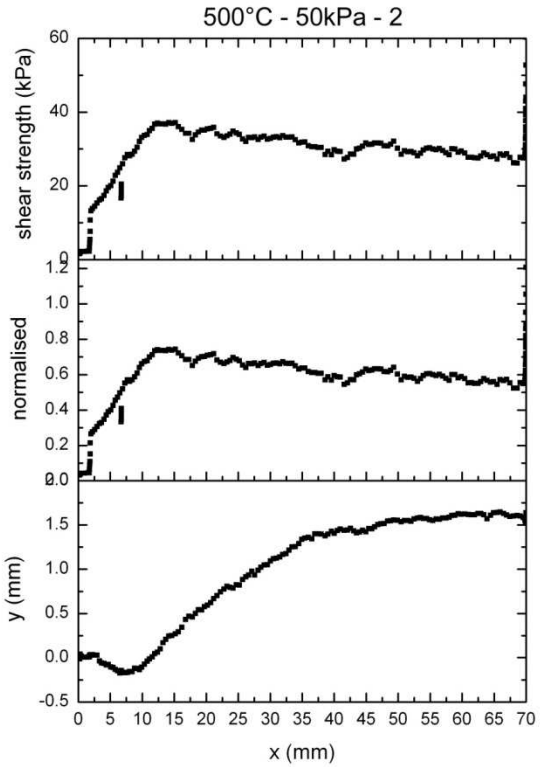

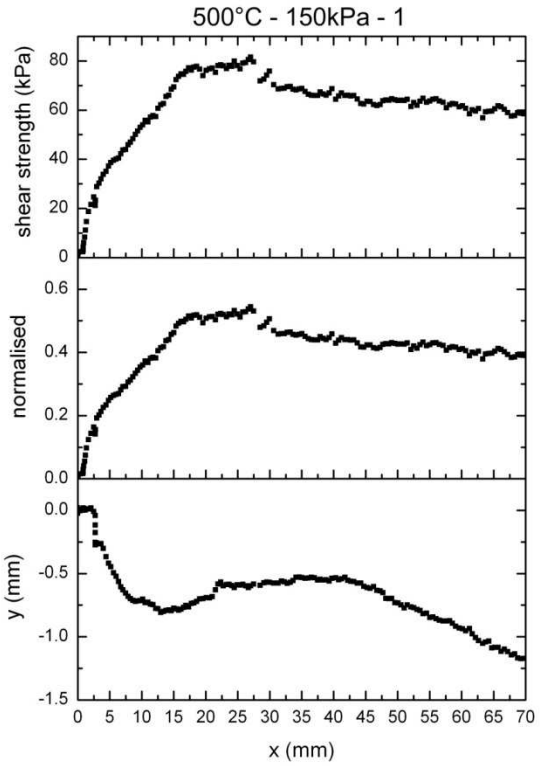

500°C 50kPa 2: dilatant behaviour inflection point not in line with peak shear stress value

500°C 150kPa 1: no dilatant inflection point

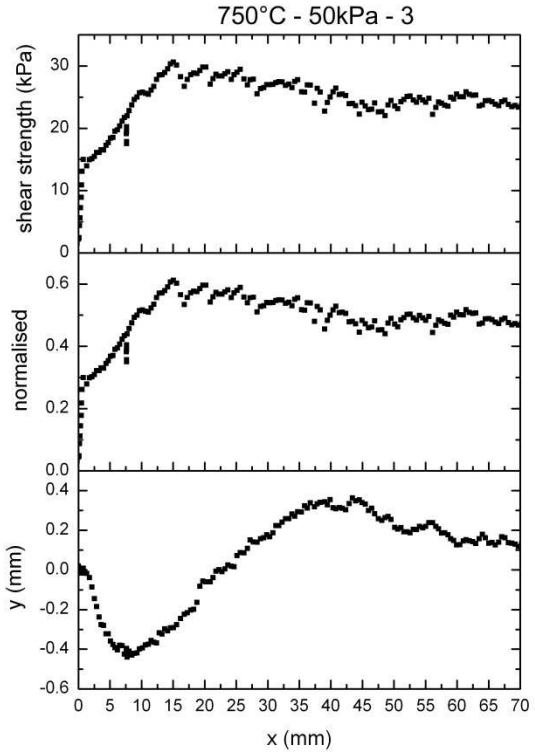

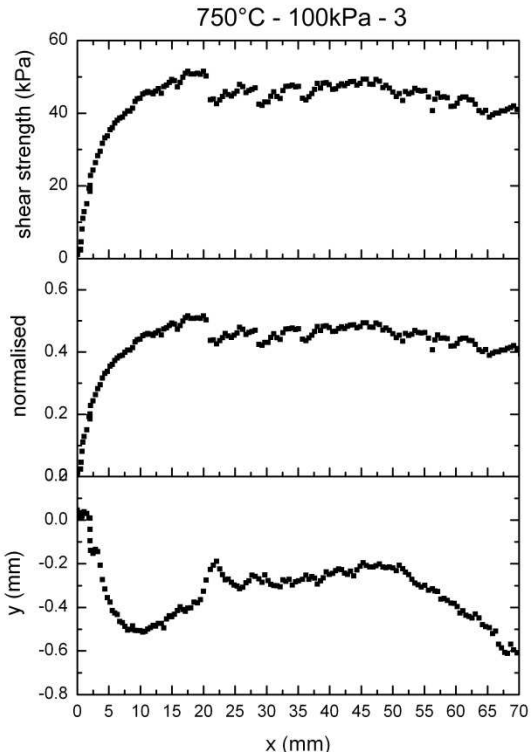

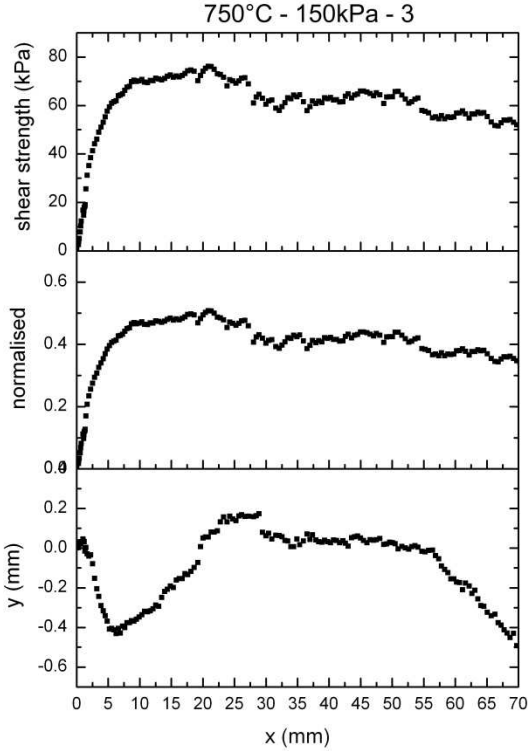

750°C 50kPa 3: dilatant inflection point not in line with peak shear stress

750°C 100kPa 3: inconsistent dilatant behaviour

750°C 150kPa 3: drop in shear stress at 25mm displacement

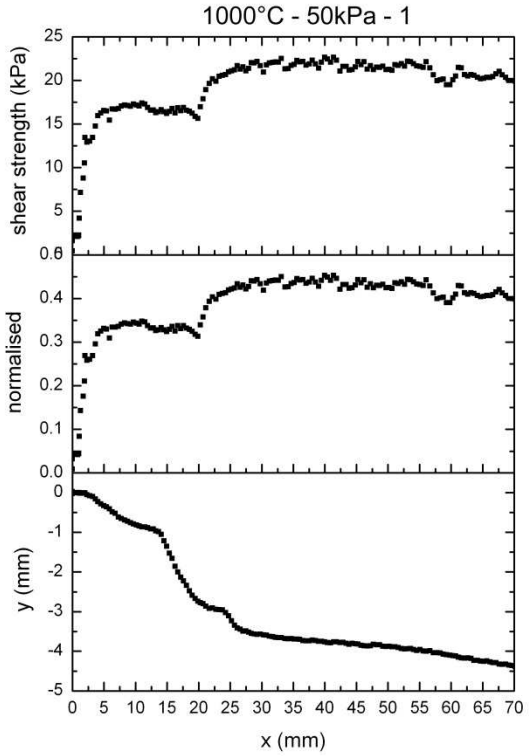

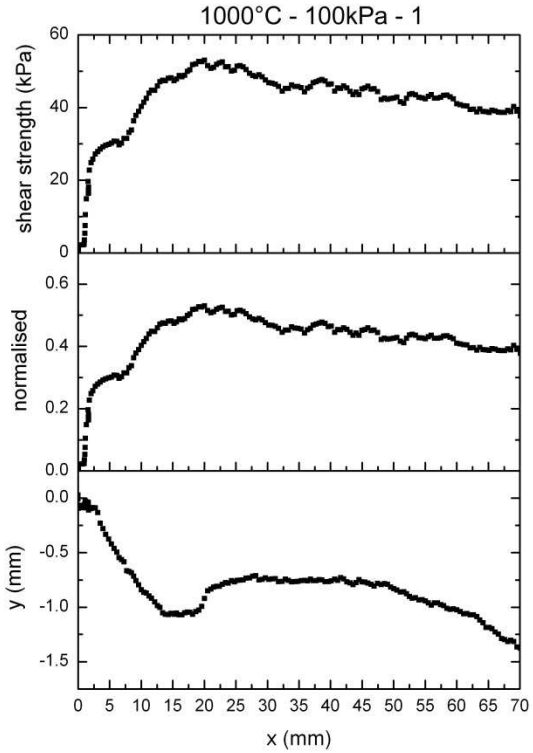

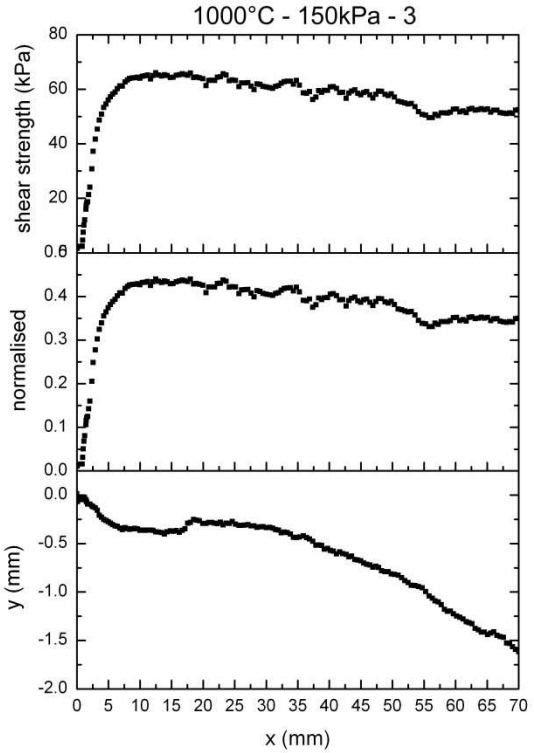

1000°C 50kPa 1:no dilatant inflection point

1000°C 100kPa 1: no dilatant inflection point

1000°C 150kPa 3: no dilatant inflection point

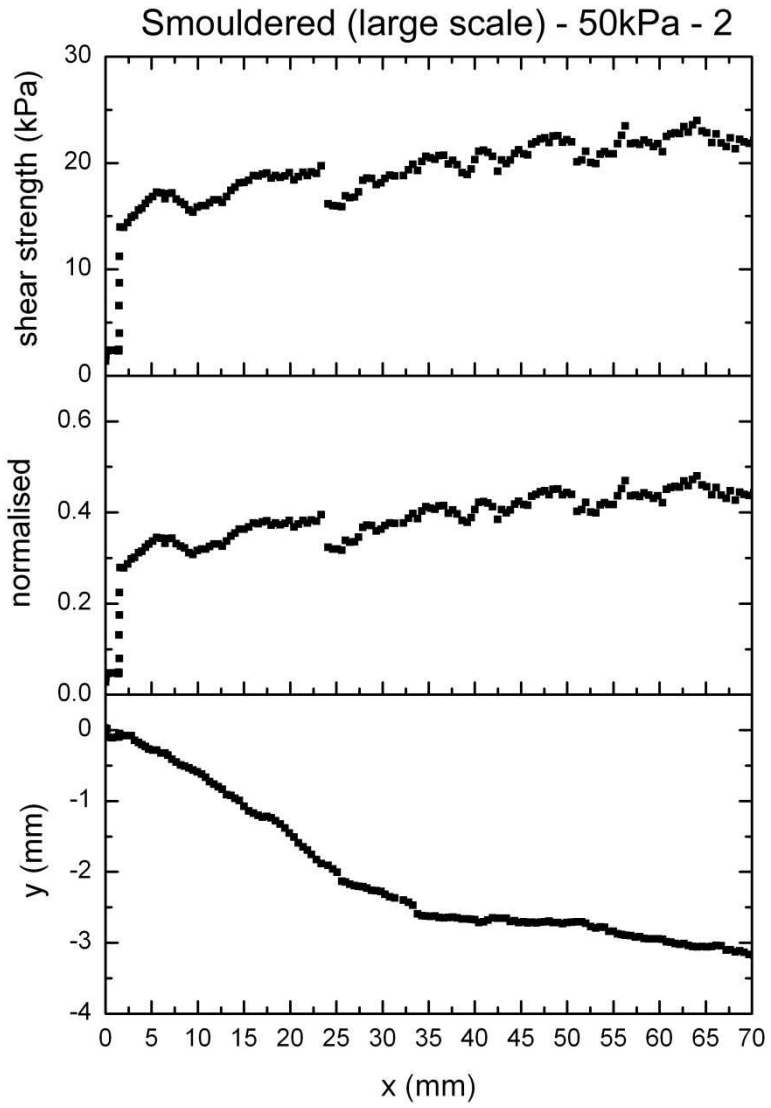

Smouldered (large scale) 50kPa 2: no peak shear stress